

**Sources and sinks of branched tetraether lipids and
bacteriohopanepolyols in a major river system
(Yenisei River – Kara Sea)**

Implications for their application as geochemical tracers

Cindy De Jonge

Colofon

ISBN:

978-94-6203-808-0

Graphic design cover and inside:

Lieselotte De Jonge

Photography:

Cover photo: Copyright Cindy De Jonge

Inside photos: Cindy De Jonge and Alina Stadnitskaia

Printed by:

CPI – Koninklijke Wöhrmann, Zutphen

**Sources and sinks of branched tetraether lipids and bacteriohopanepolyols
in a major river system
(Yenisei River – Kara Sea)
Implications for their application as geochemical tracers**

**Bronnen, afbraak en opslag van vertakte tetraether lipiden en
bacteriohopanepolyolen in een uitgebreid rivierbekken en zijn monding
(Yenisei – Kara Zee)
Implicaties voor hun toepassing als geochemische indicatoren
(met een samenvatting in het Nederlands)**

**Источники формирования и исчезновения разветвлённых
глицеролдиалкил- глицеролтетраэфиров и бактериальных
гопанопиолов в крупной речной системе (Енисей - Карское море)
Результаты их применения в качестве геохимических индикаторов
(С кратким изложением на русском языке)**

Proefschrift

ter verkrijging van de graad van doctor aan de Universiteit Utrecht op gezag
van de rector magnificus, prof. dr. G.J. van der Zwaan, ingevolge het besluit
van het college voor promoties in het openbaar te verdedigen op vrijdag 20
maart 2015 des middags te 2.30 uur

door

Cindy De Jonge

geboren op 31 december 1987
te Gent, België

Promotor: Prof. dr. J. S. Sinninghe Damsté

This work has been financially supported by the Research Council for Earth and Life Sciences of the Netherlands Organization for Scientific Research (NWO-ALW), the European Research Council (ERC) and the Royal Netherlands Institute for Sea Research (NIOZ).

Voor Rob, Ralph en Margaux

CONTENTS

Chapter 1.	Introduction	p. 9
------------	--------------	------

Part I 6-methyl brGDGTs and their implication for palaeoclimate reconstructions

Chapter 2.	Identification of novel penta- and hexamethylated branched glycerol dialkyl glycerol tetraethers in peat using HPLC–MS ² , GC–MS and GC–SMB-MS	p. 27
------------	---	-------

De Jonge et al., Org. Geochem 54, 78-82 (2013)

Chapter 3.	Occurrence and abundance of 6-methyl branched glycerol dialkyl glycerol tetraethers in soils: implications for palaeoclimate reconstruction	p.37
------------	---	------

De Jonge et al., Geochim. Cosmochim. Acta 141, 97-112 (2014)

Part II Sources, transport and degradation of bacterial lipids in the Yenisei River system and Kara Sea

Chapter 4.	In situ produced branched glycerol dialkyl glycerol tetraethers in suspended particulate matter from the Yenisei River, Eastern Siberia	p. 81
------------	---	-------

De Jonge et al., Geochim. Cosmochim. Acta 125, 476-491 (2014)

De Jonge et al. Geochim. Cosmochim. Acta 150, 345-346 (2015)

Chapter 5.	Tracing riverine branched glycerol dialkyl glycerol tetraethers in the outflow of the Selenga River in Lake Baikal (Russia)	p.107
------------	---	-------

De Jonge et al., submitted to Org. Geochem.

Chapter 6.	Drastic changes in distributions of branched tetraether lipids in suspended matter and sediments from the Yenisei River and Kara Sea (Siberia): Implications for the use of GDGT-based proxies in coastal marine sediments	p.129
------------	--	-------

De Jonge et al., submitted to Geochim. Cosmochim. Acta

Chapter 7.	Bacteriohopanepolyols in Yenisei River and Kara Sea suspended particulate matter and sediments trace terrigenous organic matter input and submerged permafrost	p. 173
------------	--	--------

Chapter 8.	Downcore variations in brGDGTs record rising sea levels in the Kara Sea and indicate changing sources	p. 201
------------	---	--------

References	p. 227
------------	--------

Summary	p. 244
Samenvatting	p. 246
Резюме	p. 249

Acknowledgments	p. 252
-----------------	--------

Curriculum Vitae	p. 254
------------------	--------



Photo by Cindy De Jonge

Introduction and outline

1

1. The need for palaeoclimate reconstruction

Understanding and predicting climate variability is a major scientific challenge, especially as climate-induced environmental change will impact on human society. Models to predict future climates are increasingly complex, and partly based on what we know of the climate in the past, both from the recent instrumental and historical records as well as from geological climate archives such as lacustrine and marine sediments, ice cores, speleothems, corals, and tree rings. Especially with the current (and accelerating) rise in the concentration of greenhouse gasses in the atmosphere (Hartmann et al., 2013), that cause the warming of the globe, an understanding of warm climate systems of the past can be useful when developing models for what to expect in the future. As continental air temperature has a direct impact on (human) life, a large effort has been made to reconstruct temperatures of the past. Moreover, as terrigenous environments occupy one third of the Earth's surface, they are a crucial factor in the global climate system (Hartmann et al., 2013). The temperature of the atmosphere directly impacts the prevailing vegetation types, but also affects the energy budget of the weather system, impacting on evaporation and precipitation intensities. The direct interaction between biosphere and atmosphere also results in changing amounts of greenhouse gasses (e.g. Chapin et al., 2008; Anderson-Teixeira et al., 2012). This is not limited to vegetation, also the carbon stored in soils can contribute in a temperature-dependent way to the amount of atmospheric greenhouse gasses (e.g. Davidson and Janssens, 2006; Smith et al., 2008; Chapin et al., 2009). Furthermore, as global ocean currents are driven by prevailing winds, temperature differences within the atmosphere also influence the redistribution of warmth stored in oceanic water masses, further influencing the global climate.

As the climate system has not shown large variations since the start of instrumental records (air temperature has only been recorded since ca. 1850), climate reconstructions have to be performed over larger timescales. For this purpose, indicators called proxies are used to estimate past temperatures. The development of a palaeoclimate proxy is based on the calibration of a measurable property to modern environmental conditions. For biological entities, this can happen on several scales, from variations in species assemblies, to variations in the size and chemical composition of organisms or specific organs, and by changes in the chemical structure and even in the stable isotopic values of molecules and atoms. So far, continental temperature reconstructions are hampered by a lack of quantitative temperature proxies and, consequently, are often qualitative rather than quantitative. Commonly used biological proxies for the reconstruction of continental air temperature include pollen analysis (e.g. Davis and Shaw, 2001), the width of tree rings (Cook and Kairiūkštis, 1990), and the morphological properties of fossilized leaves (e.g. Bailey and Sinnot, 1915; Peppe et al., 2011). However, as these proxies are based on vegetation type, they are also influenced by the amount of precipitation (e.g. Jordan, 1997; Adams and Kolb, 2005), migration patterns and extinction of species (e.g. Davis

and Shaw, 2001) and increases in the CO₂ concentration (e.g. Cowling et al., 1999). A second group of continental palaeothermometers is based on the $\delta^{18}\text{O}$ signal of meteoric water, as it varies with the atmospheric temperature. This signal can be recorded directly in ice cores (e.g. Johnsen et al., 2001), and is also reflected in authigenic and biogenic carbonates (e.g. Leng and Marshall, 2004), diatomaceous silica (e.g. Leng and Barker, 2006), speleothems (e.g. McDermott, 2004) and in mammal bone phosphate (e.g. Longinelli, 1984). However, the stable isotopic composition of the source of the meteoric water can change through time, complicating the interpretation of the measured $\delta^{18}\text{O}$ values in the record.

As the temperature of lake water is closely connected to the overlying air temperature, proxies that reconstruct the lake water temperature can record a local air temperature signal. In this respect, fossilized skulls of chironomids can be used to quantitatively trace palaeotemperatures (e.g. Walker et al., 1991). The TEX₈₆, a lipid-based proxy that relies on the temperature-dependent incorporation of cyclopentane moieties in membrane-spanning tetraether lipids of freshwater archaea (Schouten et al., 2002), has been shown to vary with air temperature in lake settings (e.g. Powers et al., 2004, 2010; Tierney et al., 2008; Blaga et al., 2013). However, the application of TEX₈₆ is limited to a subset of lakes due to confounding factors such as inputs from the watershed, multi-species production, or the absence of the compounds of interest (e.g. Blaga et al., 2009). Recently, the structural diversity of long-chain diols in lake sediments has shown potential for reconstructing lake-water temperatures (Rampen et al., 2014). Membrane-spanning branched tetraether lipids, produced by bacteria, have also been found to respond to prevailing temperature, both in soils as in lakes (see Schouten et al., 2013a for a review). I will elaborate on this proxy in the following sections.

2. Branched tetraether lipids: Structural diversity.

The research on branched Glycerol Dialkyl Glycerol Tetraethers (GDGTs) was initiated when advances in high performance liquid chromatography-mass spectrometry (HPLC-MS) methods (Hopmans et al., 2000) allowed the analysis of GDGT compounds. These rigid compounds have been described to be components of prokaryotic membranes (e.g. Chong, 2010 and references therein). Although membrane-spanning GDGT lipids were previously thought to be characteristic of hyperthermophilic archaea, because of their temperature- and mechanically resistant structure (e.g. van de Vossenberg et al., 1998), application of the HPLC-MS technique to environmental samples revealed that abundant membrane spanning GDGT lipids, both isoprenoid and branched, occur in low-temperature marine environments (marine sediments) and terrigenous environments (Schouten et al., 2000).

The first structural identification of two branched GDGTs (brGDGTs Ia and IIa, see Fig. 1 for structures) was done by Sinninghe Damsté et al. (2000), after isolation of these components from a Dutch peat followed by structural identification using 2D Nuclear Magnetic Resonance (NMR) spectroscopy. Cleavage of the ether bonds with HI produced two dominant hydrocarbons. The EI mass spectrum of the C₃₀ and C₃₁ branched alkanes, revealed the presence of di- or trimethyl branched C₂₈ linear chains, with methyl branching at C13 and C16, and a possible third methyl group at C5. This was confirmed by the co-elution of an authentic 13,16-dimethyloctacosane standard (Chappe et al., 1979).

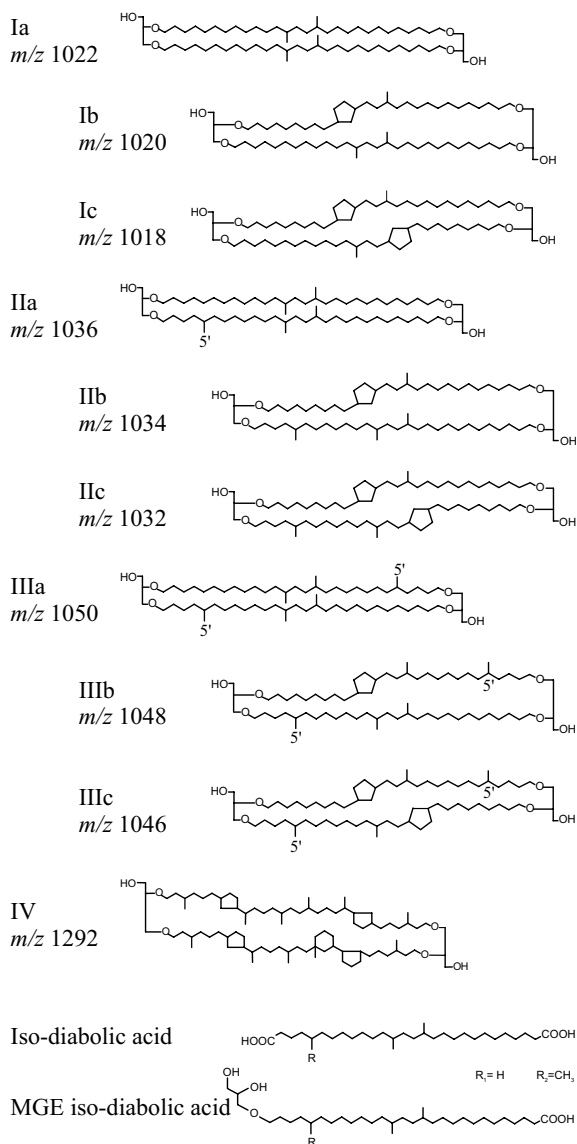


Fig. 1. Chemical structures of branched GDGTs (I-III) and crenarchaeol (IV), brGDGT core lipids that are found ubiquitously in the environment. BrGDGTs Ia, Ib and Ic are referred to as 'tetramethylated', brGDGTs IIa, IIb and IIc are referred to as 'pentamethylated', brGDGTs IIIa, IIIb and IIIc are referred to as 'hexamethylated' brGDGTs. Iso-diabolic acid and the Monoalkyl Glycerol Ether (MGE) iso-diabolic acid are found in hydrolized fractions of Acidobacterial cultures, with two (R1) or three (R2) branches.

The alkyl chains that form the backbone of the brGDGT lipid, are thus not comprised of isoprenoid moieties, as in the case of the known archaeal GDGTs (De Rosa et al., 1986 and references therein), but are straight chains with a variable number of methyl groups. Although brGDGTs with cyclopentane moieties were tentatively identified by Schouten et al. (2000), based on the EI mass spectrum of alkyl chains containing one and two cyclopentane moieties, the presence of the internal cyclization was unequivocally confirmed by Weijers et al. (2006) after isolation of the brGDGT Ib, followed by NMR characterization. Furthermore, this study gave the first molecular evidence of their bacterial origin. The stereochemistry of the glycerol backbone was found to be the bacterial 1,2-di-O-alkyl-sn-glycerol stereoconfiguration and not the 2,3-di-O-alkyl-sn-glycerol stereoconfiguration as in archaeal membrane lipids. As the number of methyl groups per alkyl chain can vary from 2 to 4 (4 to 6 methyl groups per brGDGT lipid), and the brGDGT lipids can contain up to two cyclopentane moieties after internal cyclization, this results in the existence of nine structures (Fig. 1). In the environment, brGDGTs encountered as these structures are referred to as the core lipids (CL).

Intact polar lipid (IPL) brGDGTs, that have a polar headgroup attached to the CL brGDGT structure, have also been described from environmental samples (Liu et al., 2010; Peterse et al., 2011a). The described structural variability within the polar headgroups of brGDGTs currently encompasses a glucose or glucuronyl head group (Liu et al., 2010), a hexose and a glycuronic acid moiety, a phospho-hexose moiety and a hexose-phosphoglycerol moiety as headgroup (Peterse et al., 2011a). The presence of these IPL brGDGTs in the environment (e.g. Zell et al., 2013) has been attributed to living or recently living bacteria as the polar headgroup was assumed to degrade rapidly after cell death (e.g. White et al., 1979). Studying the abundance and variability of the IPL brGDGT thus allows to discuss a fresh and possibly in-situ produced brGDGT signal, while CL brGDGTs allow to evaluate the ‘fossilized fraction’.

3. Potential biological sources of brGDGTs

BrGDGTs are ubiquitous lipids in the environment, and both CL and IPL brGDGTs have been found in peat, soils, freshwater systems and marine systems (Schouten et al., 2013a and references therein). The ecological niche of the brGDGT source organism has been studied based on the concentration of CL and IPL brGDGTs in the environments, and their stable isotopic composition. Pancost and Sinninghe Damsté (2003) analyzed the stable carbon isotopic signature ($\delta^{13}\text{C}$) of brGDGT-derived alkyl chains in peat, and inferred that the source organism is a heterotrophic organism. Also based on the $\delta^{13}\text{C}$ values of the alkyl chains, a similar conclusion was made by Oppermann et al. (2010) and Weijers et al. (2010) for soil brGDGTs. The abundance of brGDGT lipids was found to increase in anoxic environments; in the catotelm layer of peat (CL brGDGTs in Weijers et al., 2009a; CL and IPL brGDGTs in Peterse et al., 2011a), in the suboxic water layer of stratified lakes (Sinninghe Damsté et al., 2009; Buckles et al., 2014a) and in subsurface sediments (Tierney et al., 2012). This indicates that the source organisms possibly have an affinity with anoxic or suboxic environments, although enhanced preservation in less oxic environments may also explain the observed distributions. Furthermore, the brGDGT source organisms are not limited to these environments, as they are produced in soils globally (Weijers et al., 2007a), and in oxygenated surface waters (e.g. Loomis et al., 2014a).

In peat, the environment where CL brGDGTs are found in the highest concentrations, 16S rRNA gene sequencing showed that the bacterial community exists almost exclusively of Acidobacteria (Weijers et al., 2009a). Furthermore, IPL brGDGT abundances in a long-term pH manipulation plot were found to decrease with increasing pH, supporting the hypothesis that Acidobacteria are a dominant source of these compounds (Peterse et al., 2010). Environmental genome sequencing has established that Acidobacterial sequences are particularly abundant in soils, comprising 10 to 50% of the total bacterial 16S rRNA gene sequences in clone libraries (e.g. Dedysh et al., 2006; Fracchia et al., 2006; Janssen, 2006; Lee et al., 2008).

Acidobacteria are furthermore present in soils that differ greatly in physical and chemical characteristics, e.g. agricultural soils, arid soils, but also in heavily contaminated soils (Buckley and Schmidt, 2003; Dunbar et al., 1999, 2002; Barns et al., 2007). In surface soils, their phylogenetic variance and abundance seems to be dominantly controlled by soil pH (e.g. Fierer and Jackson, 2006; Fierer et al., 2007; Lauber et al., 2009). Acidobacteria are also present in river sediments (e.g. Branco et al., 2005; Hu et al., 2014), and occur in lower abundance in the overlying water column (Hu et al., 2014). They were found to be a minor component (i.e. <2.6 %) of the bacterioplankton in lake epilimnia (Newton et al., 2011) but can represent an abundant component (up to 31%) of the microbial ecosystem in lacustrine sediments (e.g. Barns et al., 1999; Dong et al., 2006). Acidobacteria are also encountered in the marine system, where they can occupy a range of environments; sediments (e.g. Barns et al., 1999; Polymenakou et al., 2005), deep-sea corals (Penn et al., 2006) and hydrothermal vents (e.g. Sievert et al., 2000). The widespread abundance of these proposed source organisms fits with the ubiquitous presence of brGDGTs.

These observations have led to the detailed characterization of the lipids of Acidobacteria. However, so far only one brGDGT (i.e. Ia) has been identified to be present in trace amounts in two strains of Acidobacteria of subdivision (SD) 1 (Sinninghe Damsté et al., 2011). Nevertheless, the hydrolized Acidobacterial cultures contain abundant amounts of 13,16-dimethyl octacosanedioic acid (iso-diabolic acid), a compound that is structurally related to the branched alkane chains of brGDGTs (Fig. 1; Sinninghe Damsté et al., 2011, 2014). While the majority of mono-glycerol iso-diabolic acid chains in the Acidobacterial SD 1 contained an ester-bond between the alkyl chain and the glycerol moiety, ether-bound branched alkyl chains (monoalkyl glycerol ethers) are dominant in the cultures studied in SD 4 of the Acidobacteria (Sinninghe Damsté et al., 2014). Furthermore, iso-diabolic acid moieties with a methylation on the C5 position (Fig. 1), i.e. the alkyl backbone of the penta- and hexamethylated brGDGTs II and III, were observed in this subdivision. The intermittent presence (6 out of 7 strains studied) of the C₃₀ and C₃₁ branched alkanes within SD 4, and the absence of trimethyl C₂₈ alkanes in SD 1 and 3, indicate that the production of the GDGT alkyl chains has a genetic component.

4. BrGDGT-based palaeoenvironmental reconstructions

Studying the fractional abundance of brGDGTs in a dataset of globally distributed soils (n = 134), the relative distribution of the nine brGDGTs was shown to vary with soil pH and the mean annual air temperature (MAT) by Weijers et al. (2007a). A biochemical mechanism was proposed to explain the observed correlations. In warmer soils the increase in fractional abundance of tetramethylated brGDGTs was inferred to be a homeoviscous adaptation

mechanism to counteract the temperature-induced increased fluidity of the bacterial membrane. The incorporation of cyclopentane-containing brGDGTs in high pH soils, was proposed to influence the permeability of the bacterial membrane, in reaction on a changing cross-membrane pH gradient. However, the recent understanding on the irregular presence of only a few of the brGDGT-related alkyl chains within the Acidobacterial cultures studied (Sinninghe Damsté et al., 2011, 2014), indicates that the observed changes may possibly also be caused by a shift in the bacterial community, that is induced by changes in the soil MAT and pH.

Weijers et al. (2007a) summarized the brGDGT distribution in two indices; the Cyclization of Branched Tetraethers (CBT [Eq. 1]) and the Methylation of Branched Tetraethers (MBT [Eq. 2]).

$$\text{CBT} = -\log[(\text{Ib}+\text{IIb})/(\text{Ia}+\text{IIa})] \quad [\text{Eq. 1}]$$

$$\text{MBT} = (\text{Ia}+\text{Ib}+\text{Ic})/(\text{Ia}+\text{Ib}+\text{Ic}+\text{IIa}+\text{IIb}+\text{IIc}+\text{IIIa}+\text{IIIb}+\text{IIIc}) \quad [\text{Eq. 2}]$$

The CBT followed a first-order function with measured soil pH, with an associated residual standard mean error (RSME) of 0.7 pH units [Eq. 3].

$$\text{CBT} = 3.33 - 0.38 \times \text{pH} \quad (r^2 = 0.70) \quad [\text{Eq. 3}]$$

The MBT was shown to vary both with soil pH and MAT. This resulted in a second-order correlation with MAT with an associated RSME of 4.8 °C [Eq. 4].

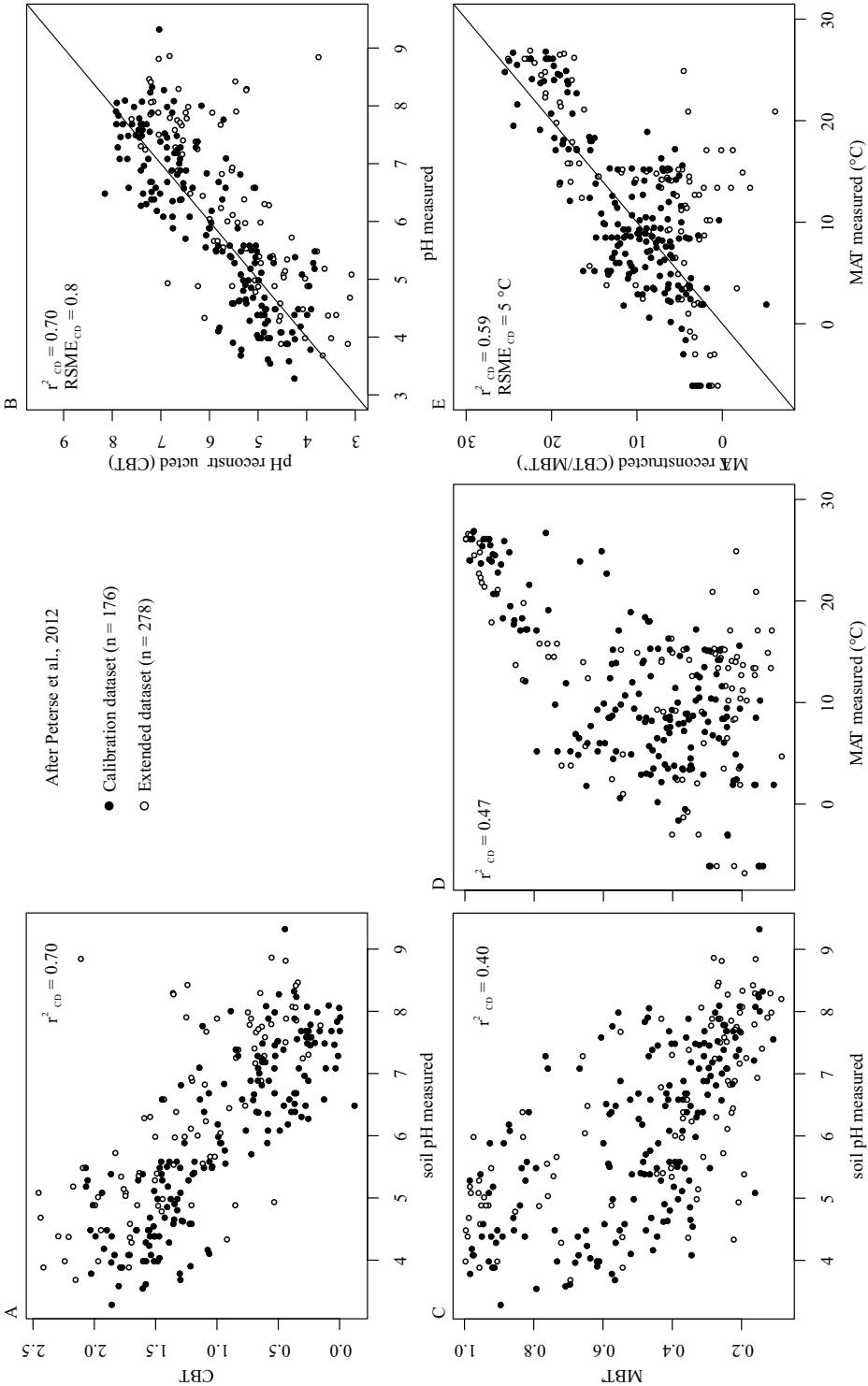
$$\text{MBT} = 0.122 + 0.187 \times \text{CBT} + 0.020 \times \text{MAT} \quad (r^2 = 0.77) \quad [\text{Eq. 4}]$$

A follow-up study (Peterse et al., 2012) was performed on an extended dataset that included 278 surface soils (Fig. 2). Although the calibration dataset ($n=176$) was subjected to a rigorous statistical analysis, the CBT and MBT indices could not be significantly improved. However, the MBT proxy was simplified (i.e. the MBT'), excluding two minor brGDGT compounds (IIIc and IIIc'). The CBT still showed a good correlation with soil pH (Fig. 2A; $r^2=0.70$), and the MBT' with the soil pH and MAT (Fig. 2C, D; $r^2=0.40$ and 0.47 , respectively). Revised calibrations were developed [Eq. 5, 6], that were associated with an RSME of 0.8 pH units (Fig. 2B) and 5.0 °C (Fig. 2E), respectively.

$$\text{pH} = 7.90 - 1.97 \times \text{CBT} \quad (r^2 = 0.70) \quad [\text{Eq. 5}]$$

$$\text{MAT} = 0.81 - 5.67 \times \text{CBT} + 31.0 \times \text{MBT}' \quad (r^2 = 0.59) \quad [\text{Eq. 6}]$$

However, this study also highlighted the large error associated with the MAT reconstruction of temperate soils and the problematic MAT reconstruction of arid soils, where the reconstructed MAT underestimated the measured MAT with up to 20 °C. This offset, referred to as the “cold bias”, was afterwards confirmed by several studies (Dirganchi et al., 2013; Menges et al., 2013).



◀ Fig. 2. The CBT [Eq. 1] and the MBT' [modified after Eq. 2] indices are calculated based on the datasets as defined in Peterse et al., 2012, where both the values for the calibration dataset (black symbols) and extended dataset (white symbols) are reported. The reported correlation of these indices with the measured soil pH (A and C) and the measured MAT (D) is illustrated. In panel B and E the reconstructed pH [Eq. 5] and the reconstructed MAT [Eq. 6] are plotted against the measured values. In each panel, the squared pearson correlation coefficient (r^2) is reported for the calibration dataset, and the 1/1 ratio is indicated in the panels B and E.

The brGDGT-based palaeoclimate proxies (CBT and MBT/MBT') have been used to reconstruct temperature and pH variations in a number of settings; palaeosoils (e.g. Peterse et al., 2011b), speleothems (e.g. Blyth and Schouten, 2013a), lacustrine sediments (e.g. Niemann et al., 2012), but firstly in marine sediments. For this application as a palaeoclimate proxy, the downcore diversity of brGDGTs in river fan sediments was assumed to represent an average signal of the soils present in the entire river watershed, which was brought to the coastal marine sediments following soil erosion and transport by rivers. This was confirmed by preliminary studies on the presence of brGDGTs in river sediments (e.g. Kim et al., 2006; 2007), and the observation that the concentration of brGDGT lipids decreases with increasing distance from river mouth (Hopmans et al., 2004; Herfort et al., 2006; Kim et al., 2006). Correspondingly, the temperature and pH evolution of the Congo Basin during the last deglaciation has been reconstructed by Weijers et al. (2007b; 2009b), while the temperature evolution of the Amazon River Basin during the last 37 ka has been reconstructed by Bendle et al. (2010). Older samples allowed the reconstruction of the temperature changes in the Arctic during the Paleocene-Eocene (Weijers et al., 2007c) and Eocene-Oligocene boundary (Schouten et al., 2008). Donders et al. (2009) reconstructed a cooling trend in Miocene Northern Europe, while Pross et al. (2012) used CBT/MBT to reconstruct temperatures along the Atlantic coast during the early Eocene.

As brGDGT lipids were found to be present in the highest abundance in soils, their presence in the marine environment was assumed to trace soil-derived OM. For this purpose, the Branched and Isoprenoid Tetraether (BIT) index was developed, contrasting the abundance of three major brGDGTs against the marine archaeal marker crenarchaeol. As crenarchaeol is characteristic for marine Thaumarchaeota (Sinninghe Damsté et al., 2002), it is present in low levels in soils, and the resulting BIT-index in soils is generally close to unity (>0.7 ; Schouten et al., 2013a). This proxy correlates well with traditional biomarker proxies for terrigenous transport, such as lignin, odd-numbered n-alkanes (Hopmans et al., 2004), and with bulk OM proxies, both $\delta^{13}\text{C}_{\text{org}}$ values (Hopmans et al., 2004) and C/N ratios. As GDGT lipids are conserved in the sedimentary archive, changes in the BIT values can be interpreted as changes in soil (bacterial) OM delivered to the site and, consequently, in the reconstruction of the discharge of river systems in the past (Ménot et al., 2006).

Recent studies have indicated that this approach is probably over-simplified since the production of brGDGTs is not limited to soil and peat environments. Although a variable fraction of the brGDGTs encountered in rivers, lakes and the marine system is derived from soils, recent studies found evidence of the production of brGDGTs both in freshwater and marine aquatic environments. Based on the different brGDGT distribution and concentration

between lake systems and their watershed soils, aquatic brGDGTs were found to be produced in lakes (e.g. Tierney and Russell, 2009; Loomis et al., 2011; 2014ab; Tierney et al., 2012; Wang et al., 2012; Buckles et al., 2014ab) and rivers (e.g. Tierney and Russell, 2009; Zell et al., 2013, 2014a; Buckles et al., 2014b). Overall, hexamethylated and cyclopentane-containing brGDGTs are enriched in lakes compared to the surrounding soils, resulting in relatively colder reconstructed temperatures and increased reconstructed pH values, based on the lacustrine brGDGT distribution. Although the brGDGT distribution of lakes differs from the surrounding soils, lacustrine sedimentary brGDGT distributions formed under different temperature regimes (e.g. along an altitudinal gradient; Loomis et al., 2012, or along a latitudinal gradient; Pearson et al., 2011; Sun et al., 2011) reveal that the distribution of aquatic brGDGTs also varies with temperature, although the temperature dependence may be different than the one observed in soils. Several authors have developed temperature calibrations based on brGDGT distributions from lake sediments (e.g. Tierney et al., 2010; Pearson et al., 2011; Sun et al., 2011; Loomis et al., 2012). The influence of the lake water pH and lake depth on cyclopentane-containing brGDGTs is less well constrained (e.g. Pearson et al., 2011; Loomis et al., 2012).

In-situ production in coastal and offshore marine sediments was shown to increase the fractional abundance of cyclopentane-containing brGDGTs, which is possibly related to the generally higher pH (± 8.5) of the marine sedimentary pore waters (e.g. Peterse et al., 2009a; Zhu et al., 2011a; Zell et al., 2014a, 2014b; Weijers et al., 2014).

5. Bacteriohopanepolyols: an independent tracer for soil-derived bacterial OM

Recently, an independent tracer for soil-derived, river-transported bacterial OM in the marine environment was developed, based on bacteriohopanepolyols (BHPs). BHPs are structurally diverse lipids that contain a ring system that is formed by an intramolecular cyclization of squalene by the enzyme squalene-hopene-cyclase (e.g. Rohmer et al., 1993). Additional methyl groups can be present on the A-ring, at C-2 and C-3 positions (Fig. 3). The side-chain, an n-alkyl polyfunctionalized C_5 unit is covalently attached to the C-29 of the hopane skeleton. Additional moieties can be linked at C-35, via an ether or amino link (Fig. 3). BHPs containing an extra functionality at C-35 may play a role in the formation of lipid rafts within the cell membrane (e.g. Sáenz, 2010).

Rohmer et al. (1984) were the first to describe the apparent widespread distribution of BHPs in Bacteria, although more recent work by Pearson et al. (2007) indicated that BHPs are only produced by ca. 10% of all bacterial species. Early work on the biological function of these lipids has indicated that certain BHPs are produced in response to environmental stressors on the bacterial membrane, such as pH and increased growth temperature (Langworthy et al., 1976). The biosynthesis of BHPs in response to changes in the bacterial lipid membrane is now widely accepted (e.g. Poralla et al., 2000). Some BHPs were also found to have a chemotaxonomic-specific occurrence, such as for methylotrophic bacteria (Neunlist and Rohmer, 1985a), cyanobacteria (Bisseret et al., 1985; Talbot et al., 2008), purple non-sulphur bacteria (Neunlist and Rohmer, 1985b), acetic acid bacteria (Herrmann et al., 1996), methanotrophic bacteria (Talbot et al., 2001), planctomycetes (Sinninghe Damsté et al., 2004), and sulfate-reducing

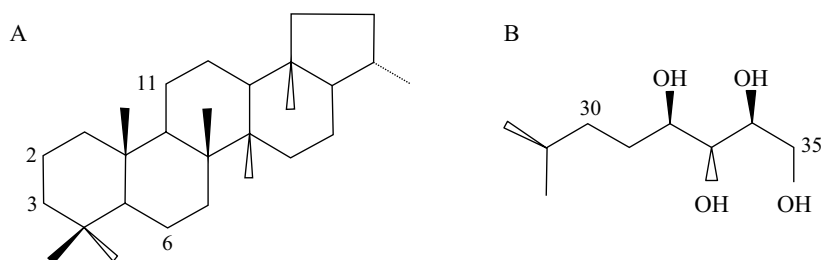


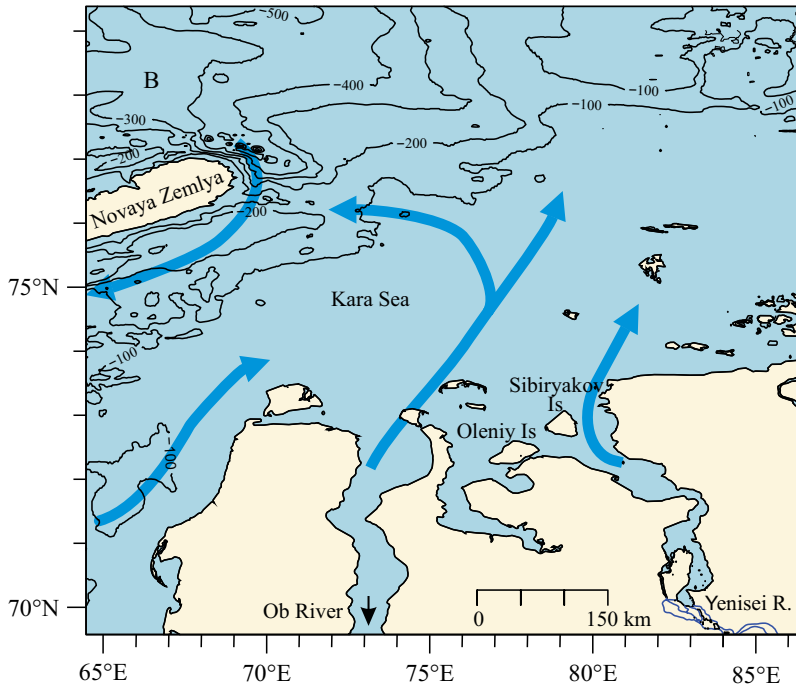
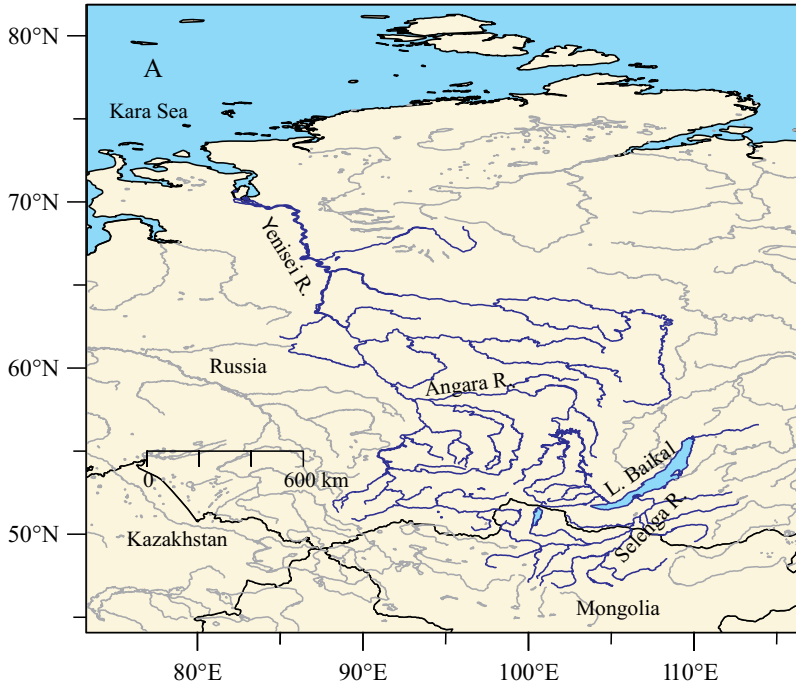
Fig. 3. Ring system (A) and the side chain (B), as described for bacteriohopanetetrol (BHT).

bacteria (Blumenberg et al., 2006). Furthermore, the study of BHPs in the environment has allowed identifying BHP distributions typical for soils (Cooke et al., 2010a, b; Rethemeyer et al., 2010), and for the marine environment (e.g. Zhu et al., 2011b). This has led to the development of two ratios (the R_{soil} and the R'_{soil}) that trace the transport of soil-derived bacterial OM, by evaluating the concentration of three groups of soil-marker BHPs, relative to the pseudo-marine end-member bacteriohopanetetrol (e.g. Zhu et al., 2011b; Doğrul Selver et al., 2012).

6. The Yenisei River and Kara Sea

The study of the delivery of terrigenous organic matter (OM) to the marine system is of paramount importance in the study of the global carbon cycle (e.g. Blair and Aller, 2012). It is a critical component for models of elemental cycling in the modern coastal ocean and for models of atmospheric compositions over geologic time (e.g. Berner et al., 2004). This is even more relevant for the OM transported into the Arctic, as its watersheds contain large areas of permafrost, where up to 33% of global soil OM is stored, predominantly present in taiga and tundra soils (Waelbroeck et al., 1997; Oechel et al., 2000). This is one of the so-called vulnerable carbon pools (Field and Raupach, 2004) as climate warming will cause the mobilization of this “old” terrestrial OC (Schuur et al., 2009). Studying the export of OM from the Arctic region is furthermore important as climate models forecast an amplification of global warming in this region (e.g. Zwiers, 2002), and there is already evidence for increasing river discharge and changes in the hydrological regime in the Eurasian continent (e.g. Peterson, 2002). These changes will also have an effect on the hydrology of the Arctic Ocean and its shelf seas. The formation of a freshwater lid on the Arctic Ocean, that is mainly derived from rivers, is essential for sea-ice formation and for sustaining the strong stratification of near-surface water masses of the Arctic Ocean (Aagaard and Carmack, 1989), which in turn can have a positive feedback effect on the climatic system, as a weaker stratification leads to less CO₂ trapped in the abyss, possibly amplifying global warming (e.g. Sigman et al., 2004).

The Yenisei River watershed (2.6 x 106 km²) covers a large part of Mongolia and Russian Siberia (Telang et al., 1991; Fig. 4A). The headwaters of the Yenisei River originate in the



◀ Fig. 4. Maps of the Yenisei River watershed and Kara Sea. A) The Yenisei River and its tributaries (e.g. Angara River, Selenga River) are indicated in blue, delineating the Yenisei River watershed. B) The river mouth of the Ob and Yenisei River are indicated, and the dominant surface currents present in the Kara are drawn in blue, after Pavlov and Pfirman (1995).

Sayan Mountains in the Asian Tuva, where also the Selenga River originates, before it flows down towards Lake Baikal. Lake Baikal has one outflow, the Angara River, that joins the Yenisei River in Krasnojarsk, as its major tributary (25% of the flow). The Yenisei River flows further north, west of the Siberian plateau, where the majority of its tributaries originate. Here, its major tributary is the Lower Tunguska (20% of the flow). The Yenisei River watershed spans a large latitudinal gradient that, together with the observed height differences, implies the presence of different climate systems and corresponding biomes. Mountainous areas and Mongolian steppe are present in the Southern part of the watershed, while large stretches of temperate broadleaf forests in the temperate areas are replaced by coniferous and shrubby taiga on the Siberian plateau, and shrubby tundra in the northern realm of the watershed.

The Kara Sea (Fig. 4B), where the Yenisei River Mouth is located, is the second largest shelf area of the Arctic Ocean, partially enclosed to the west by the large island Novaya Zemlya and the archipelago Franz Josef Land and to the south by the Siberian mainland. To the east it is partly confined by the archipelago Zevenaya and the Taimyr Peninsula, while the Kara Sea shelf is open to the Arctic Ocean to the north. About one third of the total freshwater discharge into the Arctic Ocean occurs through river run-off (Aagaard and Coachman, 1975). The Kara Sea drains a fifth of the continental run-off of the Eurasian continent into the Arctic Ocean (Lammers et al., 2001). The Yenisei River ranks ninth globally in terms of discharge ($630 \text{ km}^3 \cdot \text{year}^{-1}$; Bobrovitskaya et al., 1996). This water consists of 50% snowmelt, 35% rain water and approximately 15% groundwater (Pavlov and Pfirman, 1995). The Yenisei River is characterized by a pronounced discharge peak in June and relatively low water flow between September and April, with more than 30% of the annual discharge occurring in June (Stedmon et al., 2011). However, although this Siberian river has an extended catchment, the low thickness of weathered crust and low particulate matter wash-off from the surface of taiga and tundra leads to a low discharge of sediments. Indeed, the particulate matter run-off rate amounts up to only $4\text{--}9 \times 10^3 \text{ kg} \cdot \text{km}^{-2} \cdot \text{yr}^{-1}$, which is much below the annual average of $150 \times 10^3 \text{ kg} \cdot \text{km}^{-2} \cdot \text{yr}^{-1}$ (Milliman, 1991). Gebhardt et al. (2004) estimate that the Yenisei River yearly delivers $5.03 \times 10^9 \text{ kg}$ sediments, $0.57 \times 10^9 \text{ kg}$ particulate organic carbon and $0.084 \times 10^9 \text{ kg}$ particulate nitrogen to the Kara Sea. However, the majority (90%; Lobbes et al., 2000) of the OM delivered to the Kara Sea system is in the form of dissolved organic carbon (DOC).

The Kara Sea circulation is characterized by a strong seasonality. During the summer months, the surface currents in the Kara Sea follow a cyclonic circulation. The Greenland current enters the Kara Sea from the north, and passes along the east coast of the island Novaya Zemlya, flowing southwards. This water body is then joined by the discharge of the Ob and Yenisei

Rivers, before flowing further to the northeast (Fig. 4B, after Pavlov and Pfirman, 1995). From mid-October to mid-May, when only 10-15% of the river discharge happens (e.g. Pavlov and Pfirman, 1995), the Kara Sea and Yenisei River estuary are almost entirely ice-covered. The ice protects the uppermost water layers against wind mixing, and therefore the freshwater layer extends for a large distance under the ice, dispersing the little material delivered over a large distance (Lisitsyn, 1995). Between June and September, when most of the discharge happens (ca. 80%, e.g. Pavlov and Pfirman, 1995), the bulk of suspended load is deposited in front of the estuaries (Lisitsyn, 1995). This causes concentrations of suspended load to decrease by an order of magnitude between the surface isohaline of 2 and 20 psu (Lisitsyn, 1995). The high discharge period is characterized by a strong thermal stratification. Below the warm, fresh surface water, a salt-water tongue is present at 6-8 m in the inner Kara Sea, flowing onshore (Pavlov and Pfirman, 1995). Present sedimentation rates in the southern Kara Sea are estimated to range between approximately 0.2 to 1 mm . yr⁻¹, with the exception of shallow areas that are subjected to winnowing (Polyak et al., 2000). Sediment trap studies showed that sedimentation fluxes are highest in autumn and during the ice-covered months (Gaye et al., 2007).

7. Scope of this thesis

The reconstruction of past climates of Siberia, a region that seems to be sensitive to global climate change, is of paramount importance. Therefore, testing lipid-based tracers for bacterial OM delivered by the Yenisei River to the Kara Sea (BIT-index, R'_{soil}), and constraining the sources of the brGDGTs conserved in the marine sediments, will allow informed palaeoclimate reconstructions of the Yenisei River watershed in particular, but also of Siberian watersheds in general. In this thesis, we evaluate whether brGDGT present in the Yenisei River watershed are dominantly sourced from watershed soils and peat, or whether they are influenced by riverine in-situ production. Furthermore, the fate of riverine brGDGTs after their introduction in the marine (Kara Sea) and lacustrine environment (Lake Baikal) is reconstructed. The performance of the BIT-index as a tracer for terrigenous and riverine bacterial organic matter is tested, both in recent sediments as during a period that was characterized by eustatic changes in sea level. The findings in recent sediments are contrasted with an independent set of bacterial lipids that can trace terrigenous bacterial OM and specific bacterial groups, the bacteriohopanepolyols.

While studying the brGDGTs in the Yenisei River, novel brGDGTs were discovered and identified. This has an impact on the interpretation of currently used brGDGT palaeoclimate proxies. This latter aspect is described in Part 1 (Chapters 2 and 3) of the thesis, whereas the regional application of brGDGTs and BHPs is described in Part 2 of the thesis (Chapters 4 to 8).

Chapter 2 describes how novel 6-methyl hexamethylated brGDGTs, and their traditional 5-methyl counterparts, were isolated from a Siberian Peat. After preparative HPLC, we obtained two chromatographic peaks that previously co-eluted as brGDGT IIIa, and a pure fraction of brGDGT IIa. Using multistage HPLC, gas chromatography-supersonic molecular beam-mass spectrometry (GC-SMB-MS) and GC-MS, we determined that both a symmetrical and assymetrical hexamethylated brGDGT was present in each brGDGT IIIa peak. The different elution behavior was due to the position of the outer branches, that were present in the α and/or ω -5 position in the earlier elution peak (brGDGT IIIa), and in the α and/or ω -6 position in the later elution peak. Also brGDGT IIa was shown to contain two isomers, with a methylation on the C-5 and C-6 positions, respectively. **Chapter 3** describes an improved HPLC-based chromatographic method, using a sequence of four Alltima Silica columns, that allowed to quantify a total of six 6-methyl brGDGTs. Studying the dataset of globally distributed soils that was also used by Peterse et al. (2012) for the CBT/MBT' calibration, allowed us to assess the abundance and variability of the novel 6-methyl brGDGTs and to study whether their separate quantification has an effect on the accuracy of the brGDGT-based palaeoclimate proxies. The 6-methyl brGDGTs were shown to be abundant (on average 24% of brGDGTs), as they were present in 93% of all soils. The fractional abundance of the 6-methyl brGDGTs was shown to vary with soil pH, but not with the MAT. Furthermore, the separate quantification of the 5- and 6-methyl brGDGTs results in a pH-independent MBT', the so-called MBT'_{5ME}. The absence of a CBT-based correction for pH already resulted in a significantly improved accuracy for MBT'5ME-based temperature reconstruction, especially for arid soils. Further statistical analysis allowed the development of the CBT', a logarithmic ratio that included all six 6-methyl brGDGTs and allowed to reconstruct the soil pH with a RSME of 0.5. Calibrating a multiple linear regression, the MAT_{mr}, with the measured MAT, the RSME of the temperature

reconstruction could be decreased to 4.6 °C. Furthermore, a simplified multiple linear regression was formulated, based only on the fractional abundances of the major brGDGTs Ia, IIa and IIIa (i.e. the MAT_{mrs}).

Chapter 4 describes the brGDGT abundance and diversity in the suspended particulate matter (SPM) of the Yenisei River. As the Yenisei River crosses a large gradient in MAT, we aimed to elucidate whether the input of soil-derived brGDGTs that were produced under different temperature regimes, could be traced in the Yenisei River. Also, using a single Prevail silica column, we were able to separate the hexamethylated 6-methyl brGDGTs in the Yenisei River SPM, and showed them to be abundant brGDGTs. Based on the offset between the watershed soil pH and brGDGT-based reconstructed pH, and the absence of a latitudinal trend in reconstructed temperatures, it was concluded that soils were not the dominant source of brGDGTs in the Yenisei River SPM. Furthermore, the reconstructed pH was close to the measured river water pH, and using a calibration that is based on the temperature dependence of aquatic brGDGTs (Pearson et al., 2011), the reconstructed temperature was close to the mean summer temperature imposed on the Yenisei River. In-situ production in the Yenisei River was thus concluded to be the dominant source of brGDGTs in the Yenisei River SPM.

Chapter 5 describes the study of the inflow of Selenga River, the river that drains the southernmost part of the Yenisei River watershed, in Lake Baikal, the largest freshwater lake worldwide. The aim of this study was to assess whether the signature of brGDGTs that is delivered to the lake is comparable to the signal that will be exported downstream, both in the outflow of Lake Baikal and in the Yenisei River. Lake Baikal water was found to have a contrasting brGDGT distribution to Selenga River. The Selenga River mixing zone indicated the impact of preferential degradation or in-situ production on the brGDGT distribution, although the latter was found to be more likely, based on the increase in the brGDGT abundance. The cyclopentane-containing brGDGT Ic and highly methylated brGDGTs IIa and IIIa may be produced in-situ in the Selenga Outflow system. However, as the lacustrine brGDGT distribution is not recognized in the Yenisei River SPM, both the brGDGTs encountered in the Selenga River and in Lake Baikal are not assumed to contribute significantly to the brGDGT distribution transported to the marine system by the Yenisei River.

Chapter 6 discusses the observed changes in the distribution of CL and IPL brGDGTs of the SPM and sediments in the Yenisei River and its outflow into the Kara Sea. This study first presents the re-analysed dataset of the Yenisei River, reporting the presence of all fifteen brGDGTs. Application of the novel soil pH-calibration (the CBT') confirms our earlier assessment that the brGDGT lipids are produced at a neutral pH, as the reconstructed pH values fall between 6.9 and 7.9. Evaluating the brGDGT distributions, large shifts are observed in the river outflow system. The contribution of coastal cliff-derived brGDGTs and brGDGTs delivered to the system during the spring freshet is invoked to explain the offset between the Yenisei River and the River Mouth distributions. Further downstream, marine in-situ production plays a role, but it cannot explain the strong increase in the fractional abundance of the 'warm' brGDGT Ia. Preferential conservation of a pre-aged brGDGT pool can possibly explain the observed distribution, although the nature of this brGDGT pool can not be fully constrained.

Following up on this detailed description of the brGDGTs in the Yenisei River and Kara Sea, **Chapter 7** describes the bacteriohopanepolyol (n=22) concentration and distribution in the same SPM and sediment samples. Supporting the proposed river transport mechanism, soil-marker BHPs are present in the Yenisei River SPM and the Yenisei River Mouth sediments. Their abundance was found to decrease downstream in the marine system. Several other BHPs that showed the same distribution were identified as having a dominant terrigenous source. The downstream distribution of BHT implies that it is probably in-situ produced. Furthermore, BHPentol cyclitol ether was found to increase in abundance in the most offshore marine samples, reflecting a possible cyanobacterial source. The concentrations of biomarkers for methanotrophic bacteria (aminotetrol, aminopentol) were increased in the marine sediments in the Yenisei Gulf, indicating the in-situ production of these BHPs in the marine environment. Methane in the Kara Sea sediments is possibly sourced from submerged permafrost and its consumption can have a mitigating effect on the escape to the atmosphere of this greenhouse gas.

As the distribution of bacterial lipids in modern SPM and sediments of the Yenisei River and Kara Sea is strongly modified with increasing distance from the river mouth, we studied the brGDGT distributions of a core in the St. Anna Through (northern Kara Sea) in **Chapter 8**. This core allowed to evaluate changes in the brGDGT distribution and the BIT-index in marine sediments (0 – 13.3 ka) that have been deposited during the retreat of the palaeo Yenisei River Mouth, caused by the eustatic sea level rise. The contribution of marine in-situ produced brGDGTs (i.e. Ib, Iib, Iic, IIib, IIic, Iib', Iic', IIIa', IIib' and IIic') and the concentration of crenarchaeol increases in recent sediments, tracking the sea level rise. In deeper sediments, the shifts in brGDGT distribution and abundance indicate a shift in the terrigenous brGDGT sources. Although temperature reconstructions are still possible in sediments influenced by marine in-situ production, using the MAT_{mss}, changes in the terrigenous sources of brGDGTs can strongly influence palaeoclimate reconstructions. This has important implications for global brGDGT-based palaeoclimate reconstructions at sites where mixed sources of brGDGTs (i.e. riverine in-situ produced and soil-derived brGDGTs) contribute to the sedimentary brGDGT distribution. Here, the enrichment of a terrigenous brGDGT subpool through increased erosion, or the preferential degradation of more labile brGDGT pools will result in distributional shifts that are unrelated to changes in palaeotemperature and pH.

Overall, studying the abundance and diversity of brGDGTs and BHPs in the Yenisei River and its outflow in the Kara Sea, has resulted in new insights concerning the diversity, and the environmental dependence of these lipids. Furthermore, riverine, lacustrine and marine in-situ production and preferential degradation of brGDGTs was shown to act on the brGDGT distribution during their transport to the marine sediments. Knowledge of the possible impact of these mechanisms highlights the importance of abolishing the concept that river fan brGDGTs per se reflect an average of the river's watershed. However, the MAT can still be reconstructed at sites where marine in-situ production is the only confounding factor, using the novel simplified MAT calibration (i.e. MAT_{mss}). Thus, brGDGT-based palaeoclimate reconstructions can still be performed, although the complexity of sedimentary brGDGTs sources has to be taken into account.



Photo by Cindy De Jonge

2

Identification of novel penta- and hexamethylated branched glycerol dialkyl glycerol tetraethers in peat using HPLC-MS², GC-MS and GC-SMB-MS

Cindy De Jonge, Ellen C. Hopmans,
Alina Stadnitskaia, W. Irene C. Rijpstra,
Ron Hofland, Erik Tegelaar,
Jaap S. Sinninghe Damsté

Published in Organic Geochemistry 54, January 2013

ABSTRACT

A Siberian peat contains high abundances of three unknown isomers of hexamethylated branched (br) GDGTs, of which two are present as a second peak eluting shortly after the known hexamethyl br GDGT containing two 5,13,16-trimethyloctacosanyl moieties. Tandem high performance liquid chromatography-mass spectrometry (HPLC-MS²) did not reveal substantial differences in the MS² spectrum of the two peaks. HPLC isolation of the two peaks of the hexamethylated br GDGT followed by ether cleavage and characterization of the hydrocarbons formed by GC-MS using supersonic molecular beam (SMB) ionization revealed that the second peak was mainly composed of a novel hexamethyl br GDGT, possessing two 6,13,16-trimethyloctacosanyl moieties. In addition, both chromatographically separated hexamethylated br GDGTs contained a smaller quantity (20-33%) of a non-symmetrical isomer, with one 13,16-dimethyloctacosanyl and one tetramethyloctacosanyl (either 5,13,16,24- or 6,13,16,23-) moiety. Hexamethylated br GDGTs thus consist of four structural isomers. Furthermore, the pentamethylated br GDGT was also isolated and shown to contain both 5,13,16- and 6,13,16-trimethyloctacosanyl moieties and is thus composed of two structural isomers. These assignments reveal why environmental distributions of br GDGT are sometimes complex and may have implications for the use of br GDGTs in palaeoclimate reconstruction.

1. Introduction

Branched glycerol dialkyl glycerol tetraethers (br GDGTs) are abundant lipids in soil, peat, lake and coastal marine sediments. They are derived from bacteria and possess 4 to 6 methyl substituents attached to the linear C₂₈ alkyl chains and up to two cyclopentanyl moieties formed by internal cyclization (Sinninghe Damsté et al., 2000; Weijers et al., 2006a). With decreasing temperature, the number of methyl substituents increases and with higher soil pH the degree of cyclization increases. This is expressed in the ratios of methylation of branched tetraethers (MBT) and cyclisation of branched tetraethers (CBT) (Weijers et al., 2007a), which can be used as continental palaeoclimate proxies. Application of the MBT index, which uses the fractional abundances of tetra-, penta- and hexamethylated br GDGTs, is sometimes complicated as the latter component is not present as a clear distinct chromatographic peak, which may compromise accurate measurement (e.g. Weijers et al., 2007a). Here, we present data from a Siberian peat that contains a high fractional abundance of hexamethylated br GDGT isomers that elute after the traditional hexamethylated br GDGT. To elucidate their structures, both peaks were isolated and analyzed using an array of analytical techniques. Furthermore, the pentamethylated br GDGT from this peat was isolated and shown to consist of two different isomers within a single HPLC peak.

2. Material and methods

Freeze-dried material (220 g) from a peat core (340 cm) from the East Sayan Mountains, Siberia (51°96.166 N, 100°95.583 E) was extracted as described by Weijers et al. (2007a). The extracts were pooled (yielding ca. 2 g of extract) and separated over a column (2.5 x 20 cm) containing activated Al₂O₃. The fraction eluted with dichloromethane (DCM)/MeOH (95/5, v/v) and containing the br GDGTs was dried, redissolved in hexane/isopropanol (IPA) (99/1, v/v) and filtered through a 0.4 µm PTFE filter. Two stages of HPLC were used for isolation of br GDGTs. They were first separated on a semi-preparative NH₂ column according to Sinninghe Damsté et al. (2000). Fractions were collected each 1 min and analyzed off-line via flow injection analysis and atmospheric pressure chemical ionization– mass spectrometry (APCI-MS) in selected ion monitoring mode (SIM) with an Agilent 1100 MSD instrument as described by Smittenberg et al. (2002). Fractions enriched in the desired br GDGTs were injected onto a silica high performance liquid chromatography (HPLC) column (150 x 2.1 mm; 3 µm; 30 °C; 0.2 ml min⁻¹; Alltech, Deerfield, IL). Br GDGTs were eluted isocratically with hexane/IPA (97.8:2.2) for 38 min. Collected fractions (15 s) were analyzed off-line using the same chromatographic method with APCI-MS detection in SIM mode at *m/z* 1050, 1048, 1046, 1036 and 1022.

To differentiate between alkyl chains with a different degree of methylation, HPLC-MS² analysis of the isolates was carried out using a Thermo Fisher LTQ XL ion trap equipped with Ion Max source with APCI probe. The isolates (10 µg ml⁻¹) were infused at 10 µl.min⁻¹ via a T-union into 0.2 ml.min⁻¹ hexane/IPA (99:1). APCI settings were: vaporizer 450°C; capillary 275°C; discharge current 5 µA; sheath gas, auxiliary gas and sweep gas (all N₂) respectively 50, 5 and 5 arbitrary units. Spectra were collected in the full scan mode from *m/z* 650-1350. MS² spectra were obtained with a relative collision energy of 20, an isolation width of 3 and collected in full scan mode from *m/z* 350-1375.

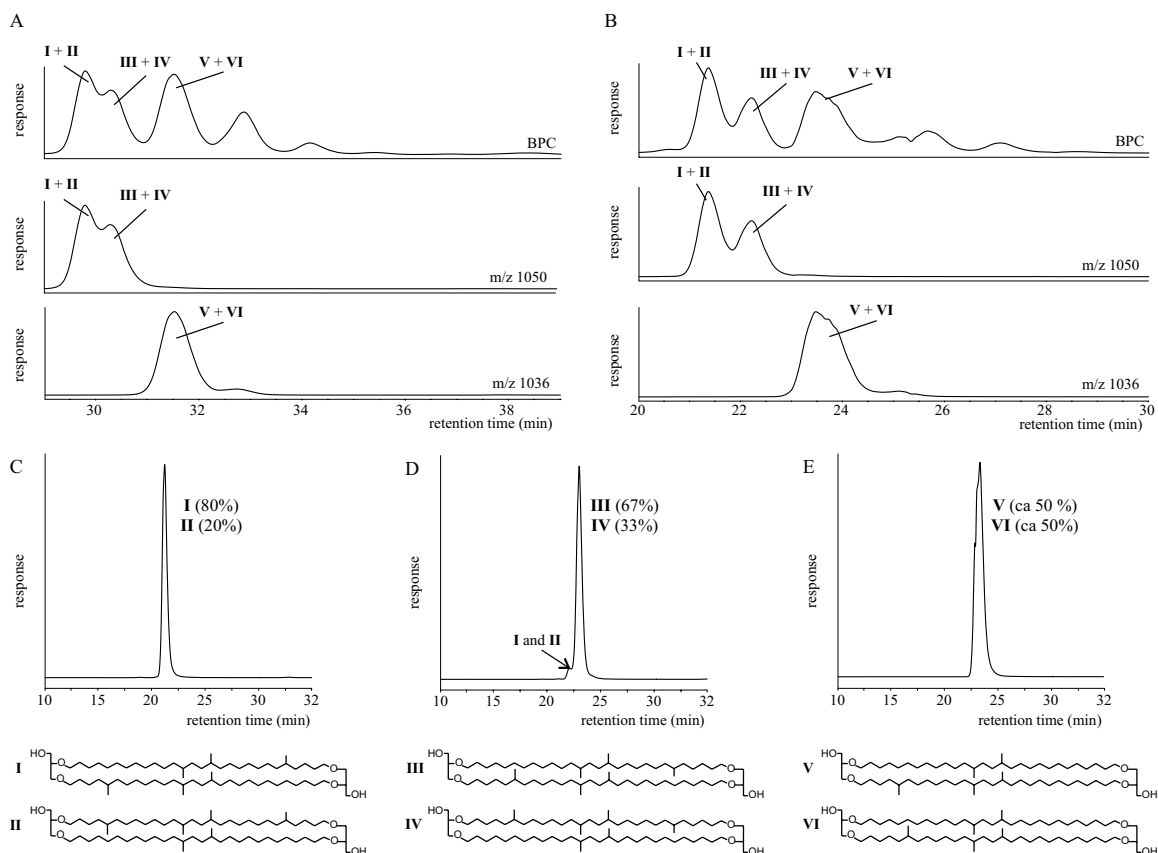


Fig. 1. Chromatograms illustrating the presence of penta- and hexamethylated br GDGTs in the Siberian peat and their isolation. Partial base peak chromatogram (BPC) and m/z 1050 and m/z 1036 chromatograms from HPLC-APCI-MS analysis of GDGTs using a cyano (A) and silica (B) column. The latter gives better separation and was used to isolate the two hexamethylated br GDGTs. (C-E) BPCs of the isolated (C) early and (D) late eluting hexamethylated br GDGT and (E) pentamethylated br GDGT using the silica column with structures of br GDGTs identified.

Aliquots of the isolated peaks of the hexamethylated br GDGTs were subjected to ether cleavage (57% HI) as described by Schouten et al. (1998). The resulting alkyl iodides were reduced to hydrocarbons with H_2/PtO_2 (Kaneko et al., 2011), which were analyzed via gas chromatography (GC) after on-column injection on a HP 6890 Series GC instrument as in Schouten et al. (1998) and in splitless mode with GC-MS using an Agilent 7890A GC instrument equipped with a Agilent 5975C VL MSD detector. A Valcobond VB-1 column was used (30 m x 0.32 mm i.d.; film thickness 0.50 μ m; He carrier gas). Samples were injected at 70°C and the GC oven was programmed to rapidly raise to 130°C, increase with 4°C.min⁻¹ until 320°C, held for 10 min. GC-SMB-MS analysis was carried out with an Agilent 7890A GC instrument, an Aviv Analytical 5975-SMB 101-09 SMB interface (cf. Fialkov et al., 2008) and an Agilent 5975C MSD. A fused silica DB-1 column (60 m x 0.25 mm; 0.25 μ m film thickness He carrier gas) was used. Samples were injected in splitless mode (injector temperature 300 °C) at 50°C and the oven temperature was increased to 320°C (held 30 min) at 4 °C.min⁻¹. For cooling, 35 ml.min⁻¹ He make-up gas was added. The compounds were ionized in a fly-through dual cage electron ionization (EI) source at 70 eV. The MSD was run in full scan mode with m/z 50–650.

3. Results and discussion

HPLC/APCI-MS analysis of the hexamethylated br GDGT from the peat showed two partially co-eluting peaks in the m/z 1050 mass chromatogram (Fig. 1A). The separation could be substantially improved by using a silica column (Fig. 1B). The first peak eluted at the position where the common (i.e. with two 5,13,16-trimethyloctacosanyl moieties) hexamethylated br GDGT (e.g. Weijers et al., 2006a) elutes, whereas the GDGTs in the second peak were unknown. We isolated both peaks of hexamethylated br GDGTs using preparative HPLC, resulting in 1.4 and 0.2 mg of the GDGTs comprising the earlier and later-eluting peak, respectively (Figs. 1C-D). Furthermore, 0.7 mg of pentamethylated br GDGTs with m/z 1036 that was present as a single peak (Figs. 1A-B) was isolated (Fig. 1E).

Tetraether lipid core structures can be revealed via tandem MS (MS²; Knappy et al., 2009). Both isolates of the hexamethylated br GDGT were analyzed using an ion trap mass spectrometer. The spectra showed a base peak at m/z 1050.0; other peaks only had an intensity of <6%. MS² spectra (Fig. 2A, B) revealed subtle differences between the two isolates. Neutral losses involving one (m/z 1032) and two (m/z 1014) water molecules, the loss of a glycerol

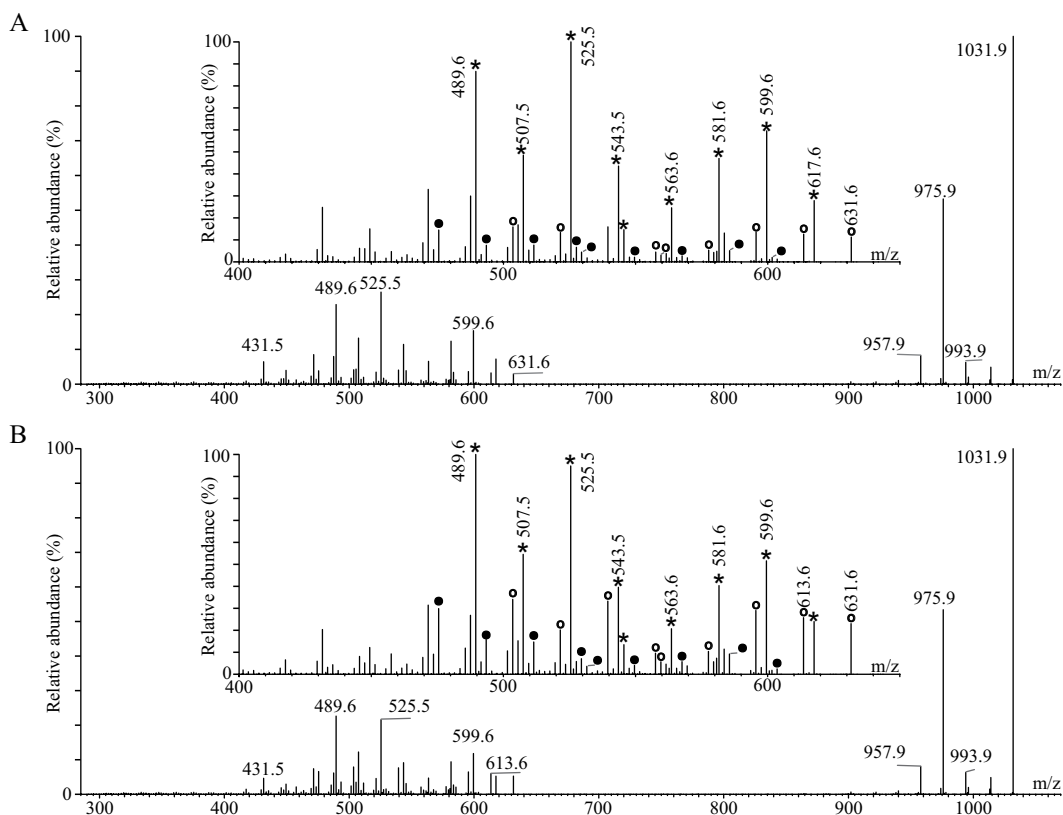


Fig. 2. HPLC-MS² spectra for the early (A) and late (B) eluting hexamethylated br GDGTs. The insets show enlargement of the *m/z* 400-650 region containing fragments ions that result from loss of one of the alkyl chains and consecutive losses of water and glycerol. Three series of fragment ions are indicated: those from loss of a dimethyloctacosanyl unit are marked with an open circle, those from loss of a trimethyloctacosanyl unit with an asterisk and those from loss of a tetramethyloctacosanyl unit with a closed circle.

moiety (m/z 994) and a glycerol moiety and one (m/z 976) and two (m/z 958) water molecules were observed in both spectra. These losses are independent of the structure of the alkyl chains and have been reported for archaeal GDGTs (Knappy et al., 2009). Other neutral losses involve loss of an alkyl chain. These losses allow differentiation between br GDGTs composed of two alkyl chains with three methyl groups (loss of C_3H_6 resulting in a fragment at m/z 617.6), and those isomers with the six methyl groups apparently distributed unevenly over the two alkyl chains, i.e. containing two (loss of $C_{30}H_{60}$, m/z 631.6) and four methyl substituents (loss of $C_{32}H_{64}$, m/z 603.6). Subsequently, these ions can lose a glycerol and/or water in addition to the alkyl chain, resulting in the fragment ions at m/z 471.6-613.6 (Fig. 2A, B). The relative abundance of the C_{31}/C_{31} and C_{30}/C_{32} br GDGT could be estimated by comparing the intensity of the fragment ions. For the earlier-eluting hexamethylated br GDGTs, the C_{31}/C_{31} isomer dominated (70-80%), while this was less so for the later-eluting br GDGT (60-70% C_{31}/C_{31}). This type of analysis cannot, however, reveal differences in the positions of methylation.

To investigate this, aliquots of the isolated br GDGTs were subjected to ether cleavage and the hydrocarbons generated were analyzed via both GC-MS using EI and a soft ionization technique using a SMB (Fialkov et al., 2008). The earlier eluting hexamethylated br GDGTs generated three hydrocarbons upon treatment (Fig. 3A); the most abundant was assigned as 5,13,16-trimethyloctacosane (c), whereas the two minor components were assigned as 13,16-dimethyloctacosane (a) and 5,13,16,24-trimethyloctacosane (e) from their EI and SMB mass spectra (Figs. 3A) and Kovats indices. The results for the first two hydrocarbons (a and c) are in good agreement with data reported by Sinninghe Damsté et al. (2000). The latter (e) was tentatively assigned by Weijers et al. (2010). Its anticipated molecular ion was confirmed by the SMB spectrum (Fig. 3H) and its Kovats index (2960) fitted with the predicted value (2959) using the additivity principle (Kissin and Feulmer, 1986). GC analysis showed that 5,13,16-trimethyloctacosane (c) represented 80% of the summed branched alkanes, whilst the two other two hydrocarbons (a and e) accounted each for 10%. The ratio of the C_{31}/C_{31} brGDGT (I in Fig. 1B) and C_{30}/C_{32} brGDGT (II) for the earlier eluting hexamethylated brGDGT was thus 4:1, in good agreement with the HPLC-MS² results.

Ether cleavage of the later-eluting peak of the hexamethylated brGDGTs also generated three branched hydrocarbons (Fig. 3B). In the gas chromatogram, the earlier eluting compound was again assigned as 13,16-dimethyloctacosane (a), identical to the structure in the early-eluting peak of hexamethylated br GDGT (Fig. 3A). However, the mass spectra of the other two hydrocarbons (b and d; Figs. 3E, 3G) showed subtle differences, most visible in the SMB spectra, from those (c and e) generated from the early-eluting br GDGTs (Figs. 3F, 3H). The main differences between the spectra of the trimethyloctacosane (b-c) are the presence of a fragment at m/z 365 and the absence of the fragments at m/z 379 and 351 in the second isolate (b), and the increased relative intensity of m/z 98 and decreased relative intensity of m/z 85 (Figs. 3E-F). The latter is even more pronounced in the spectra of the tetramethyloctacosane d-e (Figs. 3G-H) and fragment ions are present at m/z 351 and 379 instead of at m/z 365 and 393. This can be explained by the presence of a methyl at C-6 (and C-ω6 in the case of the tetramethyloctacosane) instead of at C-5 (and C-ω5) of the alkyl chain. This assignment is consistent with the measured Kovats indices for the 6,13,16-trimethyloctacosane (2905) and 6,13,16,23-tetramethyloctacosane (2949) vs. those calculated (2904 and 2948, respectively).

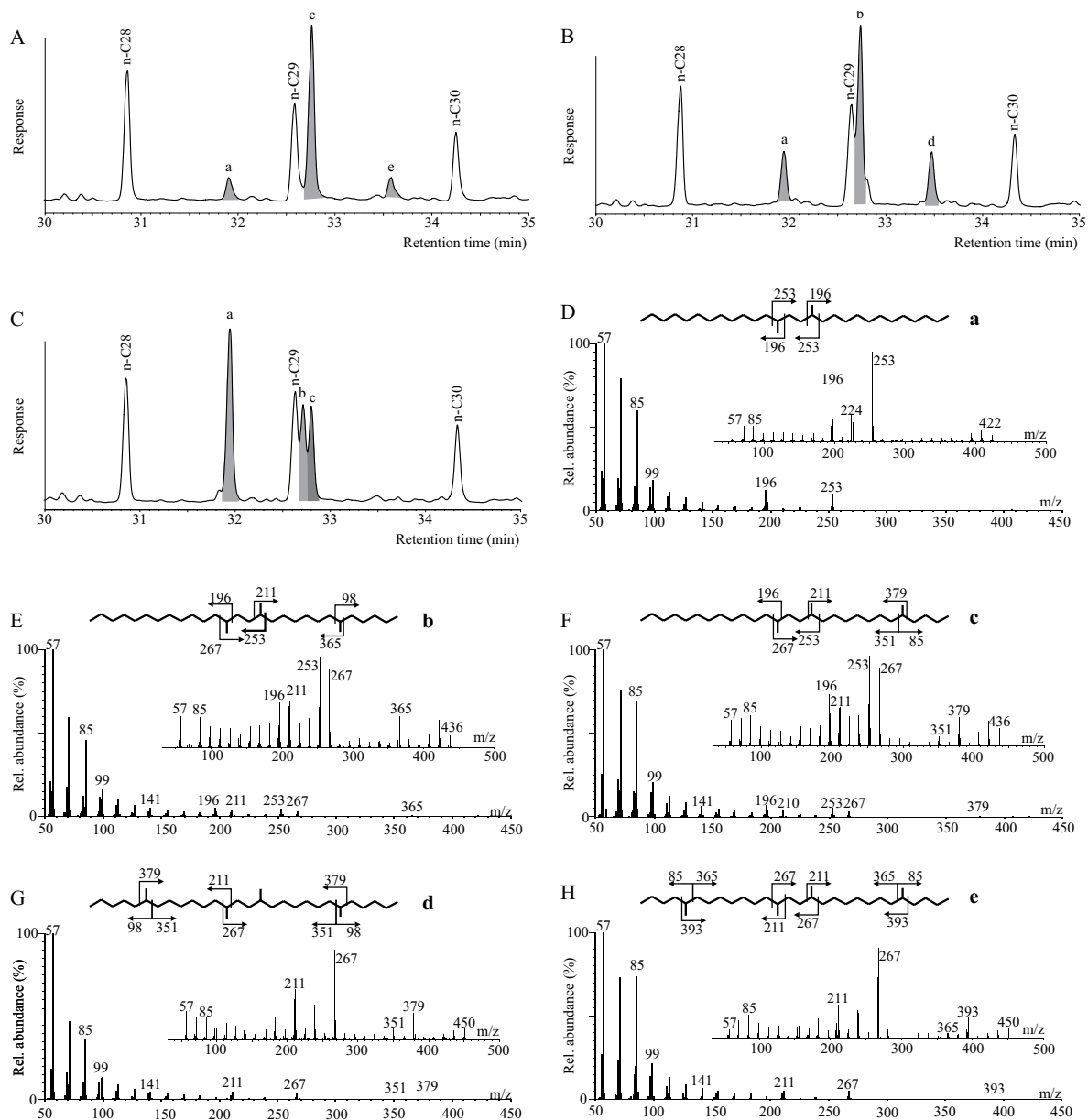


Fig. 3. Characterization of alkyl moieties in the isolated penta- and hexamethylated br GDGTs via ether cleavage and subsequent hydrocarbon characterization. (A-C) partial GC traces of the hydrocarbons (a-e) generated by ether cleavage of the isolated early- (A) and late-eluting (B) hexamethylated, and (C) pentamethylated br GDGTs. Branched hydrocarbons derived from br GDGTs are indicated in black; other peaks represent C₂₈-C₃₀ n-alkanes from a co-injected standard. (D-H) EI and SMB (inserts) mass spectra of the five hydrocarbons generated (a-e) upon ether cleavage. Structures of hydrocarbons are indicated with preferred MS fragmentations.

These are lower than those for the branched hydrocarbons in the earlier eluting hexamethylated br GDGT (2911 and 2960, respectively), as expected from the more internal position of the methyl group(s). GC analysis indicated that 6,13,16-trimethyloctacosane amounted to 67%, whilst the two other two hydrocarbons together accounted for 33% (Fig. 3B). The ratio of the C_{31}/C_{31} br GDGT (III in Fig. 1C) and C_{30}/C_{32} br GDGT (IV) for the later eluting hexamethylated br GDGT was ca. 2:1, in good agreement with the HPLC-MS² data.

The observed variation in the position of the methyl group is not limited to the hexamethylated br GDGTs, but also occurs in the trimethyloctacosane moiety of the pentamethylated br GDGTs. The EI and SMB mass spectra and the Kovats indices (2861 and 2905) of the branched alkanes formed upon ether cleavage of the isolated pentamethylated br GDGT (Fig. 3C) show the presence of 13,16-dimethyloctacosane (a) and 5,13,16-trimethyloctacosane (c), in good agreement with data reported by Sinninghe Damsté et al. (2000). However, based on the EI and MSB mass spectra and the Kovats index (2910) we conclude that 6,13,16-trimethyloctacosane (b) is present as an alkyl moiety of the pentamethylated br GDGTs (Fig. 3C). GC analysis showed that 13,16-trimethyloctacosane represented 50% of the summed branched alkanes, whilst the two other hydrocarbons accounted each for 25%. The ratio of the pentamethylated brGDGTs V and VI (Fig. 1E) is thus roughly 1:1.

In the assignments of structures I-VI, we assume that all GDGTs possess the parallel stereo configuration, whereas for crenarchaeol and other isoprenoid GDGTs, it has been demonstrated that they can also occur in the anti-parallel form (Sinninghe Damsté et al., 2002). In addition, I-VI contain various chiral carbons in the alkyl moieties, extending the possibility for stereoisomerism although previous NMR studies (Sinninghe Damsté et al., 2000; Weijers et al., 2006a) suggest that the configuration is fixed in the bacterial biosynthesis of these br GDGTs.

The presence of abundant isomers that co-elute with the traditional br GDGTs may have large implications for the use of the CBT/MBT proxies. In the soil dataset used by Weijers et al. (2007a) that includes a number of peats, a second peak of the hexamethylated brGDGTs (III and IV) was present only as a minor component and thus not incorporated in the development of the CBT/MBT proxy. However, this study indicates that the abundance of these GDGT isomers may vary widely in the environment. At this stage, it is unclear if GDGTs III and IV comprising this second peak are biosynthesized independently to GDGTs I and II comprising the first peak, or represent an alternative expression of the traditionally used hexamethylated br GDGT. It thus requires further investigation whether hexamethylated br GDGTs III and IV should be incorporated when calculating the CBT/MBT indices. With the current chromatographic separation, the asymmetrical isomers of hexamethylated br GDGTs and the two pentamethylated br GDGT isomers (V and VI) cannot be quantified separately. A re-calibration of the CBT/MBT proxy using the abundance of the separate isomers can possibly eliminate part of the substantial calibration error that still characterizes these proxies (Weijers et al., 2007a; Peterse et al., 2012).

4. Conclusions

The hexamethylated br GDGTs in the Siberian peat are actually composed of at least four structural isomers (I-IV). The results aid in the understanding of the sometimes complex distribution of hexamethylated brGDGTs in environmental samples, for instance the strong increase in hexamethylated br GDGTs in lake environments. The pentamethylated br GDGT reveals the presence of two structural isomers (V-VI). Follow-up studies will need to address the distribution of novel penta- and hexamethylated br GDGTs (II-VI) and if the presence of these compounds reveals specific environmental information. At this stage, it is unclear if the CBT/MBT indices should be recalibrated using the relative abundance of the isomers I-VI.

Acknowledgments

We acknowledge A. Fedotov (Limnological Institute, Siberian Branch of Russian Academy of Science) for help in the collection of the peat, G. Cherkoshev (VNIIOkeangeologia) for help in logistics and support, and R.D. Pancost and P. Schaeffer for insightful comments on an earlier draft of this paper. This work, performed in the framework of the memorandum NIOZ-VNIIOkeangeologia for Arctic research, was funded by research project 819.01.013, financed by the Netherlands Organization for Scientific Research (NWO) and the European Research Council under the EU Seventh Framework Programme (FP7/2007-2013) / ERC grant agreement n° [226600].



Photo by Cindy De Jonge

Occurrence and abundance of 6-methyl branched glycerol dialkyl glycerol tetraethers in soils: implications for palaeoclimate reconstruction.

3

Cindy De Jonge, Ellen C. Hopmans,
Claudia I. Zell, Jung-Hyun Kim,
Stefan Schouten, Jaap S. Sinninghe Damsté

Published in *Geochimica et Cosmochimica Acta* 141,
September 2014

ABSTRACT

The distribution of branched glycerol dialkyl glycerol tetraethers (brGDGTs) in soils has been shown to correlate with the soil pH and the mean annual air temperature (MAT). This has been used to perform palaeoclimate reconstructions based on brGDGTs recovered from palaeosoils, freshwater, and marine sedimentary archives. Recently described 6-methyl brGDGTs were shown to co-elute with the 5-methyl brGDGTs that are used to calculate the CBT and MBT' indices used as palaeoclimate proxies. The impact of these 6-methyl brGDGTs on the established palaeoclimate proxies is unknown and will depend on their abundance in soils. Using improved chromatography, we quantified the fractional abundance of 6-methyl brGDGTs in globally distributed soils and show that they are abundant components, comprising on average 24% of the total amount of brGDGTs. All penta- and hexamethylated brGDGTs (i.e. with zero to two cyclopentane moieties) were shown to comprise both 5- and 6-methyl isomers. The fractional abundances of the six 6-methyl brGDGTs correlate positively with each other, suggesting a common biological source in most soils, and correlate strongly with soil pH. The presence of the 6-methyl brGDGTs introduced scatter in the original MBT'/CBT-MAT calibration and caused a dependence on soil pH of the MBT'. Exclusion of the 6-methyl brGDGTs from the MBT', i.e. the newly defined MBT'_{SME}, shows that it is no longer related to soil pH. The correlation with MAT is improved, reducing the residual mean error (RMSE) from 6.2 to 4.8°C. Also, the correlation of the CBT after the exclusion of the 6-methyl brGDGTs (defined as CBT_{SME}) with soil pH slightly improved. Furthermore, the separate quantification of the 6-methyl brGDGTs allows the definition of new indices. The CBT', which comprises the 6-methyl brGDGTs, is a substantially improved alternative to the CBT_{SME}, reducing the RMSE from 0.8 to 0.5 pH units. Also, the accuracy of MAT reconstructions can be improved using a multiple linear regression, the MAT_{mrs}, decreasing the RMSE further to 4.6°C. Furthermore, we introduce an index that allows the reconstruction of MAT in sites where only the ubiquitous brGDGT Ia, IIa and IIIa are present, the MAT_{mrs}. Our results imply that separate quantification of the 6- and 5-methyl brGDGT is essential for accurately quantifying brGDGTs in environmental samples and results in substantially improved MAT and soil pH reconstructions.

1. Introduction

A challenge in continental palaeoclimate research is the development of quantitative climate proxies that can be applied in continuous records. These archives can be found, for example, in calcite deposits in caves (e.g. Gascoyne, 1992) or in lakes, where undisturbed sedimentation can occur over long timespans, up to 6.7 Ma (Kravchinsky et al., 2003). A large part of the continental temperature records is indeed retrieved from lake sediments, where climate indicators like pollen may be preserved, together with chironomids or diatoms, whose community changes record the temperature of the lake water (e.g. Smol and Cumming, 2000; Broström et al., 2008; Eggermont and Heiri, 2012). The number of proxies that can estimate past continental air temperatures, however, is relatively limited.

The distribution of a set of 9 bacterial lipids, branched glycerol dialkyl glycerol tetraethers (brGDGTs), has been demonstrated to show a relationship with mean annual air temperature (MAT) and soil pH (Weijers et al., 2007a). This observation has led to the development of a continental palaeoclimate proxy, with applications in palaeosoils (Peterse et al., 2009b; Peterse et al., 2011b) and speleothems (Blyth and Schouten, 2013). Following soil erosion and run-off through rivers, the soil-derived brGDGTs can also be recovered from marine and lake sediments (e.g. Weijers et al., 2007b; Niemann et al., 2012), where their incorporation in sediments creates a continuous palaeoclimate archive. BrGDGT lipids are stable components that can persist in the environment up to at least 55 Ma (Weijers et al., 2011a).

Our knowledge of the structural diversity of brGDGTs has been developed just over the past decade (Schouten et al., 2013a). In 2000, the structure of the two dominant brGDGTs has been elucidated using NMR (Sinninghe Damsté et al., 2000; Ia and IIa; see Fig. 1 for structures), after their isolation from a Dutch Holocene peat bog. Unlike the GDGTs of archaea, the alkyl core chain was not isoprenoidal, but shown to be a straight chain comprising two to three methyl groups. These alkyl core chains can undergo internal cyclization, resulting in the presence of one or two cyclopentane moieties (Weijers et al., 2006a; Ib-c, IIb-c, IIIb-c). Both the non-isoprenoidal structure and the stereo-configuration of the glycerol moieties indicated a bacterial origin (Weijers et al., 2006a). Acidobacteria, that occur in substantial cell numbers in soil and peat (e.g. Fierer et al., 2007), were proposed as likely candidates (Weijers et al., 2009). The observation that brGDGT concentrations in soils are higher at lower pH fits with the higher abundance of subdivision 1 Acidobacteria in soil at lower pH (Peterse et al., 2010). Recently, brGDGT Ia has been detected in two cultured Acidobacterial strains from subdivision 1 (Sinninghe Damsté et al., 2011). However, although usually a full suite of 9 brGDGTs is present in the environment, only one brGDGT has been recovered from a bacterial culture so far and this mismatch still remains to be explained.

BrGDGTs are abundant lipids found in soils and peat across the globe (Weijers et al., 2006a; Peterse et al., 2010; Yang et al., 2013). As the precursor organisms thrive in highly contrasting soil conditions, the composition of the lipid membrane is variable in order to adjust the membrane fluidity to different environments. The relative distribution of the nine brGDGTs in a global soil dataset, expressed in the Methylation of Branched Tetraethers (MBT) and Cyclisation of Branched Tetraethers (CBT) ratios, was shown to correlate with the ambient MAT and soil pH (Weijers et al., 2007a). These authors hypothesized that the temperature has a direct effect on membrane fluidity, while the soil pH will affect the proton gradient

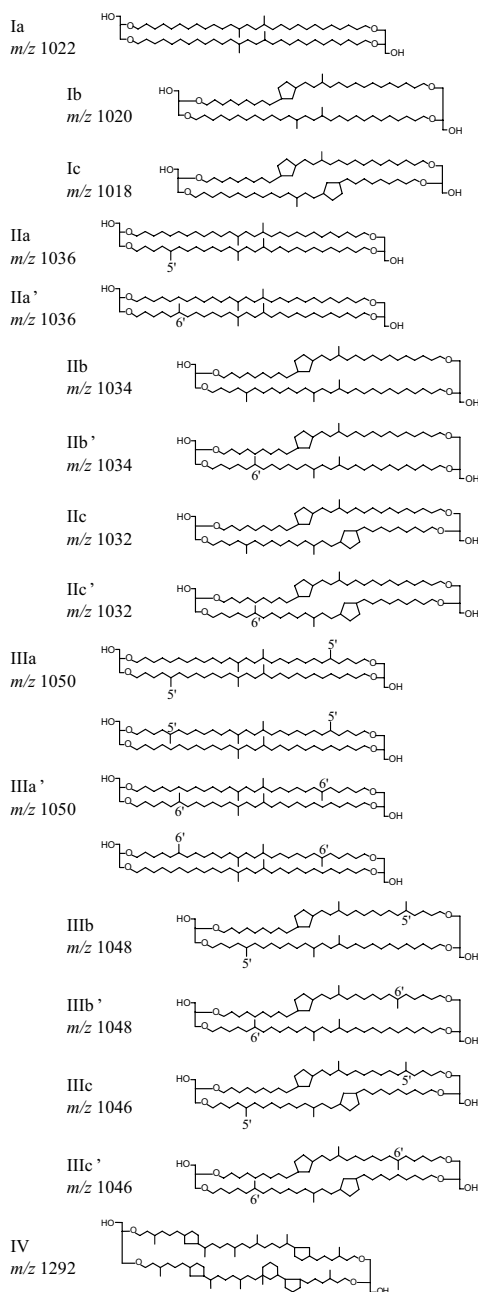


Fig. 1. Chemical structures of branched GDGTs (I-III) and crenarchaeol (IV). BrGDGTs Ia, Ib and Ic are referred to as 'tetramethylated', brGDGTs IIa, IIa', IIb, IIb', IIc and IIc' are referred to as 'pentamethylated', brGDGTs IIIa, IIIa', IIIb, IIIb', IIIc and IIIc' are referred to as 'hexamethylated' brGDGTs. The compounds that have one or two methyl groups at the α and/or ω -6 position are indicated with a prime symbol, and are referred to as 6-methyl brGDGTs. The compounds that have one or two methyl groups in the α and/or ω -5 position are referred to as 5-methyl brGDGTs. The chemical structures of the hexa- and pentamethylated brGDGTs with cyclopentyl moiety(ies) IIb', IIc', IIIb' and IIIc' are tentative.

across the membrane. Based on an extended soil dataset (Peterse et al., 2012), the MBT was simplified by removing two minor components (brGDGT IIIb and IIIc) and redefined as the MBT'. However, when reconstructing the MAT using the MBT'/CBT ratios, a considerable amount of scatter was still present, as indicated by the relatively low r^2 value (0.59). This scatter was mainly attributed to soils in arid regions that apparently react differently to the ambient temperature conditions. The problematic reconstruction of arid soils was confirmed in a number of studies targeting the brGDGT distributions in arid settings (Dirghangi et al., 2013; Menges et al., 2013). Recently, a new set of brGDGT isomers that differ in the position of the methyl groups on the branched carbon skeleton have been identified by De Jonge et al. (2013). Two isomers of the major hexamethylated brGDGT were found, where one component is characterized by the methyl at position 5, as originally identified by Sinninghe Damsté et al. (2000) (IIIa), while a second component contains two alkyl chains with a methyl at position 6 (IIIa'). Similarly, the pentamethylated brGDGT was shown to contain both a 5-methyl (IIa) and 6-methyl isomer (IIa'). Until now the abundance of the hexamethylated isomers had only been described in a Siberian Holocene peat (De Jonge et al., 2013) and in Siberian river suspended particulate matter (De Jonge et al., 2014a). The presence of 6,13,16-trimethyloctacosanyl chains in hexamethylated brGDGTs has also been reported in a pooled marine sediment (Liu et al., 2012).

It is unclear how widely distributed the 6-methyl brGDGTs are considering that, if the commonly used Prevail cyano column is used for high-performance liquid chromatography (Schouten et al., 2007a), these compounds co-elute with the 'traditional' 5-methyl brGDGTs (De Jonge et al., 2013). Here we investigated the presence of the 6-methyl brGDGTs in a global soil dataset of 239 soils (from Peterse et al., 2012) using a modified chromatographic HPLC method that enables to separate the 5- and 6- methyl brGDGTs. We discuss the dependence of the 6-methyl brGDGTs on environmental parameters and evaluate the bias introduced by these components in the existing MBT'/CBT calibrations and present improved soil pH and MAT calibrations.

2. Material and methods

2.1. Soil dataset compilation

The dataset is comprised of the globally distributed surface soils analyzed by Weijers et al. (2007a) for the original MBT/CBT calibration, complemented with the soils added for the revised MBT'/CBT calibration of Peterse et al. (2012). Compared to the dataset of Peterse et al. (2012), 39 samples did not contain sufficient brGDGTs for reanalysis. The soil collection in this study is thus composed of 239 globally distributed soils (Supp. Table 1, Fig. 2), representing 86% of the samples used in the Peterse et al. (2012) dataset. The soil pH, MAT, mean annual precipitation (MAP) and organic carbon content (Corg) values have been reported by Peterse et al. (2012). The approach for calculating the MAT and measuring the soil pH values is described in Weijers et al. (2007a). In short, the soil pH values were extracted from the International Soil Reference and Information Centre (ISRIC) soil database or performed in-house in an equilibrated 1:2.5 soil/water solution. The MAT reported are obtained from the Royal Dutch Meteorological Organisation (KNMI) database and represent a 30 year air temperature average. An altitude-dependent temperature correction was made between the sample location and the



Fig. 2. World map, indicating locations of soils used in this study.

weather station by linearly interpolating the temperature. If not enough climate stations were present in the World Climate Information database, data was obtained from the database of the ISRIC or from websites of local weather stations.

In addition, an independent soil dataset was used to test the performance of the novel MAT and soil pH proxies proposed, that has been described in Zell et al. (2014a). The 14 surface soils investigated were distributed along the Tagus River, on the Iberian Peninsula.

2.2. BrGDGT analysis

The soils were previously extracted as described in Weijers et al. (2007a), Kim et al. (2010b), Peterse et al. (2009a, 2009b, 2012) and Zell et al. (2014a). For this study, the polar fractions were concentrated to about 3 mg.mL^{-1} prior to analysis using an Agilent 1290 Infinity ultra high performance liquid chromatography (UHPLC) coupled to an Agilent 6130 single quadrupole mass detector. Separation of the brGDGTs was performed on four Alltima Silica columns (150 mm x 2.1 mm; W. R. Grace & Co.-Conn.; USA) at 30°C , placed in succession. GDGTs were separated isocratically using 98 % hexane and 2% isopropanol (IPA) for 140 min, with a flow rate of 0.25 mL.min^{-1} . After each analysis, the columns were cleaned by back-flushing hexane/IPA 1:9 (v/v), at a flow rate of $0.275 \text{ mL.min}^{-1}$. The maximum pressure obtained during the analysis, including backflush, was 200 bar. As this pressure is within the reach of standard HPLC systems (typically allowing maximum pressures of up to 400 bar), the method described does not require a UHPLC system.

Detection was achieved using positive ion APCI of the eluent. Source conditions were as follows; gas temperature 200°C , vaporizer temperature 400°C , drying gas (N_2) flow 6 L.min^{-1} , Neb pressure 60 psig., capillary voltage 3500 V, corona current $5.0 \mu\text{A}$. Detection was performed in selected ion monitoring (SIM) mode, targeting the protonated molecules at m/z 1050, 1048,

1046, 1036, 1034, 1032, 1022, 1020 and 1018. Quantification of the components was achieved using Chemstation software B.04.02.

2.3. Calculation of brGDGT indices

The roman numerals below refer to the brGDGTs indicated in Fig. 1. To differentiate between the 5- and 6-methyl brGDGTs, the latter are indicated by an accent. The CBT and MBT' indices were adopted from Weijers et al. (2007a) and Peterse et al. (2012). Below, we have rewritten this equation to explicitly show that in these studies the 5-methylated and 6-methylated brGDGTs were measured as co-eluting components:

$$\text{CBT} = -^{10}\log \left(\frac{(\text{Ib} + \text{IIb} + \text{IIb}')}{(\text{Ia} + \text{IIa} + \text{IIa}')} \right) \quad [\text{Eq. 1}]$$

$$\text{MBT}' = (\text{Ia} + \text{Ib} + \text{Ic}) / (\text{Ia} + \text{Ib} + \text{Ic} + \text{IIa} + \text{IIb} + \text{IIc} + \text{IIIa} + \text{IIa}' + \text{IIb}' + \text{IIc}' + \text{IIIa}') \quad [\text{Eq. 2}]$$

The here-defined CBT_{SME} and MBT'_{SME} (Supp. Table 1) are based on the 5-methyl isomers only:

$$\text{CBT}_{\text{SME}} = -^{10}\log \left(\frac{(\text{Ib} + \text{IIb})}{(\text{Ia} + \text{IIa})} \right) \quad [\text{Eq. 3}]$$

$$\text{MBT}'_{\text{SME}} = (\text{Ia} + \text{Ib} + \text{Ic}) / (\text{Ia} + \text{Ib} + \text{Ic} + \text{IIa} + \text{IIb} + \text{IIc} + \text{IIIa}). \quad [\text{Eq. 4}]$$

Prior to calculating the indices, the limit of quantification of brGDGT abundances on our system was determined following Schouten et al. (2007a). In order to avoid a large influence of brGDGTs below quantification limit, CBT_{SME} values have been calculated only if the minor components brGDGT Ib or IIb have a peak area above the quantification limit ($n=221$). Furthermore, MBT'_{SME} values have been calculated only if the area of brGDGT Ia and brGDGT IIa or IIIa were above quantification limit ($n=222$). For comparing the performance of the soil pH and MAT reconstructions, the calibrations of Peterse et al. (2012) were used. The calibration set of Peterse et al. (2012) is limited to soils that contain all brGDGTs used in the CBT and MBT' indices, and is composed of 179 soils. However, the complete dataset of Peterse et al. (2012) consists of 278 soil samples. In this study, the r^2 and RMSE reported are based on the soils that were successfully re-analyzed on the improved HPLC method and where the brGDGT abundances allow for the calculation of CBT_{SME} and MBT'_{SME} indices, minus three soils for which no CBT values could be calculated. This dataset was used to evaluate the performance of the MBT'/CBT indices and the novel proxies (r^2 denotes the pearson coefficient of determination, RMSE denotes residual mean standard error, n indicates the sample size):

$$\text{pH} = 7.9 - 1.97 * \text{CBT} \quad (r^2 = 0.59, \text{RMSE} = 0.9, n = 218) \quad [\text{Eq. 5}]$$

$$\text{MAT} (^{\circ}\text{C}) = 0.81 - 5.67 * \text{CBT} + 31.0 * \text{MBT}' \quad (r^2 = 0.58, \text{RMSE} = 5.5^{\circ}\text{C}, n = 219) \quad [\text{Eq. 6}]$$

2.4. Statistical analysis

All statistical analyses were performed using the statistical software R 3.0.1 (R Development Core Team, 2013), with the vegan (Oksanen et al., 2013), leaps (Lumley, 2009) and car packages (Fox and Weisberg, 2011). BrGDGTs are expressed as fractional abundances in all statistical analyses, as we are interested in compositional differences between sites. The recalibration of the CBT_{SME} and MBT'_{SME} indices against MAT and soil pH were performed using a linear

regression. Samples with a Bonferroni p-value < 0.05 were identified as outliers. Subsequently, these outliers were not incorporated when evaluating the calibrations. The number of outliers varies between regressions but are relatively small compared to the total data set, amounting up to 0.5% for the CBT_{SME}, 2.3% for the CBT' and 0.9% for the pH_{mr}. To compare the performance of the calibrations, we report the adjusted r² and RMSE. The performance of the linear model was evaluated examining the residuals. Furthermore, the complete set of 15 brGDGTs was used to calculate new indices to describe the relationship of brGDGT distributions with the MAT and pH. First, we used the approach that was previously applied on isoprenoid GDGTs in Kim et al. (2010a) and on brGDGTs in Peterse et al. (2012). Here, a calibration equation was calculated with a brGDGT index of the form:

$$\text{GDGT index} = {}^{10} \log \left(\frac{\sum k_1 Y_j}{\sum k_2 Y_j} \right) \quad [\text{Eq. 7}]$$

Y_j refers to any of the 15 brGDGT components. The summation in the numerator and the denominator is over the sets k₁ and k₂, respectively, where a set can be any possible combination of brGDGTs. For 15 brGDGT components, 32767 combinations are possible. The sets k₁ and k₂ were thus selected that the resulting index yields the largest correlation coefficient with the environmental variables. Hence, the correlations of 32767x32766/2 combinations were tested. A log-ratio is generally preferable over an ordinary ratio, since it usually makes the error structure closer to a normal distribution with constant variance (e.g. Montgomery and Peck, 2006).

Secondly, for both the MAT and soil pH, a least squares multiple linear regression was performed using the fractional abundances of the brGDGTs that showed a linear correlation with the environmental parameter (p<0.05), using a similar approach as the aquatic brGDGT calibrations from Tierney et al. (2010) and Pearson et al. (2011). The performance of the models were evaluated by examining the residual plots.

3. Results and discussion

3.1. Improved separation of 5- and 6-methyl brGDGTs

In De Jonge et al. (2013), we reported the presence of 5- and 6-methyl isomers of the hexa- and pentamethylated brGDGTs (IIa' and IIIa') in a Siberian peat. The separation on a Prevail cyano column that is typically applied in the HPLC-MS analysis of GDGTs in environmental samples (Schouten et al., 2009 and 2013b), is usually not sufficient to separate the 5- and 6-methyl isomers of the penta- and hexamethylated brGDGTs (Fig. 3A). Recently we showed that the separation on a single silica column is sufficient to quantify the 5- and 6 methyl isomers of the hexamethylated brGDGTs (IIIa, IIIB, IIIC and IIIa', IIIB', IIIC', respectively; De Jonge et al., 2014a). This separation of the hexamethylated isomers is possible because in these brGDGTs, two methyl groups have a different position. In comparison, the 5- and 6-methyl isomers of the pentamethylated brGDGTs (IIa, IIb, IIc and IIa', IIb', IIc', respectively) are hardly separated, as they only have one methyl group at a different position. After testing several column configurations we find that after using a sequence of 4 Alltima silica columns the separation improves sufficiently to quantify the 5- and 6-methyl isomers of the pentamethylated

brGDGTs (Fig. 3B). As expected it also leads to an improved separation of the hexamethylated brGDGTs. This showed, besides the previously described IIa' and IIIa' (De Jonge et al., 2013), the presence of later eluting brGDGTs in the mass chromatograms of the protonated molecules of the hexa- and pentamethylated brGDGTs IIb, IIc, IIIb and IIIc (Fig. 3B). Based on the similar shift in retention time we propose that these components are brGDGTs that have one (IIb' and IIc') or two (IIIb' and IIIc') methyl groups at the 6 and/or ω 6 position rather than the 5 and/or ω 5 position. In this study, the separation using four sequential Alltima silica columns thus enabled for the first time the quantification of six hexamethylated, six pentamethylated and three tetramethylated brGDGTs (Fig. 1). The relative retention times of the 15 brGDGTs, scaled between the retention times of crenarchaeol and brGDGT Ia, are reported in Supp. Table 2.

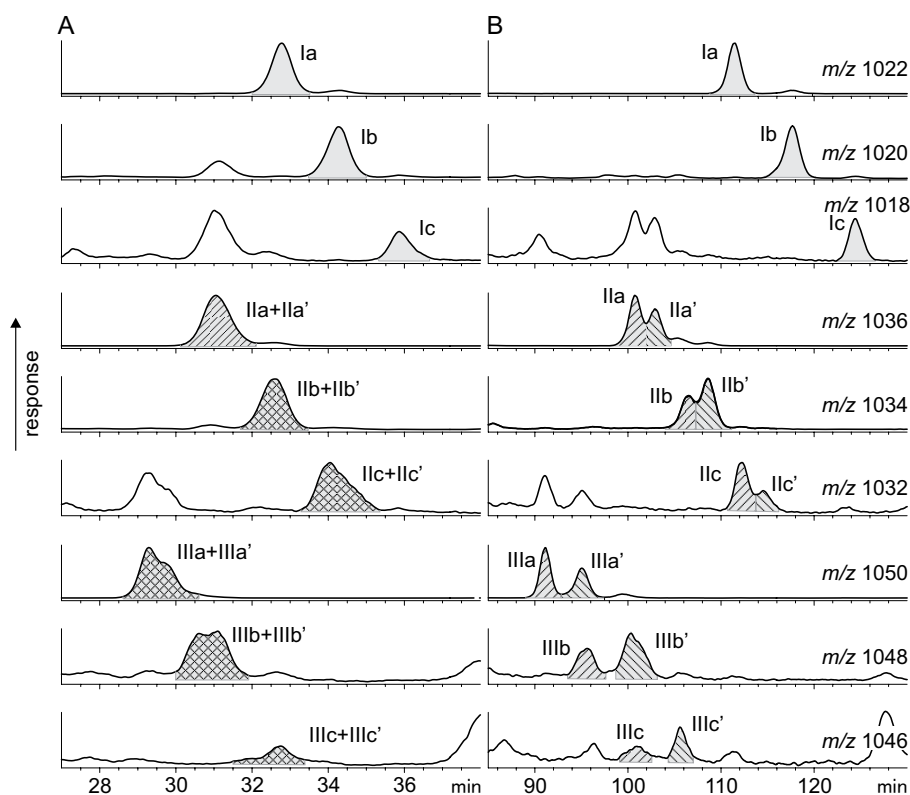


Fig. 3. Improved separation of brGDGTs, demonstrating A) the separation achieved using HPLC-MS on a Prevail cyano column after Schouten et al. (2007a) and B) the separation achieved using HPLC-MS on a sequence of 4 Alltima silica columns (this study), of the soil sample USA-17. The roman numerals refer to the structures in Fig. 1. For the penta- and hexamethylated compounds, the peaks representing 5-methyl compounds elute first (forward slanting lines), followed by the peaks representing 6-methyl compounds (backward slanting lines). Peaks that represent a co-elution of 5- and 6-methyl compounds are crosshatched. Chromatograms shown were treated with a Gaussian smooth of 0.3 minutes.

Comparing the chromatograms and the relative abundances of brGDGTs in this study with the Peterse et al. (2012) dataset, it became clear that, in the brGDGT analysis of Peterse et al. (2012), the 5- and 6-methyl isomers nearly always co-eluted and were quantified as a single peak for the large majority of the soils investigated (Fig. 4). The inconsistent quantification of these brGDGTs will have introduced some scatter in the obtained calibration, although the influence on the slope and intercept was probably negligible, as only a small number of soils allowed the exclusion of brGDGTs IIIa', IIIb' and/or IIIc'. Occasionally, the chromatography on a Prevail cyano column can allow the separate quantification of the hexamethylated 5- and 6-methyl isomers, but the separation potential of Prevail cyano columns is batch-specific and probably decreases with use. Furthermore, the complexity of the matrix possibly affects the separation (De Jonge et al., 2014). We recommend that for consistency, when using the Peterse et al. (2012) calibration, the peak area of 5- and 6-methyl hexamethylated brGDGTs should be combined, even when the achieved chromatographic separation allows to quantify them individually. Below we discuss the abundance of 6-methylated brGDGTs and their impact on the MBT'/CBT ratios.

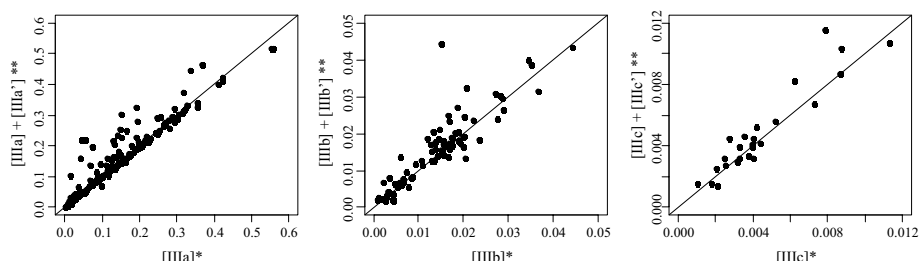


Fig. 4. Scatterplot of *) the fractional abundances of the hexamethylated brGDGTs as reported in Peterse et al. (2012), versus **) the summed amounts of the 5- and 6-methyl hexamethylated brGDGTs calculated in this study. The majority of the samples (83%) plot on the 1/1 line (plotted in black), indicating that it was not possible to separate the 5- and 6 methyl isomers in these soil samples. For samples plotting above the 1/1 line, the separation allowed to cut off a shoulder.

3.2. 6-methyl brGDGTs: Abundance and environmental controls

To evaluate the ubiquity and potential biological sources of 6-methyl brGDGTs, we calculated their fractional abundance in 239 soils previously examined by Peterse et al. (2012). The fractional abundance of all 15 brGDGTs is reported in Supp. Table 3 and the average fractional abundance is shown in Fig. 5. The 6-methyl brGDGTs were detected in 222 out of 239 soils and comprise on average 24% (Fig. 5) of the total amount of brGDGTs and can represent 80% of all brGDGTs in some soils. This shows that they are ubiquitous as well as abundant in soils worldwide.

To investigate the environmental controls on the fractional abundance of the new 6-methyl brGDGTs, the variance of the fractional abundances of all 15 individual brGDGTs was studied using principal component analysis (PCA; Fig. 6). The first three principal components (PCs) account for 40, 17 and 13% of the variance. The loadings of the 15 brGDGTs and the scores of

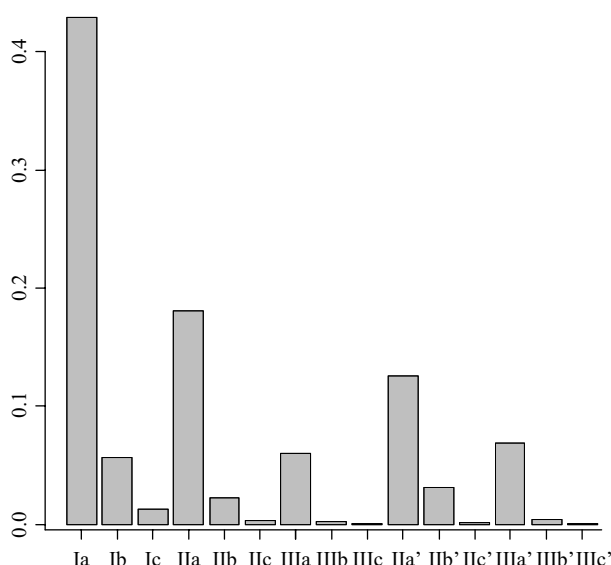


Fig. 5. Average (n=239) fractional abundance of brGDGTs in global soils.

the 239 soils on the first three principal components (PC1-PC3) are also given in Supp. Table 4. The first PC (PC1) reveals the positive correlation between the fractional abundance of all six 6-methyl brGDGTs and the 5-methyl cyclopentane-containing hexa- and pentamethylated brGDGTs. While the 5-methyl non-cyclopentane containing brGDGTs (IIa and IIIa) have a low loading on the PC1, they score high on the second PC (PC2). The fractional abundances of the tetramethylated brGDGTs (Ia, Ib and Ic) all plot negatively on the PC2. The third PC (PC3) indicates that 13% of the variation can be explained by a correlation of the fractional abundance of the 6-methyl components IIIa' and IIa', which have high loadings on PC3, and corresponding low values of the cyclopentane-containing components, especially IIc, that have large negative loadings on PC3.

The correlation of the fractional abundances of brGDGTs with the MAT, soil pH, MAP and the organic content of the soil (Corg) can be visualized when plotting the environmental parameters a posteriori in the ordination space of the PCA (Fig. 6). Soil pH is positively correlated with the largest component of the variance and plots along the PC1, correlating with the fractional abundances of the cyclopentane-containing and 6-methyl brGDGTs, while the MAT plots mainly along the PC2, correlating positively with the fractional abundance of the tetramethylated brGDGTs. The MAP plots in the same quadrant as the MAT (Fig. 6A), reflecting the positive correlation between the MAP and MAT in our data set ($r^2=0.30$). The Corg content does not seem to vary in the dataset with either the PC1 or the PC2, but does correlate with the PC3, that shows a low amount of Corg in the soils is coeval with a high fractional abundance of brGDGT IIa' and IIIa' (Fig. 6B). On this axis, a limited number of samples, all dry soils, plot separately as a cluster. These soils have relatively high fractional abundances of brGDGT IIa' and IIIa'.

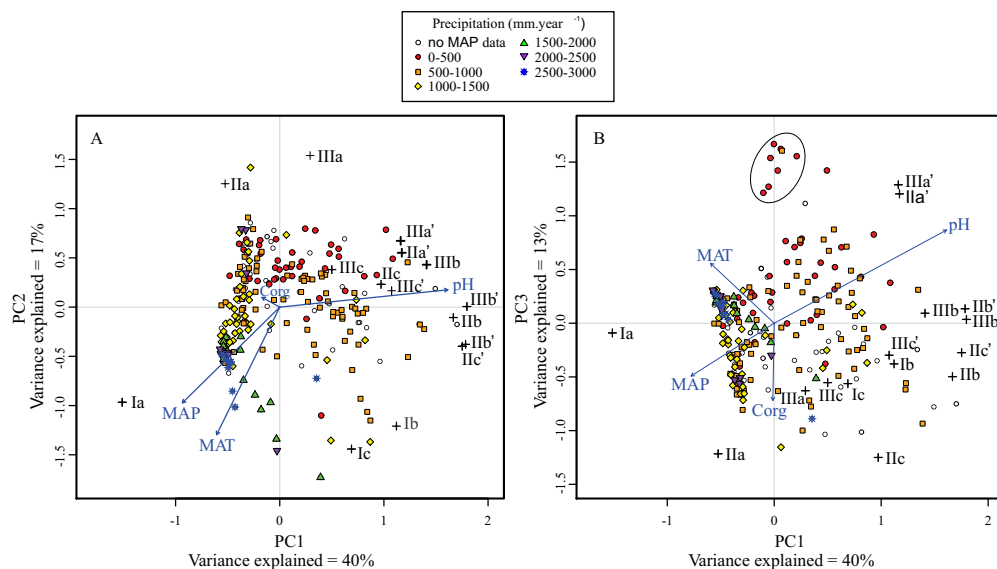


Fig. 6. Principal component analysis (PCA) of the standardized fractional abundances of the 15 brGDGTs in the surface soils of the global soil dataset ($n=239$). Panel A shows a plot of PC1 versus PC2, panel B a plot of PC1 versus PC3. The first principal component (PC) explains 40% of the variance, the second 17% and the third PC 13%. The environmental variables are plotted a posteriori, indicating the direction of the strongest linear increase. The sample site symbols are indicative of the precipitation class.

Since MAT and soil pH seem to be an important control on the relative abundance of brGDGTs, we plotted the fractional abundances of all brGDGTs against soil pH and MAT (Figs. 7 and 8, respectively). Fig. 7 shows that the tetramethylated and 5-methyl brGDGTs containing one cyclopentane moiety (Ib, IIb, IIIb) are all significantly correlated with soil pH (Fig. 7; $0.41 < r^2 < 0.55$, $p < 0.01$). The tetramethylated and 5-methyl brGDGTs with two cyclopentane moieties (Ic, IIc, IIIc) have a weak or non-significant correlation with soil pH (Fig. 7; $0.02 < r^2 < 0.22$, $0.01 < p < 0.9$). BrGDGT Ia is inversely correlated with soil pH (Fig. 7; $r^2=0.72$, $p < 0.01$). A new insight is the strong increase in the fractional abundance of all 6-methyl brGDGTs with increasing soil pH (Fig. 7; $0.41 < r^2 < 0.79$, $p < 0.01$). Furthermore, the separation of the soil pH-dependent 6-methyl brGDGT IIa' from brGDGT IIa now allows to see an inverse correlation of the latter with soil pH (Fig. 7; $r^2=0.34$, $p < 0.01$). BrGDGT IIIa, however, does not show a significant correlation with soil pH (Fig. 7; $r^2=0.05$, $p > 0.5$). This is in apparent contrast with what was observed in Peterse et al. (2012), where a correlation was observed. Likely, the co-elution of IIIa with IIIa' in the HPLC-MS method used by Peterse et al. (2012) caused a correlation with soil pH as GDGT IIIa' shows a strong correlation with soil pH.

The dependence of the fractional brGDGT abundances on MAT is shown in Fig. 8. The non-cyclopentane containing tetramethylated and 5-methyl brGDGTs (Ia, IIa and IIIa) show the strongest correlation with MAT (Fig. 8; $0.58 < r^2 < 0.65$, $p < 0.01$), as previously described by Peterse et al. (2012). However, due to the individual quantification of the 6-methyl brGDGTs, the correlation coefficients (r^2) of the fractional abundances of the brGDGTs Ia, IIa and IIIa with MAT are much higher compared to the previous study (r^2 of 0.58 vs 0.29, 0.65 vs

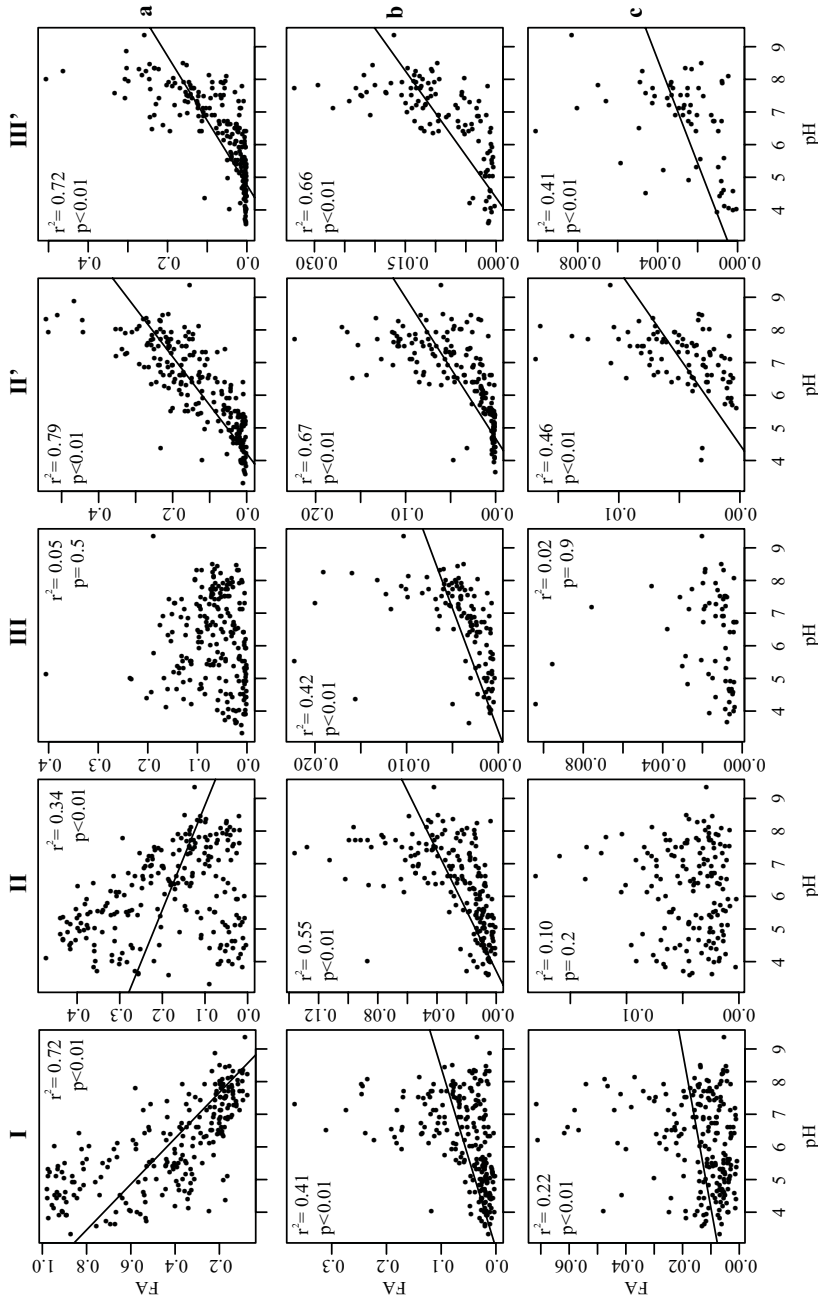


Fig. 7. Fractional abundance (FA) of branched GDGTs, plotted versus soil pH. The combination of roman numbers and letters refers to the structures in Fig. 1. Values below the limit of quantification are not included in the correlation plots. The linear regression lines of correlation with a p-value >0.05 are plotted. The Pearson's product-moment correlation regression coefficients (r^2) and p-values are indicated above each graph.

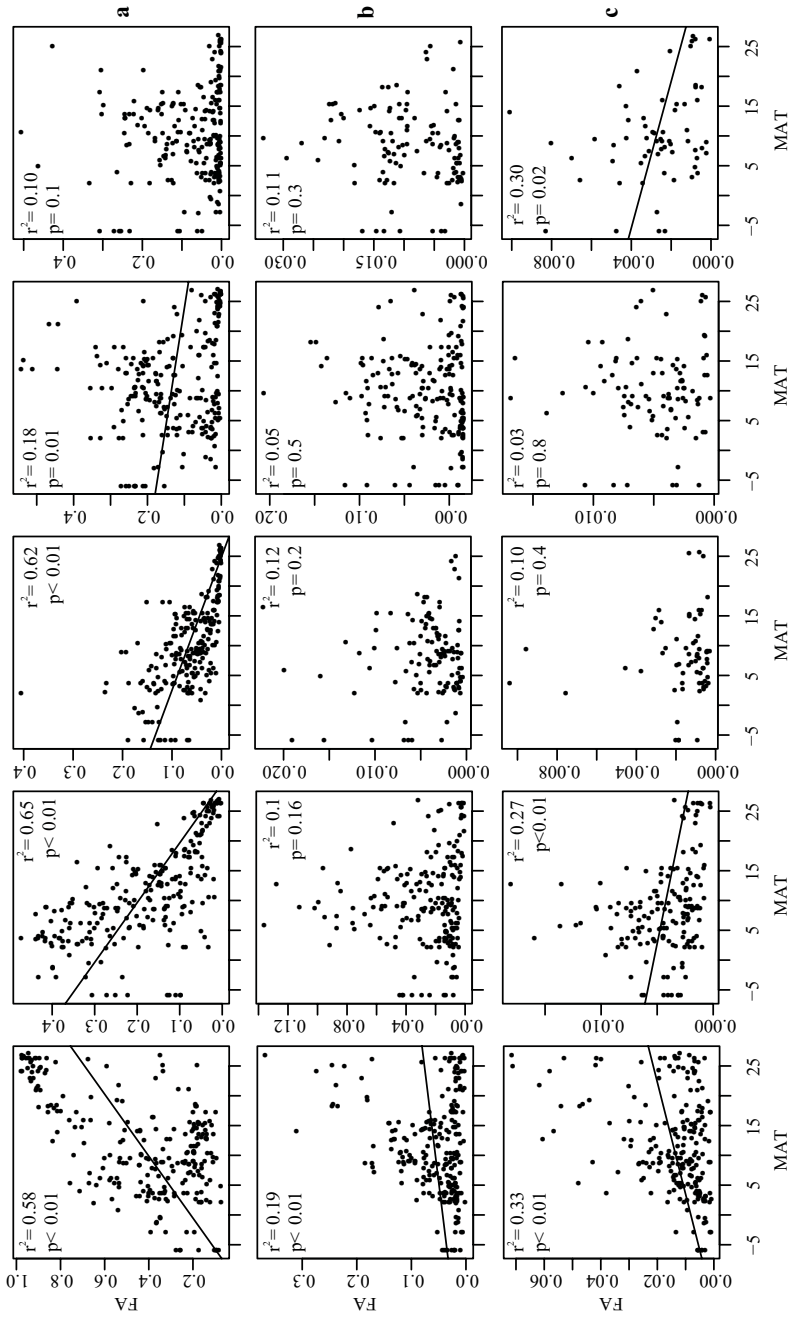


Fig. 8. Fractional abundance (FA) of branched GDGTs, plotted versus MAT. The combination of roman numbers and letters refers to the structures in Fig. 1. Values below the limit of quantification are not plotted in this figure. The regression lines are plotted and the Pearson's product-moment correlation regression coefficients (r^2) and p-values are indicated above each graph.

0.53 and 0.62 vs 0.33, respectively). In accordance with Peterse et al. (2012), the fractional abundances of the cyclopentane-containing tetramethylated brGDGTs (Ib and Ic) increase with increasing temperature, although the correlation is weaker (Fig. 8; $0.19 < r^2 < 0.33$, $p < 0.01$) than for brGDGT Ia. The other brGDGTs, i.e. all the 6-methyl and the 5-methyl cyclopentane-containing penta- and hexamethylated brGDGTs, show an absent or weak inverse correlation with MAT (Fig. 8; $0.03 < r^2 < 0.30$, $0.01 < p < 0.8$).

Based on these correlations, the most important control on the fractional abundance of the 6-methyl brGDGTs seems to be soil pH. The reason why 6-methyl brGDGTs increase with increasing soil pH is unclear at the moment. The slight structural difference between the 5- and 6-methyl brGDGTs is unlikely to have a direct effect on the proton permeability of the cell membrane, as was postulated for the pH-dependent brGDGTs with cyclopentane moieties (Weijers et al., 2007a). An alternative explanation is the increase of 6-methyl brGDGTs as a result of a pH-dependent community shift, i.e. a higher abundance of soil bacteria producing 6-methyl instead of 5-methyl brGDGTs with increasing soil pH. Presently, no bacterial cultures have been identified that produce either 5- or 6-methyl brGDGTs.

3.3. Effect of 6-methyl brGDGTs on CBT and MBT'

The relative abundance of the 6-methyl brGDGTs as well as their strong relation with soil pH, suggests that the MBT'/CBT proxy requires a reassessment. The impact of the 6-methyl brGDGTs can be evaluated by calculating the CBT_{SME} and MBT'_{SME} that are based only on the fractional abundances of the 5-methyl brGDGTs (see experimental section for formulas). Firstly, we examined the impact on the CBT-soil pH correlation. The exclusion of the 6-methyl brGDGTs results in a significant correlation of the CBT_{SME} with pH, with an r^2 of 0.60 (Fig. 9A). One outlier was observed and removed from the dataset before calibration. The calibration results in [Eq. 8], allowing the reconstruction of the pH with a RMSE of 0.84 (Fig. 9B):

$$pH = 7.84 - 1.73 * CBT_{SME} \quad (n=221, r^2 = 0.60, RMSE = 0.84, n_{outliers} = 1) \quad [Eq. 8]$$

The RMSE of this calibration is similar to that reported for the CBT in Peterse et al. (2012), i.e. 0.8 ($n=176$). However, our CBT_{SME} -based pH is calculated on a set of soils ($n=221$) that is larger than the calibration dataset of Peterse et al. (2012). Calibration of the original CBT for all soils used in this study ($n=218$, as the CBT could not be calculated for three soils), shows that this extended dataset has an associated RMSE of 0.9 and an r^2 of 0.59, i.e. larger than CBT_{SME} . The separation of the 5- and 6-methyl brGDGTs thus results in a slightly more accurate pH reconstruction (Fig. 9A-B). This incremental improvement is to be expected, as the pentamethylated brGDGTs quantified co-eluted with 6-methyl components whose abundance is also strongly dependent on pH (Fig. 7).

The original MBT and MBT' ratios correlated, besides with MAT, also with soil pH. Correlation of MBT'_{SME} with soil pH now showed no significant correlation with soil pH ($p=0.22$) with r^2 reduced to 0.05 (Fig 9E). This can be explained by the removal of the pH-dependent 6-methyl brGDGTs that were present in the denominator of the MBT' ratio [Eq. 2]. Indeed, a linear model that attempts to fit a regression between the MAT and the CBT_{SME} and MBT'_{SME} following the approach of Weijers et al. (2007a), indicates that the CBT_{SME} no longer

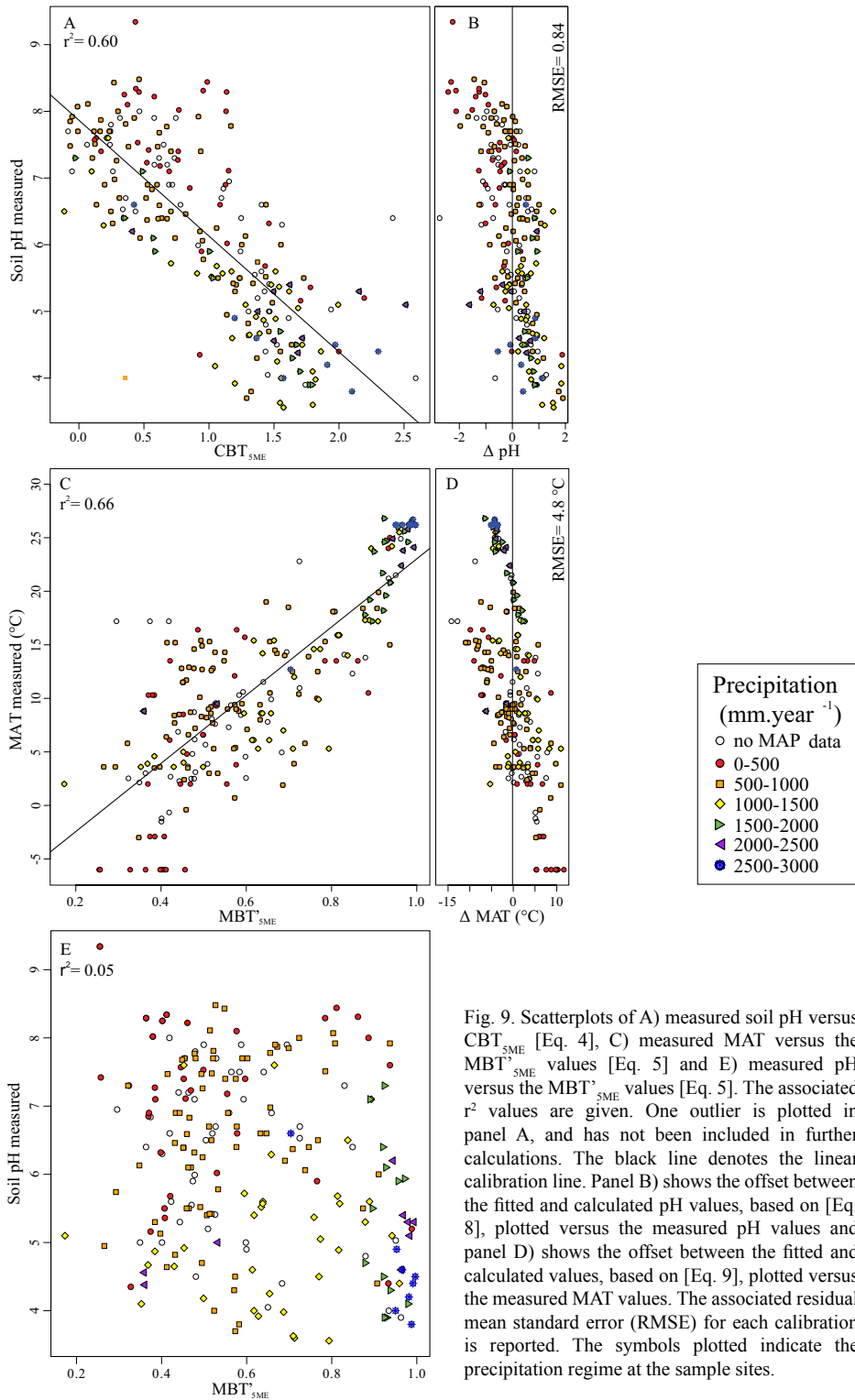


Fig. 9. Scatterplots of A) measured soil pH versus CBT_{SME} [Eq. 4], C) measured MAT versus the MBT_{SME} values [Eq. 5] and E) measured pH versus the MBT_{SME} values [Eq. 5]. The associated r^2 values are given. One outlier is plotted in panel A, and has not been included in further calculations. The black line denotes the linear calibration line. Panel B) shows the offset between the fitted and calculated pH values, based on [Eq. 8], plotted versus the measured pH values and panel D) shows the offset between the fitted and calculated values, based on [Eq. 9], plotted versus the measured MAT values. The associated residual mean standard error (RMSE) for each calibration is reported. The symbols plotted indicate the precipitation regime at the sample sites.

contributes significantly to the MAT reconstruction ($p=0.26$). A linear regression of MBT'_{SME} against MAT now resulted in the following correlation:

$$MAT = -8.57 + 31.45 * MBT'_{SME} \quad (n=222, r^2 = 0.66, RMSE = 4.8^\circ C) \quad [Eq. 9]$$

This correlation has a much lower RMSE than the MBT' -MAT correlation reported by Peterse et al. (2012) for the calibration dataset ($RMSE=5.7^\circ C$, $n=176$). In fact, the RMSE of the MBT'_{SME} -MAT calibration is similar to that of previously reported MBT' /CBT-MAT correlation based on the calibration dataset ($RMSE = 5.0^\circ C$, $n=176$), and is an improvement compared to the MBT' /CBT-MAT correlation of the extended soil dataset ($RMSE = 5.5^\circ C$, $n=219$). However, the MBT'_{SME} calibration slightly underestimates the MAT of the warmest soils in our dataset (Fig. 9D) and only allows the reconstructions of MAT up to $22.7^\circ C$ (i.e. $MBT'_{SME}=1$) and, thus, does not allow the reconstruction of MAT of tropical regions where $MAT > 25^\circ C$.

3.4. Exploring brGDGT indices for improved pH and MAT-calibrations

The individual quantification of the brGDGT 5- and 6-methyl isomers allows to improve the soil pH and MAT reconstruction by calculating the CBT'_{SME} and MBT'_{SME} ratios after exclusion of the 6-methyl brGDGTs as shown above. However, we can also attempt to define new indices, taking all 15 brGDGTs into account.

To this end, we firstly pursued an objective statistical approach to identify the indices with the highest correlation coefficients, where the indices are in the form of a common logarithm of a ratio of brGDGTs. We follow the approach of Kim et al. (2010a) applied for marine isoprenoid GDGTs and Peterse et al. (2012) applied for brGDGTs in soils. From the models with the best correlations, we then selected the index with the most straightforward structural interpretation. The here defined CBT' index yielded one of the highest correlations with soil pH (Fig. 10A-B):

$$CBT' = {}^{10}\log[(Ic+IIa'+IIb'+IIc'+IIa'+IIb'+IIc')/(Ia+IIa+IIa)]. \quad [Eq. 10]$$

$$pH = 7.15 + 1.59 * CBT' \quad [Eq. 11]$$

$$(n = 221, r^2 = 0.85, RMSE = 0.52, n_{outliers} = 5, p < 0.0001).$$

This index is distinct from the previously reported CBT-pH correlation (Peterse et al., 2012), as it includes the pH-dependent 6-methyl brGDGTs in the numerator. The accuracy of the pH-reconstruction is substantially improved compared to CBT'_{SME} , resulting in a decrease of RMSE from 0.85 to 0.52 pH units (Fig. 10B).

We also performed the same statistical analysis for correlations against the MAT. One of the highest correlations was obtained using an index of the form (Fig. 10D):

$$Index\ 1 = {}^{10}\log[(Ia+Ib+Ic+IIa'+IIa')/(Ic+IIa+IIc+IIa+IIa')] \quad [Eq. 12]$$

$$MAT = 5.05 + 14.86 * Index\ 1 \quad [Eq. 13]$$

$$(n = 222, r^2 = 0.67, RMSE = 4.7^\circ C, p < 0.0001).$$

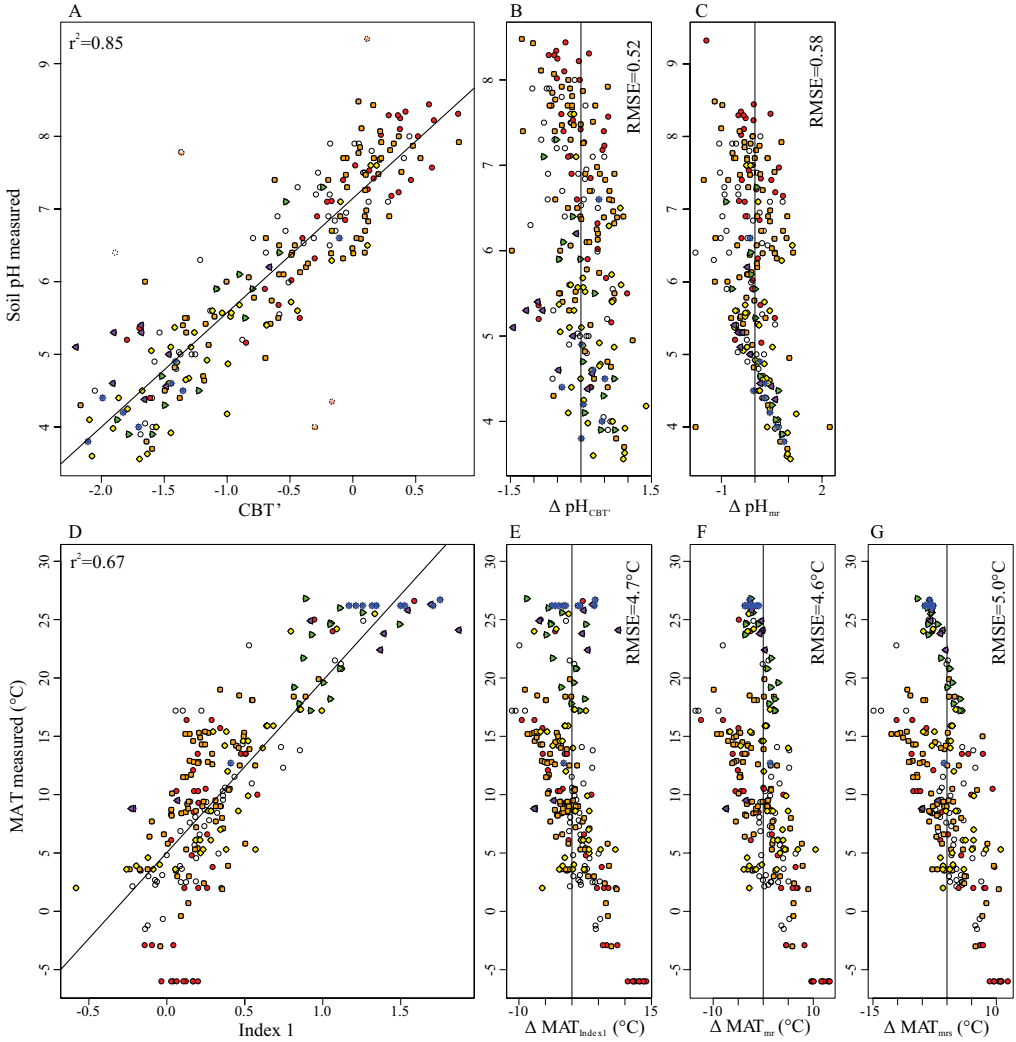


Fig. 10. A) CBT' plotted versus measured pH [Eq. 10] and D) Index 1 plotted versus measured MAT [Eq. 12]. Panel B-C show the offset between the fitted and calculated pH values, based on B) the CBT' [Eq. 10 and 11], C) pH_{mr} [Eq. 14]. Panels E-G show the offset between the fitted and calculated MAT values, based on E) Index 1 [Eq. 12 and 13], F) MAT_{mr} [Eq. 15] and G) MAT_{mrs} [Eq. 16]. The associated residual mean standard error (RMSE) for each calibration is reported. The symbols plotted indicate the precipitation regime at the sample sites.

In contrast to the MBT' and MBT'_{SME}, this index includes the two major 6-methyl penta- and hexamethylated brGDGTs in the nominator. This is somewhat surprising as their fractional abundance shows no or only a weak linear relation with the MAT (Fig. 8). Furthermore, the denominator includes two components with two cyclopentane groups (brGDGTs Ic and IIc), which are usually present as minor components (on average 6 and 1% of all brGDGTs). With the use of Index 1, the MAT reconstruction accuracy is improved only marginally compared to the MBT'_{SME} calibration, decreasing the RMSE from 4.8 to 4.7°C (Fig. 10E). We, therefore, conclude that the Index 1 does not result in a substantially improved MAT reconstruction.

Another statistical approach to find the best model to predict MAT and soil pH is by applying a least squares multiple linear correlation using linear combinations of the fractional abundances of the 15 brGDGTs, following the approach of Tierney et al. (2010) and Pearson et al. (2011). We base our calculation on the brGDGTs whose fractional abundances correlates with soil pH. If different models with a similar r^2 were found, the model using relatively abundant components was chosen. The best soil pH correlation is then given by:

$$\text{pH}_{\text{mr}} = 6.93 - 2.27*[\text{Ia}] + 4.86*[\text{Ib}] - 8.45*[\text{Ic}] - 3.00*[\text{IIa}] + 2.47*[\text{IIa}'] + 2.04*[\text{IIIa}'] + 63.4*[\text{IIIc}']$$

($n=221$, $r^2 = 0.81$, $\text{RMSE} = 0.58$, $p < 0.01$, $n_{\text{outliers}}=2$) [Eq.14]

This multiple regression (Fig. 10C) does not result in a more accurate pH reconstruction, compared to the CBT', suggesting that the latter is still the best proxy for pH reconstruction. The same approach was used for linear combinations of the fractional abundances of the brGDGTs that correlate with the MAT:

$$\text{MAT}_{\text{mr}} = 7.17 + 17.1*[\text{Ia}] + 25.9*[\text{Ib}] + 34.4*[\text{Ic}] - 28.6*[\text{IIa}]$$

($n=222$, $r^2 = 0.68$, $\text{RMSE} = 4.6^\circ\text{C}$, $p < 0.01$) [Eq. 15]

This equation reflects the positive correlation of the MAT with the fractional abundance of the tetramethylated brGDGTs Ia, Ib and Ic and the negative correlation with the fractional abundances of the pentamethylated brGDGT IIa (Fig. 8). This multiple linear regression-based MAT reconstruction (MAT_{mr}) has a small improvement in accuracy in comparison with the MBT'_{SME} (Fig. 10F). However, the range of temperatures reconstructed is larger than using the MBT'_{SME} with reconstructed temperatures $> 26^\circ\text{C}$. We, therefore, recommend using the MAT_{mr} for MAT reconstructions in palaeoclimate studies, although the reconstruction of MAT outside of the calibration range ($\sim 26^\circ\text{C}$) still has to be done with great caution.

Despite the improved MAT calibration using the MAT_{mr} (Fig. 10F) there is still a large amount of scatter. For example, we observe that the reconstructed MAT of soils with a MAT below 1°C is significantly overestimated (Fig. 10F). A possible explanation for this phenomena would be the preferential production of brGDGTs in the summer season, compared to the seasons when the soils are frozen. Although Arctic soil bacteria have been shown to produce new cell membrane components in frozen conditions (McMahon et al., 2009), it is unclear whether this production is as abundant as during the summer. Another observation is that soils from temperate areas (between ~ 12 and $\sim 20^{\circ}\text{C}$) show the largest remaining scatter. Plotting the ΔMAT based on the MAT_{mr} against the sampling latitude shows an increasing offset and increasing scatter with increasing latitude (Fig. 11), matching an increased seasonality in these soils. Weijers et al. (2011b) could not reconstruct a seasonal difference in the brGDGT distribution, probably because a small difference would have been obscured by the fossil brGDGT lipids already present in the soils. Another cause for the remaining temperature offset (also discussed in Peterse et al., 2012), is the offset between the air MAT and the in-situ soil MAT.

One potential issue with the MAT_{mr} is that it requires the measurement of all 15 brGDGTs, as it is based on fractional abundances. Therefore, we assessed whether MAT can be reconstructed using only the three most abundant and omnipresent brGDGTs Ia, IIa and IIIa, in the form of the Multiple linear Regression Simple index (MAT_{mrs}) (Fig. 10G). In the following formula, the abundances of brGDGT Ia and IIa are fractional to the combined amounts of brGDGT Ia, IIa and IIIa:

$$MAT_{mrs} = 5.58 + 17.91 * [Ia] - 18.77 * [IIa] \quad [\text{Eq. 16}]$$

($n=231$, $r^2 = 0.62$, $RMSE = 5.0^{\circ}\text{C}$, $p < 0.01$)

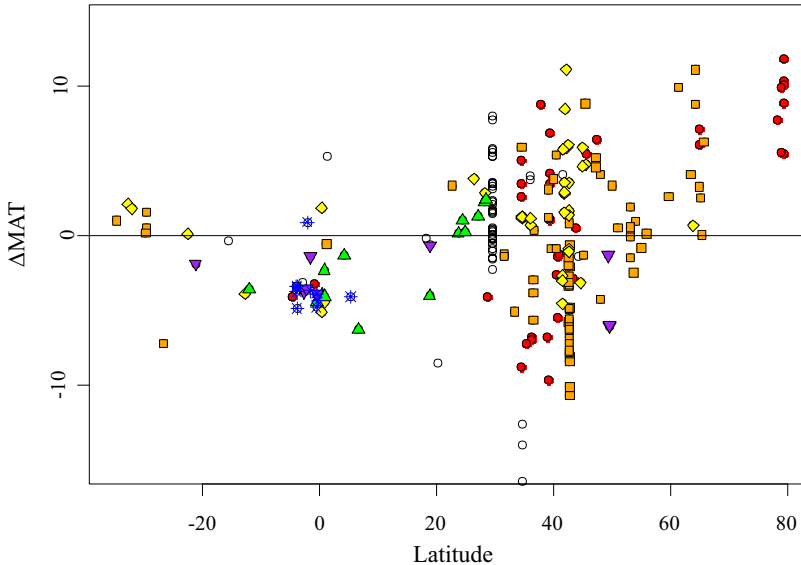


Fig. 11. The residual errors (ΔMAT) based on the MAT_{mr} plotted versus the latitude at which the sample was taken. The symbols plotted indicate the precipitation regime at the sample sites.

The RMSE associated with this calibration is 5.0°C, similar to the MBT'_{SME} and only slightly higher than the MAT_{mr} . The MAT_{mr} index can thus potentially be used to reconstruct the MAT in settings where the abundance of brGDGTs is low, and the maximum temperatures are not expected to be > 23.5°C.

3.5. Palaeoclimate reconstructions in arid soils

As shown above, the accuracy of the MAT and soil pH reconstruction will be improved substantially using the CBT' and MAT_{mr} proxies and we, therefore, recommend to use these proxies in palaeoclimate reconstructions. The application of the new calibrations may potentially result in quite different temperature reconstructions.

We examined the impact of the new calibration by comparing the soil pH and MAT estimates from the soil data set using the new calibrations versus those based on the Peterse et al. (2012) calibrations (Fig. 12). Fig. 12A shows that the reconstructed MAT values plot around the 1:1 line suggesting that, in most cases, the reconstructed MAT obtained from the MBT'/CBT calibration from Peterse et al. (2012), will approximate the values we calculate based on the MAT_{mr} . However, our results indicate that the separate quantification of the 6-methyl components will result in substantially warmer reconstructed MAT values in a set

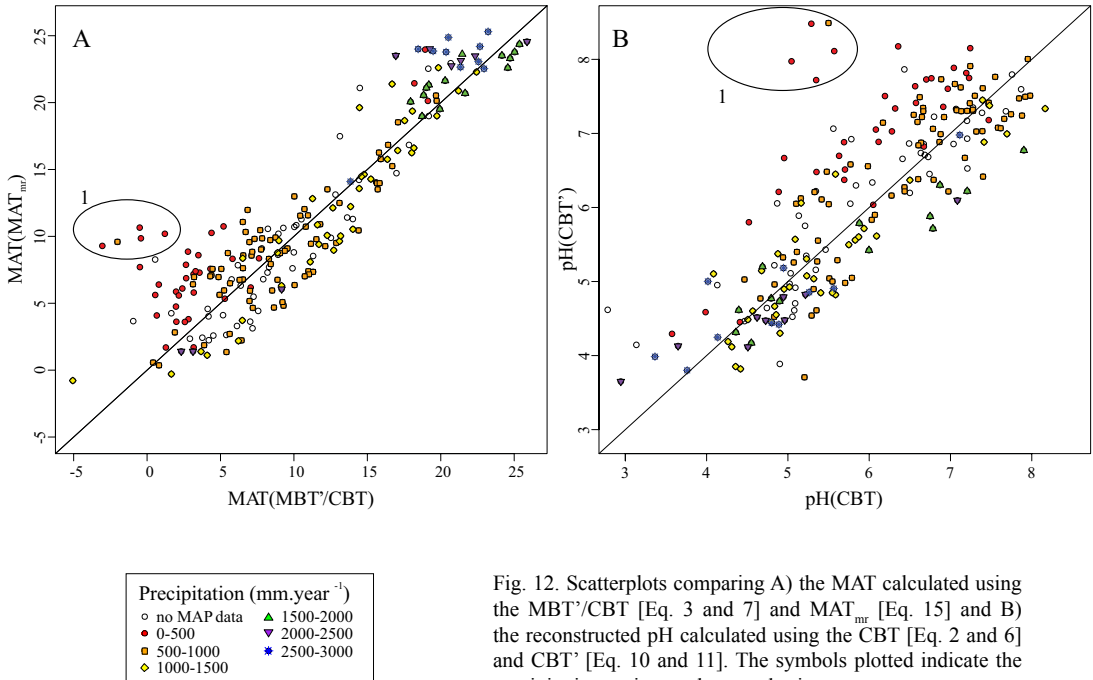


Fig. 12. Scatterplots comparing A) the MAT calculated using the MBT'/CBT [Eq. 3 and 7] and MAT_{mr} [Eq. 15] and B) the reconstructed pH calculated using the CBT [Eq. 2 and 6] and CBT' [Eq. 10 and 11]. The symbols plotted indicate the precipitation regime at the sample sites.

¹ Soil samples with an aberrant brGDGT distribution are indicated. Although not all of the samples highlighted in the PCA (Fig. 6) have sufficient amounts to calculate the pH and MAT, all these sites, and only these sites, fit in the range indicated in this scatterplot.

of arid soils (Fig. 12A, in circle). Using the MBT'/CBT calibration [Eq. 6], the MAT in these soils was underestimated significantly (RMSE of 13.1°C). Using the MAT_{mr} , the temperatures reconstructed are much more accurate (RMSE of 3.3°C). In this study, the aberrant soils all have high loadings on the PC3 (Fig. 6B). Based on the PCA, we can conclude that the 'cold bias' observed in this subset of arid soils, was due to an increase of the fractional abundance of 6-methyl brGDGTs IIIa' and IIa'. In contrast to the majority of the soils, this was not coeval with an increase in the cyclopentane-containing brGDGTs, and thus the CBT value. Calculating the MAT thus resulted in temperatures that are too cold, as the CBT-adjustment performed (Weijers et al., 2007a; Peterse et al., 2012) is not sufficient to 'correct' for the large amount of the 'cold' 6-methyl brGDGTs IIa' and IIIa' present in arid soils. The underestimation of MAT in arid soils has been observed in a number of recent studies (Dirghangi et al., 2013; Menges et al., 2013; Yang et al., 2013; Zell et al., 2014) and we surmise that this is due to the presence of 6-methyl brGDGTs. Furthermore, the increase in the fractional abundances of brGDGT IIa' will also result in an underestimation of the soil pH. Indeed, using the CBT', the RMSE of the subset of arid soils decreases from 2.9 to 0.3 pH units.

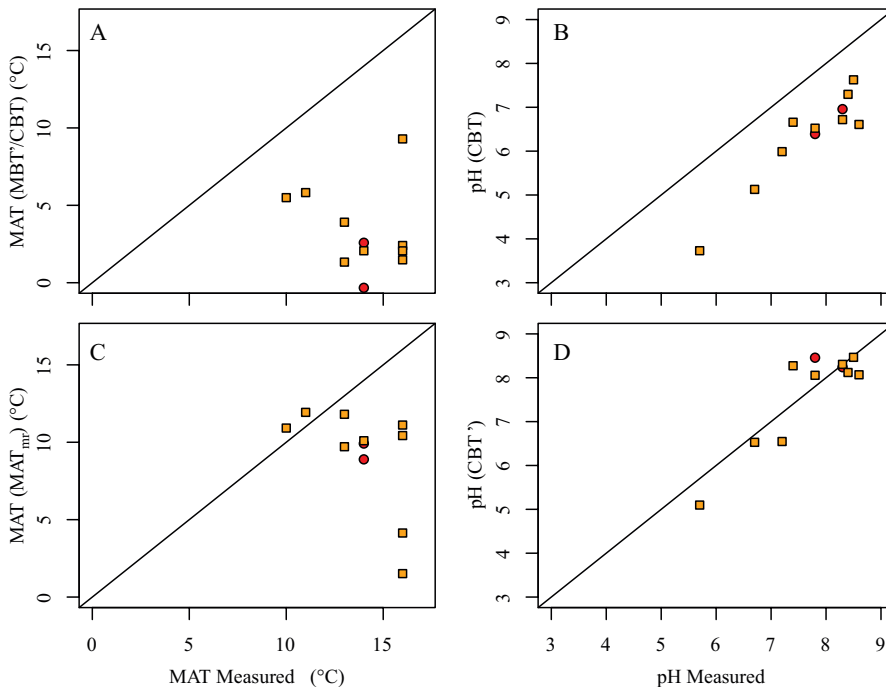


Fig. 13. Reconstructed versus measured MAT (A, C) and pH (B, D) of a set of Iberian Peninsula soils. MAT and pH reconstructed using A, B) the Peterse et al. (2012) calibration and C, D) the MAT_{mr} and CBT' calibrations developed in this paper. The symbols plotted indicate the precipitation regime at the sample sites, where red circles denote a MAP > 500 mm.year⁻¹ and orange squares denote a MAP between 500 and 100 mm.year⁻¹.

We test the potential to improve MAT and soil pH reconstructions in an independent set of 14 soils collected on the Iberian Peninsula, that were previously described in Zell et al. (2014a). The MAT of these soils was significantly underestimated using the MBT'/CBT calibration, with residual errors between 4.5 and 14.5°C, on average 10.6°C (Fig. 13A). Furthermore, all pH values reconstructed underestimate the measured soil pH (Fig. 13B). We reanalyzed this sample set with our improved separation method. After the separate quantification of the 6-methyl brGDGTs, the MAT_{mr} and CBT' indices were applied to the dataset. Firstly, the MAT and pH can now be calculated for all soils, including three soils for which the CBT values could previously not be calculated due to low abundances of the brGDGTs Ib and IIb. Here, we only compare the soils that have a MAT and pH reconstruction based on both calibrations. The MAT reconstruction improved for all soils, with the residual error being on average 5.1°C. Furthermore, the pH determination using the CBT' reconstruct measured soil pH well, with an associated RMSE of 0.4 pH units (Fig. 10B). We conclude that the use of the MAT_{mr} and CBT' indeed substantially improved the MAT and pH reconstructions for this dataset of relatively arid soils (MAP>1000 mm.year⁻¹). Palaeoclimate reconstructions are thus likely to substantially benefit from a separate quantification of the 6-methyl isomers.

4. Conclusions

The recently described 6-methyl brGDGTs are abundant brGDGTs in globally distributed soils, and their fractional abundance covaries strongly with soil pH. Excluding them from MBT' calculations, allows a pH-independent MAT reconstruction, with an improved RMSE of 4.8°C. A multiple linear regression, based on the fractional abundances of the brGDGTs Ia, Ib, Ic and IIa and defined as the MAT_{mr}, allows to reduce the RMSE further to 4.6°C. Furthermore, we defined a second linear regression, based on the abundances of only brGDGT Ia, IIa and IIIa, calculating the simple and robust MAT_{ms}, with an associated RMSE of 5.0°C. The new brGDGT index, the CBT', which includes the 6-methyl brGDGTs, allows to reconstruct soil pH with an improved RMSE of 0.5. Applying the novel calibrations on a independent soil dataset from the Iberian Peninsula, confirms the improvements in MAT and pH reconstructions. Thus, palaeoclimate MAT and pH reconstruction is substantially improved, in particular for arid regions, after the separate quantification of the 6-methyl brGDGTs, using the MAT_{mr} and the CBT' indices.

5. Acknowledgments

We acknowledge Jaap van der Meer (Royal NIOZ) for insightful discussions on the statistical methods used. We acknowledge the work of Johan Weijers and Francien Peterse in collecting the soil dataset and preparing the samples for analysis. We thank Dr. R. Smith and two anonymous referees for their helpful comments. This work was funded by research project 819.01.013, financed by the Netherlands Organization for Scientific Research (NWO) and the European Research Council under the EU Seventh Framework Programme (FP7/2007-2013) / ERC grant agreement n° [226600].

Supp. Table 1. Summarizes the measured environmental variables, the calculated indices and the reconstructed variables. The pH is reconstructed based on the CBT_{SME} [Eq. 4 and 8], the CBT' [Eq. 10 and 11] and the pH_{nr} [Eq. 14]. The MAT is reconstructed using the MBT' [Eq. 5 and 9], index 1 [Eq. 12 and 13], the MAT_{nr} [Eq. 15] and the MAT_{ms}. N.m. indicates that environmental variables are not available or measured. N.d. indicates that the amounts of the brGDGTs are not sufficient for the calculation of the indices.

ID	Soil site	MAT (°C)	Soil pH	Corg (%)	MAP (mm.year ⁻¹)	CBT _{SME}	pH CBT _{SME}	CBT'	pH CBT'	pH _{nr}	MBT' _{SME}	MAT MBT' _{SME} (°C)	Index 1	MAT Index 1 (°C)	MAT _{nr} (°C)	MAT _{ms} (°C)
1	Australia-17	13.9	6.4	n.m.	624	0.64	6.7	-0.48	6.4	7.1	0.75	14.9	0.53	12.9	14.0	13.4
2	Australia-4	19	6.6	2.9	677	1.44	5.4	-0.69	6.1	5.4	0.65	11.8	0.34	10.1	9.1	11.0
3	Brazil-1	22.9	4.5	0.95	1021	n.d.	n.d.	n.d.	n.d.	n.d.	n.d.	n.d.	n.d.	n.d.	n.d.	n.d.
4	Brazil-12	24.9	6.2	n.m.	2060	0.41	7.1	-0.66	6.1	6.1	0.94	21.1	0.92	18.8	24.6	21.6
5	Brazil-13	24.9	3.9	n.m.	n.m.	1.74	4.8	-1.69	4.5	4.7	0.96	21.7	1.26	23.8	23.0	22.1
6	Brazil-14	21.2	4	n.m.	n.m.	2.59	3.4	-1.59	4.6	4.7	0.93	20.8	1.12	21.6	21.1	21.1
7	Brazil-28	25.6	5.9	n.m.	1570	1.00	6.1	-1.09	5.4	5.2	0.97	22.0	1.26	23.7	23.5	22.5
8	Brazil-3	22.8	5.1	1.74	1177	n.d.	n.d.	n.d.	n.d.	n.d.	n.d.	n.d.	n.d.	n.d.	n.d.	n.d.
9	Brazil-6	20.8	5.2	0.83	1194	n.d.	n.d.	n.d.	n.d.	n.d.	0.94	20.9	1.12	21.7	21.4	21.2
10	Cameroon-1	21.7	6.4	3	1950	0.35	7.2	-0.58	6.2	6.4	0.92	20.4	0.88	18.1	23.3	20.5
11	Canada-14	6.1	4	n.m.	1474	1.55	5.2	-1.56	4.7	4.5	0.62	10.8	0.19	7.8	8.1	9.3
12	Canada-17	2.4	7.7	n.m.	505	0.16	7.6	0.17	7.4	7.4	0.45	5.7	0.24	8.6	8.6	5.9
13	Canada-24	9.5	5	n.m.	2031	1.38	5.5	-1.46	4.8	4.9	0.53	8.2	0.07	6.1	6.1	7.7
14	China-19	22.4	4.6	2.22	2006	1.72	4.9	-1.91	4.1	4.8	0.96	21.7	1.37	25.4	22.8	22.1
15	China-20	24.7	3.9	1.87	1600	1.77	4.8	-1.60	4.6	4.7	0.93	20.7	1.05	20.7	21.4	20.9
16	China-23	18.2	4.5	0.58	1590	1.67	4.9	-1.23	5.2	5.2	0.92	20.4	1.05	20.6	20.6	20.9
17	China-25	17.2	5.5	0.82	1670	1.03	6.1	-0.86	5.8	5.5	0.9	19.6	0.92	18.8	19.5	19.9
18	China-27	17.8	4.7	5.18	1590	1.55	5.2	-1.52	4.7	4.9	0.88	19.1	0.85	17.7	19.0	19.1
19	China-31	19.6	6.1	4.22	1720	0.57	6.9	-0.90	5.7	6.0	0.93	20.6	1.00	20.0	22.6	20.7
20	China-32	20.8	4.3	1.36	1690	1.64	5.0	-1.50	4.8	4.8	0.94	20.9	1.11	21.5	21.7	21.4
21	China-4	17.2	4.9	1.2	1422	n.d.	n.d.	n.d.	n.d.	n.d.	0.91	20.0	0.99	19.8	19.6	20.3
22	China-49	14	6.5	3.66	1210	-0.11	8.0	0.12	7.3	7.6	0.83	17.8	0.61	14.2	19.0	14.7
23	China-6	19.2	7.1	2.93	1876	0.49	7.0	-0.53	6.3	6.3	0.89	19.4	0.82	17.2	20.7	19.2

ID	Soil site	MAT (°C)	Soil pH	Corg (%)	MAP (mm.year ⁻¹)	CBT _{SME}	pH CBT _{SME}	CBT ⁺	pH CBT ⁺	pH _{mr}	MBT ⁺ _{SME}	MAT _{MBT⁺_{SME}} (°C)	Index 1	MAT Index 1 (°C)	MAT _{mr} (°C)	MAT _{ms} (°C)
24	China-MG1180	14.32	7.9	n.m.	n.m.	0.74	6.6	-0.18	6.9	6.8	0.69	13.3	0.49	12.3	11.3	12.6
25	China-MG1220	14.08	7.3	n.m.	n.m.	0.62	6.8	-0.44	6.5	6.4	0.83	17.5	0.73	15.9	16.9	17.2
26	China-MG1515	12.31	6.4	n.m.	n.m.	2.41	3.7	-1.89	4.1	4.6	0.85	18.1	0.75	16.1	17.5	18.1
27	China-MG1645	11.53	7.5	n.m.	n.m.	0.06	7.7	0.09	7.3	7.5	0.63	11.6	0.43	11.5	13.1	10.7
28	China-MG1740	10.96	6.7	n.m.	n.m.	0.36	7.2	-0.14	6.9	6.9	0.72	14.2	0.55	13.1	14.2	14.3
29	China-MG1800	10.6	7.1	n.m.	n.m.	0.26	7.4	0.13	7.3	7.5	0.59	10.1	0.37	10.6	10.6	9.5
30	China-MG1850	10.3	7.5	n.m.	n.m.	0.24	7.4	0.08	7.3	7.4	0.58	9.8	0.36	10.4	10.7	8.8
31	China-MG1915	9.91	6.9	n.m.	n.m.	0.72	6.6	-0.60	6.2	5.9	0.66	12.1	0.36	10.4	11.3	10.6
32	China-MG1973	9.562	7.7	n.m.	n.m.	-0.08	8.0	0.41	7.8	8.0	0.52	8.1	0.36	10.4	10.6	8.5
33	China-MG2005	9.37	7.5	n.m.	n.m.	0.65	6.7	-0.28	6.7	6.5	0.56	9.2	0.25	8.8	8.8	8.1
34	China-MG2115	8.71	7.1	n.m.	n.m.	-0.05	7.9	0.28	7.6	7.9	0.46	6.4	0.24	8.7	10.2	6.4
35	China-MG2160	8.44	7.9	n.m.	n.m.	0.32	7.3	0.01	7.2	7.3	0.58	9.9	0.32	9.8	10.8	8.9
36	China-MG2220	8.08	6.6	n.m.	n.m.	0.78	6.5	-0.31	6.7	6.4	0.52	7.8	0.18	7.8	7.3	6.7
37	China-MG2300	7.6	6.7	n.m.	n.m.	1.10	5.9	-0.54	6.3	5.9	0.53	8.0	0.15	7.2	6.8	7.5
38	China-MG2350	7.3	6.9	n.m.	n.m.	0.69	6.6	-0.19	6.8	6.7	0.55	9.0	0.24	8.6	8.6	8.2
39	China-MG2420	6.88	7.2	n.m.	n.m.	0.68	6.7	-0.18	6.9	6.7	0.44	5.3	0.09	6.4	6.3	5.1
40	China-MG2470	6.58	7.9	n.m.	n.m.	0.58	6.8	0.05	7.2	7.2	0.49	7.1	0.21	8.2	7.9	6.7
41	China-MG2540	6.16	7.8	n.m.	n.m.	0.25	7.4	0.15	7.4	7.6	0.47	6.5	0.20	8.0	9.1	7.6
42	China-MG2620	5.68	6.5	n.m.	n.m.	0.44	7.1	-0.18	6.9	6.9	0.5	7.3	0.18	7.7	9.0	7.0
43	China-MG2742	4.948	4.4	n.m.	n.m.	1.43	5.4	-1.60	4.6	4.7	0.68	12.9	0.33	10.0	11.4	12.4
44	China-MG2764	4.816	5.9	n.m.	n.m.	1.24	5.7	-1.08	5.4	5.1	0.47	6.3	0.00	5.0	4.4	5.7
45	China-MG2808	4.552	5	n.m.	n.m.	1.30	5.6	-1.25	5.2	4.9	0.6	10.2	0.19	7.9	8.6	9.7
46	China-MG2920	3.88	5.2	n.m.	n.m.	1.37	5.5	-0.88	5.8	5.0	0.51	7.4	0.08	6.3	3.1	5.2
47	China-MG2960	3.64	7.2	n.m.	n.m.	0.58	6.8	-0.29	6.7	6.3	0.46	6.0	0.10	6.5	7.7	5.6
48	China-MG3049	3.106	4.5	n.m.	n.m.	1.52	5.2	-2.05	3.9	4.7	0.48	6.5	-0.03	4.6	3.6	5.9
49	China-MG3065	3.01	6.4	n.m.	n.m.	1.25	5.7	-0.69	6.1	5.6	0.36	2.9	-0.12	3.3	2.3	3.4
50	China-MG3119	2.686	5.6	n.m.	n.m.	1.40	5.4	-1.13	5.3	5.1	0.42	4.7	-0.08	3.9	2.7	4.6

ID	Soil site	MAT (°C)	Soil pH	Corg (%)	MAP (mm·year ⁻¹)	CBT _{SME}	pH CBT _{SME}	CBT ⁺	pH CBT ⁺	pH _{mr}	MBT ⁺ _{SME}	MAT MBT ⁺ _{SME} (°C)	Index 1	MAT Index 1 (°C)	MAT _{mr} (°C)	MAT _{ms} (°C)
51	China-MG3140	2.56	4.9	n.m.	n.m.	1.61	5.1	-1.58	4.6	4.7	0.6	10.3	0.19	7.8	7.6	9.5
52	China-MG3145	2.53	7.3	n.m.	n.m.	0.74	6.6	-0.26	6.7	6.8	0.32	1.6	-0.06	4.1	4.0	3.2
53	China-MG3188	2.272	5.3	n.m.	n.m.	1.43	5.4	-1.54	4.7	4.9	0.44	5.4	-0.07	4.0	3.3	5.4
54	China-MG3209	2.146	5	n.m.	n.m.	1.46	5.3	-1.28	5.1	5.2	0.35	2.4	-0.22	1.8	2.4	4.1
55	China-MG3676	-0.656	6.6	n.m.	n.m.	1.40	5.4	-0.79	5.9	5.5	0.42	4.6	-0.03	4.7	4.6	6.0
56	China-MG3769	-1.214	6.3	n.m.	n.m.	1.56	5.1	-1.21	5.2	5.1	0.4	4.1	-0.12	3.2	2.4	4.5
57	China-MG3819	-1.514	5	n.m.	n.m.	1.47	5.3	-1.37	5.0	5.0	0.4	4.0	-0.14	3.0	2.6	4.6
58	Colombia-12	13.8	4.8	n.m.	n.m.	1.44	5.4	-1.40	4.9	4.9	0.88	19.1	0.85	17.7	19.0	19.1
59	Colombia-14	6.6	5.5	n.m.	750	1.07	6.0	-1.32	5.1	5.1	0.46	6.0	-0.02	4.8	4.7	5.9
60	Colombia-7	26.2	4.2	n.m.	2900	1.91	4.5	-1.83	4.2	4.7	0.98	22.3	1.50	27.3	23.8	22.9
61	Colombia-9	26.2	3.8	n.m.	2900	2.10	4.2	-2.11	3.8	4.7	0.99	22.5	1.71	30.4	23.9	23.0
62	Ecuador-19	12.7	6.6	n.m.	2900	0.42	7.1	-0.11	7.0	6.5	0.7	13.6	0.41	11.1	14.1	12.1
63	Ecuador-6	26.2	4.9	n.m.	2900	1.20	5.8	-1.41	4.9	5.1	0.95	21.4	1.21	23.1	22.6	21.7
64	Ecuador-7	26.2	4.6	n.m.	2900	1.37	5.5	-1.44	4.9	4.9	0.97	21.8	1.32	24.6	23.1	22.3
65	Egypt-1	25	7.6	n.m.	30	0.13	7.6	0.02	7.2	7.5	0.94	20.9	0.95	19.1	20.1	21.3
66	Egypt-2	25	n.m.	n.m.	30	n.d.	n.d.	n.d.	n.d.	n.d.	n.d.	n.d.	n.d.	n.d.	n.d.	n.d.
67	Finland-2	3.9	3.7	36.4	547	n.d.	n.d.	n.d.	n.d.	n.d.	0.71	13.8	0.39	10.9	11.8	13.4
68	France-15	8.3	4.7	6	664	1.46	5.3	-1.19	5.3	5.0	0.49	7.0	0.03	5.5	4.7	6.5
69	France-TESOI	4	4.92	n.m.	1009	1.36	5.5	-1.16	5.3	5.0	0.45	5.7	-0.05	4.4	3.7	5.2
70	France-TESOI0	8.4	6.46	n.m.	758	0.82	6.4	0.00	7.1	7.0	0.43	5.0	0.09	6.4	6.4	5.4
71	France-TESOI1	12.9	6.83	n.m.	556	0.56	6.9	0.12	7.3	7.3	0.46	6.1	0.15	7.2	7.6	5.9
72	France-TESOI2	11.7	6.59	n.m.	719	0.62	6.8	0.06	7.3	7.2	0.46	5.9	0.16	7.4	7.1	5.6
73	France-TESOI3	12.8	6.32	n.m.	568	0.26	7.4	-0.08	7.0	6.9	0.47	6.4	0.20	8.1	8.8	5.3
74	France-TESOI4	12.8	7.68	n.m.	552	0.62	6.8	0.21	7.5	7.4	0.44	5.5	0.17	7.6	7.0	5.1
75	France-TESOI4B	12.8	7.81	n.m.	552	0.36	7.2	0.30	7.6	7.8	0.52	7.8	0.26	9.0	8.8	7.9
76	France-TESOI5	11.5	6.39	n.m.	770	0.68	6.7	0.00	7.2	7.0	0.45	5.6	0.12	6.9	7.0	5.5
77	France-TESOI6	11.5	6.39	n.m.	770	0.61	6.8	-0.17	6.9	6.6	0.45	5.6	0.10	6.6	6.8	4.6

ID	Soil site	MAT (°C)	Soil pH	Corg (%)	MAP (mm·year ⁻¹)	CBT _{SME}	pH CBT _{SME}	CBT ⁺	pH CBT ⁺	pH _{mr}	MBT ⁺ _{SME}	MAT _{MBT⁺_{SME}} (°C)	Index I	MAT Index I (°C)	MAT _{mr} (°C)	MAT _{ms} (°C)
78	France-TESO18	10.1	5.52	n.m.	959	1.44	5.4	-1.10	5.4	5.1	0.49	6.9	0.03	5.5	5.2	6.9
79	France-TESO19	14.2	7.87	n.m.	633	0.17	7.5	0.48	7.9	7.9	0.66	12.6	0.44	11.6	11.1	13.9
80	France-TESO2	3.9	4.67	n.m.	1053	1.39	5.4	-1.30	5.1	5.0	0.37	3.0	-0.20	2.1	1.1	3.1
81	France-TESO22B	14.3	8.48	n.m.	637	0.46	7.0	0.04	7.2	7.3	0.52	8.0	0.22	8.4	8.9	7.4
82	France-TESO24	14.6	7.77	n.m.	648	0.68	6.7	0.04	7.2	7.1	0.47	6.5	0.17	7.6	7.6	6.8
83	France-TESO25	14.5	7.9	n.m.	646	0.43	7.1	0.33	7.7	7.7	0.67	12.4	0.42	11.4	10.3	12.1
84	France-TESO26	14.9	7.26	n.m.	648	0.29	7.3	0.10	7.3	7.5	0.49	7.0	0.21	8.2	9.0	6.0
85	France-TESO28	13.5	8.43	n.m.	633	0.27	7.4	0.16	7.4	7.4	0.54	8.7	0.29	9.4	9.9	8.6
86	France-TESO3	3.6	4.65	n.m.	1052	1.31	5.6	-1.33	5.0	4.9	0.43	4.9	-0.09	3.8	2.2	4.2
87	France-TESO30	14.3	7.4	n.m.	637	0.71	6.6	-0.20	6.8	6.6	0.55	8.7	0.25	8.7	8.3	8.0
88	France-TESO31	15.3	7.51	n.m.	634	0.12	7.6	0.39	7.8	8.0	0.78	16.1	0.50	12.4	13.0	15.5
89	France-TESO33	15.3	7.78	n.m.	638	1.17	5.8	-1.36	5.0	4.8	0.66	12.0	0.27	9.0	10.5	11.0
90	France-TESO34	15.3	8.11	n.m.	617	0.07	7.7	0.07	7.3	7.1	0.51	7.6	0.21	8.1	10.7	5.9
91	France-TESO36	15.4	7.47	n.m.	577	0.38	7.2	0.10	7.3	7.3	0.49	7.0	0.24	8.7	8.6	7.3
92	France-TESO4	3.6	4.1	n.m.	1052	1.80	4.7	-2.09	3.8	4.8	0.35	2.5	-0.26	1.2	-0.3	2.7
93	France-TESO43	15.2	6.9	n.m.	605	0.53	6.9	-0.10	7.0	6.9	0.43	5.1	0.15	7.2	6.8	5.1
94	France-TESO43B	15.2	7.47	n.m.	605	0.61	6.8	-0.06	7.1	7.0	0.41	4.5	0.12	6.8	6.0	3.9
95	France-TESO47	10.5	6.98	n.m.	549	0.27	7.4	0.11	7.3	7.4	0.65	12.0	0.40	11.0	12.1	11.6
96	France-TESO48	6.4	4.64	n.m.	728	1.31	5.6	-1.18	5.3	5.1	0.41	4.4	-0.11	3.4	2.7	4.3
97	France-TESO49	7.7	4.82	n.m.	790	1.30	5.6	-1.42	4.9	4.8	0.43	5.0	-0.10	3.6	2.2	4.1
98	France-TESO5	3.6	4.18	n.m.	1098	1.05	6.0	-1.00	5.6	5.4	0.49	7.1	0.05	5.9	6.3	7.0
99	France-TESO51	8.5	6.9	n.m.	613	0.60	6.8	0.09	7.3	7.3	0.44	5.3	0.12	6.9	7.0	5.1
100	France-TESO6	4.6	4.87	n.m.	1054	1.42	5.4	-0.99	5.6	5.2	0.38	3.5	-0.12	3.3	1.4	3.3
101	France-TESO7	12.6	7.48	n.m.	553	-0.07	8.0	0.20	7.5	7.6	0.51	7.7	0.29	9.4	11.6	8.6
102	France-TESO8	9.2	5.42	n.m.	574	1.34	5.5	-0.66	6.1	5.5	0.52	7.7	0.13	7.0	6.0	7.2
103	Gabon-1	23.7	3.3	3.27	1781	n.d.	n.d.	n.d.	n.d.	n.d.	0.9	19.7	0.93	18.9	20.1	19.9
104	Gabon-2	24.1	5.3	0.22	2007	2.16	4.1	-1.90	4.1	4.8	0.99	22.7	1.87	32.9	24.0	23.3

ID	Soil site	MAT (°C)	Soil pH	Corg (%)	MAP (mm·year ⁻¹)	CBT _{SME}	pH CBT _{SME}	CBT ⁺	pH CBT ⁺	pH _{mr}	MBT ⁺ _{SME}	MAT MBT ⁺ _{SME} (°C)	Index I	MAT Index I (°C)	MAT _{mr} (°C)	MAT _{ms} (°C)
105	Gabon-3	24.1	4.7	5.25	2007	n.d.	n.d.	n.d.	n.d.	n.d.	n.d.	n.d.	n.d.	n.d.	n.d.	n.d.
106	Gabon-4	25.8	5.3	2.73	2158	1.50	5.2	-1.68	4.5	4.9	0.98	22.2	1.55	28.0	23.5	22.7
107	Gabon-5	26.3	5.1	2.22	2158	2.51	3.5	-2.20	3.6	4.7	0.98	22.4	1.69	30.2	23.5	22.9
108	Gabon-6	26	5.9	2.45	1969	0.58	6.8	-0.80	5.9	6.0	0.96	21.5	1.11	21.5	23.8	22.1
109	Galapagos	24	4.4	n.m.	451	2.00	4.4	-1.61	4.6	4.6	0.93	20.8	1.06	20.9	21.5	21.0
110	Germany-G1	5.4	7.4	n.m.	805	0.94	6.2	-0.62	6.2	5.9	0.57	9.5	0.20	8.0	9.5	10.6
101	France-TES07	12.6	7.48	n.m.	553	-0.07	8.0	0.20	7.5	7.6	0.51	7.7	0.29	9.4	11.6	8.6
102	France-TES08	9.2	5.42	n.m.	574	1.34	5.5	-0.66	6.1	5.5	0.52	7.7	0.13	7.0	6.0	7.2
103	Gabon-1	23.7	3.3	3.27	1781	n.d.	n.d.	n.d.	n.d.	n.d.	0.9	19.7	0.93	18.9	20.1	19.9
104	Gabon-2	24.1	5.3	0.22	2007	2.16	4.1	-1.90	4.1	4.8	0.99	22.7	1.87	32.9	24.0	23.3
105	Gabon-3	24.1	4.7	5.25	2007	n.d.	n.d.	n.d.	n.d.	n.d.	n.d.	n.d.	n.d.	n.d.	n.d.	n.d.
106	Gabon-4	25.8	5.3	2.73	2158	1.50	5.2	-1.68	4.5	4.9	0.98	22.2	1.55	28.0	23.5	22.7
107	Gabon-5	26.3	5.1	2.22	2158	2.51	3.5	-2.20	3.6	4.7	0.98	22.4	1.69	30.2	23.5	22.9
108	Gabon-6	26	5.9	2.45	1969	0.58	6.8	-0.80	5.9	6.0	0.96	21.5	1.11	21.5	23.8	22.1
109	Galapagos	24	4.4	n.m.	451	2.00	4.4	-1.61	4.6	4.6	0.93	20.8	1.06	20.9	21.5	21.0
110	Germany-G1	5.4	7.4	n.m.	805	0.94	6.2	-0.62	6.2	5.9	0.57	9.5	0.20	8.0	9.5	10.6
111	Germany-G2	5.8	7.3	n.m.	805	0.10	7.7	-0.05	7.1	7.0	0.31	1.5	0.01	5.1	7.6	4.8
112	Germany-H1	8.7	6.1	n.m.	768	0.47	7.0	-0.59	6.2	5.9	0.47	6.2	0.03	5.5	7.4	3.6
113	Ghana-2	27	6	0.33	810	n.d.	n.d.	n.d.	n.d.	n.d.	0.57	n.d.	n.d.	n.d.	n.d.	9.3
114	Greece-13	12.1	5.4	n.m.	458	1.55	5.2	-1.65	4.5	4.8	n.d.	9.4	0.17	7.6	7.0	n.d.
115	Greece-5	15.7	7.4	3.74	446	0.17	7.5	0.46	7.9	7.9	0.6	10.2	0.34	10.1	10.8	11.5
116	Greenland-5	-0.4	5.5	n.m.	984	1.24	5.7	-0.59	6.2	5.8	0.46	5.9	0.09	6.4	5.6	6.8
117	Iceland-6	3.5	6.1	6.59	706	0.74	6.6	-0.55	6.3	5.9	0.46	6.0	0.06	5.9	6.0	4.6
118	Iceland-sa	3.5	5.3	n.m.	706	1.20	5.8	-1.33	5.0	5.1	0.38	3.5	-0.17	2.5	1.4	3.0
119	Ireland-9	8.8	3.8	24	928	1.32	5.5	-1.64	4.5	4.6	0.58	9.7	0.14	7.1	7.4	8.6
120	Italy-1	14	6.2	2.9	811	0.93	6.2	-0.37	6.6	6.2	0.69	13.1	0.46	11.9	11.6	12.8
121	Italy-11	15.4	5.4	1.94	1007	1.48	5.3	-0.69	6.1	5.5	0.62	10.9	0.30	9.5	8.8	10.6

ID	Soil site	MAT (°C)	Soil pH	Corg (%)	MAP (mm·year ⁻¹)	CBT _{SME}	pH CBT _{SME}	CBT ⁺	pH CBT ⁺	pH _{mr}	MBT ⁺ _{SME}	MAT _{MBT⁺_{SME}} (°C)	Index 1	MAT Index 1 (°C)	MAT _{mr} (°C)	MAT _{ms} (°C)
122	Italy-14	14.2	5.6	3.69	1007	1.17	5.8	-0.44	6.5	6.0	0.64	11.5	0.37	10.6	9.7	11.2
123	Italy-17	15.4	7.6	1.63	1007	0.21	7.5	0.14	7.4	7.3	0.66	12.3	0.38	10.7	12.8	12.9
124	Netherlands-B	9.5	7.7	n.m.	761	-0.01	7.9	0.54	8.0	8.0	0.57	10.0	0.31	9.7	10.5	9.9
125	Netherlands-T5	9.4	4	n.m.	752	n.d.	n.d.	n.d.	n.d.	n.d.	0.63	11.3	0.24	8.6	9.3	10.7
126	Netherlands-T7	9.4	3.7	n.m.	752	1.29	5.6	-1.60	4.6	4.7	0.57	9.5	0.14	7.1	7.2	8.7
127	Nigeria-15	26.7	4.4	3.08	2811	2.30	3.9	-1.99	4.0	4.7	0.99	22.6	1.75	31.1	24.0	23.2
128	Nigeria-19	26.8	7.3	2.2	1507	-0.03	7.9	-0.24	6.8	7.5	0.92	20.5	0.89	18.3	24.4	20.8
129	Norway-1	5	7.6	1.85	1048	0.23	7.4	0.19	7.5	7.4	0.45	5.7	0.22	8.3	8.4	6.1
130	Norway-3	5.3	4.3	5.98	892	1.37	5.5	-2.17	3.7	4.7	0.57	9.4	0.12	6.9	7.0	8.5
131	Peru-1	26.2	4.5	n.m.	2900	1.97	4.4	-1.35	5.0	4.5	1	22.8	1.34	25.0	24.9	23.4
132	Peru-10	25.5	4.4	n.m.	1350	1.86	4.6	-1.86	4.2	4.7	0.96	21.6	1.33	24.9	22.6	22.2
133	Peru-13	26.2	n.m.	n.m.	2900	1.50	5.2	-1.24	5.2	4.5	1	22.8	1.26	23.7	25.3	23.4
134	Peru-14	26.2	n.m.	n.m.	2900	1.53	5.2	-1.72	4.4	4.7	0.99	22.4	1.53	27.7	24.2	23.1
135	Peru-4	26.2	4	n.m.	2900	1.57	5.1	-1.70	4.4	4.7	0.95	21.3	1.17	22.4	22.7	21.8
136	Rarotonga	23.8	5.4	n.m.	2112	1.62	5.0	-1.68	4.5	4.8	0.97	21.9	1.39	25.7	23.2	22.5
137	Scotland-D	8.2	5.4	n.m.	991	1.21	5.7	-1.35	5.0	4.9	0.51	7.4	0.03	5.5	4.8	6.2
138	Seychelles	26.6	5.2	n.m.	235	2.19	4.0	-1.80	4.3	4.6	0.99	22.5	1.59	28.6	24.0	23.1
139	South Africa-12	18.4	5.5	2.91	759	1.73	4.8	-1.33	5.0	4.8	0.87	18.9	0.81	17.1	18.6	18.8
140	South Africa-16	19.9	6	2.75	759	1.25	5.7	-1.00	5.6	5.2	0.91	20.1	0.97	19.5	20.2	20.3
141	South Africa-3	18.4	4.4	3.29	759	1.55	5.2	-1.38	5.0	4.7	0.91	19.9	0.89	18.3	20.6	20.0
142	South Africa-7	18	5.5	1.76	1015	n.d.	n.d.	n.d.	n.d.	n.d.	n.d.	n.d.	n.d.	n.d.	n.d.	n.d.
143	Spain-6	16.4	6.6	0.8	486	1.09	6.0	-0.40	6.5	6.2	0.58	9.6	0.29	9.3	8.4	9.4
144	Spain-7	16.4	5.5	3.88	486	n.d.	n.d.	n.d.	n.d.	n.d.	0.47	6.7	0.13	6.9	4.0	6.2
145	Svalbard-LB1	-6	4.35	n.m.	190	0.93	6.2	-0.17	6.9	6.7	0.32	1.7	0.04	5.6	3.6	2.7
146	Svalbard-MP1	-6	7.11	n.m.	190	1.15	5.8	-0.17	6.9	6.6	0.45	5.8	0.17	7.6	5.8	6.3
147	Svalbard-MP2	-6	8.29	n.m.	190	0.46	7.0	0.29	7.6	7.8	0.36	2.9	0.12	6.9	6.9	4.8
148	Svalbard-MP3	-6	5.5	n.m.	190	1.23	5.7	-0.42	6.5	6.1	0.41	4.2	0.06	6.0	3.8	4.4

ID	Soil site	MAT (°C)	Soil pH	Corg (%)	MAP (mm·year ⁻¹)	CBT _{SME}	pH CBT _{SME}	CBT ⁺	pH CBT ⁺	pH _{mr}	MBT ⁺ _{SME}	MAT MBT ⁺ _{SME} (°C)	Index 1	MAT Index 1 (°C)	MAT _{mr} (°C)	MAT _{ms} (°C)
149	Svalbard-MP4	-6	8.34	n.m.	190	0.44	7.1	0.42	7.8	7.9	0.4	4.4	0.20	8.0	7.2	4.9
150	Svalbard-MP5	-6	8.25	n.m.	190	0.35	7.2	0.38	7.7	8.0	0.38	4.1	0.17	7.5	7.3	5.1
151	Svalbard-MP6	-6	9.34	n.m.	190	0.43	7.1	0.11	7.3	7.9	0.25	-0.6	-0.03	4.5	6.1	3.5
152	Svalbard-NA1	-6	7.42	n.m.	190	0.54	6.9	0.17	7.4	7.6	0.25	-0.5	0.03	5.5	5.6	3.6
153	Svalbard-NA2	-6	6.32	n.m.	190	1.46	5.3	-0.30	6.7	6.3	0.4	3.9	0.11	6.6	4.1	4.9
154	Sweden-15	0.7	4.5	2.13	569	1.64	5.0	-1.50	4.8	4.7	0.57	9.4	0.14	7.1	6.8	8.7
155	Sweden-17	1.9	4.5	0.61	569	n.d.	n.d.	n.d.	n.d.	n.d.	0.69	13.0	0.36	10.3	10.9	12.4
156	Sweden-4	7.7	7.7	0.92	578	0.24	7.4	0.23	7.5	7.6	0.52	7.8	0.31	9.7	9.6	9.0
157	Sweden-B	5.3	4	n.m.	641	0.36	7.2	-0.30	6.7	6.3	0.52	7.9	0.18	7.7	9.8	6.1
158	the Netherlands-A	9	6.7	n.m.	720	0.31	7.3	0.10	7.3	7.5	0.57	9.6	0.35	10.2	9.9	8.7
159	the Netherlands-F	9	6.7	n.m.	720	0.52	6.9	-0.17	6.9	6.9	0.51	7.5	0.23	8.4	7.9	6.1
160	the Netherlands-J	9	6.4	n.m.	720	0.34	7.2	0.09	7.3	7.5	0.57	9.5	0.34	10.1	9.7	8.4
161	the Netherlands-M	9	6.9	n.m.	720	0.20	7.5	0.29	7.6	7.8	0.55	8.9	0.31	9.7	9.8	8.9
162	Turkey-12	10.4	8	1.05	547	0.30	7.3	0.37	7.7	7.9	0.71	14.2	0.40	11.0	12.0	16.5
163	Turkey-8	10.5	8	1.06	340	1.13	5.9	0.52	8.0	8.1	0.84	19.3	0.25	8.7	10.7	19.8
164	Uganda-1	12	3.6	n.m.	1483	1.80	4.7	-2.07	3.9	4.6	0.71	13.8	0.39	10.9	12.2	13.4
165	Uganda-2	2	5.1	n.m.	1483	1.99	4.4	-1.29	5.1	5.5	0.17	-3.1	-0.58	-3.6	-0.8	1.2
166	Uganda-3	24	7.1	n.m.	1483	0.10	7.7	-0.10	7.0	7.2	0.89	19.5	0.80	16.9	20.9	19.2
167	Uruguay-7	17.3	5.6	0.39	1133	1.51	5.2	-1.12	5.4	5.0	0.89	19.4	0.85	17.7	19.4	19.6
168	Uruguay-8	17.3	5.3	3.72	1133	1.62	5.0	-1.26	5.1	4.9	0.88	19.1	0.86	17.8	18.7	19.1
169	USA-10	24.2	5.1	3.98	1093	1.28	5.6	-1.45	4.8	4.9	0.94	21.0	1.09	21.2	22.3	21.4
170	USA-13	10	5.9	2.11	493	0.94	6.2	-0.70	6.0	5.8	0.77	15.5	0.58	13.7	14.1	14.9
171	USA-17	-2.9	7.1	3.98	277	0.69	6.6	-0.20	6.8	6.8	0.38	3.5	0.04	5.7	5.4	3.9
172	USA-BB1	6.1	4.25	12.84	1200	1.52	5.2	-1.79	4.3	4.7	0.65	12.0	0.28	9.2	10.1	11.5
173	USA-BB2	6.1	4.6	5.22	1200	1.18	5.8	-1.46	4.8	5.0	0.61	10.7	0.21	8.2	9.0	9.9
174	USA-BF1	7.8	4.05	6.44	1000	1.45	5.3	-1.65	4.5	4.8	0.65	11.9	0.27	9.1	9.9	11.2
175	USA-BP1	6.6	7.53	3.1	450	0.45	7.1	0.13	7.4	7.3	0.49	7.1	0.26	8.9	8.3	6.8

ID	Soil site	MAT (°C)	Soil pH	Corg (%)	MAP (mm.year ⁻¹)	CBT _{SME}	pH CBT _{SME}	CBT ⁺	pH CBT ⁺	pH _{mr}	MBT ⁺ _{SME}	MAT _{MBT⁺_{SME}} (°C)	Index 1	MAT Index 1 (°C)	MAT _{mr} (°C)	MAT _{ms} (°C)
176	USA-BZ2	-2.9	5.16	3.03	260	1.70	4.9	-0.85	5.8	5.3	0.37	3.2	-0.09	3.6	1.7	3.8
177	USA-BZ3	-2.9	5.36	3.73	260	1.78	4.8	-1.70	4.5	4.8	0.41	4.3	-0.14	2.9	1.7	4.4
178	USA-CA1	10.3	7.27	1.67	400	0.76	6.5	0.12	7.3	7.3	0.38	3.5	0.17	7.6	5.9	3.5
179	USA-CA2	10.3	8.02	2.15	400	0.77	6.5	0.22	7.5	7.6	0.38	3.4	0.20	8.0	6.4	4.3
180	USA-CC1	5.8	6.06	1.91	720	0.95	6.2	-0.83	5.8	5.6	0.74	14.6	0.50	12.5	13.5	14.0
181	USA-CF1	5.3	3.92	2.56	1300	1.20	5.8	-1.45	4.8	4.9	0.63	11.2	0.23	8.5	9.7	10.4
182	USA-CF2	5.3	3.63	4.06	1300	1.55	5.2	-1.63	4.6	4.7	0.71	13.7	0.38	10.7	12.2	13.2
183	USA-CF3	5.3	3.56	4.33	1300	1.57	5.1	-1.70	4.5	4.7	0.79	16.4	0.57	13.5	15.8	16.2
184	USA-CL1	15.9	5.68	2.33	1250	1.06	6.0	-0.90	5.7	5.4	0.81	17.0	0.64	14.6	16.3	16.7
185	USA-CL2	15.9	5.57	2.27	1250	1.10	5.9	-1.04	5.5	5.3	0.82	17.2	0.68	15.2	16.6	17.0
186	USA-CL3	15.9	4.89	1.21	1250	1.51	5.2	-1.40	4.9	5.0	0.82	17.1	0.64	14.6	16.4	17.0
187	USA-CM1	18.5	7.85	2.99	850	-0.07	8.0	0.06	7.2	7.6	0.69	13.4	0.46	11.9	15.8	11.1
188	USA-CO1	-3	6.13	1.59	600	1.28	5.6	-0.42	6.5	6.0	0.35	2.4	-0.04	4.4	2.8	2.8
189	USA-CO2	6.1	5.68	1.81	350	1.43	5.4	-0.59	6.2	5.8	0.42	4.7	0.03	5.5	3.6	4.8
190	USA-CO3	9.3	6.02	0.82	322	1.14	5.9	-0.49	6.4	5.9	0.53	8.1	0.20	8.1	6.2	7.3
191	USA-DF1	14.6	5.37	2.78	1100	1.54	5.2	-1.42	4.9	4.8	0.76	15.3	0.49	12.3	14.3	15.0
192	USA-DF3	14.6	5.05	1.7	1100	1.69	4.9	-1.60	4.6	4.7	0.77	15.8	0.52	12.8	14.7	15.3
193	USA-GB2	2	7.57	6.89	400	0.12	7.6	0.63	8.2	8.3	0.43	5.4	0.20	8.1	8.9	9.6
194	USA-GB3	2	7.18	5.71	400	0.62	6.8	0.31	7.6	8.0	0.54	8.9	0.35	10.3	8.6	9.8
195	USA-GB4	2	6.85	3.62	400	0.85	6.4	-0.06	7.1	6.9	0.37	3.0	0.11	6.7	5.6	4.4
196	USA-GB5	4.8	8.22	1.68	400	0.58	6.8	0.65	8.2	8.3	0.43	5.9	0.16	7.4	7.7	7.7
197	USA-GB6	2	7.23	2.24	400	0.52	6.9	0.36	7.7	7.8	0.46	6.2	0.26	8.9	7.9	7.3
198	USA-HF2	7	3.98	9.55	1100	1.82	4.7	-1.91	4.1	4.6	0.69	13.0	0.34	10.1	10.9	12.4
199	USA-HI3	22.8	6.53	18.24	1000	0.34	7.3	-0.39	6.5	6.7	0.72	14.2	0.53	12.9	14.7	12.5
200	USA-HJ1	9.4	5.41	6.95	2000	1.46	5.3	-0.69	6.1	6.0	0.52	8.0	0.15	7.3	6.8	8.2
201	USA-IE2	8.6	5.52	4.07	1200	1.02	6.1	-0.97	5.6	5.3	0.63	11.4	0.28	9.3	10.1	10.4
202	USA-IE3	8.6	5.72	6.41	1200	0.71	6.6	-0.49	6.4	6.0	0.59	10.1	0.27	9.0	9.4	8.4

ID	Soil site	MAT (°C)	Soil pH	Corg (%)	MAP (mm·year ⁻¹)	CBT _{SME}	pH CBT _{SME}	CBT ⁺	pH CBT ⁺	pH _{mr}	MBT ⁺ _{SME}	MAT MBT ⁺ _{SME} (°C)	Index 1	MAT Index 1 (°C)	MAT _{mr} (°C)	MAT _{ms} (°C)
203	USA-IE4	8.6	6.29	3.27	1200	0.19	7.5	-0.17	6.9	7.1	0.66	12.1	0.46	11.9	13.6	10.8
204	USA-IE5	8.6	5.57	5.29	1200	0.91	6.3	-0.97	5.6	5.3	0.64	11.5	0.28	9.3	10.6	10.4
205	USA-IT1	3	5.78	6.31	750	0.96	6.2	-0.79	5.9	5.5	0.53	8.2	0.14	7.2	6.4	6.9
206	USA-IT2	3	5.42	3.91	750	1.19	5.8	-1.17	5.3	5.1	0.51	7.6	0.07	6.1	5.1	6.6
207	USA-KP1	12.5	6.37	6.12	835	0.52	6.9	-0.49	6.4	6.2	0.71	13.7	0.47	12.0	14.0	12.6
208	USA-KP2	12.5	6.5	4.62	835	0.71	6.6	-0.59	6.2	6.0	0.77	15.6	0.57	13.5	15.3	14.9
209	USA-LQ2	21.5	5.03	4.11	3500	1.94	4.5	-1.38	5.0	4.6	0.95	21.3	1.08	21.1	22.6	21.7
210	USA-MD3	21	7.9	0.12	150	n.d.	n.d.	n.d.	n.d.	n.d.	n.d.	n.d.	n.d.	n.d.	n.d.	n.d.
211	USA-MD4	21	8.86	0.12	150	n.d.	n.d.	n.d.	n.d.	n.d.	n.d.	n.d.	n.d.	n.d.	n.d.	n.d.
212	USA-MP1	8.8	4.56	10.7	2200	1.50	5.2	-1.48	4.8	5.0	0.36	2.7	-0.21	1.9	1.4	3.7
213	USA-MP2	8.8	4.38	9.87	2200	1.69	4.9	-1.66	4.5	5.0	0.36	2.8	-0.23	1.7	1.4	3.9
214	USA-R-1	8	6.6	n.m.	918	0.14	7.6	0.03	7.2	7.5	0.63	11.3	0.35	10.3	13.5	10.9
215	USA-R-2	8.6	6.5	n.m.	876	0.25	7.4	-0.46	6.4	6.6	0.52	7.7	0.19	7.8	9.5	5.0
216	USA-R-3	7.1	7.7	n.m.	815	0.12	7.6	-0.05	7.1	7.1	0.6	10.4	0.36	10.4	12.5	8.9
217	USA-R-4	7.2	7.7	n.m.	719	0.23	7.4	-0.08	7.0	7.1	0.47	6.5	0.19	7.9	8.9	5.3
218	USA-R-5	3.8	8.1	n.m.	307	0.37	7.2	0.37	7.7	7.8	0.56	9.6	0.29	9.4	10.3	13.4
219	USA-R-6	8.5	7.4	n.m.	419	0.76	6.5	-0.08	7.0	7.0	0.45	5.6	0.17	7.6	7.6	7.4
220	USA-RT1	18.1	7.92	3.94	840	-0.05	7.9	0.23	7.5	7.6	0.8	16.8	0.55	13.2	16.8	13.7
221	USA-RT2	18.1	8.07	3.75	840	-0.01	7.9	0.22	7.5	7.6	0.8	16.7	0.55	13.2	16.3	13.3
222	USA-SA1	10.3	6.9	2.29	400	1.13	5.9	-0.28	6.7	6.5	0.37	3.1	0.06	6.0	4.8	4.9
223	USA-SB1	15	7.92	2.65	550	0.92	6.2	0.84	8.5	8.6	0.94	20.9	0.49	12.4	9.6	22.2
224	USA-SN1	3.6	4.95	4.25	600	1.14	5.9	-0.70	6.0	5.9	0.27	-0.2	-0.24	1.5	0.4	0.6
225	USA-SN3	3.6	5.74	1.66	600	1.37	5.5	-0.65	6.1	5.7	0.29	0.6	-0.17	2.5	0.6	1.6
226	USA-SP1	12.7	6.25	1.68	650	1.06	6.0	-0.36	6.6	6.3	0.5	7.0	0.20	8.0	6.5	7.2
227	USA-SP2	3.6	5.13	8.1	750	1.49	5.3	-1.15	5.3	5.1	0.4	3.9	-0.12	3.2	1.9	3.9
228	USA-SR1	17.2	6.84	4.59	500	1.11	5.9	-0.14	6.9	6.7	0.37	3.2	0.10	6.6	4.3	3.8
229	USA-SR2	17.2	8	1.46	500	0.47	7.0	0.45	7.9	8.1	0.41	4.6	0.22	8.3	8.3	8.9

ID	Soil site	MAT (°C)	Soil pH	Corg (%)	MAP (mm·year ⁻¹)	CBT _{5ME}	pH CBT _{5ME}	CBT ⁺	pH CBT ⁺	pH _{mr}	MBT ⁺ _{5ME}	MAT MBT ⁺ _{5ME} (°C)	Index 1	MAT Index 1 (°C)	MAT _{mr} (°C)	MAT _{ms} (°C)
230	USA-SR3	17.2	6.95	3.3	500	1.16	5.8	-0.05	7.1	7.0	0.3	0.7	0.06	5.9	3.7	2.3
231	USA-SV1	13.5	8.31	0.3	210	0.96	6.2	0.84	8.5	8.7	0.86	18.5	0.48	12.1	9.3	20.8
232	USA-SV2	13.5	8.44	0.23	210	0.99	6.1	0.61	8.1	8.3	0.81	16.9	0.51	12.6	9.9	17.8
233	USA-SV3	13.5	8.31	0.3	210	n.d.	n.d.	n.d.	n.d.	n.d.	0.42	4.7	0.20	8.0	7.4	6.3
234	USA-SV4	13.5	8.29	0.27	210	1.14	5.9	0.36	7.7	7.9	0.78	16.1	0.50	12.5	10.2	16.5
235	USA-VC1	2.5	5.55	5.67	500	1.35	5.5	-0.58	6.2	5.8	0.47	6.2	0.09	6.4	4.1	5.5
236	USA-VC2	2.5	5.99	3.44	500	0.92	6.3	-0.51	6.3	5.9	0.48	6.5	0.12	6.9	5.5	5.5
237	USA-W	9.9	4.5	n.m.	1239	1.72	4.9	-1.68	4.5	4.7	0.77	15.6	0.52	12.8	14.5	15.4
238	Zaire-1	24.6	3.9	n.m.	1871	1.79	4.7	-1.78	4.3	4.7	0.92	20.5	1.05	20.6	21.1	20.8
239	Zaire-2	24.6	4.1	1.26	1871	1.70	4.9	-1.87	4.2	4.7	0.98	22.2	1.49	27.2	23.6	22.7

(Next page)

Supp. Table 3. Overview of the fractional abundances of individual soils. Abundances below the limit of quantification are quantified as 0.

Supp. Table 2. Relative retention times (RRT) and their standard deviations, based on the elution time of peak tops, scaled between crenarchaeol, with a relative retention time of 0 and brGDGT Ia, with a relative retention time of 1. ▼

brGDGT	RRT	σ_{RRT}
IIIa	0.654	0.002
IIIa'	0.722	0.004
IIIb	0.734	0.010
IIIb'	0.809	0.008
IIIc	0.821	0.005
IIIc'	0.905	0.010
Ila	0.819	0.003
Ila'	0.853	0.003
Ilb	0.914	0.007
Ilb'	0.951	0.004
Ilc	1.012	0.003
Ilc'	1.054	0.003
Ia	1.000	0.000
Ib	1.105	0.004
Ic	1.221	0.004

ID	Relative abundances of brGDGTs (%)													
	Ia	Ib	Ic	IIa	IIa'	IIb	IIb'	IIc	IIc'	IIIa	IIIa'	IIIb	IIIb'	IIIc
1	45	13	1	16	15	1	3	0	0	3	2	0	0	0
2	52	2	0	26	13	1	1	0	0	3	3	0	0	0
3	92	1	0	5	2	0	0	0	0	0	0	0	0	0
4	59	22	7	3	4	2	2	0	0	0	1	0	0	0
5	93	2	2	4	0	0	0	0	0	0	0	0	0	0
6	91	0	0	6	2	0	0	0	0	0	0	0	0	0
7	82	8	3	2	3	0	1	0	0	0	0	0	0	0
8	94	2	1	3	1	0	0	0	0	0	0	0	0	0
9	91	1	1	6	1	0	0	0	0	0	0	0	0	0
10	54	24	6	5	6	2	3	0	0	1	1	0	0	0
11	57	2	3	36	0	1	0	0	0	2	0	0	0	0
12	14	9	1	13	21	9	11	0	1	6	14	1	1	0
13	49	3	1	36	1	1	0	0	0	8	1	0	0	0
14	93	2	1	4	1	0	0	0	0	0	0	0	0	0
15	89	2	1	7	1	0	0	0	0	0	0	0	0	0
16	86	2	1	6	4	1	0	0	0	1	1	0	0	0
17	73	7	1	8	8	1	1	0	0	1	1	0	0	0
18	83	2	0	11	2	0	0	0	0	1	0	0	0	0
19	66	18	3	5	4	1	1	0	0	1	1	0	0	0
20	89	2	1	5	1	0	0	0	0	1	1	0	0	0
21	86	1	0	8	5	0	0	0	0	1	1	0	0	0
22	20	31	6	6	10	3	16	0	1	2	3	1	1	0
23	54	18	4	7	11	2	2	0	0	1	1	0	0	0
24	37	8	0	15	24	1	5	0	0	4	7	0	0	0
25	51	13	2	10	14	2	5	0	0	1	2	0	0	0
26	83	0	0	14	1	0	0	0	0	1	0	0	0	0
27	20	17	3	10	17	8	11	1	1	4	7	1	2	0
28	33	14	2	10	17	5	8	0	1	3	5	0	1	0
29	20	11	2	11	23	6	9	1	1	4	10	0	1	0
30	20	12	2	12	21	6	11	1	1	5	8	1	1	0
31	43	10	2	23	11	2	2	0	0	3	2	0	0	0
32	11	12	2	7	23	10	13	1	1	4	13	1	2	0
33	31	8	2	22	16	4	5	1	0	4	6	0	1	0
34	11	11	3	9	17	11	13	1	2	6	12	1	3	0
35	22	11	3	14	20	6	8	1	1	5	9	1	1	0
36	30	6	2	25	17	3	4	1	0	6	7	0	0	0
37	37	4	1	28	13	1	2	0	0	8	6	0	0	0
38	29	7	2	20	18	3	5	1	0	5	9	0	1	0
39	22	5	1	22	15	4	5	1	0	10	12	1	1	0
40	20	6	1	16	22	4	7	1	1	6	15	0	1	0

ID	Relative abundances of brGDGTs (%)													
	Ia	Ib	Ic	IIa	IIa'	IIb	IIb'	IIc	IIc'	IIIa	IIIa'	IIIb	IIIb'	IIIc
41	16	8	1	11	16	8	11	1	1	7	14	1	3	1
42	23	9	3	19	15	6	5	1	1	8	8	1	1	0
43	64	3	1	27	1	1	0	1	0	3	0	0	0	0
44	40	3	1	38	5	1	0	1	0	10	1	0	0	0
45	53	3	1	31	3	1	0	1	0	6	1	0	0	0
46	42	3	1	42	8	1	0	0	0	0	3	0	0	0
47	24	7	4	23	15	6	3	2	0	10	6	0	1	0
48	46	2	1	42	0	1	0	1	0	8	0	0	0	0
49	28	2	0	36	8	2	2	0	0	15	5	0	1	0
50	37	2	0	40	5	1	1	1	0	12	1	0	0	0
51	57	2	0	34	1	1	0	0	0	4	1	0	0	0
52	19	3	1	25	12	5	5	1	0	15	13	1	1	0
53	41	2	0	40	2	1	0	0	0	13	0	0	0	0
54	31	2	0	37	4	1	0	0	0	24	1	0	0	0
55	35	1	0	31	10	1	0	0	0	18	3	0	0	0
56	36	1	0	40	4	1	0	0	0	16	1	0	0	0
57	37	2	0	40	3	1	0	0	0	17	1	0	0	0
58	81	3	1	11	3	0	0	0	0	0	0	0	0	0
59	40	3	1	37	2	3	0	0	0	11	1	0	0	0
60	96	1	1	2	0	0	0	0	0	0	0	0	0	0
61	97	1	1	1	0	0	0	0	0	0	0	0	0	0
62	30	13	6	13	18	3	8	2	0	3	4	0	0	0
63	86	6	1	4	2	0	0	0	0	0	0	0	0	0
64	90	4	1	3	2	0	0	0	0	0	0	0	0	0
65	34	25	4	2	21	2	8	0	1	0	3	0	1	0
66	18	0	0	0	39	0	0	0	0	0	43	0	0	0
67	71	0	0	26	0	0	0	0	0	2	0	0	0	0
68	44	2	1	38	4	1	0	0	0	9	1	0	0	0
69	39	2	1	39	4	1	0	0	0	12	1	0	0	0
70	19	4	1	18	19	2	2	0	0	10	24	0	0	0
71	16	5	1	15	21	3	4	1	0	8	24	0	1	0
72	18	5	1	17	23	3	3	0	0	8	21	0	1	0
73	18	11	2	18	18	9	7	1	0	7	7	0	1	0
74	14	4	1	14	26	2	5	0	0	7	24	0	1	0
75	14	7	1	10	26	4	10	0	1	6	20	0	2	0
76	19	5	1	18	20	3	5	0	0	9	19	0	1	0
77	21	7	2	23	18	4	3	1	0	10	12	0	1	0
78	43	2	0	35	5	1	0	0	0	11	1	0	0	0
79	14	8	2	4	33	4	11	0	0	3	18	1	2	0
80	33	2	1	43	3	1	0	0	0	16	1	0	0	0

ID	Relative abundances of brGDGTs (%)													
	Ia	Ib	Ic	IIa	IIa'	IIb	IIb'	IIc	IIc'	IIIa	IIIa'	IIIb	IIIb'	IIIc
81	20	8	1	15	21	4	6	1	0	7	16	0	1	0
82	19	5	1	16	22	3	6	0	0	9	19	0	1	0
83	18	7	1	7	31	2	11	0	1	3	16	0	2	0
84	16	10	2	14	20	6	9	1	1	8	13	0	2	0
85	17	9	1	11	23	6	8	0	0	6	15	0	2	0
86	38	3	1	43	3	1	0	1	0	10	1	0	0	0
87	29	7	1	20	20	3	6	0	0	7	9	0	0	0
88	17	14	1	4	26	1	15	0	1	4	15	0	2	0
89	58	5	2	29	0	1	1	0	0	3	1	0	0	0
90	14	14	4	13	13	10	10	1	2	7	10	1	2	0
91	18	7	1	13	24	6	8	0	1	7	15	0	0	0
92	34	1	0	47	0	1	0	0	0	16	1	0	0	0
93	20	6	1	20	20	5	6	0	0	9	10	1	1	0
94	18	6	1	21	21	4	7	0	0	9	12	0	1	0
95	22	12	2	10	21	5	9	0	1	4	11	0	2	0
96	36	3	1	40	4	1	0	0	0	14	1	0	0	0
97	38	3	1	44	2	2	0	1	0	9	1	0	0	0
98	40	5	1	32	5	2	0	1	0	11	2	1	0	1
99	16	5	1	16	20	3	4	1	0	9	23	0	1	0
100	33	2	1	42	7	1	0	0	0	13	1	0	0	0
101	14	13	3	9	16	13	10	1	1	5	11	1	2	0
102	40	2	1	31	12	1	1	0	0	8	3	0	0	0
103	87	1	1	9	1	0	0	0	0	1	0	0	0	0
104	97	1	1	1	0	0	0	0	0	0	0	0	0	0
105	98	0	1	1	0	0	0	0	0	0	0	0	0	0
106	93	3	1	2	1	0	0	0	0	0	0	0	0	0
107	97	0	0	2	0	0	0	0	0	0	0	0	0	0
108	68	17	4	3	5	1	1	0	0	0	0	0	0	0
109	90	1	1	6	1	0	0	0	0	0	0	0	0	0
110	44	3	1	22	6	4	3	1	0	8	6	0	1	0
111	12	7	1	13	11	14	5	1	1	15	16	2	2	0
112	25	12	4	30	7	6	2	1	0	9	3	0	0	0
113	95	3	1	1	1	0	0	0	0	0	0	0	0	0
114	53	0	0	32	6	0	0	0	0	7	2	0	0	0
115	12	7	3	5	34	5	7	0	0	6	22	0	0	0
116	35	2	1	28	16	2	0	1	0	13	3	0	0	0
117	28	8	2	31	12	3	2	1	0	10	3	0	0	0
118	33	4	1	44	2	1	0	1	0	14	1	0	0	0
119	53	3	2	36	0	1	0	1	0	4	0	0	0	0
120	44	6	1	17	21	2	2	0	0	4	4	0	0	0

ID	Relative abundances of brGDGTs (%)													
	Ia	Ib	Ic	IIa	IIa'	IIb	IIb'	IIc	IIc'	IIIa	IIIa'	IIIb	IIIb'	IIIc
121	50	2	0	26	13	1	1	0	0	6	3	0	0	0
122	44	4	0	21	20	1	1	0	0	5	4	0	0	0
123	21	12	3	7	18	5	11	1	1	5	12	1	2	0
124	9	10	1	5	20	4	22	1	1	5	17	1	3	0
125	60	2	2	32	0	2	0	1	0	3	0	0	0	0
126	53	3	1	35	1	2	0	1	0	4	1	0	0	0
127	98	1	1	1	0	0	0	0	0	0	0	0	0	0
128	35	37	7	3	8	3	6	0	1	0	1	0	0	0
129	14	8	1	12	21	8	11	1	1	7	15	1	2	0
130	53	3	1	36	0	1	0	1	0	6	0	0	0	0
131	94	1	4	0	0	0	0	0	0	0	0	0	0	0
132	93	1	1	3	1	0	0	0	0	0	0	0	0	0
133	92	3	5	0	0	0	0	0	0	0	0	0	0	0
134	94	3	2	1	0	0	0	0	0	0	0	0	0	0
135	91	2	2	4	0	0	0	0	0	0	0	0	0	0
136	93	2	1	3	1	0	0	0	0	0	0	0	0	0
137	44	4	1	39	2	1	0	0	0	7	1	0	0	0
138	97	1	1	1	0	0	0	0	0	0	0	0	0	0
139	82	2	1	12	3	0	0	0	0	1	0	0	0	0
140	79	4	1	7	7	1	0	0	0	1	1	0	0	0
141	84	3	2	9	1	0	0	0	0	0	0	0	0	0
142	90	0	0	8	2	0	0	0	0	0	0	0	0	0
143	38	4	0	23	21	1	1	0	0	7	5	0	0	0
144	38	0	0	34	17	0	0	0	0	6	2	2	0	0
145	17	3	0	25	23	2	3	1	0	13	11	2	0	0
146	26	2	0	22	25	1	2	0	0	9	11	0	0	0
147	10	4	0	11	24	4	8	0	0	10	27	1	1	0
148	28	2	0	31	21	1	1	1	0	11	5	0	0	0
149	9	4	1	10	27	3	13	0	1	7	23	1	2	0
150	10	4	1	10	23	4	11	0	1	7	25	2	1	0
151	8	3	1	12	15	4	6	0	1	19	26	1	2	0
152	9	2	0	13	21	4	3	0	0	16	31	1	1	0
153	26	1	0	27	26	1	1	0	0	12	6	0	0	0
154	54	1	1	36	2	1	0	1	0	4	0	0	0	0
155	65	2	0	27	3	0	0	0	0	3	0	0	0	0
156	16	8	1	9	25	7	11	0	1	6	14	0	1	0
157	25	12	5	22	12	9	5	1	0	6	4	0	0	0
158	20	11	1	13	23	5	9	0	1	5	11	0	1	0
159	23	9	1	21	20	4	6	0	0	7	7	0	1	0
160	20	10	1	13	24	5	8	0	1	5	11	0	1	0

ID	Relative abundances of brGDGTs (%)													
	Ia	Ib	Ic	IIa	IIa'	IIb	IIb'	IIc	IIc'	IIIa	IIIa'	IIIb	IIIb'	IIIc
161	15	9	1	9	24	6	11	0	1	5	17	0	2	0
162	19	8	1	3	30	4	5	0	0	4	25	1	1	0
163	20	2	1	2	23	0	0	0	0	1	51	1	0	0
164	69	1	1	26	0	1	0	0	0	2	0	0	0	0
165	16	0	0	38	3	0	0	0	0	41	2	0	0	0
166	34	27	6	4	13	3	10	0	1	1	2	0	1	0
167	80	3	1	9	5	0	0	0	0	2	1	0	0	0
168	81	2	1	11	4	0	0	0	0	1	0	0	0	0
169	86	5	2	5	1	0	0	0	0	0	0	0	0	0
170	58	7	0	17	12	1	1	0	0	2	2	0	0	0
171	19	5	1	23	17	3	6	1	0	13	9	1	1	0
172	62	2	0	29	1	1	0	0	0	4	0	0	0	0
173	54	5	1	31	2	1	0	0	0	5	1	0	0	0
174	61	3	1	30	1	1	0	0	0	4	0	0	0	0
175	17	7	1	14	27	4	7	0	0	7	14	0	1	0
176	32	1	0	39	11	1	0	0	0	15	1	0	0	0
177	39	1	0	43	1	1	0	0	0	14	0	0	0	0
178	13	4	1	17	32	2	5	0	0	10	15	0	0	0
179	12	3	1	14	35	2	4	0	0	10	19	0	1	0
180	58	7	1	19	9	1	1	0	0	3	1	0	0	0
181	56	5	1	30	2	1	0	1	0	5	0	0	0	0
182	67	2	1	26	1	1	0	0	0	2	0	0	0	0
183	76	2	1	18	0	1	0	0	0	1	0	0	0	0
184	66	6	1	15	6	1	2	0	0	1	2	0	0	0
185	70	6	1	14	6	1	1	0	0	2	1	0	0	0
186	76	3	1	16	2	0	0	0	0	2	1	0	0	0
187	19	24	5	9	15	8	9	0	1	4	6	1	1	0
188	23	2	1	32	18	1	1	0	0	15	6	0	0	0
189	31	2	0	33	16	0	0	0	0	13	4	0	0	0
190	37	4	0	29	18	1	2	0	0	6	4	0	0	0
191	70	2	1	20	2	0	0	0	0	3	0	0	0	0
192	73	2	1	20	1	0	0	0	0	2	1	0	0	0
193	7	3	2	3	27	5	9	0	0	7	33	1	2	0
194	16	4	0	9	35	2	7	0	0	6	18	0	1	1
195	17	3	1	20	28	2	3	1	0	13	12	0	0	0
196	7	2	1	5	27	1	3	0	0	5	46	2	1	0
197	12	4	1	9	33	3	7	1	0	7	23	1	1	0
198	67	1	0	28	1	0	0	0	0	2	0	0	0	0
199	37	19	2	15	12	5	5	0	0	2	2	0	1	0
200	41	2	0	28	13	0	0	0	0	11	3	0	0	1

ID	Relative abundances of brGDGTs (%)													
	Ia	Ib	Ic	IIa	IIa'	IIb	IIb'	IIc	IIc'	IIIa	IIIa'	IIIb	IIIb'	IIIc
201	52	6	2	28	6	2	0	0	0	4	1	0	0	0
202	37	9	2	25	14	3	3	0	0	5	3	0	0	0
203	27	19	3	14	16	8	6	1	0	3	4	0	1	0
204	50	7	2	27	6	2	1	0	0	4	1	0	0	0
205	40	6	1	33	9	2	2	0	0	6	2	0	0	0
206	44	4	0	38	4	1	1	0	0	7	1	0	0	0
207	42	14	3	17	13	4	2	0	0	3	2	0	0	0
208	52	11	2	15	12	2	1	0	0	2	2	0	0	0
209	90	1	3	5	1	0	0	0	0	0	0	0	0	0
210	27	3	0	5	44	0	0	0	0	2	20	0	0	0
211	22	1	0	0	47	0	0	0	0	0	30	0	0	0
212	34	1	0	41	2	1	0	0	0	19	1	0	0	0
213	34	1	0	42	2	1	0	0	0	20	0	0	0	0
214	19	17	2	7	18	2	14	1	1	12	5	0	1	0
215	24	17	2	25	9	10	4	1	0	5	3	0	0	0
216	21	17	3	13	15	10	9	0	1	4	6	0	1	0
217	18	12	2	18	16	9	8	1	1	7	9	1	1	0
218	16	4	2	4	29	5	5	0	1	7	26	1	1	0
219	22	4	1	16	25	3	3	0	0	13	14	0	0	0
220	18	25	5	6	16	3	17	0	1	3	5	1	1	0
221	19	24	5	6	17	2	17	0	1	3	5	0	1	0
222	23	2	0	24	24	1	2	0	0	17	8	0	0	0
223	12	1	0	0	54	0	3	0	0	1	30	0	0	0
224	18	4	0	38	11	0	0	0	0	23	5	0	0	0
225	22	1	1	38	13	1	0	0	0	19	4	0	0	0
226	32	3	0	25	22	2	2	0	0	10	5	0	0	0
227	35	2	1	42	5	1	0	0	0	14	1	0	0	0
228	20	2	0	24	27	1	3	0	0	12	11	0	0	0
229	10	3	0	5	34	2	4	0	0	11	31	1	1	0
230	14	2	0	23	29	1	2	0	0	15	15	0	0	0
231	11	1	0	0	54	0	2	0	0	2	30	0	0	0
232	15	2	1	2	51	0	3	0	0	2	24	0	0	0
233	14	5	0	12	28	5	5	0	0	9	23	0	0	0
234	23	2	0	5	44	0	2	0	0	2	22	0	0	0
235	35	2	0	34	14	1	1	0	0	8	4	0	0	0
236	32	5	1	31	16	3	1	1	0	7	3	0	0	0
237	74	1	1	21	1	1	0	0	0	1	0	0	0	0
238	89	2	1	7	1	0	0	0	0	1	0	0	0	0
239	95	2	1	2	0	0	0	0	0	0	0	0	0	0

Supp. Table 4. The loadings of the 15 brGDGT components and the scores of the 239 soils on the first three principal components (PC1-PC3) are given.

	PC1	PC2	PC3
Ia	-0.311	-0.307	-0.032
Ib	0.23	-0.384	-0.136
Ic	0.142	-0.458	-0.202
IIa	-0.108	0.398	-0.436
IIa'	0.241	0.176	0.432
IIb	0.342	-0.034	-0.179
IIb'	0.367	-0.12	0.048
IIc	0.2	0.073	-0.449
IIc'	0.36	-0.126	-0.098
IIIa	0.06	0.489	-0.226
IIIa'	0.238	0.214	0.463
IIIb	0.29	0.137	0.033
IIIb'	0.369	0.002	0.013
IIIc	0.103	0.121	-0.199
IIIc'	0.221	0.053	-0.107
1	0.009	-0.021	-0.005
2	-0.049	0.011	0.022
3	-0.072	-0.046	0.039
4	-0.003	-0.189	-0.039
5	-0.063	-0.067	0.019
6	-0.068	-0.044	0.035
7	-0.045	-0.096	0.012
8	-0.07	-0.064	0.033
9	-0.058	-0.044	0.022
10	-0.004	-0.173	-0.023
11	-0.052	-0.019	-0.062
12	0.09	0	0.02
13	-0.041	0.045	-0.066
14	-0.071	-0.058	0.035
15	-0.068	-0.06	0.025
16	-0.048	-0.039	0.021

	PC1	PC2	PC3
17	-0.049	-0.056	0.032
18	-0.067	-0.04	0.025
19	-0.031	-0.116	0.004
20	-0.066	-0.055	0.031
21	-0.07	-0.032	0.04
22	0.112	-0.177	-0.048
23	-0.011	-0.125	-0.006
24	-0.016	0.001	0.066
25	-0.004	-0.065	0.018
26	-0.072	-0.028	0.022
27	0.124	-0.071	-0.045
28	0.066	-0.056	-0.022
29	0.097	-0.02	-0.005
30	0.108	-0.027	-0.025
31	-0.013	-0.031	-0.017
32	0.173	-0.022	-0.032
33	0.043	-0.005	-0.056
34	0.22	-0.023	-0.097
35	0.099	-0.02	-0.067
36	0.024	0.02	-0.045
37	-0.017	0.035	-0.01
38	0.051	0.011	-0.035
39	0.058	0.047	-0.034
40	0.078	0.027	-0.012
41	0.193	0.024	-0.101
42	0.106	0.018	-0.131
43	-0.048	-0.008	-0.049
44	-0.037	0.043	-0.08
45	-0.04	0.012	-0.063
46	-0.043	0.025	-0.038
47	0.061	0.004	-0.134
48	-0.045	0.054	-0.078
49	-0.011	0.086	-0.053
50	-0.039	0.07	-0.073
51	-0.055	0.023	-0.036

	PC1	PC2	PC3		PC1	PC2	PC3
52	0.081	0.09	-0.077	88	0.088	-0.032	0.092
53	-0.042	0.073	-0.069	89	-0.041	-0.021	-0.048
54	-0.036	0.111	-0.069	90	0.159	-0.066	-0.072
55	-0.039	0.082	-0.036	91	0.05	-0.001	0.029
56	-0.049	0.082	-0.058	92	-0.05	0.098	-0.075
57	-0.044	0.084	-0.069	93	0.056	0.042	-0.005
58	-0.056	-0.034	-0.006	94	0.052	0.04	0.014
59	-0.029	0.054	-0.068	95	0.098	-0.049	0.009
60	-0.068	-0.07	0.024	96	-0.044	0.066	-0.067
61	-0.072	-0.062	0.035	97	-0.038	0.051	-0.104
62	0.046	-0.094	-0.115	98	0.008	0.095	-0.149
63	-0.061	-0.073	0.026	99	0.051	0.044	0.028
64	-0.061	-0.072	0.02	100	-0.039	0.073	-0.061
65	0.051	-0.142	0.01	101	0.179	-0.029	-0.121
66	0	0.049	0.216	102	-0.043	0.034	0.001
67	-0.072	0.002	0	103	-0.07	-0.045	0.025
68	-0.052	0.044	-0.041	104	-0.065	-0.06	0.032
69	-0.048	0.044	-0.053	105	-0.073	-0.061	0.038
70	0.015	0.056	0.045	106	-0.065	-0.063	0.033
71	0.041	0.036	0.05	107	-0.074	-0.055	0.04
72	0.027	0.037	0.057	108	-0.023	-0.135	-0.005
73	0.078	-0.015	-0.063	109	-0.069	-0.062	0.025
74	0.032	0.041	0.1	110	0.03	0.034	-0.056
75	0.093	0.019	0.063	111	0.159	0.059	-0.08
76	0.034	0.037	0.037	112	0.034	-0.03	-0.129
77	0.027	0.02	-0.014	113	-0.068	-0.073	0.034
78	-0.049	0.053	-0.038	114	-0.062	0.041	-0.003
79	0.072	-0.007	0.113	115	0.033	-0.015	0.102
80	-0.041	0.085	-0.085	116	-0.028	0.064	-0.037
81	0.058	0.018	0.014	117	0.005	0.01	-0.082
82	0.029	0.039	0.074	118	-0.041	0.072	-0.086
83	0.066	-0.012	0.087	119	-0.045	-0.001	-0.079
84	0.107	-0.002	-0.03	120	-0.03	-0.003	0.043
85	0.077	-0.004	0.045	121	-0.049	0.027	0.021
86	-0.038	0.061	-0.093	122	-0.038	0.017	0.039
87	-0.007	0.009	0.039	123	0.106	-0.043	0.013

	PC1	PC2	PC3
124	0.174	-0.023	0.04
125	-0.047	-0.004	-0.073
126	-0.047	0.011	-0.064
127	-0.069	-0.063	0.034
128	0.051	-0.224	-0.067
129	0.095	0.01	0.023
130	-0.053	0.022	-0.061
131	-0.059	-0.11	0.012
132	-0.064	-0.048	0.009
133	-0.056	-0.131	0.004
134	-0.064	-0.08	0.02
135	-0.062	-0.074	0.01
136	-0.064	-0.062	0.016
137	-0.046	0.025	-0.064
138	-0.071	-0.071	0.033
139	-0.067	-0.044	0.023
140	-0.057	-0.059	0.03
141	-0.063	-0.074	0.014
142	-0.073	-0.037	0.037
143	-0.028	0.034	0.037
144	-0.005	0.089	0.026
145	0.044	0.101	0.004
146	-0.003	0.061	0.037
147	0.073	0.066	0.068
148	-0.024	0.07	-0.023
149	0.105	0.041	0.056
150	0.14	0.064	0.049
151	0.132	0.102	-0.005
152	0.032	0.103	0.097
153	-0.026	0.081	0.012
154	-0.045	0.022	-0.086
155	-0.067	0.006	0
156	0.094	-0.002	0.037
157	0.044	-0.063	-0.1
158	0.078	-0.013	0.026
159	0.035	0.007	0

	PC1	PC2	PC3
160	0.066	-0.006	0.033
161	0.104	-0.008	0.054
162	0.06	0.007	0.101
163	0.027	0.06	0.201
164	-0.056	-0.003	-0.019
165	-0.036	0.183	-0.085
166	0.064	-0.175	-0.033
167	-0.062	-0.046	0.028
168	-0.066	-0.04	0.029
169	-0.058	-0.078	0.01
170	-0.044	-0.018	0.031
171	0.062	0.07	-0.049
172	-0.054	0.011	-0.039
173	-0.045	0.014	-0.043
174	-0.051	0.008	-0.039
175	0.049	0.012	0.057
176	-0.042	0.089	-0.052
177	-0.051	0.083	-0.062
178	0.015	0.041	0.074
179	0.025	0.053	0.092
180	-0.045	-0.021	0.015
181	-0.038	0.009	-0.077
182	-0.053	-0.013	-0.042
183	-0.056	-0.034	-0.026
184	-0.039	-0.03	-0.007
185	-0.05	-0.032	0.013
186	-0.054	-0.022	0.002
187	0.1	-0.12	-0.032
188	-0.023	0.073	-0.025
189	-0.045	0.075	0.005
190	-0.038	0.037	0.025
191	-0.056	-0.012	-0.021
192	-0.067	-0.021	0.006
193	0.12	0.042	0.107
194	0.073	0.077	0.041
195	0.015	0.072	0

	PC1	PC2	PC3
196	0.064	0.082	0.184
197	0.056	0.051	0.073
198	-0.062	0.002	-0.024
199	0.027	-0.077	-0.015
200	-0.007	0.101	-0.08
201	-0.043	-0.012	-0.021
202	-0.011	-0.022	-0.015
203	0.059	-0.07	-0.054
204	-0.036	-0.022	-0.029
205	-0.03	0.02	-0.026
206	-0.045	0.036	-0.037
207	-0.003	-0.065	-0.016
208	-0.021	-0.056	0.004
209	-0.064	-0.087	0.016
210	-0.013	0.03	0.157
211	-0.005	0.038	0.199
212	-0.042	0.101	-0.073
213	-0.048	0.103	-0.068
214	0.081	-0.044	-0.019
215	0.042	-0.049	-0.093
216	0.09	-0.083	-0.034
217	0.097	-0.009	-0.055
218	0.081	0.021	0.091
219	-0.006	0.052	0.057
220	0.113	-0.149	-0.018
221	0.109	-0.138	-0.007
222	-0.024	0.088	0.033
223	0.009	0.041	0.208
224	-0.039	0.118	-0.029
225	-0.033	0.103	-0.023
226	-0.029	0.047	0.031
227	-0.037	0.084	-0.082
228	-0.008	0.078	0.056
229	0.037	0.071	0.144
230	-0.016	0.093	0.066
231	0.008	0.052	0.21

	PC1	PC2	PC3
232	0.004	0.036	0.184
233	0.014	0.053	0.099
234	-0.007	0.036	0.164
235	-0.029	0.062	-0.011
236	-0.014	0.032	-0.042
237	-0.062	-0.02	-0.013
238	-0.07	-0.051	0.027
239	-0.07	-0.069	0.032



Photo by Cindy De Jonge

In situ produced branched glycerol
dialkyl glycerol tetraethers in
suspended particulate matter from
the Yenisei River, Eastern Siberia.

4

Cindy De Jonge, Alina Stadnitskaia,
Ellen C. Hopmans, Georgy Cherkashov,
Andrey Fedotov, Jaap S. Sinninghe Damsté

Published in *Geochimica et Cosmochimica Acta* 1425,
January 2014

Corrigendum published in *Geochimica et
Cosmochimica Acta* 150, February 2015

ABSTRACT

Soil-derived branched glycerol dialkyl glycerol tetraethers (brGDGTs) in marine river fan sediments have a potential use for determining changes in the mean annual temperature (MAT) and pH of the river watershed soils. Prior to their incorporation in marine sediments, the compounds are transported to the marine system by rivers. However, emerging evidence suggests that the brGDGTs in freshwater systems can be derived from both soil run-off and in situ production. The production of brGDGTs in the river system can complicate the interpretation of the brGDGT signal delivered to the marine system. Therefore, we studied the distribution of brGDGT lipids in suspended particulate matter (SPM) of the Yenisei River. Chromatographic improvements allowed quantification of the recently described hexamethylated brGDGT isomer, characterized by having two methyl groups at the 6/6' instead of the 5/5' positions, in an environmental dataset for the first time. This novel compound was the most abundant brGDGT in SPM from the Yenisei. Its fractional abundance correlated well with that of the 6-methyl isomer of the hexamethylated brGDGT that contains one cyclopentane moiety. The Yenisei River watershed is characterized by large differences in MAT ($>11^{\circ}\text{C}$) as it spans a large latitudinal range ($46\text{--}73^{\circ}\text{N}$), which would be expected to be reflected in brGDGT distributions of its soils. However, the brGDGT distributions in the SPM show little variation. Furthermore, the reconstructed pH values are high compared to the watershed soil pH. We, therefore, hypothesize that the brGDGTs in the Yenisei River SPM are predominantly produced in situ and not primarily derived from erosion of soil. This accounts for the absence of a change in the temperature signal, as the river water temperature is more stable. Using a lake calibration, the reconstructed temperature values agree with the mean summer temperatures (MST) recorded. The brGDGTs delivered to the sea by the Yenisei River during this season are thus not soil-derived, possibly complicating the use of brGDGTs in marine sediments for palaeoclimate reconstructions.

1. Introduction.

Branched glycerol dialkyl glycerol tetraethers (brGDGTs) are ubiquitous membrane lipids in peat and soils. They are derived from bacteria and possess 4 to 6 methyl substituents ('branches') on the linear C₂₈ alkyl chains and up to two cyclopentyl moieties formed by internal cyclization (Fig. 1; Sinninghe Damsté et al., 2000; Weijers et al., 2006a). The distribution of the different brGDGTs depends on the prevailing mean annual temperature (MAT) and soil pH (Weijers et al., 2007a). With decreasing temperature, the number of methyl groups in the alkyl chains increase and with a higher soil pH the prevalence of the cyclopentyl moieties will increase. A global soil calibration is thus based on the Methylation of Branched Tetraethers (MBT) and Cyclisation of Branched Tetraethers (CBT) ratios (Weijers et al., 2007a). This calibration was recently extended by Peterse et al. (2012), proposing a modified MBT ratio, the MBT'.

Branched GDGTs have also been found in coastal marine sediments, where they are likely deposited by rivers, after erosion and transport of soil particles (Hopmans et al., 2004). The amounts of soil-derived bacterial brGDGTs and the marine Thaumarchaeotal isoprenoid GDGT (iGDGT) crenarchaeol (Sinninghe Damsté et al., 2002) can be expressed in the Branched Isoprenoid Tetraether (BIT) index, which has been used to estimate the amount of soil-derived material in aquatic environments (Hopmans et al., 2004). Furthermore, the distribution of soil-derived brGDGTs in river fan sediments can be used to reconstruct the continental MAT and soil pH of the watershed of the river and this principle has been successfully used for palaeoclimate reconstructions (Weijers et al., 2007a). However, complications can arise if the watershed is affected by changes in the supply of organic matter and the source area of the sediments (Bendle et al., 2010). Furthermore, overestimations of MAT have been reported (Schouten et al., 2008; Donders et al., 2009). Recently, structural isomers that partially co-elute with the brGDGTs that are used for these proxy calculations have been described (De Jonge et al., 2013; IIa, IIa', IIIa, IIIa'; Fig. 1). The abundance and variability of these isomers in the environment is currently unknown, as is their impact on MAT and pH reconstructions based on CBT/MBT indices.

BrGDGTs also occur ubiquitously in lake sediments (e.g. Blaga et al., 2009; 2010) and, since they were thought to be derived from erosion of surrounding soils, the sedimentary record of the BIT index has been applied as an indicator of past variations in the intensity of rainfall in an equatorial lake (Verschuren et al., 2009). The CBT/MBT indices of sedimentary brGDGTs have subsequently also been applied to a variety of lakes, to reconstruct local MAT and pH changes in their watershed (e.g. Tierney et al., 2010, 2012; Niemann et al., 2012; Wang et al., 2012). However, in these studies the CBT/MBT -inferred temperatures using soil-based calibrations often considerably underestimated MAT. The discrepancy between soil and lake brGDGT distributions points to potential in-situ production of brGDGTs in lakes (Tierney and Russell, 2009; Sinninghe Damsté et al., 2009; Loomis et al., 2011). Since the prevailing lake temperature still controls the distributions of the brGDGTs in the surface sediments of the lakes this has led to alternative (aquatic) calibrations being created (Tierney et al., 2010; Sun et al., 2011; Pearson et al., 2011; Loomis et al., 2012).

Although rivers are the main pathway for the transport of brGDGTs to ocean sediments, there is a remarkable lack of studies that assess the potential effect of in-situ production in

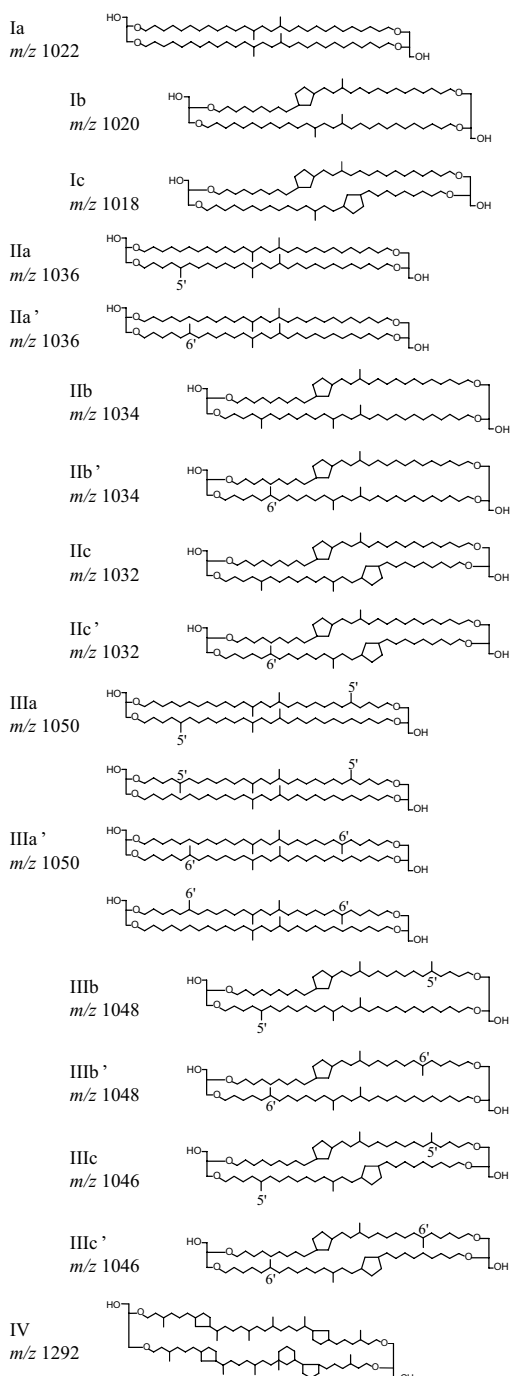


Fig. 1. Chemical structures of branched GDGTs (I-III) and crenarchaeol (IV). The chemical structures of the penta- and hexamethylated brGDGTs with cyclopentyl moiety(ies) IIb', IIc', IIIb' and IIIc' are tentatively assigned.

ivers. The occurrence of branched GDGTs and crenarchaeol has been reported in suspended particulate material (SPM) from the European rivers Rhine, Meuse, Niers, and Berkel (Herfort et al., 2006) as well as in the Têt and Rhone rivers in France (Kim et al., 2007). BrGDGTs have also been shown to occur in three East-Siberian rivers, the Lena, Indigirka and Kolyma Rivers (van Dongen et al., 2008). A small set of sediments from a tropical river system (Tierney and Russell, 2009), showed an offset between the prevailing soil and river CBT/MBT values. Kim et al. (2012) compared the brGDGT distributions in the Amazon River SPM and sediments and soils from the Amazon watershed and concluded that aquatic in-situ production contributed to the riverine brGDGT pool. Zell et al. (2013) also described a different brGDGT distribution in soil and river brGDGTs in the Amazon River basin, characterized by a higher abundance of brGDGT Ia in soils. Furthermore, they investigated the intact polar lipid (IPL) precursors of brGDGTs. In living or recently living cells brGDGTs are present as IPLs which, after cell death, are relatively quickly degraded into core lipids (CL) (White et al., 1979) that are the compounds used in the CBT/MBT proxies. Both the presence of IPLs with a labile phosphatidyl headgroup and the similar distribution of the IPL-derived core lipids and the core lipids present in the SPM indicated riverine in-situ production of brGDGTs.

Table 1. Weather stations; weather station code, coordinates and elevation. Climate data from the period 1963-2012 from the online NOAA database; Mean Annual Temperature (MAT), Mean Summer Temperature (MST), averaged from June to September.

Weather station	Latitude (°N)	Longitude (°E)	Elevation (m)	MAT (°C)	MST (°C)
W1 Bayanhongor	46° 07' 48"	100° 40' 48"	1859	0.0	15.4
W2 Ulaanbatar	47° 55' 12"	106° 52' 12"	1306	-1.6	15.4
W3 Tosontsengel	48° 43' 48"	98° 12' 00"	1723	-6.1	12.7
W4 Hatgal	50° 25' 48"	100° 09' 00"	1668	-4.6	10.6
W5 Irkutsk	52° 16' 12"	104° 21' 00"	498	-0.2	14.3
W6 Minusinsk	53° 43' 12"	91° 42' 00"	254	0.9	16.1
W7 Zhigalovo	54° 48' 00"	105° 10' 12"	418	-5.7	12.7
W8 Nizhneudinsk	54° 52' 48"	99° 01' 48"	411	0.7	13.9
W9 Krasnojarsk	56° 01' 48"	92° 45' 00"	276	0.9	14.8
W10 Kirensk	57° 46' 12"	108° 04' 12"	259	-3.9	13.9
W11 Vanavara	60° 19' 48"	102° 16' 12"	260	-5.7	12.7
W12 Erbogacen	61° 16' 12"	108° 01' 12"	291	-6.7	12.6
W13 Bor	61° 36' 00"	90° 01' 12"	58	-3.6	13.2
W14 Bajkit	61° 40' 12"	96° 22' 12"	262	-6.4	12.0
W15 Tura	64° 16' 12"	100° 13' 48"	168	-9.0	11.7
W16 Turuhansk	65° 46' 48"	87° 55' 48"	38	-6.4	11.4
W17 Dikson	73° 30' 00"	80° 24' 00"	47	-11.4	2.9

In this study we examine for the first time the distribution of brGDGTs and crenarchaeol in the Yenisei River, the world's sixth largest river in terms of discharge that crosses Mongolia and Siberian Russia in a south to north direction. The large latitudinal range of the river (5500 km) allows us to evaluate changes in SPM brGDGT compositions that possibly derive from soil input from a watershed that crosses several climatic zones and vegetation types, i.e. the arid Mongolian steppe, the vast Russian boreal forest (Taiga and Tundra) and the Arctic. We sampled upstream tributaries and the main stream before and after major tributaries enter. The CBT/MBT'-derived pH and temperatures of the SPM are compared with soil pH and with the climate gradients present on the Eurasian continent. The amounts and distribution of IPL-derived CL are also evaluated. In addition, the environmental abundance of recently described hexamethylated isomers was assessed for the first time.

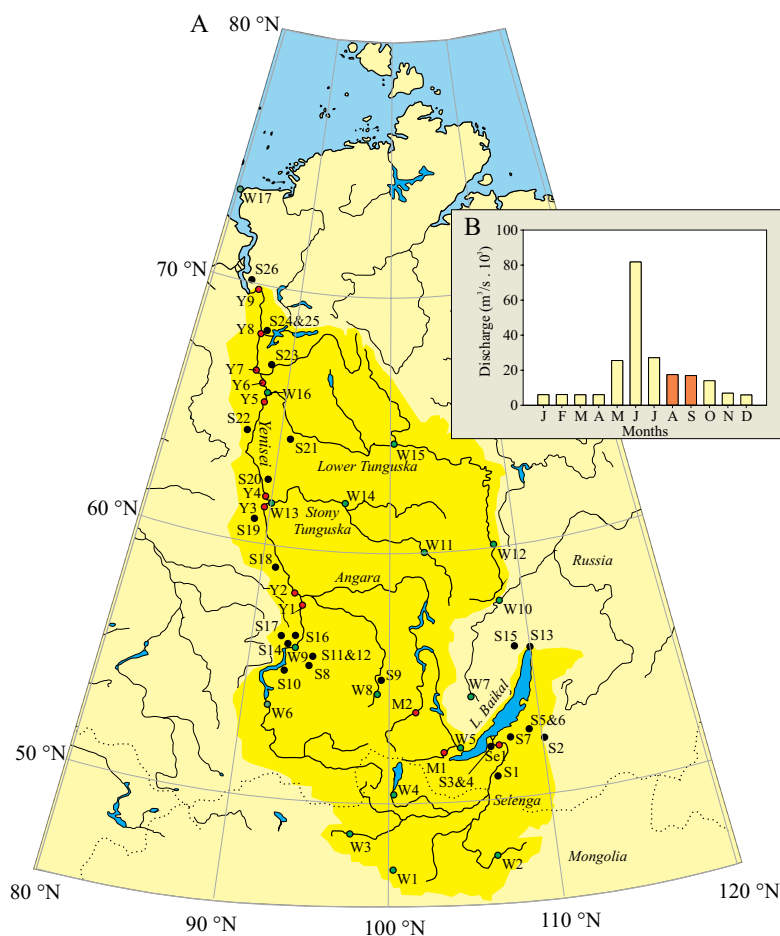


Fig. 2. A) The Yenisei River and its catchment (indicated in dark yellow), located in Russian Siberia and Mongolia. Sampling stations (Table 2; S₁, M1-M2, Y1-Y9) are indicated with red dots, weather stations (Table 1; W1-W17) are indicated with green dots, soils included in the pH database (Table 3; S1-S26) are indicated with black dots. B) Discharge regime of the Yenisei River. Months of sampling are indicated in orange.

2. Study area

The Yenisei is the largest river in Russia and one of the largest rivers in Asia (Fig. 2A). The topographical properties are described in Telang et al. (1990). The river starts in Northern Mongolia and flows through the Central Siberian Plateau into the Kara Sea and the Arctic Ocean. Two large man-made lakes, the Krasnoyarsk reservoir and Sayano-Shushenskaya reservoir are situated in the upper reaches of the Yenisei. The river here has a high flow speed, a small riverbed width and little sedimentation. Further north, its most important tributary (25% of flow), the Angara River, joins the Yenisei. Angara River drains Lake Baikal, a large freshwater lake that is fed dominantly (50% of flow) by the Selenga River that drains large parts of Mongolia. The second important tributary for the Yenisei River is the Lower Tunguska (20% of flow). In the lower reaches of the river the Yenisei River flow becomes smooth, the riverbed width reaching several kilometers.

The mean annual discharge is estimated at 19800 m³/s. In this respect, the Yenisei takes ninth place among rivers worldwide (Telang et al., 1990). Dissolved organic carbon (DOC) is by far the dominant (> 90%) form of organic carbon transported to the Arctic Ocean by the

Table 2. Overview of the SPM sample stations in the Yenisei River catchment and their characteristics; sample codes, coordinates and sampling dates. The measured pH, surface water temperature and the particulate (>0.7 µm) organic carbon (POC) concentration per L are also given. N.d. indicates not determined values

Station		Latitude (°N)	Longitude (°E)	Date sampled	Water T (°C)	Water pH	POC (mg · L ⁻¹)
Se1	Selenga River	51°43'41.8"	107°27'46.4"	06-07-2010	n.d.	8.4	6.4
M1	Irkut River	51°56'43.2"	100°47'18.2"	11-07-2010	10.8	5.6	0.1
M2	Uda River	54°51'22.7"	99°07'13.7"	30-06-2010	16.9	7.7	1.6
Y1	Yenisei River - Strelka	58°00'21.4"	93°55'48.3"	25-08-2009	12.0	n.d.	0.03
Y2	Yenisei River - Lesosibirsk	58°04'43.9"	92°55'28.2"	29-09-2009	11.0	n.d.	0.09
Y3	Yenisei River - Monastirsky Island	61°16'33.6"	90°54'0.18"	27-08-2009	n.d.	n.d.	0.2
Y4	Yenisei River - Stony Tunguska	61°28'30.4"	89°19'46.4"	25-09-2009	10.0	n.d.	0.03
Y5	Yenisei River - Kostino	65°11'32.4"	87°34'20.0"	29-08-2009	n.d.	n.d.	0.1
Y6	Yenisei River - Lower Tunguska	66°06'11.1"	87°08'24.0"	20-09-2009	9.0	n.d.	0.4
Y7	Yenisei River - Ledianaya Mt	66°21'19.1"	86°20'48.3"	31-08-2009	11.2	n.d.	0.2
Y8	Yenisei River - 60 km south of Dudinka	68°24'27.6"	86°09'36.9"	01-09-2009	11.2	n.d.	0.07
Y9	Yenisei River - Seljanka Cape	69°25'22.9"	84°07'30.5"	03-09-2009	n.d.	n.d.	0.1

Yenisei (Lobbess et al., 2000). The Yenisei River is characterized by a pronounced discharge peak in June and relatively low water flow between September and April, with more than 30% of the annual discharge occurring in June (Stedmon et al., 2011; Fig. 2B). The annual discharge consists of 50% snowmelt, 35% rain water and approximately 15% groundwater (Pavlov and Pfirmann, 1995).

The Yenisei River water catchment area equals $2.6 \cdot 10^6$ km². It extends for 5,500 km in a south-north direction, covering different climate zones and biomes. Climate data, based on 13 Russian and 4 Mongolian weather stations that report daily temperature data, are summarized in Table 1. The climate is continental, with large seasonal temperature differences and a low mean annual temperature (MAT) over most of the territory. In the southernmost area, the MAT goes down to -6°C, because of the high altitude. This increases slightly as the altitude effect decreases (Krasnoyarsk, MAT= 0.9°C). Further north, the MAT decreases steadily, with a MAT of -11.4°C in the most northern areas. Summer temperatures (June – September) decrease steadily from 15.4°C in Mongolia to 2.9 °C in the north. Precipitation varies from >1000 mm.yr⁻¹ in the Sayan and Pytorana mountains and 300-600 mm.yr⁻¹ on the middle Siberian plateau.

3. Material and methods

3.1. Collection of SPM samples

Table 2 lists the river SPM samples investigated in this study and the sampling stations are shown in Fig. 2A. Surface water (<2m depth) of the river (5-150 L) was collected and filtered (GF/F glass fiber filters, 0.7 µm pore size) at 12 locations distributed throughout Siberia. In August-September 2009, SPM from the Yenisei River water was collected with an in-situ pump (McLane Large Volume Water Transfer System Sampler) employed from the R/V Sovetskaya Arktika, at 9 stations distributed along the Yenisei River. In 2010, three more SPM samples were obtained in tributaries of the Angara and in the Selenga River. Surface water was collected in canisters after wading several meters into the river and filtered using the same filters, a peristaltic pump and a titanium tripod system. Care was taken to sample flowing water in the river, avoiding zones with stagnant water. The water temperature (n=9) and pH (n=3) were measured immediately after collecting the water.

3.2. Lipid extraction and GDGT analyses

The freeze-dried filters were extracted using a modified Bligh and Dyer method as described by Pitcher et al. (2009). The filters were ultrasonically extracted three times for 10 min using a single-phase solvent mixture of MeOH/DCM/phosphate buffer 10:5:4 (v/v/v). The extract was separated into a core lipid (CL) and intact polar lipid (IPL) fraction over a small silica column, using a procedure modified from Pitcher et al. (2009), using hexane/ethyl acetate 1:1, v/v as eluent. An aliquot of the IPL fraction was analyzed directly for CL to check for potential carry-over into the IPL fraction. In order to analyze the IPL as CL, the extract was refluxed for a minimum of 2 h in 1.5 N HCl in MeOH. The amount of CL in this IPL-derived fraction was corrected for the amount of CL brGDGTs carried-over. All GDGTs were quantified against a

Table 3. Descriptions and locations of soils samples used for describing the pH of the watershed soils.

	Soil type	Latitude (°N)	Longitude (°E)	Soil:water ratio	pH	Sour b
S1	Cropland	51° 24'	107° 00'	1:5	6.4 ^a	1
S2	Bog	52° 00'	110° 00'	1:5	6.5 ^a	1
S3	Cropland	52° 00'	106° 25'	1:5	6.1 ^a	1
S4	Forest	52° 00'	106° 24'	1:5	5.7 ^a	1
S5	Cropland	55° 18'	109° 00'	1:5	6.3 ^a	1
S6	Forest	55° 18'	109° 00'	1:5	6.7 ^a	1
S7	Forest	55° 18'	108° 00'	1:5	4.5 ^a	1
S8	Cropland	55° 00'	95° 00'	1:5	6.7 ^a	1
S9	Forest	55° 00'	99° 24'	1:5	4.2 ^a	1
S10	Meadow	55° 11'	92° 18'	1:5	6.2 ^a	1
S11	Cropland	55° 18'	95° 00'	1:5	6.8 ^a	1
S12	Meadow	55° 18'	95° 00'	1:5	6.8 ^a	1
S13	Bog	55° 29'	109° 32'	1:5	3.0 ^a	1
S14	Meadow	56° 00'	92° 18'	1:5	6.4 ^a	1
S15	Forest	56° 40'	108° 00'	1:5	6.4 ^a	1
S16	Pine Forest	56° 24'	93° 00'	1:2	5.1	2
S17	Forest	56° 27'	91° 18'	1:5	4.6 ^a	1
S18	Pine Forest	59° 24'	90° 00'	1:2	4.2	2
S19	Pine Forest	60 ° 30'	89° 00'	1:2	4.1	2
S20	Mixed Taiga	62° 30'	89° 00'	1:2	4.3	2
S21	Forest	64° 00'	92° 00'	1:5	5.7 ^a	1
S22	Mixed Taiga	64° 18'	87° 30'	1:2	4.0	2
S23	Forest	67° 00'	90° 00'	1:5	4.0 ^a	1
S24	Mixed Taiga	68° 05'	86° 42'	1:2	3.6	2
S25	Tundra	68° 05'	86° 42'	1:2	3.1	2
S26	Forest	70° 00'	84° 00'	1:5	4.8 ^a	1

^a Depending on the soil:water ratio used, the pH has been corrected with -0.5 units.

^b Source of pH data: 1 = soils from the online database composed by Stolbovoi and McCallum (2002) and 2 = the soils described in Santruckova et al. (2003).

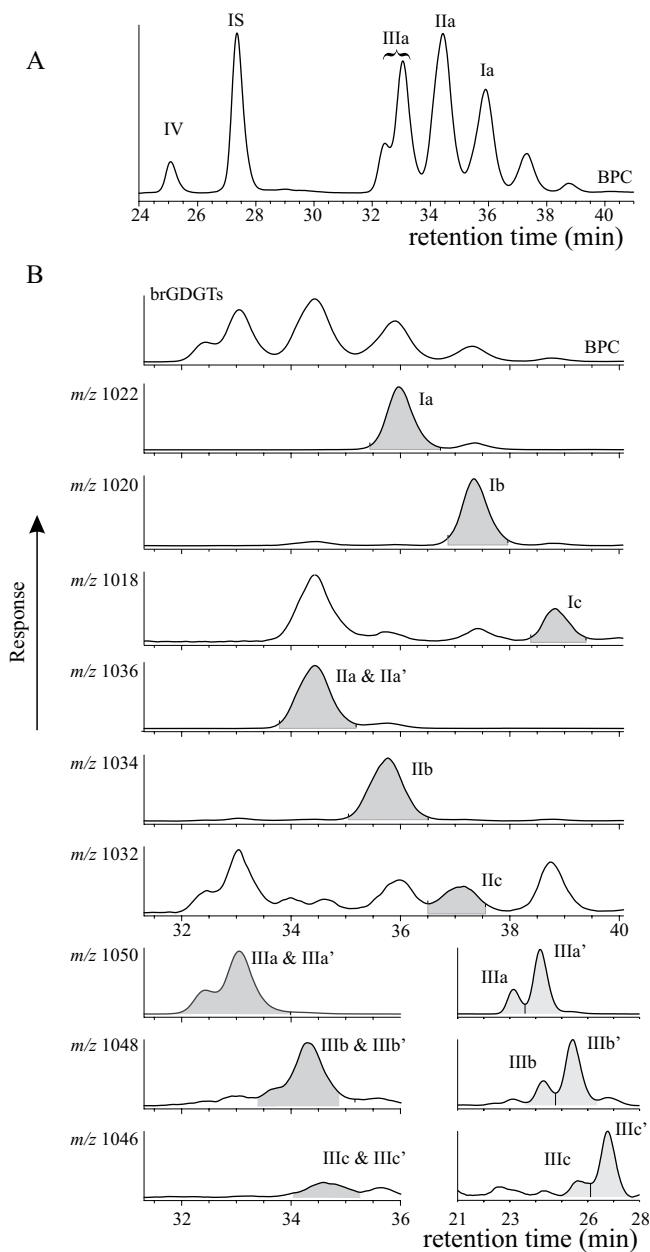


Fig. 3. A) The base peak chromatogram of the SPM at station Se1; the compounds indicated are crenarchaeol (IV), internal standard (IS) and the brGDGTs Ia, IIa, IIIa and IIIa' and B) Base peak chromatogram and separate mass traces of the brGDGTs discussed in the text, after separation on a Prevail cyano (CN) column. C) Base peak chromatogram and separate mass traces of the brGDGTs discussed in the text, after separation on a Prevail silica (Si) column. Note that the hexamethylated brGDGT isomers can be quantified using this method. Furthermore, the pentamethylated brGDGTs show a broader peak compared to the tetramethylated compounds, indicating the presence of a co-eluting compound.

Table 4. The amounts of crenarchaeol and the total amount of brGDGTs expressed per L filtered (in $\text{ng} \cdot \text{L}^{-1}$) or expressed per amount of particulate OC (in $\mu\text{g} \cdot \text{g POC}^{-1}$). The amount of the IPL fraction is expressed relative to the total amount of CL and IPL (%). n.d. is not detected.

Station	crenarchaeol ($\text{ng} \cdot \text{L}^{-1}$)	Σ brGDGT ($\text{ng} \cdot \text{L}^{-1}$)	crenarchaeol ($\mu\text{g} \cdot \text{g POC}^{-1}$)	Σ brGDGT ($\mu\text{g} \cdot \text{g POC}^{-1}$)	crenarchaeol IPL (%)	Σ brGDGT IPL (%)
Se1	3.1	69	0.5	11	41	5
M1	0.013	3.0	0.1	25	40	9
M2	0.057	4.8	0.03	2.9	45	12
Y1	0.017	0.63	0.7	25	26	10
Y2	0.025	4.3	0.3	47	34	10
Y3	0.060	5.3	0.4	31	21	9
Y4	n.d.	0.25	n.d.	7.5	n.d.	20
Y5	0.033	4.4	0.3	36	31	8
Y6	0.14	16	0.3	40	34	13
Y7	n.d.	4.3	n.d.	24	n.d.	11
Y8	0.014	1.7	0.2	24	23	7
Y9	0.041	1.7	0.1	16	22	6

known amount of C_{46} GDGT standard (Huguet et al., 2006) that was added to each fraction before filtration through a $0.45 \mu\text{m}$ PTFE filter.

Samples were analyzed using a high performance liquid chromatography–mass spectrometry (HPLC-MS) method (Schouten et al., 2007a). GDGTs were analyzed using an Agilent 1100 series / 1100 MSD series instrument, with auto-injection system and HP-Chemstation software (Agilent Technologies). Injection volume was $10 \mu\text{L}$. The HPLC system was fitted with a Prevail Cyano column ($150 \times 2.1 \text{ mm}$; $3 \mu\text{m}$; Grace Discovery Sciences, USA). Separation was achieved at 30°C with a flow-rate of $0.2 \text{ mL} \cdot \text{min}^{-1}$ and the following gradient profile; 5 min hexane/isopropanol (99:1) with a gradual increase to hexane/isopropanol (98:2) after 45 min. The column was cleaned (back-flushing) for 10 min with hexane/isopropanol (90:10). Detection was achieved in selected ion monitoring mode (SIM; Schouten et al., 2007a) using m/z 744 for the internal standard, m/z 1292 for crenarchaeol and m/z 1050, 1048, 1046, 1036, 1034, 1032, 1022, 1020 and 1018 for branched GDGTs. Agilent Chemstation software was used to integrate peak areas in the mass chromatograms of the protonated molecule ($[\text{M}+\text{H}]^+$) (Fig. 3B).

For an improved separation of the different isomers of the hexamethylated brGDGTs (De Jonge et al., 2013), a second HPLC-MS run was performed on an Agilent 1100 HPLC set-up, using a Prevail Silica column ($150 \times 2.1 \text{ mm}$; $3 \mu\text{m}$; Grace Discovery Sciences, USA) at 30°C with a flow rate of $0.2 \text{ mL} \cdot \text{min}^{-1}$. Elution was isocratically with hexane/isopropanol (97.8:2.2) for 38 min. The column was backflushed for 5 min with hexane/isopropanol (90:10). MS analysis was carried out on an Agilent 1100 MSD, in SIM mode, targeting m/z 1050, 1048, 1046, 1036, 1034, 1032, 1022, 1020 and 1018 for brGDGTs (Fig. 3C). The ratio between respectively IIIa and IIIa', IIIb and IIIb' and IIIc and IIIc' was calculated based on the latter analysis. Subsequently, the obtained ratios were used to divide the the total amount of co-eluting brGDGTs, determined with the analysis performed on the cyano column according to Schouten et al. (2007a).

Both datasets were integrated according to the NIOZ integration protocol (Schouten et al., 2009), where brGDGT isomers that are present as ‘shoulders’ are excluded from calculations. Careful evaluation of the chromatographic runs underlying the Weijers et al. (2007a) and Peterse et al. (2012) calibrations showed that for soils the resolution on the cyano columns was not sufficient to identify, and thus quantify separately, brGDGT IIIa’, although analysis on a silica column revealed the presence of often abundant brGDGT hexamethylated isomers (Fig. 4). Therefore, the soil-derived MBT/MBT’ ratio actually used the combined relative abundance of brGDGT IIIa and IIIa’. In contrast, analysis of SPM from a Siberian lake and the Selenga river showed that the second isomer in aquatic environments can be partly separated on a cyano column (fig 4). Therefore, the aquatic brGDGT calibrations (e.g. Pearson et al., 2011) are typically calculated using only IIIa but not IIIa’. The reason for this difference in chromatographic behavior is currently unknown, but is perhaps due to the difference in matrix between soil and aquatic samples.

3.3. Calculation of GDGT-based ratios and proxies

The relative amounts of the novel hexamethylated isomers are expressed as the isomer ratio (IR):

$$IR_{IIIx'} = IIIx' / (IIIx + IIIx'), \text{ where } x = a, b, \text{ or } c.$$

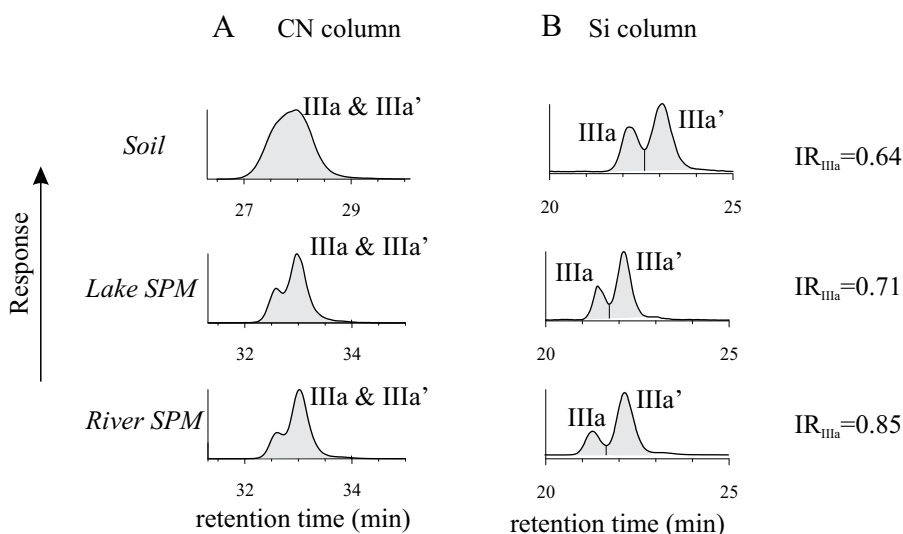


Fig. 4. The SIM chromatograms of the m/z 1050 of a soil (USA-CA2 from Peterse et al., 2012), lake SPM (Siberian “IL-Chir” lake, 51 °N 96.166, 100 °E 95.583) and river SPM (Se1); A) contrasting the elution characteristics on a cyano column (Weijers et al., 2006 and Peterse et al., 2012) and B) showing the similar $IR_{IIIa'}$ after elution on a silica column.

The BIT index was calculated according to Hopmans et al. (2004):

$$\text{BIT index} = (\text{Ia} + \text{IIa} + \text{IIIa}) / (\text{Ia} + \text{IIa} + \text{IIIa} + \text{IV}).$$

The roman numerals refer to the GDGTs indicated in Fig. 1. Ia, IIa, and IIIa are brGDGTs and IV is the isoprenoid GDGT (iGDGT) crenarchaeol (specific GDGT for Thaumarchaeota; Sinninghe Damsté et al., 2000). The CBT and MBT' indices (Peterse et al., 2012) were calculated as follows:

$$\text{CBT} = -\log ((\text{Ib} + \text{IIb}) / (\text{Ia} + \text{IIa}))$$

and

$$\text{MBT}' = (\text{Ia} + \text{Ib} + \text{Ic}) / (\text{Ia} + \text{Ib} + \text{Ic} + \text{IIa} + \text{IIb} + \text{IIc} + \text{IIIa} + \text{IIIa}').$$

The MBT' was calculated using both brGDGT IIIa and IIIa', as the area of the peak of brGDGT IIIa as integrated by Peterse et al. (2012) represents the combined peak area of brGDGT IIIa and IIIa'.

For the calculation of pH and mean annual temperature (MAT), the global soil calibration of Peterse et al., 2012 was used (RSME denotes residual standard mean error):

$$\text{pH} = 7.9 - 1.97 * \text{CBT} \quad (\text{RSME} = 0.8)$$

and

$$\text{MAT} (^{\circ}\text{C}) = 0.81 - 5.67 * \text{CBT} + 31.0 * \text{MBT}' \quad (\text{RSME} = 5.7^{\circ}\text{C})$$

The mean summer temperature (MST) was calculated using a lake calibration (Pearson et al., 2011):

$$\text{MST} (^{\circ}\text{C}) = 20.9 + 98.1 * [\text{Ib}] - 12 * [\text{IIa}] - 20.5 * [\text{IIIa}] \quad (\text{RSME} = 2.4^{\circ}\text{C})$$

The square brackets in this formula indicate that the value is relative to the sum of the brGDGTs (Ia+IIa+IIIa+Ib+IIb+IIIb+Ic+IIc+IIc).

3.4. Environmental parameters and bulk geochemical analysis

Soil pH data (Table 3) were obtained from published results (Santruckova et al., 2003), and accessible databases (Stolbovoi and Sheremet, 2002). The pH measurements reported in the Russian soil database were performed in a 1:5 soil/water mix, which results in pH values 0.1–0.5 units higher than those obtained from 1:2.5 soil/water ratios (Stolbovoi and Sheremet, 2002). We corrected for this offset by subtracting 0.5 pH units from the values provided. The particulate organic carbon (POC) content of river SPM samples on the filter was measured using a Flash 2000 Organic Elemental Analyzer.

3.5. Numerical analysis

The principal component analysis based on the correlation matrix was performed using the R software package for statistical computing. We performed an unconstrained Q-mode PCA on the standardized relative brGDGT values, excluding the relative amount of brGDGT IIIc and IIIc', as the low abundance of these compounds did not allow quantification in several samples. The brGDGT scores are calculated proportional to the eigenvalues, and the site scores are calculated as the weighted sums of the species scores. The linear correlation coefficient between the IR_{IIIa'} and IR_{IIIb'} was calculated and the regression line plotted using the R software package for statistical computing.

Table 5. Overview of BIT, CBT, MBT, reconstructed pH, reconstructed MAT using the soil calibration (Peterse et al., 2012) and reconstructed MST using the lake calibration (Pearson et al., 2011).

Station	Lipid type	BIT	CBT	MBT'	Calc pH	Calculated MAT (°C)	Calculated MST (°C)
						Soil calibration	Lake calibration
Se1	CL	0.92	0.48	0.16	7.0	2.9	19.6
	IPL	0.48	0.47	0.14	7.0	2.5	18.2
M1	CL	0.99	0.88	0.10	6.2	-1.2	10.5
	IPL	0.96	0.89	0.13	6.1	-0.2	11.3
M2	CL	0.98	0.85	0.14	6.2	0.5	12.1
	IPL	0.90	0.83	0.15	6.3	0.8	13.4
Y1	CL	0.95	0.67	0.14	6.6	1.5	16.6
	IPL	0.83	0.72	0.10	6.5	-0.1	16.0
Y2	CL	0.99	0.53	0.08	6.8	0.4	14.9
	IPL	0.93	0.54	0.09	6.8	0.6	16.2
Y3	CL	0.97	0.67	0.14	6.6	1.4	16.5
	IPL	0.93	0.61	0.11	6.7	0.8	15.8
Y4	CL	1.00	0.64	0.13	6.6	1.1	15.6
	IPL	1.00	0.57	0.15	6.8	2.2	16.9
Y5	CL	0.98	0.64	0.14	6.6	1.4	16.3
	IPL	0.92	0.57	0.12	6.8	1.4	15.9
Y6	CL	0.98	0.59	0.12	6.7	1.1	14.2
	IPL	0.93	0.54	0.13	6.8	1.9	17.1
Y7	CL	1.00	0.73	0.13	6.5	0.7	15.1
	IPL	1.00	0.72	0.10	6.5	-0.1	14.5
Y8	CL	0.99	0.75	0.16	6.4	1.5	14.6
	IPL	0.94	0.71	0.14	6.5	1.1	15.1
Y9	CL	0.99	0.78	0.16	6.4	1.3	14.2
	IPL	0.94	0.73	0.13	6.5	0.8	14.3

4. Results

4.1. Measured water parameters

Table 2 shows that the Yenisei River water temperature varied between 9.0°C and 12°C, with similar values for the mountainous Irkut River (10.8 °C) and higher values for the southern Selenga River (16.9°C). The pH was measured only in three Yenisei tributaries and varied between 5.6 and 8.4.

4.2. Abundance of crenarchaeol and brGDGTs

In the CL fraction of Yenisei River SPM the concentration of crenarchaeol (0.0-3.1 ng.L⁻¹ and 0.0-6.6 ng.g⁻¹ POC) was an order of magnitude lower than that of the brGDGTs (0.3-69 ng . L⁻¹ and 29-470 ng.g⁻¹ POC) (Table 4). The dominance of brGDGTs in the SPM was reflected in high BIT index values, between 0.92 and 1.00 (Table 5). Crenarchaeol IPL percentages fluctuated between 21 and 45 % in the river SPM. The IPL percentage of brGDGTs was generally lower, ranging from 5 to 20% (Table 4). The BIT value of the IPL fraction was between 0.0 and 0.44 units lower than the BIT values of the CL fraction (Table 5).

4.3. Distribution of brGDGTs

The relative abundances of individual brGDGTs in the CL and IPL fractions are given in Table 6. Fig. 3A illustrates a typical distribution of brGDGTs in the Yenisei SPM. BrGDGT CL distributions were dominated by brGDGTs without cyclopentane moieties. In the CL fractions of the river SPM, the recently described hexamethylated brGDGT IIIa' (De Jonge et al., 2013) was the most abundant brGDGT in 6 out of 13 river SPM samples and second or third in abundance in the others (Table 6). In the IPL fraction, the brGDGT IIIa' was the most abundant in 9 out of 13 samples. In the remaining samples, brGDGT IIa was the most abundant brGDGT. Application of a silica column for the separation of GDGTs (De Jonge et al., 2013) resulted in an improved separation of the hexamethylated brGDGT isomers (Fig. 3C). It is important to note that the pentamethylated brGDGT (IIa) has been shown to consist of two co-eluting isomers in a Siberian soil (De Jonge et al., 2013). Although the resolution was not good enough for separate quantification on the silica column (Fig. 3C), we observed a broad peak compared to the tetramethylated brGDGT and some separation, indicating the presence of a mixture of the two pentamethylated brGDGT isomers (IIa and IIa') in Yenisei SPM.

The GDGT ratios were calculated according to Peterse et al. (2012), taking into account that for this calibration study the hexamethylated brGDGTs were not separated (see experimental). The MBT' value of both the CL and IPL fraction varied between 0.09 and 0.16. CBT values of the river SPM varied between 0.48 and 0.88 for the CL fraction and between 0.47 and 0.89 for the IPL fraction (Table 5).

5. Discussion

5.1. The brGDGT distribution in Yenisei river SPM

The presence of an abundant partially co-eluting peak with brGDGT IIIa has been reported in Siberian Pleistocene loess-paleosol sequences by Zech et al. (2012). A second peak was also observed in a Siberian peat, collected in a lake floodplain, where the hexamethylated brGDGTs were shown to consist of four structurally distinct isomers (De Jonge et al., 2013). The first eluting peak contains the compound brGDGT IIIa as described by Weijers et al. (2006a), with two 5,13,16-trimethyloctacosane moieties and an asymmetrical molecule containing a 13,16-dimethyl octacosane and a 5,13,16,24-tetramethyl octacosane moiety. The second eluting peak (brGDGT IIIa') contains two hexamethylated compounds, a brGDGT that possesses two 6,13,16-trimethyloctacosane moieties and an asymmetrical isomer containing a 13,16-dimethyl octacosane and a 6,13,16,23-tetramethyl octacosane moiety (De Jonge et al., 2013).

An improved chromatographic separation allowed us to quantify the brGDGTs IIIa' in an environmental dataset for the first time. The relative abundance of brGDGT IIIa' in the SPM of the Yenisei is 22-51% of total of brGDGTs. Furthermore, the hexamethylated brGDGTs containing one and two cyclopentane moieties were also revealed as two peaks (Fig. 3B). These isomers are found in varying amounts (0.5-2.7% and 0.0-0.4% of total brGDGTs). A cross-plot of the $IR_{IIIa'}$ vs. $IR_{IIIb'}$ reveals a significant correlation (Fig. 5; p -value < 0.05). Although the $IR_{IIIc'}$ values plot closely to the $IR_{IIIb'}$ values, the dataset is too small to observe a significant correlation with $IR_{IIIa'}$. Because of this and the similar elution characteristics, we postulate that the hexamethylated brGDGTs with cyclopentyl moieties (IIIb and IIIc) also have later eluting isomers (IIIb' and IIIc') that are characterized by methyl groups at the $\alpha 6$ and $\omega 6$ position of the alkyl chains and are probably derived from the same biological source as IIIa'.

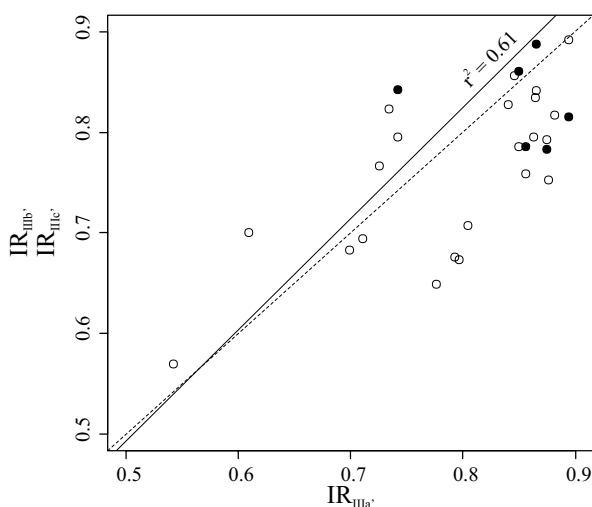


Fig. 5. A cross-plot comparing the isomer ratios (IR) of the brGDGT IIIa' versus the IR of brGDGT IIIb' (white symbols) and IIIc' (black symbols). The linear regression line between $IR_{IIIa'}$ and $IR_{IIIb'}$ is plotted with a full line and the corresponding correlation coefficient (r^2) value given. The 1:1 ratio is plotted with a dotted line.

To investigate the general relationships between the branched GDGTs after quantification of all hexamethylated isomers using our improved chromatographic separation, we performed a principal component analysis (PCA) on the standardized relative abundances of the river SPM brGDGTs. The relative amounts of brGDGTs IIIc and IIIc' have not been included, as they are present below the limit of quantification in the majority of the samples. The first three principal components represent 36, 21 and 14% of the total variance, respectively (Fig. 6A, 6B). The scores provide us with a summary of the relationship between the stations and the variables (Fig. 6C, 6D).

Table 6. Overview of the relative abundance of individual brGDGTs of the CL and IPL fractions. N.d. is not detected.

Station	Lipid type	Relative amount per compound (%)											
		Ia	Ib	Ic	IIa ^a	IIb ^a	IIc ^a	IIIa	IIIa'	IIIb	IIIb'	IIIc	IIIc'
Se1	CL	10.3	4.3	0.6	32.0	9.7	0.6	5.8	34.4	0.5	1.6	0.1	0.2
	IPL	9.2	3.9	0.5	30.8	9.5	1.6	9.3	32.4	0.9	1.7	n.d.	n.d.
M1	CL	7.8	1.7	0.2	30.0	3.3	2.8	28.1	25.3	0.4	0.5	n.d.	n.d.
	IPL	10.5	2.0	0.3	31.4	3.4	0.6	26.5	23.3	0.7	1.3	n.d.	n.d.
M2	CL	11.9	2.0	0.3	30.2	4.0	0.5	22.9	27.0	0.5	0.6	n.d.	n.d.
	IPL	12.3	2.2	0.4	29.5	4.0	1.8	19.1	29.7	0.3	0.7	n.d.	n.d.
Y1	CL	10.2	3.0	1.0	27.4	5.1	0.8	10.6	40.5	0.4	0.9	n.d.	n.d.
	IPL	9.0	2.1	n.d.	25.3	4.4	0.9	7.0	49.8	0.4	1.1	n.d.	n.d.
Y2	CL	6.1	1.8	0.2	32.0	9.4	0.3	6.4	41.0	0.4	2.1	0.0	0.3
	IPL	6.8	2.2	0.1	22.5	6.2	0.7	7.9	50.6	0.5	2.7	n.d.	n.d.
Y3	CL	11.3	2.0	0.4	27.1	6.1	0.4	5.3	44.6	0.2	2.1	0.1	0.3
	IPL	8.9	1.8	0.3	25.1	6.5	0.9	6.4	47.4	0.5	2.2	n.d.	n.d.
Y4	CL	9.6	2.0	0.8	24.6	5.8	0.5	8.7	45.6	0.4	2.1	n.d.	n.d.
	IPL	11.7	2.7	n.d.	24.4	6.9	1.1	10.2	39.9	1.0	2.1	n.d.	n.d.
Y5	CL	10.7	2.1	0.4	27.2	6.6	0.4	6.2	43.4	0.5	1.9	0.1	0.3
	IPL	9.1	2.4	0.5	26.0	7.1	1.4	10.0	41.0	0.8	1.8	n.d.	n.d.
Y6	CL	8.8	2.0	0.4	24.4	6.6	0.4	14.0	40.1	0.6	2.2	0.1	0.4
	IPL	10.0	2.5	0.4	24.1	7.3	0.9	8.0	43.5	0.5	2.7	n.d.	n.d.
Y7	CL	10.4	1.8	0.3	26.8	5.1	0.3	7.9	44.8	0.5	1.7	0.0	0.3
	IPL	8.2	1.5	0.2	25.2	4.8	0.4	7.8	49.1	0.6	2.2	n.d.	n.d.
Y8	CL	13.0	2.2	0.4	29.6	5.4	0.5	12.9	34.2	0.4	1.4	n.d.	n.d.
	IPL	10.9	2.6	0.1	28.6	5.0	0.7	13.2	36.6	0.4	1.8	n.d.	n.d.
Y9	CL	13.2	2.0	0.4	29.8	5.1	0.5	13.6	33.5	0.6	1.3	n.d.	n.d.
	IPL	10.6	2.4	0.1	28.7	5.0	0.5	15.2	35.2	0.8	1.6	n.d.	n.d.

^a In a Siberian peat in the Yenisei watershed, IIa was shown to consist of two isomers that co-elute (De Jonge et al., 2013). In this study, the contribution of isomers to the areas of IIa, IIb and IIc is probable but remains to be proven.

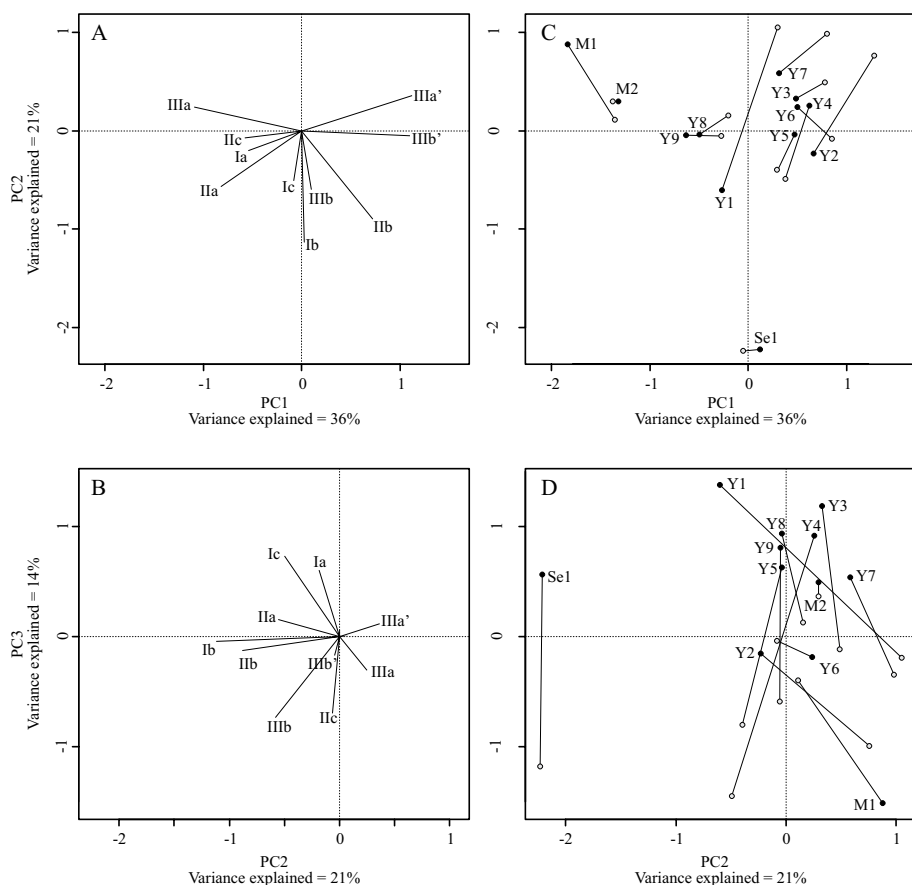


Fig. 6. Biplot of the principal component analysis based on the relative abundance of the river SPM brGDGTs. The loadings of the variables (A, B) and the scores of the sites (C, D) are plotted on the first three components. The first component accounts for 36% of the variance, the second component for 21%, the third component for 14%. The score of each station is calculated using the relative abundance of each compound per station and its loading on the PC. Scores based on a CL fraction are indicated with a black symbol and per station connected with the scores based on the IPL fraction, indicated with a grey symbol.

The first principal component reflects the strong correlation between the relative abundance of the novel brGDGT isomers IIIa' and IIIb' (Fig. 6A) and illustrates their negative correlation with the relative abundance of brGDGT IIIa. SPM from the mountainous source area (M1 and M2) scores negatively on the first principal component (Fig. 6C), in line with the relatively low abundance of the novel brGDGT isomers IIIa', IIIb' and also brGDGT IIb (Fig. 6C) and high relative abundance of IIIa (Table 6). SPM collected from the main stream of the Yenisei River (Y2-Y7) scores higher on principal component 1 (Fig. 6C) and contains higher relative abundances of IIIa' and IIIb' (Table 6).

The pH and MAT were previously shown to explain most of the variation within the brGDGT distributions in soils globally (Weijers et al., 2007a; Peterse et al., 2012). Also, earlier studies on

the distribution of brGDGTs in freshwater environments have shown that mostly MAT/MST, but also pH to a varying degree, explain part of the variation in freshwater brGDGTs (Tierney et al., 2010; Pearson et al., 2011; Zhu et al., 2011a). Our environmental dataset is incomplete and based on point-measurements, so it is impossible to assess to what extent the variation we observe is explained by pH and water temperature. However, the scores of the various brGDGTs on PC2 and PC3 seem to reflect their dependency on MAT and pH as described in the soil and lake calibrations studies. Weijers et al. (2007a) and Peterse et al. (2009a) have described an increase in cyclization of brGDGTs as a response to pH. This seems to be captured by the second principal component, where brGDGTs Ib, IIb and IIIb, all with one cyclopentane moiety, score high on the second principal component, as does the brGDGT Ic with two cyclopentane moieties. Especially the Selenga River SPM (Se1) scores high on this component, which is possibly related to differences in its watershed soil or water chemistry (Fig. 6D). The pH of the water sample at this station was indeed much higher than at other stations (Table 2), although there is only a single measurement. A high relative abundance of tetramethylated brGDGTs has been shown to be positively correlated to the MAT for a global soil dataset (Weijers et al., 2007a, Peterse et al., 2012). This seems to be captured on the third principal component, where the tetramethylated brGDGTs Ia and Ic have a high positive loading while most hexamethylated brGDGTs and pentamethylated brGDGT IIc have negative loadings (Fig. 6C). Consistent with this hypothesis, the high mountainous station M1 plots separately on this component, indicating a cold signal (Fig. 6D). The IPL fractions typically score more negative than the corresponding CL fraction, consistent with the often lower relative abundance of brGDGT Ia and Ic in the IPL fraction (Table 5). We hypothesize that the offset in the living or recently living material is caused by the colder temperature in September compared to July/August for the Yenisei samples. The SPM collected at site Se1 may carry a warmer CL signal from the downstream Mongolian steppe.

5.2. Sources of brGDGTs in the Yenisei River

Analysis of the river SPM shows the presence of the full suite of brGDGTs in the river SPM, in both the core lipid (CL) and intact polar lipid (IPL) fractions. Their presence fits with the hypothesis that transport of brGDGTs by rivers is a mechanism for the delivery of these lipids to coastal marine sediments (Hopmans et al., 2004). The BIT indices of the CL fraction of the riverine SPM ranged from 0.94 to 0.99 (Table 5), at least as high as BIT-values encountered in global soils (Hopmans et al., 2004; Weijers et al., 2006b; Schouten et al., 2013a). The BIT-index reported here is comparable to the values encountered in the Amazon River SPM (Kim et al., 2012; Zell et al., 2013) and Yangtze River sediments, China (Zhu et al., 2011a; Yang et al., 2013) and higher than values reported from the Têt and Rhone River, France (Kim et al., 2007) and the Rhine and Meuse, N-Europe (Herfort et al., 2006). However, when comparing BIT values, it is important to keep in mind that absolute values can vary between labs (Schouten et al., 2009).

BrGDGTs in aquatic systems can be derived from two major sources. First, they are eroded from watershed soils and transported with run-off (Weijers et al., 2007a). Secondly, brGDGTs are produced by micro-organisms living within fresh and marine water systems (Tierney and Russell, 2009; Peterse et al., 2009a). The resulting distribution will thus often be a mixture of

both sources, complicating the interpretation of MBT/CBT proxies. Previous studies on the brGDGT distributions have recognized systems that are dominated by soil input (Niemann et al., 2012), by in-situ production (e.g. Tierney et al., 2012) or by a mixture of these end members (e.g. Zell et al., 2013). For the Yenisei River, distributions dominated by soil-input would be expected to reflect the low pH of the catchment soils (Table 3) and the strong temperature gradient imposed on the soils (Table 1). On the other hand, brGDGTs produced in situ in the river water should reflect its characteristics: the absence of a strong temperature gradient and a stable pH of ca. 7.

The PCA analysis revealed that variations in the brGDGT distributions may partly be explained by changes in pH and temperature as has been reported before for other environmental datasets. Therefore, it is a logical approach to calculate pH and temperature from the brGDGT composition to shed light on their origin. We have reconstructed variations in MAT and pH using both soil (Peterse et al., 2012) and lake calibrations (Pearson et al., 2011). A complication in this respect is the relatively high abundance of 6-methyl isomers of the hexamethylated brGDGTs in Yenisei SPM (Table 6), since the presence of these components was unknown at the time of these calibrations. Since all published studies on soil calibrations used LC separation methods that did not separate these isomers (see experimental), we used the summed relative abundance of the 5- and 6-methyl isomers in these calculations. The lake calibration is based on the abundance of brGDGT IIIa after exclusion of brGDGT IIIa', according to commonly adopted integration protocols (Schouten et al., 2009). For the aquatic calibration, we thus use only the area of brGDGT IIIa but not of IIIa'.

Based on the chromatograms (Fig. 3), it is likely that, next to the presence of large amounts of hexamethylated brGDGT isomers, a substantial amount of 6-methyl isomers of the pentamethylated compounds (IIa, IIb and IIc) is present. The effect of the presence of these pentamethylated isomers on the proxy calculations is possibly large, as this isomer of brGDGT IIa was shown to equal 50% of the total amount of brGDGT IIa in a Siberian peat, collected in a lake floodplain (De Jonge et al., 2013).

5.2.1. The CBT-index and reconstructed river pH

Based on the global soil calibration by Peterse et al. (2012), the reconstructed pH varies between 6.1 and 6.9 for the CL fraction (Table 5). The pH is uniform downstream, with slightly lower values in SPM originating closer to the mountainous source area of the Yenisei and at high latitudes (Table 5, Fig. 7A). The IPL fraction-based pH (6.1-7.0) mimics that of the CL fraction closely, with a maximum offset of 0.15 pH units. Overall, the pH values are substantially higher than those of soils in the Yenisei watershed (pH 3.0-6.8, Table 3, Fig. 8).

Taking into account the pH reconstruction calibration error of 0.8 (Peterse et al., 2012), only soils with pH values >5.3 are likely sources of these brGDGTs. However, such soils are only encountered in the southern part of the watershed (between 52 and 56°N), in agriculturally more developed and forested areas (Table 3). However, the northern part of the watershed (an extensive area of low pH peatland that typically contains high amounts of brGDGTs (cf. Weijers et al., 2006a)) is expected to contribute brGDGTs with a low degree of cyclisation (resulting from the low pH), as it sources two major tributaries of the Yenisei River. However,

a decrease of the reconstructed pH from brGDGTs in riverine SPM after the inflow of these tributaries is not evident and, therefore, it is unlikely that the brGDGTs in the riverine SPM are predominantly soil-derived. We propose that the brGDGTs in the Yenisei River SPM are primarily derived from in-situ production since the reconstructed pH is close to that of the river water. The similar reconstructed pH values of the IPL fraction supports this hypothesis, as this value is likely to reflect living or recently living biomass.

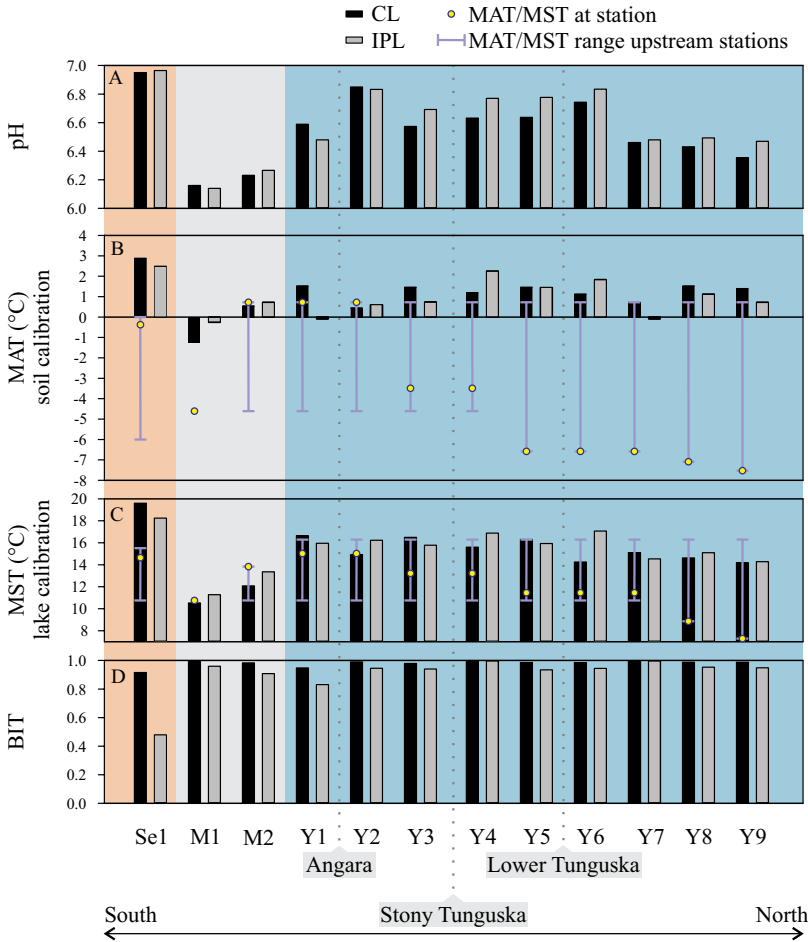


Fig. 7. Barplots showing the variation in GDGT-based proxies, from south to north. Black bars are values based on the CL fraction, grey bars are the values based on the IPL fraction. Background colors denote tributaries from different parts of the watershed. Orange; Selenga watershed. Grey; Angara watershed. Blue; Yenisei River samples. The dotted grey line shows where major tributaries drain in the Yenisei river. A) reconstructed pH, B) Reconstructed MAT, based on the soil calibration, represented by the black and grey bars. The MAT of all upstream weather stations is summarized by the purple line. The yellow dot indicates the MAT at the station. C) Reconstructed MST, based on the lake calibration, represented by the black and grey bars. The MST of all upstream weather stations is summarized in the purple line. The yellow dot indicates the MST at the station. D) BIT-index.

CBT-reconstructed pH values have been previously reported for riverbed sediments and match river water pH (Tierney and Russell, 2009; Tierney et al., 2010; Zhu et al., 2011a; Yang et al., 2013). The pH of the Yenisei River is reported to be constant downstream and over time (Sorokovikova, 1997), with values between 7.0 and 7.3 (± 0.2) along the river. The reconstructed pH values (between 6.1 and 6.8) are only slightly lower than the Yenisei River water pH. This offset is larger for the more alkaline upstream rivers. Here, the measured pH values are more variable and reconstructed pH values do not reflect the magnitude of these variations well (Table 5; Fig. 7A). This larger offset is most probably due to the variation in pH (up to 2 pH units daily) that has been encountered in weakly buffered alkaline streams (Nimick et al., 2011).

5.2.2. Reconstruction of temperatures

Similar to the pH values, MBT⁺/CBT-reconstructed temperatures using the soil calibration along the main part of the Yenisei River are remarkably constant (Fig. 7B). They do not reflect the large changes in MAT imposed on the soils from south to north (from 0.9 to -10°C; Table 1). The reconstructed Yenisei SPM MAT varies between -1.2 and 2.9°C, which is up to 9°C higher than the observed MAT imposed on local and upstream soils (Fig. 7B). Thus, both the absolute values of MAT reconstructed and the absence of a north-south trend do not fit with the MAT imposed on the soils of the watershed. To test whether the distributions fit with a freshwater source, we use a global lake calibration that is based on the MST (Pearson et al., 2011). The reconstructed temperatures of the main stream are between 14.2°C and 17.1°C for both the IPL and CL fractions (Table 5; Fig. 7C), which is only slightly higher than the measured temperatures at the time of sampling (Table 2). The absolute values of this MST reconstruction fit the MST temperatures of weather stations in the area of the upper reaches of the Yenisei River (Fig. 7). The MST of weather stations at higher latitudes is somewhat lower than the reconstructed MST but this is in line with the fact that warmer river water is transported towards higher latitudes before it can adjust to the colder MST downstream. In-situ production of brGDGTs in the river water can thus account for the absence of a latitudinal gradient in the brGDGT distributions. The temperatures reconstructed for the mountainous upstream rivers also give a reliable temperature estimate. The mountainous rivers that flow into the Angara River and the SPM downstream the inflow of the Angara River shows a contribution of a colder signal (Table 5, Fig. 7B).

5.2.3. Importance of in-situ produced versus soil-derived brGDGTs

Based on the distribution of brGDGTs, this study thus indicates that the Yenisei River is an example of a river system where brGDGTs are dominantly produced in-situ. This is in contrast with previous studies by Kim et al. (2012) and Zell et al. (2013) on the Amazon River that concluded that soils are the dominant source of brGDGTs (70-80%). On the other hand, Zhu et al. (2011a) concluded that the brGDGT signal of the Yangtze River catchment was overprinted by brGDGTs produced in-situ. Based on a study in a hydroplant lake situated on the same river, Yang et al. (2013) endorsed this conclusion. The relative contribution of in-situ produced brGDGTs is thus variable between river systems.

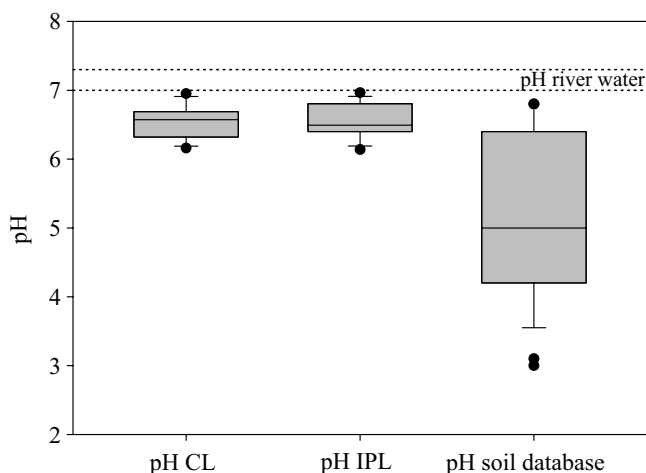


Fig. 8. Comparison of boxplots of the reconstructed pH based on the CL fraction and IPL fraction with the pH values from the soil database and the Yenisei River water. The first, second and third quartiles are indicated.

We postulate that the contribution of in-situ produced brGDGTs is dominant in the Yenisei River because of the relatively low amounts of soil-derived brGDGTs. However, the brGDGT concentration in the Yenisei River (Table 4) is comparable to other river systems. The concentration of brGDGTs in the Selenga River is comparable to previous studies of rivers in France and Northern Europe (Herfort et al., 2006; Kim et al., 2007), but it is up to an order of magnitude lower than found in the Amazon River (Kim et al., 2012). The concentration of GDGTs at the other stations is lower, only comparable to the Têt and Rhone rivers during time periods other than flood events (Kim et al., 2007). The higher brGDGT concentration in the Selenga River corresponds with a high amount of POC. Normalized on the POC content, the brGDGT concentrations are similar at all stations (Table 4). In this way, brGDGT concentrations at all stations exceed the lowest values reported from the European Rivers (Herfort et al., 2006; Kim et al., 2007), and are comparable to the POC-normalized concentrations reported for the Amazon River during the low water season (Kim et al., 2012; Zell et al., 2013) and are only one order of magnitude lower than the values reported for the high water season (Kim et al., 2012).

The niche of the aquatic brGDGT source organisms can be two-fold; first, it can be derived from the water-logged wetlands around shallow lakes that source the Yenisei River water. Water-logged soils have been described to have a brGDGT distribution more alike lakes (Loomis et al., 2011). We have described one peat, sampled in a lake's floodplain, in De Jonge et al. (2013), whose brGDGT distributions are very similar to the river SPM at site M1, sampled slightly downstream (pH reconstructed=6.7, MAT reconstructed=0.7). Or, the brGDGTs can be produced in the river channel. The residence time of the SPM can be estimated based on the propagation speed and the length of the river. Using the propagation speed of the Lena River, a major Siberian River located east of the Yenisei, of 88km.day⁻¹ (Smith and Pavelsky, 2008), we can calculate a water transport time of 62 days, from source to the river mouth. This is a

minimum for the residence time of the SPM, as all natural river channels contain “dead zones”, or areas of low velocity. Mixing processes carry suspended sediment into these low-velocity zones where particles settle out and accumulate until they are resuspended and transported further downstream. Thus, these zones can act as a source area for the bacterial population. Furthermore, bacterial cells and lipids can be sourced from the hyporheic zone, the layer of saturated sediments and surface water beneath the river channel (Dobson, 1998). During the summer season, turnover times for attached and free-living bacteria in rivers have been reported in eg. Edwards and Meyer (1986), with an average of two weeks. This is significantly shorter than the residence time. The time required for the IPL fraction to be (partly) degraded to CL strongly depends on the polar headgroup. BrGDGT lipids with a labile phosphatidyl headgroup have been described in the Amazon River SPM by Zell et al. (2013), where they indicate freshly produced material.

The low amount of soil-derived brGDGTs in the Yenisei River can be explained by a low amount of horizontal run-off during the sampling season. The SPM samples were taken several months after the freshet, when the precipitation that accumulated as a snow layer during autumn, winter and spring is released as a large meltwater pulse into the Kara Sea. About 30% of the total annual water budget and 42% of the total annual sediment budget are discharged in June (Lammers and Shiklomanov, 2000). This indicates that the brGDGT signal in the Yenisei River SPM may thus be very different during the freshet, and an integrated annual signal may possibly match the soil brGDGT signature better.

6. Conclusions

This study represents the first comprehensive record of brGDGT distribution in a river that crosses several climatic zones in a north-south direction, revealing insights in the site of their production. At all stations, in both the CL and IPL fraction, the full suite of brGDGTs is present. The brGDGT distribution is very uniform downstream, in contrast to the strong climate gradients crossed. As the reconstructed pH is too high for the surrounding soils and the gradient in MAT of the Yenisei watershed is not reconstructed, we conclude that brGDGTs in the SPM of the Yenisei River and tributaries do not reflect the watershed soil characteristics. The absence of strong changes in the distribution can be explained if the brGDGTs are produced in the river water, as it has a relatively constant pH and temperature downstream. The pH of the river water is reconstructed well using the soil calibration and the MST is reconstructed well using a lake calibration. The brGDGTs in the Yenisei River and tributary SPM thus likely reflect an in-situ produced aquatic signal. The absence of a soil-derived signal can be due to the low soil input at the time of sampling (end of summer). We hypothesize that SPM signal of the Yenisei River may be very seasonal, as much more soil material will be transported in the river during the freshet. To assess these seasonal changes, further research is required.

The exceptional brGDGT distribution was shown to be dominated by the newly described brGDGT IIIa'. This compound was shown to be an important constituent of the brGDGTs in the SPM (between 22 to 51% of all brGDGTs). The chromatographically similar isomers brGDGTs IIIb' and IIIc' are tentatively identified as having the same shift in methylation from the $\alpha 5$ and/or $\omega 5$ to the $\alpha 6$ and/or $\omega 6$ position. Also, the chromatography of the pentamethylated brGDGT

Ila and IIb in the dataset suggests the presence of an isomer with methylation at the $\alpha 6$ and/or $\omega 6$ position.

At the moment it is unclear if both isomeric forms are biosynthesized independently, or if isomers with a methylation on the $\alpha 6$ position are produced as an alternative to the corresponding isomer with a methylation on the $\alpha 5$ position of the alkyl chain. If they are biosynthesized independently, whether these compounds react to environmental factors is unknown. The hexamethylated brGDGT isomers have been included in soil calibration as defined in Weijers et al. (2007a) and Peterse et al. (2012) and excluded from lake calibrations (Pearson et al., 2011), following integration protocols. Using an improved chromatographic method, this study and previous studies indicate that these isomers can be abundant in the environment. Improving the separation and quantifying the hexa- and pentamethylated isomers will be required to assess the relevance of these isomers for the pH and temperature reconstruction. The logical next step will be to recalibrate the soil and lake calibrations and to evaluate if the exclusion or inclusion of hexa- and pentamethylated brGDGT isomers can explain some of the scatter observed in these calibrations.

7. Acknowledgments

The three anonymous reviewers are thanked for providing constructive comments that have improved this manuscript. This work, performed in the framework of the memorandum NIOZ-VNIIOkeangeologia for Arctic research, was funded by research project 819.01.013, financed by the Netherlands Organization for Scientific Research (NWO) and the European Research Council under the EU Seventh Framework Programme (FP7/2007-2013) / ERC grant agreement n° [226600].



Photo by Cindy De Jonge

Impact of riverine suspended
particulate matter on the branched
glycerol dialkyl glycerol tetraether
composition of lakes: The outflow
of the Selenga River in Lake
Baikal (Russia)

5

Cindy De Jonge, Alina Stadnitskaia,
Andrey Fedotov, Jaap S. Sinninghe Damsté

Submitted to Organic Geochemistry

ABSTRACT

Branched glycerol dialkyl glycerol tetraethers (brGDGTs) are bacterial membrane lipids occurring in several environments, including soils, rivers and lakes, whose distribution varies with temperature and pH, although this dependence is apparently not the same for the different producing environments. Mixing of brGDGT sources may thus complicate palaeoenvironmental reconstruction. The extent to which brGDGTs in a lake outflow reflect the brGDGT distribution delivered by upstream rivers was studied for Lake Baikal (Russia), one of the largest freshwater lakes worldwide. Fifteen brGDGTs were quantified in suspended particulate matter (SPM) of the Selenga River and its outflow in the lake. The river and lake SPM had rather different brGDGT distributions. The riverine brGDGT distribution was still apparent in the SPM of the lake surface water 5 km from the river mouth, but shifts in the brGDGT distribution were already apparent in the SPM of the surface water after 1 km. Based on the brGDGT distributions of the SPM of the Selenga outflow and that of the lake, conservative mixing between the river and the lake brGDGT distributions could not fully explain the observed shifts in brGDGT distributions. Both preferential degradation and in situ production of brGDGTs in the surface and, especially, bottom water of the river outflow were potentially responsible. This implies that a riverine signal delivered to a lake can be modified prior to being transported downstream. The lacustrine brGDGT distribution, that possibly reflected a mixture of mountainous and Selenga River SPM, was not recognized in downstream Yenisei River SPM. The watershed of Lake Baikal thus does not seem to contribute to the brGDGTs transported to the marine system. As many large rivers have major lakes in their watershed, this has implications for palaeoclimate reconstruction from river fan sediments globally.

1. Introduction

Branched glycerol dialkyl glycerol tetraethers (brGDGTs) are bacterial membrane lipids found in a variety of settings: soils, lacustrine and marine suspended particulate matter (SPM) and sediments and hot springs. Their source organisms probably fall within the Acidobacteria, based on environmental (Weijers et al., 2009a; Peterse et al., 2010) and culture studies (Sinninghe Damsté et al., 2011; 2014). Their main application is as palaeoclimate proxies. In a dataset of global soils, the structural diversity of the brGDGT components was shown to correlate with the prevailing soil pH and mean annual air temperature (MAT; Weijers et al., 2007a). Nine brGDGT components were described that possess 4 to 6 methyl substituents (branches) on the linear C₂₈ alkyl chains (Sinninghe Damsté et al., 2000) and contain up to two cyclopentyl moieties formed by internal cyclization (Fig. 1; Schouten et al., 2000; Weijers et al., 2006a). The cyclization of branched tetraethers (CBT) and methylation of branched tetraethers (MBT) are two brGDGT indices (Weijers et al., 2007a) that have been successfully applied to reconstruct the palaeoclimatic changes in palaeosoils (e.g. Peterse et al., 2011), speleothems (Blyth and Schouten, 2013), lake sediments (e.g. Niemann et al., 2012), but initially in marine sediments (e.g. Weijers et al., 2007b; Bendle et al., 2010). Prior to their incorporation into marine and lacustrine sediments, they were understood to be eroded from soils and transported by rivers through upstream lakes. The brGDGT distribution was thus assumed to reflect the distribution present in watershed soils and to remain unaltered during this process.

Contrasting brGDGT distributions between lake systems and their surrounding soils provided the first indications for in situ production of brGDGTs in aquatic systems (e.g. Tierney and Russell, 2009). Although the temperature dependence is different from that in soils, the distribution of aquatic brGDGTs also varies with prevailing MAT, and to some extent with depth and pH (e.g. Tierney et al., 2010; Pearson et al., 2011; Sun et al., 2011; Loomis et al., 2012, 2014b). There is thus a growing body of evidence supporting in situ production of brGDGTs in lakes, but the niche of the source organism has not been constrained. The concentration of lacustrine brGDGTs was shown to increase below the lake thermocline, pointing towards a preference for environments with low O₂ concentration (e.g. Sinninghe Damsté et al., 2009; Buckles et al., 2014a). However, a recent study of brGDGTs in a temperate lake (Loomis et al., 2014a) found that brGDGTs were produced throughout the water column. Further possible mechanisms influencing the brGDGT distributions are shifts in bacterial community, possibly prompted by a large shift in nutrients or by the transition between river and lake biomes (Loomis et al., 2014a and references therein). Although in situ production of brGDGTs has been described to occur in rivers (e.g. Kim et al., 2012; Zell et al., 2013, 2014; De Jonge et al., 2014a), a lacustrine in situ produced signal may be significantly different from that of its inflowing river (Tierney and Russell, 2009; Buckles et al., 2014b). As large lakes are often present in large river drainage basins, lacustrine in situ production may result in the introduction of lacustrine brGDGTs in downstream rivers and ultimately in marine sediments. Large lakes in the drainage basin of river systems may thus have an effect on palaeoclimate brGDGT reconstruction for river fan marine sediments.

The aim of this study was to investigate the extent to which the brGDGT distribution delivered by a river can propagate in a large lake and to compare this effect with the brGDGT distribution exported from the lake by river outflow. Furthermore, we tried to constrain the environmental

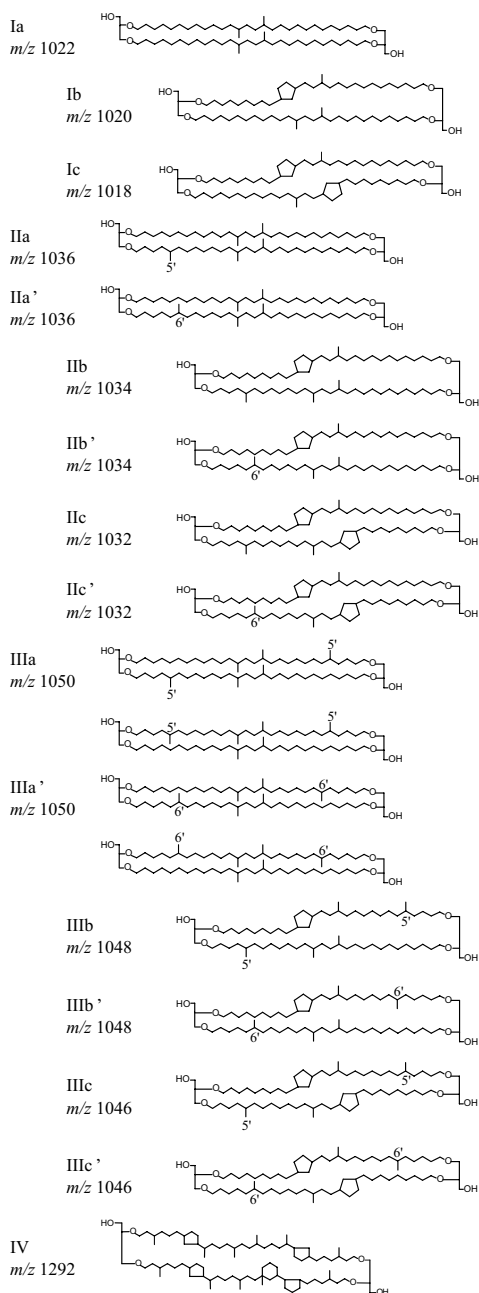


Fig. 1. Chemical structures of branched GDGTs (I-III) and crenarchaeol (IV). The chemical structures of the hexa- and pentamethylated brGDGTs with cyclopentyl moiety(ies) IIb', IIc', IIb' and IIIc' are tentatively assigned.

parameters that influence lacustrine in situ production of brGDGTs. Although in situ production of brGDGTs in lakes has been extensively documented (e.g. Tierney and Russell, 2009; Loomis et al., 2011, 2014a; Buckles et al., 2014a), this is the first study to evaluate the delivery and export of riverine brGDGTs to and from a lake system. Furthermore, the above previous studies are all based on a dataset of nine brGDGTs, as the analytical procedure used did not allow separating the recently described 6-Me brGDGTs (De Jonge et al., 2013). The abundance of these novel brGDGTs was recently shown to be high in a Siberian River system (De Jonge et al., 2014a) and to be highly variable in a set of globally distributed soils (De Jonge et al., 2014b).

This study describes the full suite of fifteen brGDGTs in a major river (Selenga River) that drains northern Mongolia and southern Siberia before and after its inflow to the world's largest freshwater lake (Lake Baikal). We evaluate the brGDGT concentration and distribution in the Selenga River outflow, where in situ production and preferential degradation could possibly affect the lacustrine brGDGT distributions. Furthermore, the signal exported from the lake was compared with the brGDGT distribution in both Selenga River and the mountainous Irkut River, to evaluate whether or not riverine brGDGTs alone could explain the brGDGT signal exported.

2. Geographical setting

The Selenga River originates in the mountainous parts of Mongolia, draining large parts of Mongolia and southern Siberia (442 000 km²; Fig. 2b). It is the main tributary of Lake Baikal, with a drainage area 82% of the total drainage area of the lake. It transports 57.8 km³ · yr⁻¹, which accounts for ca. 50% (Votintsev et al., 1985) of the total water input to the lake. Furthermore, it contributes ca. 80% of the total suspended solids delivered by the tributaries to the lake (Votintsev et al., 1985). The other tributaries (Fig. 2b) drain the steep, mountainous watershed that borders the lake on the North and the East. The lake is one of the largest in the world, containing ca. 20% of the Earth's fresh liquid surface water (23,000 km³). The lake water is well mixed and aerated. The chemical and biological parameters of the Selenga River outflow have been studied by Maksimenko et al. (2008) and Sorokovikova et al. (2012). The mixing zone was described to be biologically very active, fueled by the riverine NO₃⁻ and PO₄³⁻. Based on changes in water chemistry and the phyto- and bacterioplankton, the latter authors concluded that, during the summer months, the mixing zone extends from 1–3 km downstream off the Selenga River mouth, after which a lake signature dominates. Maksimenko et al. (2008) studied the microbial communities of the Selenga River outflow and concluded that a fully lacustrine composition occurs between 5 and 7 km downstream of the river mouth.

3. Material and methods

3.1. Collection of suspended particulate matter (SPM)

Table 1 lists the SPM samples investigated and the locations of the sampling stations are shown in Fig. 2. In July 2010, 100 l of Lake Baikal water was sampled from the shoreline at the point where it drains into the Angara River (Ba), further referred to as 'Lake Baikal outflow'. Between 10–20 L of the Selenga River outflow into Lake Baikal (SRM, S1, S3, S5, B1, B3, B5) were sampled later in July 2010 (Fig. 2a). It was sampled at the surface at the river mouth (Harauz tributary; SRM), and surface and bottom waters were sampled at 1 (S1 and B1), 3 (S3

and B3) and 5 km (S5 and B5) from the river mouth. The remaining samples were filtered using the same type of 0.7 μm GF/F glass fiber filters. The bulk parameters of the riverine sites Y1, Y2, MIR and SR (Fig. 2) have been discussed by De Jonge et al., 2014a and the GDGT contents have been described by De Jonge et al. (Chapter 6).

3.2. Lipid extraction and analysis

The freeze-dried filters were extracted using a modified Bligh and Dyer method as described by Pitcher et al. (2009). The samples were ultrasonically extracted 3x for 10 min using a MeOH/dichloromethane (DCM)/phosphate buffer 10:5:4 (v/v/v). The extract was separated into a core lipid (CL) fraction and intact polar lipid (IPL) fraction over a small silica column,

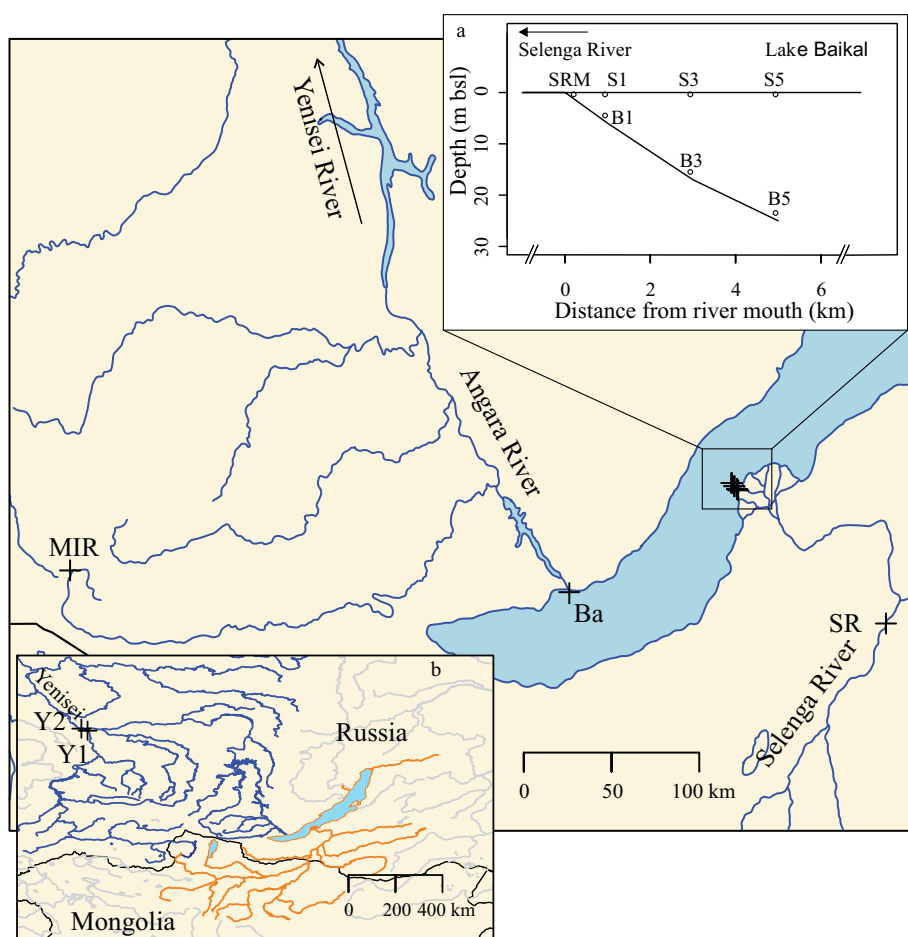


Fig. 2. Map of the Southern part of Lake Baikal, with the sample sites indicated. Insert a shows the distribution of the SPM samples collected in the Selenga River outflow. Insert b shows, i) the extent of the watershed of Lake Baikal, where all rivers that drain into Lake Baikal are indicated in orange and ii) the Southern part of the Yenisei River watershed, where all rivers that drains into the Yenisei River (and the Yenisei River itself) are indicated in blue.

using a procedure modified from Pitcher et al. (2009), using hexane/EtOAc 1:1, v/v as eluent. An aliquot of the IPL fraction was analyzed directly for CLs to check for potential carryover into the IPL fraction. In order to analyze IPLs as CLs, half of the extract was refluxed for a minimum of 2h in 1.5 N HCl in MeOH. However, IPL-derived brGDGTs were often below the limit of detection, indicating that the amount of IPLs was insufficient for quantification, so we refrain from reporting the IPL brGDGTs composition of Selenga River and Lake Baikal. All brGDGTs were quantified against a known amount of C₄₆ GDGT standard (Huguet et al., 2006) added to the CL fraction before filtration through a 0.45 µm PTFE filter and to the IPL fraction before the separation preceding the acid hydrolysis.

Fractions were analyzed using high performance liquid chromatography-atmospheric pressure chemical ionization-mass spectrometry (HPLC-APCI-MS), as described by De Jonge et al. (2014a). Detection was achieved in selected ion monitoring mode (SIM; Schouten et al., 2007a) using *m/z* 744 for the internal standard, *m/z* 1292 for crenarchaeol and *m/z* 1050, 1048, 1046, 1036, 1034, 1032, 1022, 1020 and 1018 for brGDGTs. Agilent Chemstation software was used to integrate peak areas in the mass chromatograms of the [M+H]⁺ ions.

3.3. Calculation of GDGT-based ratios and proxies

The isomer ratio (IR) represents the fractional abundance of the penta- and hexamethylated 6-methyl (6-Me) brGDGTs vs. the total penta- and hexamethylated brGDGTs (modified after De Jonge et al., 2014a):

$$IR = (IIa', b', c' + IIIa', b', c') / (IIa, b, c + IIIa, b, c + IIa', b', c' + IIIa', b', c') \quad 1$$

The roman numerals refer to the GDGTs indicated in Fig. 1. The index includes the non-cyclopentane containing and the cyclopentane containing components of brGDGTs II, III, II' and III'.

The branched and isoprenoid tetraether (BIT) index was calculated according to Hopmans et al. (2004):

$$BIT \text{ index} = (Ia + IIa + IIIa + IIa' + IIIa') / (Ia + IIa + IIIa + IIa' + IIIa' + IV) \quad 2$$

Ia, IIa, IIIa, IIa' and IIIa' are brGDGTs and IV is the isoprenoid GDGT (iGDGT) crenarchaeol, a source-specific GDGT for mesophilic Thaumarchaeota (Sinninghe Damsté et al., 2002; Pearson et al., 2004).

We calculated a reconstructed pH using the modified cyclization of branched tetraether CBT' index (De Jonge et al., 2014b):

$$CBT' = {}^{10}\log[(Ic + IIa' + IIb' + IIc' + IIIa' + IIIb' + IIIc') / (Ia + IIa + IIIa)]. \quad 3$$

$$pH = 7.15 + 1.59 \times CBT' \quad 4$$

Mean summer temperature (MST) is calculated as an approximation for the summer lake water temperature recorded by aquatic brGDGT distributions. To this end, we applied the calibration developed by Pearson et al. (2011):

$$\text{MST } (^{\circ}\text{C}) = 20.9 + 89.1 \times [\text{Ib}] - 12 \times ([\text{IIa}] + [\text{IIa}']) - 20.5 \times [\text{IIIa}] \quad 5$$

Here, we explicitly state that the fractional abundances of IIa and IIa' have to be summed, as these brGDGTs co-eluted under the chromatographic conditions used by Pearson et al. (2011). However, conditions did allow separation of brGDGTs IIIa and IIIa', and only the first eluting one (IIIa) was used in the calibration dataset (E. Pearson, personal communication). The square brackets in Eq. 5 indicate that we used the fractional abundance, i.e. the value relative to the sum of all the brGDGTs ($\text{Ia} + \text{Ib} + \text{Ic} + \text{IIa} + \text{IIa}' + \text{IIb} + \text{IIb}' + \text{IIc} + \text{IIc}' + \text{IIIa} + \text{IIIa}' + \text{IIId} + \text{IIId}' + \text{IIIe} + \text{IIIe}'$).

3.4. Environmental parameters and bulk geochemical analysis

The pH and temperature of the river and lake water were measured immediately after sampling, except for the sample SR, whose parameters were measured after transport. The particulate organic carbon (POC) and $\delta^{13}\text{C}_{\text{POC}}$ content of the river and lacustrine SPM samples were measured on the filter using a Flash 2000 Organic Elemental Analyzer.

3.5. Numerical analysis

Principal component analysis (PCA) based on the correlation matrix was performed using the R software package for statistical computing. We performed an unconstrained Q-mode PCA on the standardized relative brGDGT values in SPM from the Selenga River, Lake Baikal and mountainous Irkut River, using 11 brGDGTs. The brGDGTs IIc, IIIc, IIc' and IIIc' were excluded from this analysis, as they were absent from 4 to 7 sample sites. The brGDGT scores were calculated proportional to the eigenvalues, and the site scores were calculated as the weighted sum of the species scores. The environmental parameters (point measurement of water pH and temperature) were plotted a posteriori in the resulting ordination space, in case a significant correlation ($p < 0.05$) with the principal components (PCs) was present.

4. Results

The brGDGT distribution of the SPM in the Selenga River was determined, before and after its outflow into Lake Baikal. The river SPM was collected ca. 150 km before its inflow into the lake (SR). The transect in the outflow comprised 7 sites, the Selenga River Mouth (SRM), the surface water at 1, 3 and 5 km from the outflow (S1, S3, S5) and the bottom water at 1, 3 and 5 km from the outflow (B1, B3, B5). A shoreline SPM sample from a site in Lake Baikal (Ba) not directly influenced by the river, close to the point where the lake water flows into the Angara River, allowed contrasting the Lake Baikal distribution exported with the Yenisei river system further downstream, before (Y1) and after (Y2) the contribution of the Angara River. Furthermore, the brGDGT distribution of the SPM of a mountainous river (i.e. the Irkut River; MIR) was evaluated to constrain the influence that similar mountainous rivers that drain into

the lake may have on the lacustrine brGDGT distribution. The sites and bulk parameters for the organic matter (OM) in SR, MIR, Y1 and Y2 have been reported by De Jonge et al. (2014a), while the GDGT concentrations and distributions have been reported previously by De Jonge et al. (Chapter 6).

4.1. Environmental and bulk OM parameters

The Selenga River, Lake Baikal and the mountainous Irkut River are contrasting waterbodies, as reflected in both the temperature and bulk POC content, and to a lesser extent in the pH and bulk $\delta^{13}\text{C}_{\text{POC}}$ values (Table 1). The inflow of Selenga River into the lake is characterized by a strong gradient in water temperature (Fig. 3A), decreasing from 25 °C in the river and 22.5 °C at the river mouth to 11.3 °C at S5. The bottom water is on average 6°C colder than the surface water. The coldest water in the Selenga outflow system (5.2 °C) was the bottom water at 5 km distance. The Lake Baikal outflow sample (Ba) had a temperature of 6.7 °C. The pH remained more constant in the Selenga River outflow (Fig. 3B), with a river water pH of 8.4, while the outflow system had a pH that varied around 8.0 pH units. The POC varied between 6.4 and 1.1 mg/l, with the highest values in the river. A clear downstream trend was observed (Fig. 3C), POC decreasing as the river flows further in Lake Baikal. The POC content of the bottom water (2.5-1.1 mg/l) was always lower than for the corresponding surface water, although the difference was most pronounced near the shore. The $\delta^{13}\text{C}_{\text{POC}}$ values (Fig. 3D) showed that the lake bottom water to have an increasingly depleted signal downstream (down to -29.7 ‰) compared with the river SPM (-27.6 ‰). Surface water in the outflow system also had more

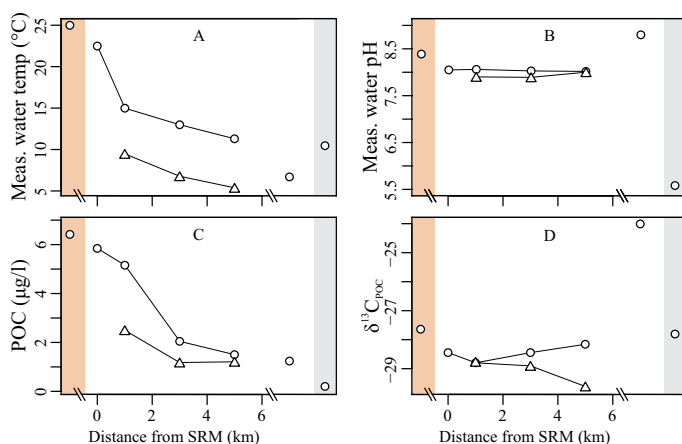


Fig. 3. Figure plotting the environmental variables of Lake Baikal and its inflowing rivers; measured water temperature (°C, A), measured water pH (B), measured concentration of POC (µg/l, C) and the stable carbon isotopic value of the bulk OM, $\delta^{13}\text{C}_{\text{POC}}$ (‰, D). The shaded areas indicate riverine samples, where orange denotes the Selenga River, and grey denotes the Irkut River. Surface water is indicated by round symbols, bottom water is indicated with triangles. Please note that the x-axis, where the distance to the Selenga River Mouth is plotted is broken, as to allow the Selenga River, the Lake Baikal sample and the Mountain River to be plotted on the same axis. Selenga outflow samples, collected in the same sampling campaign, are connected.

negative $\delta^{13}\text{C}_{\text{POC}}$ signal than the river, except for the sites 3 and 5 km from the river mouth, that had a comparable signal to the river mouth (-28.6 to -28.4 ‰). The shoreline lake site had an offset, much less negative $\delta^{13}\text{C}_{\text{POC}}$ value (-24.0 ‰). The mountainous Irkut River differed from the lowland Selenga River, as it has the lowest POC content in the (0.1 mg/l), a much lower pH (5.6) and a lower water temperature (10.8°C). On the other hand, the $\delta^{13}\text{C}_{\text{POC}}$ value of -27.8 ‰ was comparable to that in the Selenga River. The Yenisei River before and after the inflow of the Angara River had a neutral pH (7.5-7.9), a temperature between 11 and 12 °C, and the one measured $\delta^{13}\text{C}_{\text{POC}}$ value (-30.5 ‰) was slightly more negative than for both the Selenga River and Lake Baikal systems.

4.2. GDGT amounts and distribution

The amounts and distribution of crenarchaeol and the brGDGTs are listed in Table 2. SPM of the Selenga River and the river mouth had a low amount of crenarchaeol (0.3-0.5 $\mu\text{g/g}$ POC; Fig. 4B), which increased slightly in the outflow surface water (up to 0.5 $\mu\text{g/g}$ POC). SPM of the bottom waters contained a higher amount of crenarchaeol (0.9-3 $\mu\text{g/g}$ POC), with the highest amount 3 km from the delta. The lake outflow and the Yenisei River SPM had a low crenarchaeol concentration, between 0.2 and 0.3 $\mu\text{g/g}$ POC. The amount of brGDGTs was highest at the Selenga River Mouth (10-12 $\mu\text{g/g}$ POC; Fig. 4A), substantially higher than in the river itself (4 $\mu\text{g/g}$ POC), although this was measured in a different month and can thus not be directly compared. The brGDGT concentration decreased in the surface water of the outflow system to 0.6 $\mu\text{g/g}$ POC. The mountainous Irkut River had the highest POC-normalized brGDGT concentration at 15 $\mu\text{g/g}$ POC). The brGDGTs in the bottom water varied between 2 and 10 $\mu\text{g/g}$ POC, with the highest values 3 km from the Selenga River Mouth. The lake outflow had the lowest amount of brGDGTs, with 0.1 $\mu\text{g/g}$ POC. The abundance in the Yenisei River SPM varies between 10 and 21 $\mu\text{g/g}$ POC (De Jonge et al., 2014b).

Typical examples of brGDGT distributions in the SPM are shown in Fig. 5. The distribution

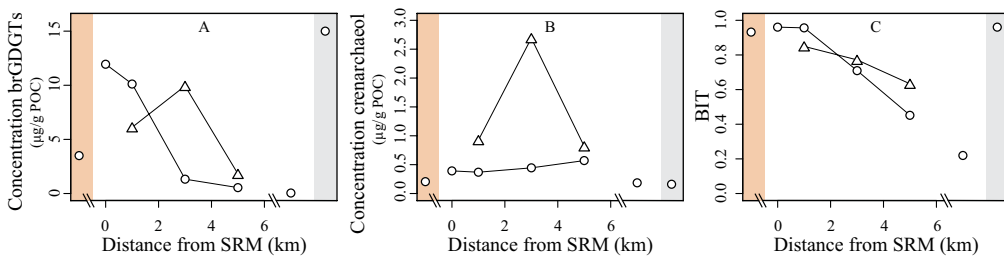


Fig. 4. The concentration of CL brGDGTs ($\mu\text{g/g}$ POC, A) and crenarchaeol ($\mu\text{g/g}$ POC, B) and the BIT-index values (C), in Lake Baikal and its inflowing rivers. The shaded areas indicate riverine samples, where orange denotes the Selenga River, and grey denotes the Irkut River. Surface water is indicated by round symbols, bottom water is indicated by triangles. Please note that the x-axis, where the distance to the Selenga River Mouth is plotted is broken, as to allow the Selenga River, the Lake Baikal sample and the mountainous Irkut River to be plotted on the same axis. Selenga outflow samples, collected in the same sampling campaign, are connected.

Table 1, Sampling station data (n.d., not determined; n.a., not available).

Site	Latitude (°N)	Longitude (°E)	Depth bsl (m) ^a	Distance SRM (km) ^b	Sampling date	Measured pH	Measured temp (°C)	POC (mg/l)	$\delta^{13}\text{C}_{\text{POC}}$ (‰)
SR ^c	51.72833	107.4628	0.5	-150	06-07-2010	8.4	25.0	6.4	-27.6
SRM	52.27318	106.2547	0.5	0	20-07-2010	8.1	22.5	5.9	-28.4
S1	52.27852	106.2444	0.5	1	20-07-2010	8.1	15.0	5.1	-28.8
S3	52.29025	106.2226	0.5	3	22-07-2010	8.1	13.0	2.0	-28.4
S5	52.30313	106.1998	0.5	5	28-07-2010	8.0	11.3	1.5	-28.2
B1	52.27852	106.2444	6	1	20-07-2010	7.9	9.3	2.5	-28.8
B3	52.29025	106.2226	17	3	20-07-2010	7.9	6.6	1.1	-29.0
B5	52.30313	106.1998	25	5	28-07-2010	8.0	5.2	1.3	-29.7
Ba	51.89194	104.8233	0.5	105	01-07-2010	8.8	6.7	1.3	-24.0
MIR ^c	51.94533	100.78839	0.5	n.a.	11-07-2010	5.6	10.8	0.1	-27.8
Y1 ^c	58.00992	93.11680	2.0	n.a.	25-8-2009	n.d.	12.0	0.03	b.d.l.
Y2 ^c	58.13147	92.75405	3.0	1500	29-9-2009	n.d.	11.0	0.09	-30.5

a Below surface water level; b estimated downstream distance relative to Selenga River mouth, so upstream samples thus have negative values; c samples reported by De Jonge et al., 2014b and De Jonge et al., Chapter 6.

in the Selenga River Mouth (Fig. 5A) was dominated by 6-Me pentamethylated brGDGTs, and relatively abundant cyclopentane-containing brGDGTs (17%). It was markedly different from that in the lake outflow (Fig. 5E), which was dominated by 5-Me and 6-Me hexamethylated brGDGTs, and a lower contribution of cyclopentane-containing brGDGTs (5%). The brGDGTs in the Selenga outflow seemed to have intermediate distributions (Fig. 5B-D), while the mountain river had a distribution comparable with that of the lake outflow (Fig. 5E-F). The distribution in the Yenisei River samples (Fig. 5G-H) was dominated by 6-Me brGDGTs, the hexamethylated compounds in particular dominated.

To study the variance in the brGDGT distribution of the lake and the rivers in its watershed (Selenga and Irkut), a PCA was performed, based on the fractional abundances of brGDGTs in the Selenga River, Lake Baikal and the mountainous Irkut River ($n = 10$). Most brGDGTs containing two cyclopentanes, i.e. IIc, IIc', IIIc and IIIc' were excluded, as they were absent from 4 to 7 samples. The first three PCs accounted for a large part of the variance (almost 90%), being 41%, 25% and 21%, respectively. The first PC highlighted the correlation of a group of minor brGDGTs with positive values on PC1 (Ib, Ic, IIb, IIIb, IIa', IIb', IIIb') and, to a lesser extent, brGDGT Ia (Fig. 6A). The brGDGTs IIa and IIIa had negative values on PC1. PC2 revealed that brGDGT IIIa', and to a lesser extent IIa' and IIb', showed a negative correlation with Ic, IIb and IIIb (Fig. 6A). BrGDGT Ia had a positive score on PC3, while IIIb and IIIb' had a negative score (Fig. 6C). The similarity in the brGDGT distributions at each site could be evaluated comparing their scores on the first three PCs. The similar scores for the Selenga River, Selenga River Mouth and the surface water 1 km from the river mouth, indicated that the brGDGT distributions were similar (Fig. 6B, D). Moving downstream (S3, S5) the scores

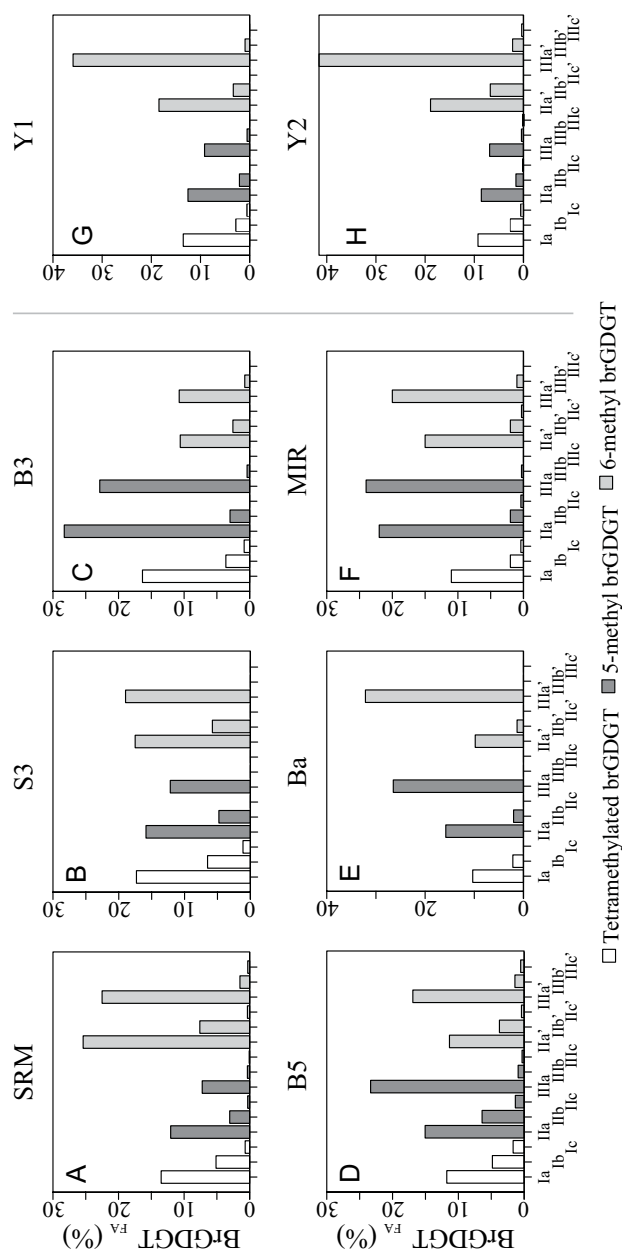


Fig. 5. The fractional abundance (FA), expressed as the percentage of the total of the 15 brGDGT compounds, of the CL (A-F) fraction of selected samples: Selenga River Mouth (SRM, A), the surface water at 3 km distance from the outflow (S3, B), the bottom water at 3 km from the outflow (B3, C), the bottom water at 5 km from the outflow (B5, D), the shoreline Lake Baikal setting (Ba, E), the Mountainous Irkut River (MIR, F), the Yenisei River before (Y1, G) and after the Angara River inflow (Y2, H). The color of the bars refers to the structure of the brGDGTs, and is referred to in the legend.

on PC1 decreased, and the scores on PC2 and, especially, PC3 increased. The distribution for S3 (Fig. 5B) indeed showed increased fractional abundances of the 5-Me brGDGTs Ia, IIa and IIIa, at the expense of decreased fractional abundances of 6-Me brGDGTs. This was also apparent from the IR ratio (Table 2; Fig. 8A) that decreased downstream in the Selenga outflow surface water. Compared with the overlying surface water, SPM of the bottom water had an increased score on PC2, reflecting a decrease in brGDGT IIIa', coupled with an increase in brGDGTs IIa and IIIa, that dominated the distributions of B3 and B5, respectively (Fig. 5C, 5D). This resulted in lower IR values (Table 2; Fig. 8A) of the bottom water vs. the overlying surface water. The brGDGT distribution in the lake outflow, was most similar to that in the mountainous Irkut River, as reflected in the similar scores on PC1 and PC3. However, on PC2, the lake outflow sample had more negative values, caused by a larger fractional abundance of IIIa and IIIa' (Fig. 5E).

The point measurement of water temperature had a significant correlation with the PCs ($p < 0.05$) and were plotted a posteriori in the PCA. The water temperature values had a positive score on PC1, and a negative one on PC2. The point measurements of water pH showed no significant correlation with the PCs ($p > 0.05$).

5. Discussion

5.1. Characteristics of Selenga River outflow

During the sampling period (September 2011), the Selenga outflow system was characterized by a warmer surface layer that extended to at least 5 km in Lake Baikal. Although a strong thermal bar is usually present during the start of the summer (Sorokovikova et al., 2012), its stability generally breaks down later in summer. The temperature profile shows that there was no complete stratification of the Selenga River outflow water during the sampling, and partial mixing caused the bottom water temperature to warm, especially near the shoreline (Fig. 3A). The $\delta^{13}\text{C}_{\text{POC}}$ values of the Selenga River and River Mouth SPM (-27.5 to -28.5‰) are indicative of a dominant terrigenous signature, probably derived from soil or terrigenous vegetation. Although large blooms of phytoplankton were described to be present in the mixing zone of the river inflow (Sorokovikova et al., 2012), this apparently has little impact on the $\delta^{13}\text{C}_{\text{POC}}$ values in the Selenga outflow surface SPM (Fig. 3D). This may be due to the similar $\delta^{13}\text{C}$ signature of the lake phytoplankton and the terrigenous organic matter (OM), as the former varies between -27 and -29.5‰ (Yoshii et al., 1999). Bottom water SPM, however, shows increasingly depleted values of $\delta^{13}\text{C}_{\text{POC}}$, possibly reflecting the slightly depleted values of $\delta^{13}\text{C}_{\text{POC}}$ of lacustrine phytoplankton, as the highest abundance of lake phytoplankton was in the bottom waters at 5 km distance (Sorokovikova et al., 2012). Alternatively, this may be caused by a shift in the microbial community (Maksimenko et al., 2008; Sorokovikova et al., 2012), possibly with an increased contribution of organotrophic bacteria. Increased amounts of such bacteria in the bottom water have been described, with maximum abundance in the bottom water at 5-10 (Maksimenko et al., 2008) or 14 km from the Selenga River mouth (Sorokovikova et al., 2012). They may thrive on the easily hydrolysable OM entering the near-bottom layers from decomposition of the spring algae (Votintsev et al., 1975). The shoreline lake SPM probably does not reflect an open water lacustrine end member. Here, the POC is substantially more enriched in ^{13}C , but this probably reflects the contribution of a isotopically enriched OM

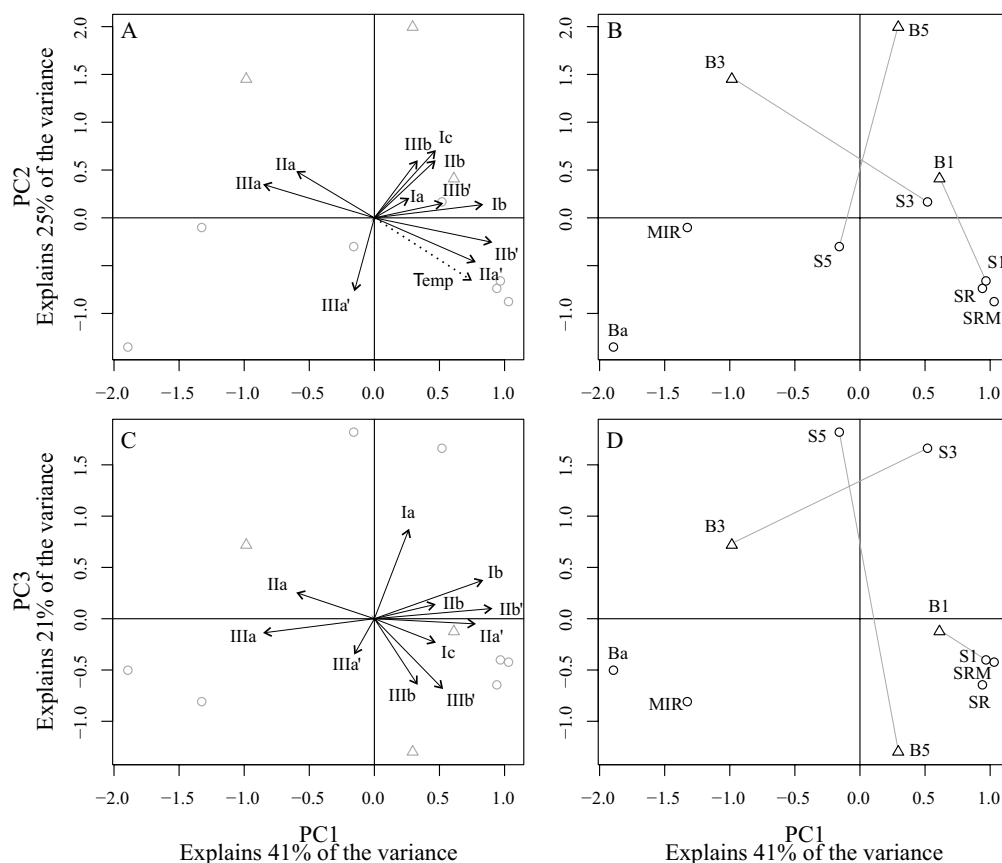
Site	Fractional abundance (%)													BrGDGTs ($\mu\text{g/g POC}$)	Crenarchaeol ($\mu\text{g/g POC}$)	IR	BIT	pH ^a	MST ^a ($^{\circ}\text{C}$)		
	Ia	Ib	Ic	IIb	IIIa	IIIb	IIIc	IIa'	IIb'	IIc'	IIIa'	IIIb'	IIIc'								
SR ^b	12	5	1	0.68	4	7.5	8	0.4	b.d.l.	24	7	0.4	24	1	b.d.l.	4	0.2	0.68	0.93	7.5	20
SRM	13	5	1	0.71	3	7.5	7	0.3	0.1	25	8	0.3	23	1	0.3	12	0.4	0.71	0.96	7.5	20
S1	14	5	1	0.70	3	7.5	8	0.4	0.05	25	7	0.3	21	1	0.3	10	0.4	0.70	0.96	7.5	19
S3	17	7	1	0.56	5	7.1	12	b.d.l.	b.d.l.	18	6	b.d.l.	19	b.d.l.	b.d.l.	1	0.4	0.56	0.71	7.1	20
S5	18	5	b.d.l.	0.52	4	7.0	16	b.d.l.	b.d.l.	17	5	b.d.l.	17	b.d.l.	b.d.l.	0.6	0.6	0.52	0.45	7.0	18
B1	14	6	1	0.56	4	7.2	12	0.5	b.d.l.	20	6	0.3	18	1	b.d.l.	6	0.9	0.56	0.84	7.2	19
B3	16	4	1	0.43	3	6.5	23	0.4	b.d.l.	11	3	b.d.l.	11	1	b.d.l.	10	2.7	0.43	0.77	6.5	15
B5	12	5	2	0.45	6	6.9	23	1	0.3	11	4	0.4	17	1	1	2	0.8	0.45	0.63	6.9	17
Ba	10	2	b.d.l.	0.44	2	7.0	26	b.d.l.	b.d.l.	10	1	b.d.l.	32	b.d.l.	b.d.l.	0.1	0.2	0.44	0.22	7.0	14
MIR ^b	11	2	0.4	0.51	2	6.9	24	0.3	b.d.l.	15	2	0.3	20	1	b.d.l.	15	0.1	0.51	0.99	6.9	13
Y1 ^b	14	3	1	0.71	2	7.5	9	0.4	0.1	18	3	b.d.l.	36	1	0.1	10	0.3	0.71	0.97	7.5	18
Y2 ^b	9	3	0.4	0.80	2	7.9	7	0.4	0.1	19	7	0.2	42	2	0.4	21	0.2	0.80	0.99	7.9	19

Fig. 6. PCA based on the standardized fractional abundances of the Lake Baikal brGDGTs and the inflowing Selenga and Irkut Rivers. Panel A and B plot principal component 1 (PC1) against PC2, panel C and D plots PC1 against PC3. The scores of the brGDGT compounds are indicated in panel A and C, and the scores of the sites are plotted in panels B and D. Surface waters are indicated with round symbols and connected with the corresponding bottom waters (triangular symbol) with a grey line. The correlation of the measured water temperature (Temp) with the PCs is plotted a posteriori in the ordination space (panel B), indicated with a dotted line. ►

Table 2. Fractional abundance (% of total) and concentrations of CL brGDGTs and crenarchaeol in SPM of Selenga River and its outflow into Lake Baikal, in the Mountainous Irkut River and in the Yenisei River (b.d.l., below detection limit).

^a reconstructed pH and MST

^b reported by De Jonge et al., 2014b and De Jonge et al., Chapter 6.



derived from macrophytes ($\delta^{13}\text{C}$ between -19 and -5‰; Yoshii et al., 1999) and benthic algae ($\delta^{13}\text{C}$ between -12 and -5‰; Yoshii, 1999), as the SPM was sampled in a shallow setting.

5.2. Changing GDGT abundance in the Selenga River outflow

As the Selenga River is the main source for SPM in Lake Baikal, its iGDGT and brGDGT distribution is expected to contribute to the lacustrine GDGT signal. The iGDGT crenarchaeol is present only in a low abundance in the river water. As it is a tracer for mesophilic Thaumarchaeota (Sinninghe Damsté et al., 2002), this fits with a reported absence of archaea from the river water (Maksimenko et al., 2008). The amount of archaea increases in the lake (Maksimenko et al., 2008) and the increase is mimicked by a slight increase in the amount of crenarchaeol in the outflow surface water (Fig. 4B). The crenarchaeol concentration in the bottom water exceeds the concentration in the surface water, especially at 3km from the outflow (i.e. a fivefold increase). The downstream trend in the brGDGT concentration in the outflow is different, being highest in the river mouth, and decreasing in the surface water of the river outflow system (Fig. 4A). The decrease in brGDGT concentration in an outflow system is similar to studies where brGDGTs are traced in river outflows in marine environments (e.g. Hopmans et al., 2004; Zell et al., 2014; De Jonge et al., Chapter 6). The decrease in POC-normalized concentration of riverine brGDGTs after their inflow into Lake Baikal can be a

result of dilution in the lacustrine environment due to in-situ produced OM, or to degradation in the active biological system of the river outflow (Maksimenko et al., 2008; Sorokovikova et al., 2012). However, the brGDGT concentration in the bottom water 3 and 5 km from the river mouth, exceeds the surface water concentration.

As no significant decrease in POC concentration was observed at B3 and B5 (Fig. 3C), we infer that the increase in GDGTs at these sites is not an artifact of the normalization to POC. Although they are produced by different source organisms, both crenarchaeol and brGDGTs have been described to be produced in-situ in the lacustrine environment. Crenarchaeol was shown to be an abundant compound in the marine environment (Sinninghe Damsté et al., 2002), but also in most medium-sized and large lakes studied (Blaga et al., 2009), as it is produced by marine and freshwater Thaumarchaeota (e.g. Sinninghe Damsté et al., 2002; Pearson et al., 2004). These NH_3 oxidizing Archaea have a preferred niche in the oxycline/thermocline and nitrocline of the water column of lakes (e.g. Pouliot et al., 2009; Llíros et al., 2010; Auguet et al., 2011; Blaga et al., 2011; Schouten et al., 2012; Woltering et al., 2012; Buckles et al., 2013), where they can outcompete NH_3 -oxidizing bacteria. The presence of an increased supply of decomposed algal matter in near-bottom water layers, resulting in increased NH_3 concentration (e.g. Jewell and McCarty, 1971), can possibly fuel the crenarchaeol production in these deeper layers. Also in situ production of brGDGTs has been observed in lacustrine environments, based on shifts in the distribution and increased abundance (e.g. Tierney and Russell, 2009). BrGDGT producers in soils are believed to be heterotrophic bacteria (e.g. Pancost and Sinninghe Damsté, 2003; Weijers et al., 2010). Thus, the in situ production at these sites can possibly be linked to enhanced heterotrophic activity in the bottom water. Indeed, the amount of organotrophic bacteria was shown to be slightly increased in the bottom water at 5-10 km from the Selenga River Mouth (Maksimenko et al., 2008).

To trace the transport of bacterial OM (soil-derived and/or river-derived) in the marine system, the BIT index was developed (Hopmans et al., 2004), expressed as the abundance of 5 major brGDGTs, relative to the abundance of crenarchaeol. In the Selenga outflow, the concentration of brGDGTs is the dominant driver for the changing BIT index (Fig. 4C), as it correlates strongly with the amount of brGDGTs ($r^2 = 0.63$). The index decreases with increasing distance from the river mouth. The decrease is to be expected, and has been observed in front of several river outflows in the marine system (e.g. Hopmans et al., 2004; Zell et al., 2014; De Jonge et al., Chapter 6). The slightly increased values in the bottom water reflect the increased amount of brGDGTs there compared with the surface outflow water. The value for the lake outflow (0.22), is lower than reported values for sediment cores from the lake, where Holocene values vary between 0.3 and 0.6 (Fietz et al., 2011), although the difference can still be related to interlaboratory differences that can influence the values obtained (Schouten et al., 2009, 2013). Overall, the brGDGT abundance decreases significantly in the river outflow, while the crenarchaeol abundance remains stable. However, in situ production of both crenarchaeol and brGDGTs within the bottom water is likely. The increase is possibly fueled by increased degradation of phytoplankton material in the bottom water.

5.3. Changing brGDGT distributions in the outflow of Selenga River and Lake Baikal

The distribution in the Selenga River and the River Mouth is distinctly different from the shoreline lake SPM that is presumably transported further downstream to the Yenisei River (Fig. 5A, F). Downstream changes in the fractional abundance of all 15 brGDGTs can be seen in the distributions (e.g. Fig. 5A-E) and the PCA based on the fractional abundances (Fig. 6). To evaluate whether the downstream changes are due exclusively to linear mixing between a riverine (SRM) and lacustrine (Ba) endmember, we plotted the data in a triplot based on the fractional abundance of three major brGDGTs (Fig. 7). It captures the majority of the variance, as the three brGDGTs have high scores on the first three PCs (brGDGTs IIIa, IIIa' and Ia, respectively). In the case that linear mixing is the only mechanism causing the shift in brGDGT distribution in the Yenisei outflow, and if the two endmembers (lacustrine, riverine) are well represented by the Ba and SRM samples, distributions that result from conservative mixing of these endmembers alone should fall on the thick black line in Fig. 7. However, both surface and bottom water SPM along the Selenga outflow transect do not fall on this mixing line. Compared with the Selenga River Mouth, the surface outflow water shows a stepwise increase in the fractional abundance of IIIa, and a decrease for Ia and IIIa'. Bottom water SPM also shows an increase in IIIa (in B1, but especially B3 and B5) and a decrease in Ia and IIIa'. The increase in IIIa correlates moderately with an increase in IIa ($r^2 = 0.36$), and correlates well with a decrease in Ib, IIa' and IIb' ($r^2 = 0.57, 0.90$ and 0.96 , respectively). The decrease in IIIa' is coeval with a weak increase in Ic ($r^2 = 0.23$).

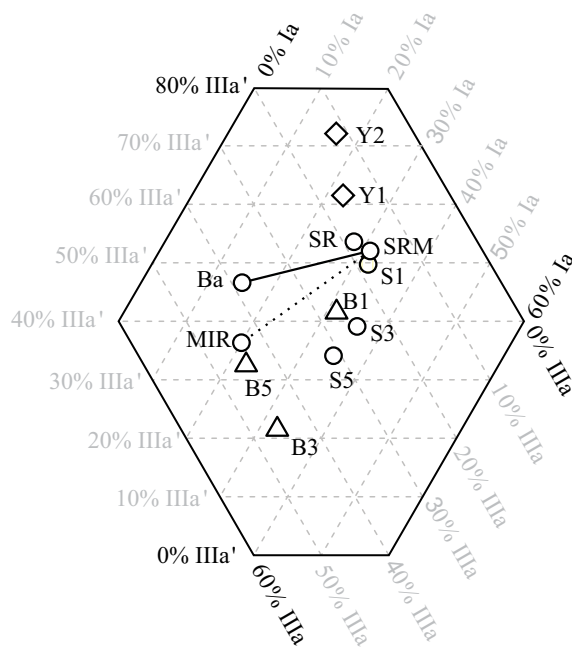


Fig. 7. Truncated triplot, based on the fractional abundances of the brGDGTs Ia, IIIa and IIIa'. The sum of the fractional abundances amounts up to 100%. The round symbols indicate surface water of Lake Baikal and inflowing rivers. The triangles indicate Lake Baikal bottom waters, while the diamonds indicate the brGDGT distribution in the Yenisei River. The full black line covers brGDGT distributions that can be explained by linear mixing between the Selenga River Mouth (SRM) distribution and the Baikal outflow (Ba) distributions. The dotted line covers brGDGT distributions that can be explained by linear mixing between the Selenga River Mouth (SRM) distribution and the mountainous Irkut River (MIR) distributions.

Possible explanations for the offset from the linear mixing line are preferential degradation of a brGDGT pool that was enriched in the Ia, Ib, IIa', IIb' and IIIa', or the in situ production of Ic, IIa and IIIa in the outflow. Although the brGDGT distribution in the river reflects a mixture dominated by in situ produced brGDGTs, a small contribution from soil-derived brGDGTs could be present. As the riverine OM will be more easily degraded (e.g. Blair and Aller, 2012), a soil-derived brGDGT sub-pool could become more dominant during degradation of the OM delivered by the river. However, especially in the bottom water, in situ production of brGDGTs is probable, based on the increased brGDGT concentration. In situ production of brGDGTs in lacustrine systems has been described in several studies, both for the lake water column or sediments. Unfortunately, these studies do not allow discussing changes in the abundance of 5- and 6-Me brGDGTs separately, although the relative abundance of the 6-Me brGDGTs, expressed as the isomer ratio (IR, Eq. 1; Fig. 8A) shows strong changes downstream. The contrasting behavior of the 5- and 6-Me brGDGTs is also reflected in their dissimilar scores in the PCA (Fig. 6A, C) and ideally they should therefore be studied separately when discussing aquatic brGDGT distributions.

Loomis et al. (2014a) have shown that cyclopentane-containing brGDGTs and penta- and hexamethylated brGDGTs can be produced in the water column of a temperate lake, both in the surface water and bottom water. A study (Buckles et al., 2014a) of the partially anoxic Lake Challa showed that penta- and hexamethylated brGDGTs were produced in the oxic part of the water column, but mainly in the suboxic part, and found some evidence suggesting their production in sediments. Furthermore, the authors showed that in situ production of IIIa (and/or IIIa') and IIb (and/or IIb') occurred in the Loch Lomond (Scotland), although they could not pinpoint whether the production was localized in the sediments or in the water column. Indications were also found for in situ production of penta- and hexamethylated brGDGTs in the suboxic sediments of Sand Pond (USA; Tierney et al., 2012). Overall, previous studies agree on the production of highly methylated and cyclopentane-containing brGDGTs by brGDGT producing bacteria occupying a variety of niches within the lacustrine environment. This is in line with the postulated in situ production of Ic, IIa and IIIa in the Selenga Outflow. As IIc, IIc', IIc and IIc' were below detection limit in 4-7 samples, an increase in their fractional abundance could not be established.

We have shown that the distribution in the Selenga River outflow can not be explained solely by mixing of a riverine end member and a lacustrine endmember. However, the source of the brGDGT distribution in the lacustrine endmember (Ba) still remains to be constrained. Besides being in situ produced, a second possible source for the brGDGT distribution in Lake Baikal is brGDGTs delivered by other rivers that account up to 50% of its water volume, and up to 20% of the total suspended solids (Votintsev et al., 1985). Although we did not sample the SPM from such rivers within the watershed, we sampled the brGDGTs in the headwater of Irkut River, a mountainous river in a nearby and similar location (Fig. 2), for which we postulate that it should approach the brGDGT distribution in the northern and eastern rivers of the watershed of the lake and in the headwaters of Selenga River. The distribution in the SPM of this mountainous river and that of the lacustrine endmember are rather similar (Fig. 5E, F), as confirmed by their similar scores on PC1 and PC3 (Fig. 6B, D). Although linear mixing (Fig. 7, dotted line) between the distributions in the mountain river and the Selenga River, approaches the lacustrine

distribution, a small decrease in the fractional abundance of Ia and IIIa, or an increase in Ic, IIa', IIb' and IIIa' is needed to explain the distribution in the lake. Unfortunately, it is impossible to determine whether preferential degradation or in situ production of brGDGTs is the more probable explanation.

Another issue is how the lake water affects the brGDGT composition of downstream Yenisei river water. The distribution in the latter (Figs. 5G-H; Fig. 7) is distinctly different from that of the lake outflow (Fig. 5E; Fig. 7) with a much larger fractional abundance of 6-Me brGDGTs. This dominance becomes even more evident after the inflow of the Angara River, that drains lake water into the Yenisei River. The signature of the latter (Figs. 5G-H; Fig. 7) is more similar to that of the Selenga River (Fig. 5A; Fig. 7). This indicates that riverine in situ production of brGDGTs, a process reported to be dominant for brGDGT distribution in the whole Yenisei River (De Jonge et al., 2014b), already operates in the Angara River. This is confirmed by the two orders of magnitude higher concentration of brGDGTs in the Yenisei River SPM than in the lake. Therefore, we postulate that the watershed of the lake, including the Selenga River watershed, should not contribute significantly to the brGDGT distribution transported by the Yenisei River and delivered to the marine system.

5.4. Environmental controls on brGDGT distributions in the Selenga River outflow

The lacustrine sedimentary brGDGT distribution of lakes covering a latitudinal or altitudinal range responds to overlying air temperature (e.g. Tierney et al., 2010; Sun et al., 2011; Pearson et al., 2011; Loomis et al., 2012) and to seasonal changes in water temperature (e.g. Loomis et al., 2014b). Similar to the soil calibrations, these authors found an increase in Ia in warmer lake settings, and a decrease of penta- and hexamethylated brGDGTs. Furthermore, some authors found evidence that pH has an influence on the brGDGT distributions (Tierney et al., 2010; Loomis et al., 2014b; Schoon et al., 2013), while others found no indication of this (Pearson et al., 2011; Loomis et al., 2014a).

The measured environmental parameters (point measurements of pH and water temperature) have been plotted a posteriori in the ordination space (Fig. 6A), in the case of significant correlation ($p < 0.05$) with the PC. The value of this vector in the ordination space is based on the correlations between the values of the environmental parameters at the sites, with the site scores on the PCs and thus revealing their relationship with individual brGDGTs. Their direction indicates for which samples their values are increased, and with which brGDGT correlations are present. The measured water temperature values correlated significantly with the site scores on the first two PCs ($p < 0.02$). The increase in fractional abundance of IIa and IIIa in the Selenga outflow results in a negative correlation with the measured water temperature as the temperature decreases strongly in the Selenga River outflow ($r^2 = 0.34$ and 0.64 , respectively). The measured water temperature follows a positive correlation with the fractional abundance of IIa' and IIb' ($r^2 = 0.75$ and 0.59 , respectively). The measured pH values do not correlate significantly with the main trends in the brGDGT distribution.

As the change in brGDGT distribution seems to be related to water temperature, we evaluate the performance of a MST calibration based on the fractional abundance of lacustrine brGDGTs (Pearson et al., 2011; Eq. 6). However, to date, no lake calibration has been based

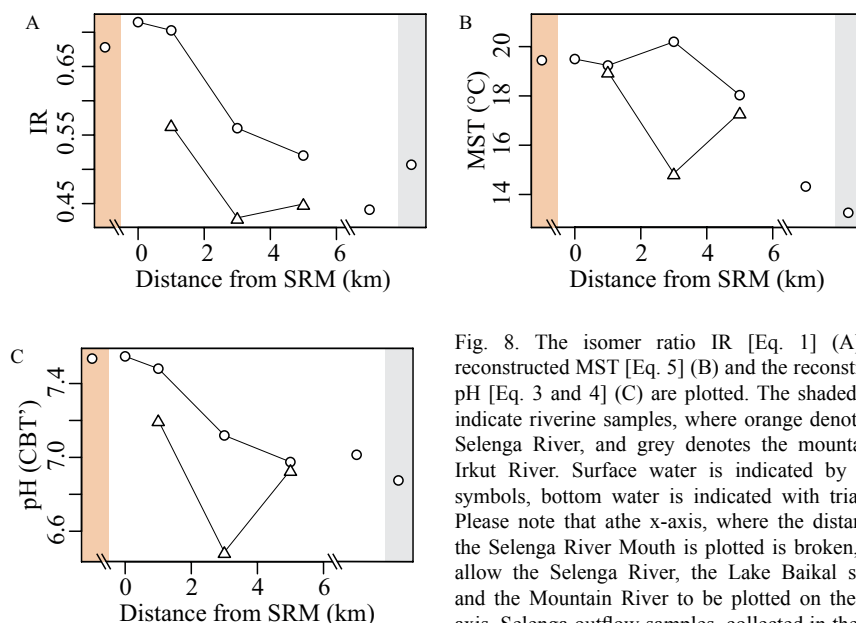


Fig. 8. The isomer ratio IR [Eq. 1] (A), the reconstructed MST [Eq. 5] (B) and the reconstructed pH [Eq. 3 and 4] (C) are plotted. The shaded areas indicate riverine samples, where orange denotes the Selenga River, and grey denotes the mountainous Irkut River. Surface water is indicated by round symbols, bottom water is indicated with triangles. Please note that the x-axis, where the distance to the Selenga River Mouth is plotted is broken, as to allow the Selenga River, the Lake Baikal sample and the Mountain River to be plotted on the same axis. Selenga outflow samples, collected in the same sampling campaign, are connected.

on the extended dataset of 15 brGDGTs. Although this calibration excluded IIIa' (E. Pearson, personal communication), it included the pentamethylated 6-Me brGDGTs, that vary strongly in the Selenga River outflow. The reconstructed MST for the outflow surface water varies between 20 and 18 °C (Fig. 8B). The bottom water values, except for sample B3 (17–19 °C; Fig. 8B), reflect the same temperature as the surface values, within the RSME of the calibration (2 °C; Pearson et al., 2011). As the absolute water temperature decreases from 25 to 12 °C (Fig. 3A), the reconstructed temperature values only give a muted response to this large decrease in temperature. The muted response to the temperature shift measured in situ is a phenomenon also recognized by Loomis et al. (2014b). Although major shifts in the fractional abundance of the penta- and hexamethylated brGDGTs occur in the Selenga outflow, this is thus not reflected in the reconstructed temperature. This is caused by the combination of 5- and 6-Me pentamethylated brGDGTs. The Pearson et al. (2011) calibration is based on the air MST, that varies between 10.6 and 15.4 °C in the Lake Baikal watershed, based on 5 climate stations (De Jonge et al., 2014a). In this respect, the reconstructed MST overestimates the MST measured in the watershed.

Although the brGDGT distribution at B3 is generally comparable with that in the other river outflow samples, it results in a substantially lower reconstructed temperature (15 °C; drop of 4 °C), because of the larger fractional abundance of IIa. This decrease in reconstructed temperature is not related to a decrease in water temperature (Fig. 3A). As strong shifts in the abundance of nutrients have shown to cause shifts in brGDGT distributions that are probably related to shifts in the microbial community (Loomis et al., 2014b), the low reconstructed temperature values can be due to the presence of a distinct brGDGT producing bacterial community associated with an increased amount of phytoplankton-derived detritus.

We also tested the performance of the most recent soil pH calibration (De Jonge et al., 2014b) in this aquatic setting. To this end, a pH reconstruction was performed using the CBT', a ratio

based on a dataset where all 15 brGDGTs were quantified separately. The reconstructed pH (Eqs. 3 and 4) has absolute values (7-7.5) that only slightly underestimate the pH measured in the river and lake water (7.9-8.9), especially when taking the residual error of 0.5 pH units into account. The reconstructed pH shows a slight decrease in the Selenga outflow surface water, that is an intensified response compared with the measured values. In the outflow system, sample B3, with a reconstructed pH of 6.5 has the largest offset with the measured pH (7.9). The brGDGT signal at the site, which is most probably influenced by an in situ produced signal, thus fails to reconstruct the in situ measured pH. Furthermore, although the mountainous Irkut River has a lower pH than the lake, the brGDGT distributions are fairly similar. Overall, this environmental dataset indicates a limited influence of pH on the aquatic brGDGT distributions, as all reconstructed pH values vary around 7-7.5, and do not correlate with the measured values.

6. Conclusions

We have traced the Selenga River brGDGT signature during its outflow into Lake Baikal and compared the signal with the outflow from Lake Baikal and the brGDGT distribution in the Yenisei River SPM. The signature for the Selenga River is characterized by a dominance of 6-Me brGDGTs IIa' and IIIa' (Selenga River endmember). Although the Selenga River delivers the largest part of the suspended matter to Lake Baikal, the brGDGT signal delivered by it is drastically different from the lacustrine brGDGT signal, that shows an increased amount of brGDGT IIIa and IIa (lacustrine endmember). As linear mixing of these two endmembers can not explain the shifts in the in the Selenga Outflow brGDGT distribution, we postulate that in situ production of brGDGTs or preferential degradation takes place in the Selenga outflow. The brGDGT distribution of the lacustrine endmember can be produced in situ in the lake, or can be caused by a contribution from brGDGTs derived from mountainous rivers in the Selenga watershed, that is dominated by non-cyclopentane containing penta- and hexamethylated brGDGTs (mountain river endmember).

Furthermore, the brGDGT distribution in the Yenisei River, both before and after the inflow of the Angara River that drains Lake Baikal, was studied. This distribution was found to be dissimilar to the lacustrine endmember, indicating only a limited contribution from the lacustrine brGDGTs to the Yenisei River distribution. The dominance of 6-Me brGDGTs, similar to the brGDGT distribution encountered in the Selenga River, indicated that the lacustrine signal is overwritten by in situ produced riverine brGDGTs. The watershed of Lake Baikal thus does not contribute significantly to the brGDGT pool transported by the Yenisei River. This study therefore has several implications for the use of lipid-based palaeoclimate proxies, both in lacustrine and marine sediments.

Acknowledgments

We acknowledge the help of I. Tomberg (Limnological Institute, Irkutsk, Siberian Branch of Russian Academy of Science), who provided the filtered Selenga River transect SPM. The work was performed in the framework of the MOU between NIOZ and VNIIOkeangeologia (St. Petersburg, Russian Federation) for Arctic research. The study was funded by research project 819.01.013, financed by the Netherlands Organization for Scientific Research (NWO) and the European Research Council under the EU Seventh Framework Programme [FP7/2007-2013]/ERC grant agreement No. 226600].



Photo by Alina Stadnitskaia

Drastic changes in the distribution of branched tetraether lipids in suspended matter and sediments from the Yenisei River and Kara Sea (Siberia)

Implications for the use of brGDGT-based proxies in coastal marine sediments

6

Cindy De Jonge, Alina Stadnitskaia,
Ellen C. Hopmans, Georgy Cherkashov,
Andrey Fedotov, Irina D. Streletskaya,
Alexander A. Vasiliev and Jaap S. Sinninghe Damsté

Submitted to *Geochimica et Cosmochimica Acta*

ABSTRACT

The distribution of branched glycerol dialkyl glycerol tetraethers (brGDGTs) in soils has been shown to correlate with pH and mean annual air temperature. Because of this dependence brGDGTs have found an application as palaeoclimate proxies in coastal marine sediments, based on the assumption that their distribution is not altered during the transport from soils to marine systems by rivers. To study the processes acting on the brGDGT distributions, we analysed the full suite of brGDGTs, including the recently described 6-Me brGDGTs, in both the suspended particulate matter (SPM) of the Siberian Yenisei River and the SPM and sediments of its outflow in the Kara Sea. The brGDGT distribution in the SPM of the Yenisei River was fairly constant and characterized by high abundances of the 6-Me brGDGTs, reflecting their production at the neutral pH of the river water. However, the brGDGT distribution showed marked shifts in the marine system. Firstly, in the Yenisei River Mouth, the fractional abundance of the 6-Me brGDGTs decreases sharply. The brGDGT signature in the Yenisei River Mouth possibly reflects brGDGTs delivered during the spring floods that may carry a different distribution. Also, coastal cliffs were shown to contain brGDGTs and to influence especially those sites without major river inputs (e.g. Khalmyer Bay). Further removed from the river mouth, in situ production of brGDGTs in the marine system influences the distribution. However, also the fractional abundance of the tetramethylated brGDGT Ia increases, resulting in a distribution that is distinct from in situ produced signals at similar latitudes (Svalbard). We suggest that this shift may be caused by preferential degradation of labile (riverine in situ produced) brGDGTs and the subsequent enrichment in pre-aged (soil) material. The offshore distribution indeed agrees with the brGDGT distribution encountered in a lowland peat. This implies that the offshore Kara Sea sediments possibly carry a soil-dominated signal, indicating potential for palaeoclimate reconstructions at this site.

Both in the river system and coastal cliffs, brGDGTs were much more abundant than crenarchaeol, an archaeal isoprenoid GDGT, resulting in high (>0.93) Branched and Isoprenoid Tetraether (BIT) index values. Moving downstream in the marine sediments, a decrease in brGDGT concentrations, coeval with an increase in crenarchaeol, resulted in decreasing BIT index values. This decrease correlates with changes in bulk proxies for terrigenous input ($\delta^{13}\text{C}_{\text{org}}$, C/N), confirming the use of the BIT index to trace the delivery of river-transported and coastal cliff-derived terrigenous organic matter.

1. Introduction

Branched glycerol dialkyl glycerol tetraethers (brGDGTs) are bacterial membrane lipids (Weijers et al., 2006; Sinninghe Damsté et al., 2011) that are ubiquitous in soils and peat (e.g. Weijers et al. 2007a, Weijers et al., 2009a). They are also found in marine river fan sediments, deposited by rivers after erosion and transport of soil particles (Hopmans et al., 2004). The amount of terrigenous brGDGTs relative to the amount of crenarchaeol, a marine Thaumarchaeotal isoprenoid GDGT (Sinninghe Damsté et al., 2002), can be expressed in the Branched Isoprenoid Tetraether (BIT) index (Hopmans et al., 2004). The BIT index has been used to trace the input of soil-derived matter in marine environments (e.g. Kim et al., 2006, Zell et al., 2014a). BrGDGTs also find an application in palaeoclimate reconstructions. They possess 4 to 6 methyl substituents ('branches') on the linear C₂₈ alkyl chains and up to two cyclopentyl moieties formed by internal cyclization (Fig. 1; Schouten et al., 2000; Sinninghe Damsté et al., 2000; Weijers et al., 2006). In a dataset of global soils, the structural diversity of nine brGDGTs was shown to correlate with the prevailing soil pH and the mean annual air temperature (MAT) (Weijers et al., 2007a). The Cyclization of Branched Tetraethers (CBT) and the Methylation of Branched Tetraethers (MBT) are two brGDGT indices that have been successfully applied to reconstruct the palaeoclimate in a variety of settings; palaeosoils (e.g. Peterse et al., 2011, 2014a, Gao et al., 2012), speleothems (e.g. Yang et al., 2011), lake sediments (e.g. Tyler et al., 2010; Niemann et al., 2012) but firstly in marine sediments. In the Congo fan, brGDGTs have been used to reconstruct continental palaeoclimate changes over the past 25 kyr B.P. (Weijers et al., 2007b). Palaeoclimatic changes since 37 kyr B.P. were reconstructed, based on Amazon River fan sediments (Bendle et al., 2010). Older samples allowed the reconstruction of the temperature changes in the Arctic during the Paleocene-Eocene (Weijers et al., 2007c) and Eocene-Oligocene boundary (Schouten et al., 2008). Donders et al. (2009) reconstructed a cooling trend in Miocene Northern Europe, while Pross et al. (2012) used CBT/MBT to reconstruct temperatures along the Atlantic coast during the early Eocene.

These previous studies have all been based on the assumption that the majority of the brGDGTs encountered in marine sediments are derived from soils. However, in situ production of brGDGTs has been shown to occur in lakes (e.g. Sinninghe Damsté et al., 2009; Loomis et al., 2011, 2014a). This process was also demonstrated in rivers: by Tierney and Russell (2009) in a set of small African rivers, by Kim et al. (2012) and Zell et al. (2013) in the Amazon River, by Zhang et al. (2012) and Yang et al. (2013) in the Chinese Yangtze River, by De Jonge et al. (2014a) in the Siberian Yenisei River and by Zell et al. (2014a) in the Portuguese Tagus River. These studies showed that an aquatic in situ produced signal can influence or even dominate the brGDGT distribution delivered by the surrounding watershed. This possibly complicates palaeoclimate reconstructions.

In situ production of brGDGTs in the marine system may also influence brGDGT distributions. This was shown by a number of recent studies that compare the brGDGT signature of recent sediments and/or suspended particulate matter (SPM) with continental and/or riverine material in coastal marine settings. Peterse et al. (2009a) made a comparison of the brGDGTs downstream a high latitude fjord (Svalbard, Norway). They showed that an increase in the amount of brGDGTs downstream and an increased fractional abundance of the cyclopentane-containing brGDGT in the marine sediments are indicative of in situ production of brGDGTs.

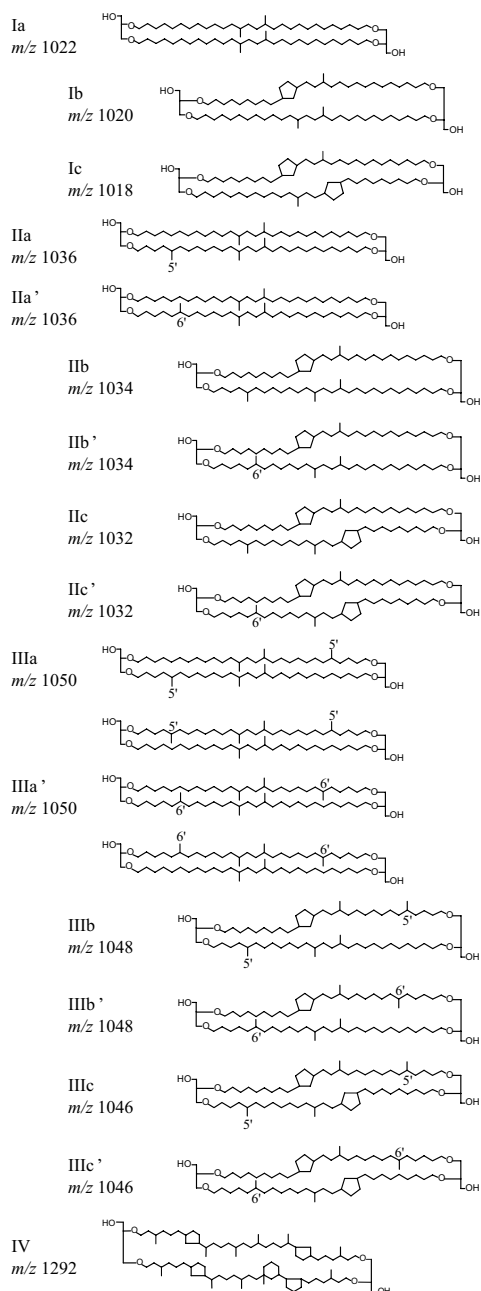


Fig. 1. Chemical structures of branched GDGTs (I-III) and crenarchaeol (IV). The chemical structures of the hexa- and pentamethylated brGDGTs with cyclopentyl moiety(ies) IIb', IIc', IIIb' and IIIc' are tentatively assigned.

Zhu et al. (2011a) also observed an increase in the brGDGT concentration offshore the Chinese Yangtze River and an increase in the cyclopentane-containing brGDGTs Ia and IIc, concluding that significant in situ production is likely. Zell et al. (2014b) observed a strong decrease in the fractional abundance of brGDGT Ia in the marine sediments that were not influenced by the Amazon River plume, coeval with an increase of the cyclopentane-containing brGDGTs. They invoked in situ production of brGDGTs in the marine sediments to explain the results from Bendle et al. (2010), who reconstructed unexpected temperature shifts based on the brGDGT distribution in the Amazon River fan sediments. A study of the brGDGT distribution in the Tagus basin and its outflow in the marine system also indicated an increase in the fractional abundance of cyclopentane-containing brGDGTs (Zell et al., 2014a).

All studies referred to above employed an HPLC-based chromatographic method, as described by Schouten et al. (2007a), that allowed quantification of nine individual brGDGTs (Fig. 1). However, using this chromatographic method, a set of novel brGDGT components recently described by De Jonge et al. (2013), is not separated. These components were shown to possess a methyl group at the 6 and/or ω 6 position, rather than at the 5 and/or ω 5 position, as had been described previously for brGDGT IIa and IIIa by Sinninghe Damsté et al. (2000). De Jonge et al. (2013) showed that in a Siberian peat both the pentamethylated and hexamethylated (non-cyclopentane containing) brGDGTs exist as a 5- and 6-Me component (respectively IIa' and IIa'' and IIIa' and IIIa''); Fig. 1). With the application of a silica HPLC column, De Jonge et al. (2014a) were able to show that the hexamethylated 6-Me brGDGTs were abundant in the Yenisei River SPM, and probably also occurred with one or two cyclopentane groups. Application of a further improved HPLC method on a set of global soils allowed to quantify six penta- and hexamethylated 6-Me brGDGTs (De Jonge et al., 2014b) and revealed that the 6-Me brGDGTs are abundant, comprising on average 24% of the total amount of brGDGTs. Evaluating the influence of the 6-Me brGDGTs on the existing CBT and MBT'-proxies, shows that exclusion of the 6-Me brGDGTs, results in an index (the MBT'_{SME}) that shows an improved correlating with MAT and is no longer dependent on pH. In contrary to the findings by Weijers et al. (2007a) and Peterse et al. (2012), a first-order correlation between the MBT'_{SME} and the MAT is now possible. De Jonge et al. (2014b) also showed that a novel brGDGT index (CBT') and a multiple linear regression of the fractional abundances of the brGDGTs (MAT_{mr}), further improved the accuracy of the reconstructed pH and MAT, respectively.

This study describes for the first time the abundance of both the 5- and 6-Me brGDGTs in a dataset of riverine and marine SPM and sediments. We compare the brGDGT distribution delivered by the river with the signal encountered in the marine sediments, and evaluate the changes in brGDGT distributions. We also evaluate the performance of the BIT-index in the Yenisei River outflow, comparing it with bulk organic matter properties ($\delta^{13}\text{C}_{\text{org}}$, C/N). To evaluate the extent to which the observed changes in brGDGT distributions can effect palaeoclimate reconstructions, we calculate the reconstructed pH and MAT using the novel CBT' and MAT_{mr} (De Jonge et al., 2014b).

2. Study area

The Kara Sea is the second largest shelf area of the Arctic Ocean, partially enclosed to the west by the Novaya Zembla and Franz Josef Land, to the south by the Siberian mainland and to the east by the Zevernaya Archipelago and the Taimyr Peninsula. To the north, the Kara Sea shelf is open to the Arctic Ocean (Fig. 2A). About one third of the total freshwater discharge into the Arctic Ocean occurs through river run-off (Aagaard and Coachman, 1975). The Kara Sea drains a fifth of the continental run-off of the Eurasian continent into the Arctic Ocean (Lammers et al., 2001). The resulting water discharges of the Ob and Yenisei River reach 400 and 630 km³/year, ranking them thirteenth and sixth in the world in terms of water discharge (Bobrovitskaya et al., 1996). The Ob and Yenisei River estuaries are separated by the Gydan Peninsula, where the narrow and deep Khalmir Bay is situated. North of its shore are a number of islands; the Oleniy and Sibiriakov Islands (Fig. 2A).

The Yenisei discharge and Kara Sea circulation are characterized by a strong seasonality. During the summer months, the surface currents in the Kara Sea follow a cyclonic circulation. The Greenland current enters the Kara Sea from the north, and passes along the east coast of Novaya Zemlya. This water body is then joined by the discharge of the Ob and Yenisei Rivers, before flowing further to the northeast (e.g. Lisitsyn, 1995; Pavlov and Pfirman, 1995). From mid-October to mid-May, when only 10-15% of the river discharge happens (e.g. Pavlov and Pfirman, 1995), the Kara Sea and Yenisei River estuary are almost entirely ice-covered. The ice preserves the uppermost water layers against wind mixing, and therefore the freshwater layer extends for a large distance under the ice, dispersing the little material delivered over a large distance (Lisitsyn, 1995). Between June and September, when most of the discharge happens (ca. 80%, e.g. Pavlov and Pfirman, 1995), the bulk of suspended load is deposited in front of the estuaries (Lisitsyn, 1995). Between the surface isohaline of 2 and 20 psu, concentrations of suspended load decrease with an order of magnitude compared to the estuary (Lisitsyn, 1995). The high discharge period is characterized by a strong thermal stratification. Below the warm, fresh surface water, a salt-water tongue is present at 6-8 m in the inner Kara Sea, flowing onshore (Pavlov and Pfirman, 1995). Present sedimentation rates in the southern Kara Sea are estimated to range between approximately 0.2 to 1 mm.yr⁻¹, with the exception of shallow areas that are subjected to winnowing (e.g. Polyak et al., 2000). Sedimentation fluxes are highest in autumn and during the ice-covered months (Gaye et al., 2007).

3. Material and methods

3.1. Collection of samples.

Table 1 lists the SPM and sediment samples investigated in this study and the location of the sampling stations are shown in Fig. 2. In August-September 2009, surface water (<10 m depth; 1-300 L) was collected and filtered at 30 locations distributed throughout the Kara Sea and at 9 locations along the Yenisei River, from the R/V Sovetskaya Arktika. At 15 sites, surface sediment samples were obtained by gravity coring. In September 2011, SPM (120-150 L) and surface sediments (obtained by box cores) were sampled at nine sites throughout the Kara Sea, from the R/V Akademik Mstislav Keldysh. The SPM from both the 2009 and 2011 expeditions was collected with an in situ pump (McLane Large Volume Water Transfer System Sampler), on

A

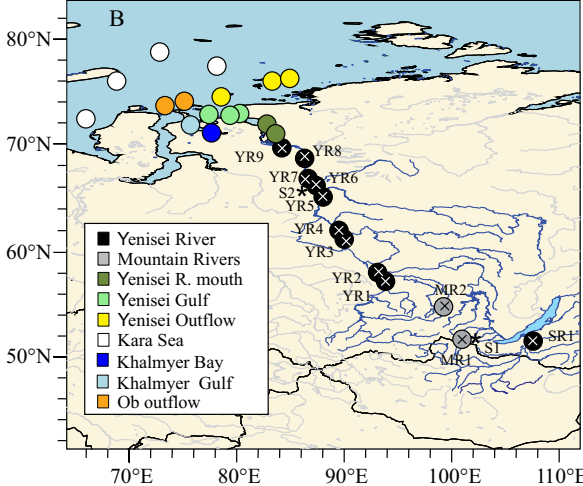


Fig. 2. A) Satellite image of the Ob River Mouth, the Khalmyer Bay and Yenisei River Mouth, showing the increase in sediment load in the Khalmyer Bay and Yenisei Gulf that can be related to coastal cliff erosion. NASA image courtesy Norman Kuring, Ocean Color Web. B) Overview map of the Yenisei River, with sample sites indicated. Asterisks indicate sites of watershed soil samples. C) Map of the Kara Sea, with sampling locations and Yenisei and Ob River Mouths and Khalmyer Bay indicated. Asterisks indicate sampling sites of coastal cliff samples. In panel B) and C) symbol colours divide the stations in geographical zones, as reflected by the legend.

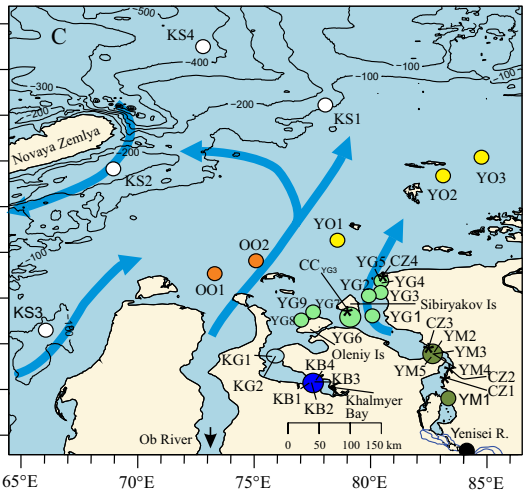


Table 1. Information on the sampled stations. The type of sample, either suspended particulate matter (SPM), sediment, coastal cliff or watershed soil sample is indicated. The coordinates and date of sampling are reported. The depth below sea level (bsl) at which the sample was taken is indicated, both for SPM and sediment samples. N.d. indicates 'not determined', while n.a. indicates 'not applicable'. ▼ ►

Sample code	Zone	Type	Latitude (°N)	Longitude (°E)	Date sampled	Depth bsl (m)
MR1	Mountain River	SPM	54.85631	99.12047	30-6-2010	0.5
MR2	Mountain River	SPM	51.94533	100.78839	11-7-2010	0.5
SR1	Yenisei River	SPM	51.72828	107.46281	6-7-2010	0.5
YR1	Yenisei River	SPM	58.00992	93.11680	25-8-2009	2.0
YR2	Yenisei River	SPM	58.13147	92.75405	29-9-2009	3.0
YR3	Yenisei River	SPM	61.46000	90.08773	27-8-2009	7.0
YR4	Yenisei River	SPM	61.79185	89.54925	25-9-2009	4.0
YR5	Yenisei River	SPM	65.32055	87.95368	29-8-2009	5.0
YR6	Yenisei River	SPM	66.17182	87.23333	20-9-2009	4.5
YR7	Yenisei River	SPM	66.59222	86.57790	31-8-2009	5.0
YR8	Yenisei River	SPM	68.67943	86.26707	1-9-2009	7.0
YR9	Yenisei River	SPM	69.70503	84.20855	3-9-2009	5.0
YM1	Yenisei River Mouth	SPM	70.86107	83.42537	20-9-2009	6.0
YM2	Yenisei River Mouth	SPM	71.87552	82.82212	18-9-2009	4.0
		Sediment				9.5
YM3	Yenisei River Mouth	SPM	71.84173	82.78483	18-9-2009	10.0
		Sediment				23.5
YM4	Yenisei River Mouth	SPM	71.81020	82.74788	19-9-2009	4.5
		Sediment				8.5
YM5	Yenisei River Mouth	SPM	71.76715	82.70532	19-9-2009	3.5
YG1	Yenisei Gulf	SPM	72.64740	80.13693	9-9-2014	7.0
		Sediment				17.0
YG2a	Yenisei Gulf	SPM	73.08272	79.98005	7-9-2009	3.0
YG2b		SPM				15.0
		Sediment				15.0
YG3	Yenisei Gulf	SPM	73.15012	80.49095	6-9-2009	3.0
		Sediment				n.d.
YG4	Yenisei Gulf	SPM	73.36032	80.49095	5-9-2009	3.0
YG5	Yenisei Gulf	SPM	73.40058	80.47580	5-9-2009	5.0
YG6	Yenisei Gulf	SPM	72.71858	79.11492	17-9-2009	1.0
YG7	Yenisei Gulf	SPM	72.55642	79.30307	17-9-2009	5.0
		Sediment				13.5

Sample code	Zone	Type	Latitude (°N)	Longitude (°E)	Date sampled	Depth bsl (m)
YG8	Yenisei Gulf	SPM	72.45150	77.05383	15-9-2009	2.0
		Sediment				4.1
YG9	Yenisei Gulf	SPM	72.61993	77.52445	16-9-2009	2.0
		Sediment				5.8
YO1	Yenisei Outflow	SPM	74.28794	78.62166	09-2012	Surface
		Sediment				28
YO2	Yenisei Outflow	SPM	75.68333	83.20000	09-2012	Surface
		Sediment				52
YO3	Yenisei Outflow	SPM	76.08627	84.86278	09-2012	Surface
		Sediment				51
KS1	Kara Sea	SPM	77.21723	78.09048	09-2012	Surface
		Sediment				126
KS2	Kara Sea	SPM	75.83585	68.91351	09-2012	Surface
		Sediment				320
KS3	Kara Sea	SPM	72.33722	65.98106	09-2012	Surface
		Sediment				139
KS4	Kara Sea	SPM	78.48321	72.79748	09-2012	Surface
		Sediment				476
KB1	Khalmyer Bay	SPM	71.17518	77.37713	12-9-2009	1.0
		Sediment				2.0
KB2	Khalmyer Bay	SPM	71.19288	77.45945	13-9-2009	2.0
		Sediment				4.0
KB3	Khalmyer Bay	SPM	71.22395	77.56670	13-9-2009	4.0
		Sediment				7.1
KB4	Khalmyer Bay	SPM	71.24463	77.68583	14-9-2009	2.0
		Sediment				4.5
KG1	Khalmyer Gulf	SPM	71.77597	75.80948	10-9-2009	3.0
		Sediment				10.5
KG2	Khalmyer Gulf	SPM	71.77742	75.97872	11-9-2009	3.0
		Sediment				6.5
OO1	Ob Outflow	SPM	73.56237	73.30226	09-2012	Surface
		Sediment				25
OO2	Ob Outflow	SPM	73.84178	75.09213	09-2012	Surface
		Sediment				22

Sample code	Zone	Type	Latitude (°N)	Longitude (°E)	Date sampled	Depth bsl (m)
S_1	Watershed soil	Soil	51.96166	100.95583	11-7-2010	n.a.
S_2	Watershed soil	Soil	66.35770	86.34261	26-8-2009	n.a.
CC_YM1	Coastal Cliff Zone 1	Coastal cliffs	71.22225	83.17480	09-2009	n.a.
CC_YM2	Coastal Cliff Zone 1	Coastal cliffs	71.22225	83.17480	09-2009	n.a.
CC_YM3	Coastal Cliff Zone 1	Coastal cliffs	71.22225	83.17480	09-2009	n.a.
CC_YM4	Coastal Cliff Zone 1	Coastal cliffs	71.22225	83.17480	09-2009	n.a.
CC_YM5	Coastal Cliff Zone 2	Coastal cliffs	71.40538	83.39623	09-2009	n.a.
CC_YM6	Coastal Cliff Zone 2	Coastal cliffs	71.40538	83.39623	09-2009	n.a.
CC_YM7	Coastal Cliff Zone 3	Coastal cliffs	71.88668	82.67953	09-2009	n.a.
CC_YM8	Coastal Cliff Zone 3	Coastal cliffs	71.88668	82.67953	09-2009	n.a.
CC_YM9	Coastal Cliff Zone 3	Coastal cliffs	71.88668	82.67953	09-2009	n.a.
CC_YG1	Coastal Cliff Zone 4	Coastal cliffs	73.51950	80.56168	09-2009	n.a.
CC_YG2	Coastal Cliff Zone 4	Coastal cliffs	73.51950	80.56168	09-2009	n.a.
CC_YG3	CC_YG3	Coastal cliffs	72.72285	79.13363	09-2009	n.a.

Sample site	POC (mg.L ⁻¹) ¹	δ ¹³ C (‰)	Sample site	POC (mg.L ⁻¹) ¹	δ ¹³ C (‰)
MR1	1.6	-28.8	YG4	0.03	-31.9
MR2	0.1	-27.8	YG5	0.04	b.d.l.
SR1	6.4	-27.6	YG6	8.1	-28.7
YR1	0.03	b.d.l.	YG7	1.2	-28.1
YR2	0.09	-30.5	YG8	2.7	-29.0
YR3	0.2	-29.3	YG9	2.0	-29.4
YR4	0.03	b.d.l.	YO1	0.06	b.d.l.
YR5	0.1	-29.0	YO2	0.09	b.d.l.
YR6	0.4	-31.4	YO3	0.06	b.d.l.
YR7	0.2	-31.3	KS1	0.08	b.d.l.
YR8	0.07	-33.3	KS2	0.1	b.d.l.
YR9	0.1	-35.0	KS3	0.1	b.d.l.
YM1	0.1	-32.6	KS4	0.1	b.d.l.
YM2	0.03	b.d.l.	KB1	0.2	-29.6
YM3	0.08	-30.2	KB2	0.2	-30.0
YM4	0.6	-28.8	KB3	0.1	b.d.l.
YM5	0.1	-29.6	KB4	1.5	-29.0
YG1	0.04	b.d.l.	KG1	0.1	b.d.l.
YG2a	0.02	b.d.l.	KG2	0.3	-29.1
YG2b	0.05	b.d.l.	OO1	0.1	b.d.l.
YG3	0.1	b.d.l.	OO2	0.1	b.d.l.

Table 3. Summarizes the total organic carbon content percentage (TOC, % dry weight), the stable carbon isotope signal ($\delta^{13}\text{C}$, ‰), the total nitrogen content (TN, % dry weight) and the stable nitrogen isotope signal ($\delta^{15}\text{N}$, ‰) of the sediments, coastal cliff and soil samples. N.d. indicates values that were not determined. ►

Sample site	TOC (%) ¹	$\delta^{13}\text{C}$ (‰)	TN (%) ¹	$\delta^{15}\text{N}$ (‰)
YM2	0.2	-25.7	0.02	3.7
YM3	0.4	-27.5	0.03	3.6
YM4	1.6	-29.1	0.1	2.7
YG1	2.5	-27.5	0.2	4.3
YG2	2.3	-27.5	0.2	5.1
YG3	2.2	-27.3	0.2	4.6
YG7	2.4	-27.4	0.2	3.9
YG8	0.4	-27.0	0.04	4.1
YG9	0.03	-26.2	0.01	5.2
YO1	1.8	-27.0	0.2	6.2
YO2	1.3	-24.8	0.2	7.3
YO3	1.2	-25.1	0.1	7.2
KS1	0.6	-24.9	0.06	7.3
KS2	1.0	-24.0	0.1	7.9
KS3	1.4	-23.9	0.2	7.8
KS4	1.4	-23.1	0.2	6.2
KB1	0.4	-27.7	0.03	2.4
KB2	0.9	-27.6	0.07	2.4
KB3	0.9	-27.0	0.09	3.1
KB4	0.7	-27.4	0.05	2.3
KG1	0.8	-27.1	0.08	4.1
KG2	0.7	-27.0	0.09	4.1
OO1	1.1	-27.3	0.1	6.5
OO2	0.3	-28.0	0.03	5.9
S_1	n.d.	n.d.	n.d.	n.d.
S_2	48	-26.4	1.0	-1.0
CC_YM1	0.7	-25.2	0.1	3.4
CC_YM2	14	-27.2	0.04	1.0
CC_YM3	0.4	-25.7	0.02	3.6
CC_YM4	1.9	-26.6	0.1	3.0
CC_YM5	n.d.	n.d.	n.d.	n.d.
CC_YM6	10	-24.4	0.2	2.5
CC_YM7	n.d.	n.d.	n.d.	n.d.
CC_YM8	0.8	-26.2	0.1	2.8
CC_YM9	1.0	-26.2	0.1	2.5
CC_YG1	1.8	-27.2	0.2	4.7
CC_YG2	1.4	-26.7	0.1	7.1
CC_YG3	0.9	-26.4	0.1	2.4

◀ Table 2. Summarizes the particulate organic carbon content (POC; mg.L⁻¹) and the stable carbon isotope signal ($\delta^{13}\text{C}$) of the SPM samples. B.d.l. indicates that the amounts measured were too low to allow the calculation of the stable carbon isotope signal.

0.7 μm pore size GF/F glass fiber filters. In 2010, three SPM samples were obtained in tributaries of the Angara River and in the Selenga River. Surface water was collected in canisters after wading several meters into the river and filtered using the same filters, a peristaltic pump and a titanium tripod system. Care was taken to sample flowing water in the river, avoiding zones with stagnant water. One surface peat sample was collected in the floodplain of a lake. The TOC-normalized concentrations of the GDGTs in the Yenisei River SPM have been previously reported in De Jonge et al. (2014a). The values reported here are obtained independently, after extraction of the remainder half of the filters. In 2009, coastal cliffs were sampled at five sites, after removal of the exposed layer. The samples were taken on the east bank on the Yenisei River Mouth and Gulf, with one sample taken on Sibiriakov Island. Furthermore, a lowland peat that overlies a buried glacier was sampled in an outcrop, 1.95 m below the surface.

3.2. Lipid extraction and GDGT analyses.

Freeze-dried filters, sediments, coastal cliffs and soils (0.5-5 g) were extracted using a modified Bligh and Dyer method as described by Pitcher et al. (2009). The samples were ultrasonically extracted three times for 10 min using a single-phase solvent mixture of MeOH/DCM/phosphate buffer 10:5:4 (v/v/v). The extract was separated into a core lipid (CL) and intact polar lipid (IPL) fraction over a small silica column, using a procedure modified from Pitcher et al. (2009), using hexane/ethyl acetate 1:1, v/v as eluent. An aliquot of the IPL fraction was analyzed directly for CLs to check for potential carry-over into the IPL fraction. In order to degrade the IPLs to CLs, half of the extract was refluxed for a minimum of 2 h in 1.5 N HCl in MeOH. The amount of CL in this IPL-derived fraction was corrected for the amount of CL brGDGTs carried-over, measured from the non-refluxed IPL fraction. All GDGTs were quantified against a known amount of C_{46} GDGT standard (Huguet et al., 2006) that was added to the CL fraction before filtration through a 0.45 μm PTFE filter and to the IPL fraction before the separation preceding the acid hydrolysis.

Samples were analyzed using a novel high performance liquid chromatography–mass spectrometry (HPLC-MS) method (De Jonge et al., 2014b). In short: GDGTs were analyzed using an Agilent 1100 series / 1100 MSD series instrument. The HPLC system was fitted with 4 Alltima Silica columns (150 x 2.1mm; 3 μm ; Grace Discovery Sciences, USA) in series. Separation was achieved isocratically using 98 % hexane and 2% isopropanol (IPA) for 140 min, with a flow-rate of 0.25 mL.min⁻¹. After each analysis, the columns were cleaned by back-flushing hexane/IPA 1:9 (v/v), at a flow rate of 0.275 mL.min⁻¹, and allowed to re-equilibrate at 98 % hexane and 2% IPA for 15 min. Detection was achieved in selected ion monitoring mode (SIM; Schouten et al., 2007a) using m/z 744 for the internal standard, m/z 1292 for crenarchaeol and m/z 1050, 1048, 1046, 1036, 1034, 1032, 1022, 1020 and 1018 for branched GDGTs. Agilent Chemstation software was used to integrate peak areas in the mass chromatograms of the protonated molecule ($[\text{M}+\text{H}]^+$).

3.3. Calculation of GDGT-based ratios and proxies.

The isomer ratio (IR) represents the fractional abundance of the penta- and hexamethylated 6-Me brGDGTs, compared to the total of penta- and hexamethylated brGDGTs (modified after De Jonge et al., 2014a):

$$IR = (IIabc' + IIIabc') / (IIabc + IIIabc + IIabc' + IIIabc'). \quad [Eq. 1]$$

The roman numerals refer to the fractional abundances of GDGTs indicated in Fig. 1, II, III are 5-Me brGDGTs, while II' and III' are 6-Me brGDGTs. Xabc means that this index includes both the non-cyclopentane containing (Xa) and the cyclopentane containing (Xb,c) components.

The BIT index was calculated according to Hopmans et al. (2004). The inclusion of 6-Me brGDGTs is mentioned explicitly:

$$BIT \text{ index} = (Ia + IIa + IIIa + IIa' + IIIa') / (Ia + IIa + IIIa + IIa' + IIIa' + IV). \quad [Eq. 2]$$

Here, Ia is a brGDGT and IV is the isoprenoid GDGT (iGDGT) crenarchaeol (specific GDGT for Thaumarchaeota; Sinninghe Damsté et al., 2002).

We calculated a reconstructed pH using the CBT' index following De Jonge et al., (2014b):

$$CBT' = {}^{10}\log[(Ic + IIa' + IIb' + IIc' + IIIa' + IIIb' + IIIc') / (Ia + IIa + IIIa)]. \quad [Eq. 3]$$

$$pH = 7.15 + 1.59 * CBT' \quad [Eq. 4]$$

The MAT_{mr} is calculated as a multiple linear regression (De Jonge et al., 2014b):

$$MAT_{mr} (^{\circ}C) = 7.17 + 17.1 * [Ia] + 25.9 * [Ib] + 34.4 * [Ic] - 28.6 * [IIa] \quad [Eq. 5]$$

The square brackets in this formula indicate that we use the fractional abundance, i.e. the value is relative to the sum of all the

$$\text{brGDGTs } (Ia + Ib + Ic + IIa + IIa' + IIb + IIb' + IIc + IIc' + IIIa + IIIa' + IIIb + IIIb' + IIIc + IIIc').$$

3.4. Environmental parameters and bulk geochemical analysis.

The pH of the river and marine water was measured on-board. The particulate organic carbon (POC) and $\delta^{13}C$ content of river SPM on the filter was measured using a Flash 2000 Organic Elemental Analyzer. The total organic carbon (TOC) and total nitrogen (TN) content and the $\delta^{13}C$ and $\delta^{15}N$ values from the sediments, coastal cliffs and soil samples were measured after decalcification of the sediments, in an overnight reaction with a surplus of a 1.5 N HCl solution. After washing the extract with bidistilled water and re-adjusting the pH to 4-5, the freeze dried sediments were analyzed using a Flash 2000 Organic Elemental Analyzer.

3.5. Numerical analysis.

The principal component analysis based on the correlation matrix was performed using the R software package for statistical computing. We performed an unconstrained Q-mode PCA on the standardized relative brGDGT values of the core lipid fraction, for those sites that have more than 8 components quantified. The brGDGT scores are calculated proportional to the eigenvalues, and the site scores are calculated as the weighted sums of the species scores. Squared Pearson correlation coefficients (r^2 values) are reported to demonstrate the performance of the linear correlations.

4. Results

In order to constrain the sources of the brGDGTs in the Yenisei River and the Kara Sea, the brGDGT abundance and distribution is investigated. The brGDGTs encountered in the SPM and sediments of the Kara Sea can be derived from several sources; they can be soil-derived and transported by the Yenisei River, they can be produced in situ in the river system, or delivered to the marine system through coastal erosion, or they can be of marine origin. To constrain the source of the bulk organic matter (OM; terrigenous versus marine), bulk geochemical parameters have also been measured on the SPM, sediments, coastal cliffs and soils.

4.1. Bulk parameters

Bulk geochemical parameters (OC content, N content, $\delta^{13}\text{C}_{\text{org}}$ and $\delta^{15}\text{N}$) were determined on SPM from the Yenisei River and the Kara Sea, surface sediments and coastal cliffs. The data obtained is listed in Tables 2 and 3. The sample stations are discussed according to the geographical zones (Table 1 and Fig. 2). The particulate organic carbon (POC) content (Table 2) of the Yenisei River has been reported before in De Jonge et al. (2014a), with low POC contents in the main stream (0.02-0.4 mg.L⁻¹), and higher values encountered in some upstream rivers (1.6-6.4 mg.L⁻¹). The POC content of the SPM of the Yenisei River Mouth is comparable to that of the main river (0.02-0.5 mg.L⁻¹), and remains stable throughout most of the Yenisei Gulf (0.02-0.1 mg.L⁻¹). Highest POC concentrations were encountered offshore Oliney Island (2.0-8.1 mg.L⁻¹). Marine water in the Kara Sea, sampled further offshore has a much lower POC content between 0.06 and 0.1 mg.L⁻¹.

The $\delta^{13}\text{C}_{\text{org}}$ of SPM (n=23) varies between -27.6 and -35.0‰ (Table 2). Highly variable values are encountered in the Yenisei River SPM (-27 to -35‰), and generally follow a latitudinal trend, with more negative values at higher latitudes. After the outflow in the Kara Sea no geographical trends are obvious, with $\delta^{13}\text{C}_{\text{org}}$ values varying between -28 and -33‰.

Surface sediments (n=24) were sampled from the Yenisei River Mouth on. The TOC content of the sediments varies between 0.03 to 2.5% of the dry weight, with TN values between 0.0 and 0.2% (Table 3). The highest TOC contents are encountered after the widening into the Yenisei Gulf (Fig. 2; up to 2.5%), while the Yenisei River Mouth and especially the Khalmeyer Bay sediments have lower TOC and TN concentrations (0.2-1.6 and 0.0-0.1%, respectively). The Yenisei outflow sediments have an intermediate TOC concentration (1.2-1.8%), while the offshore Kara Sea sediments show a variable TOC and TN content (0.6-1.4 and 0.06-0.2%, respectively).

The sedimentary $\delta^{13}\text{C}_{\text{org}}$ values vary between -23.1 and -29.1‰ (Table 3), more positive than the $\delta^{13}\text{C}_{\text{org}}$ signal of the overlying SPM. The stable nitrogen isotopic signal varies between 2.3 and 7.9‰ (Table 3). Both the $\delta^{13}\text{C}_{\text{org}}$ and the $\delta^{15}\text{N}$ show a geographical pattern, with the lightest $\delta^{13}\text{C}$ and the heaviest $\delta^{15}\text{N}$ values encountered in the sediments from the Yenisei River Mouth and Khalmir Bay.

The TOC and TN values of the coastal cliffs ($n=10$) are, in some cases, much higher compared to the marine sediments (up to 14% of the dry weight), although the majority of the measured values are comparable to the values in the marine sediments (Table 6). The TN content varies between 0.02 and 0.2%. The $\delta^{13}\text{C}_{\text{org}}$ values vary between -25.2 and -27.2‰ for the coastal cliffs along the Yenisei River Mouth, with slightly more depleted values measured in the coastal cliffs along the Yenisei River Gulf (between -26.4 and -27.2‰). The $\delta^{15}\text{N}$ values of the cliffs along the Yenisei River Mouth have a value between 1.0 and 3.6‰, while the cliffs encountered further downstream have values between 2.4 and 7.1‰. The TOC and TN content, measured on one watershed soil is significantly larger, 50% and 1% of the dry weight respectively (Table 6). The $\delta^{13}\text{C}_{\text{org}}$ value (-26.4 ‰) is comparable to that of the coastal cliffs.

4.2. Abundance of crenarchaeol and brGDGTs

The TOC-normalized concentrations of the brGDGTs and crenarchaeol in the SPM are summarized in Table 4. The concentration of crenarchaeol in the river SPM is low, varying between 0.02-0.3 $\mu\text{g.g POC}^{-1}$. The crenarchaeol concentrations in the Yenisei River Mouth are also low (0.2-1 $\mu\text{g.g POC}^{-1}$), with increased values encountered only in the Yenisei Gulf (up to 12 $\mu\text{g.g POC}^{-1}$). Further downstream, marine SPM is characterized by crenarchaeol concentrations varying between 0.1 and 1 $\mu\text{g.g POC}^{-1}$.

The concentration of the summed amounts of brGDGTs in the SPM of the Yenisei River exceeds that of crenarchaeol at all locations, varying between 1 and 20 $\mu\text{g.g POC}^{-1}$ (Table 4). This is reflected in high BIT-values, varying between 0.93 and 0.99 (Table 4). The brGDGT concentrations in the Yenisei River Mouth SPM (i.e. 20-40 $\mu\text{g.g POC}^{-1}$) are high compared to the concentrations observed in the Yenisei River SPM. In the Yenisei Gulf the concentrations are lower on average, but highly variable (5-40 $\mu\text{g.g POC}^{-1}$). Further downstream, the concentrations decrease to only 0.1 $\mu\text{g.g POC}^{-1}$. The BIT values decrease from over 0.95 in the Yenisei outflow down to 0.22 in marine SPM (Fig. 3A; Table 4).

The TOC-normalized concentration of crenarchaeol in the sediments (Table 5) shows a clear geographical distribution, with the lowest values (0.2 to 1.3 $\mu\text{g.g TOC}^{-1}$) encountered in the Yenisei River Mouth, while sediments of the Kara Sea have crenarchaeol concentrations of up to 33 $\mu\text{g.g TOC}^{-1}$. The brGDGT concentration in the sediments is highest in the Yenisei River Mouth (36 to 87 $\mu\text{g.g TOC}^{-1}$), decreasing to an average of 11 $\mu\text{g.g TOC}^{-1}$ in Kara Sea sediments (Table 5). The BIT values decrease from 0.98 in the Yenisei River Mouth to 0.76 in the Yenisei Gulf and decrease further to 0.09 in the open marine sediments (Fig. 3B; Table 5).

Although the Khalmir Bay is not part of the flow path downstream the Yenisei River, GDGT concentrations are comparable to the Yenisei River Mouth both for SPM and surface sediments. BrGDGT concentrations in SPM vary between 20 and 50 $\mu\text{g.g TOC}^{-1}$ with substantially lower crenarchaeol concentrations, resulting in BIT values of over 0.95 (Table 4). The crenarchaeol

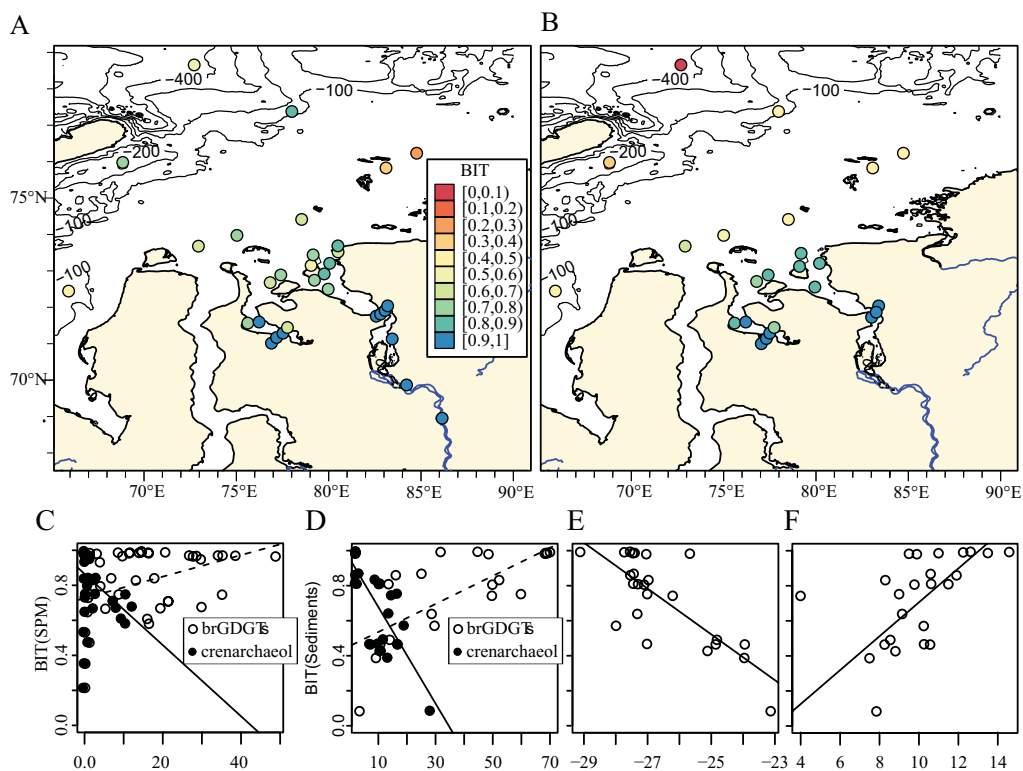


Fig. 3. A-B) Core lipid BIT values in suspended particulate matter (SPM; A) and sediments (B). Colours of the dots refer to the BIT-colour scale indicated. C-D) BIT values plotted vs. GDGT concentration, with brGDGTs plotted as closed symbols and crenarchaeol as open symbols, in both the SPM (C panel) and sediments (D panel). E-F) Sedimentary BIT-values plotted versus the sedimentary d13Corg values (E) and C/N ratio (F).

concentration is low in the Khalmyer Bay sediments (0.7 to $1.0 \mu\text{g.g OC}^{-1}$), increasing further downstream in the Khalmyer Gulf (11 to $12 \mu\text{g.g TOC}^{-1}$) (Table 5). The brGDGT concentration is high in the Khalmyer Bay sediments (50 to $80 \mu\text{g.g TOC}^{-1}$), again resulting in high BIT values (0.98 - 0.99) (Table 5).

The brGDGT concentration in the coastal cliffs (Table 6) varies between 8 and $50 \mu\text{g.g TOC}^{-1}$, with crenarchaeol abundances varying between 0.02 and $10 \mu\text{g.g TOC}^{-1}$. The resulting BIT-values vary between 0.71 and 1.00 (Table 6). The BIT-values in the watershed soils are also high (1.00), with the highest amount of brGDGTs in this dataset encountered at the site S_2 ($86 \mu\text{g.g TOC}^{-1}$).

4.3. Distribution of brGDGTs

The fractional abundances of brGDGTs are reported in Tables 4, 5, 6 and 6, for SPM, sediments and coastal cliffs and watershed soils, respectively. Fig. 4 shows the brGDGT distribution encountered in the Yenisei river and downstream samples, averaged per sampling zone, of those samples that have >8 compounds quantified. Fig. 5A-C shows the brGDGT

distribution averaged for the Khalmyer Bay and Gulf SPM and sediments. Furthermore, Fig. 5D-F shows the brGDGT distribution in the Kara Sea coastal cliffs and in the 2 watershed soils analysed. The brGDGTs present in the CL and IPL fractions are quantified separately. As the IPL brGDGTs are rapidly degraded in the environment (White et al., 1979), they can be interpreted to be indicative of living or recently living material, although archaeal IPL GDGTs with glycosidic head groups have been found fossilized in deeply buried sediments as well (Lengger et al., 2014).

The average brGDGT distribution of the Yenisei River SPM shows a dominance of the 6-Me brGDGTs (Fig. 4A; >50% of summed brGDGTs) as reported previously for the 6-Me hexamethylated brGDGTs (De Jonge et al., 2014a). The IPL fraction, comprising on average 6% of the total brGDGT pool, has a similar average distribution as the CL fraction (Fig. 4E). In contrast, in the most offshore site, the Kara Sea, both the SPM and the CL and IPL fractions of the surface sediments are dominated by the 5-Me brGDGTs (Fig. 4D, K, O; >75% of brGDGTs). Furthermore, these sites show a strong increase of the fractional abundance of brGDGT Ia. While the amount of IPLs in the SPM at these sites is below detection limit, the relative abundance of IPLs in the Kara Sea sediments is 9% of total brGDGTs on average. The distribution encountered in this fraction is similar to the CL brGDGTs (Figs. 4K and 4O). The CL fraction of both the SPM and sediments of the Yenisei River Mouth, Yenisei Gulf and Yenisei Outflow, show a brGDGT distribution that is an intermediary of the Yenisei River and Kara Sea distributions. Moving downstream, we observe decreasing fractional abundances of 6-Me brGDGTs, and increasing fractional abundances of brGDGT Ia (Fig. 4B, C, H, I, J). At these sites, the relative abundance of IPL brGDGTs in the SPM varies between 0 and 5%, with the majority of the sites having IPL brGDGTs present below detection limit. While the IPL distribution in the Yenisei River Mouth mimics the CL distribution (Fig. 4F), the distribution of IPL brGDGTs in the Yenisei Gulf (Fig. 4G) is quite different from that of the CL brGDGTs (Fig. 4C), with increased amounts of the hexamethylated brGDGTs. The amount of IPLs in the sediments is higher, on average 6%, although no major differences between the sedimentary CL and IPL brGDGT distributions are observed.

In the sedimentary brGDGT distribution in Khalmyer Bay and Gulf (Fig. 5A, C), both the CL and IPL fractions are dominated by 5-Me penta- and hexamethylated brGDGTs (Fig. 5C). IPL brGDGTs could only be quantified in the sediments, varying between 5 and 11% of total brGDGTs. The distribution in the coastal cliff samples that border the Yenisei River Mouth and Gulf is summarized in Fig. 5D. Again, the 5-Me penta- and hexamethylated brGDGTs IIa and IIIa are the most abundant compounds and, in general, the distribution is rather similar to those of the Khalmyer Bay and Gulf (Fig. 5).

Only two watershed soils were available for analysis, and neither of these soils represents a 'typical' topsoil (0-10 cm; De Jonge et al., 2014b). The first sample was collected in a lakes floodplain, and is characterized by a dominance of brGDGT IIIa, IIIa' and IIa (Fig. 5E). The second sample was collected in an outcrop, 1.95m below the surface of a peat layer. This sample is characterized by a very large abundance (65%) of the tetramethylated brGDGT Ia (Fig. 5F).

To investigate the changes in distribution of the 15 brGDGTs per site, we performed a principal component analysis (PCA) on the standardized fractional abundances of the CL

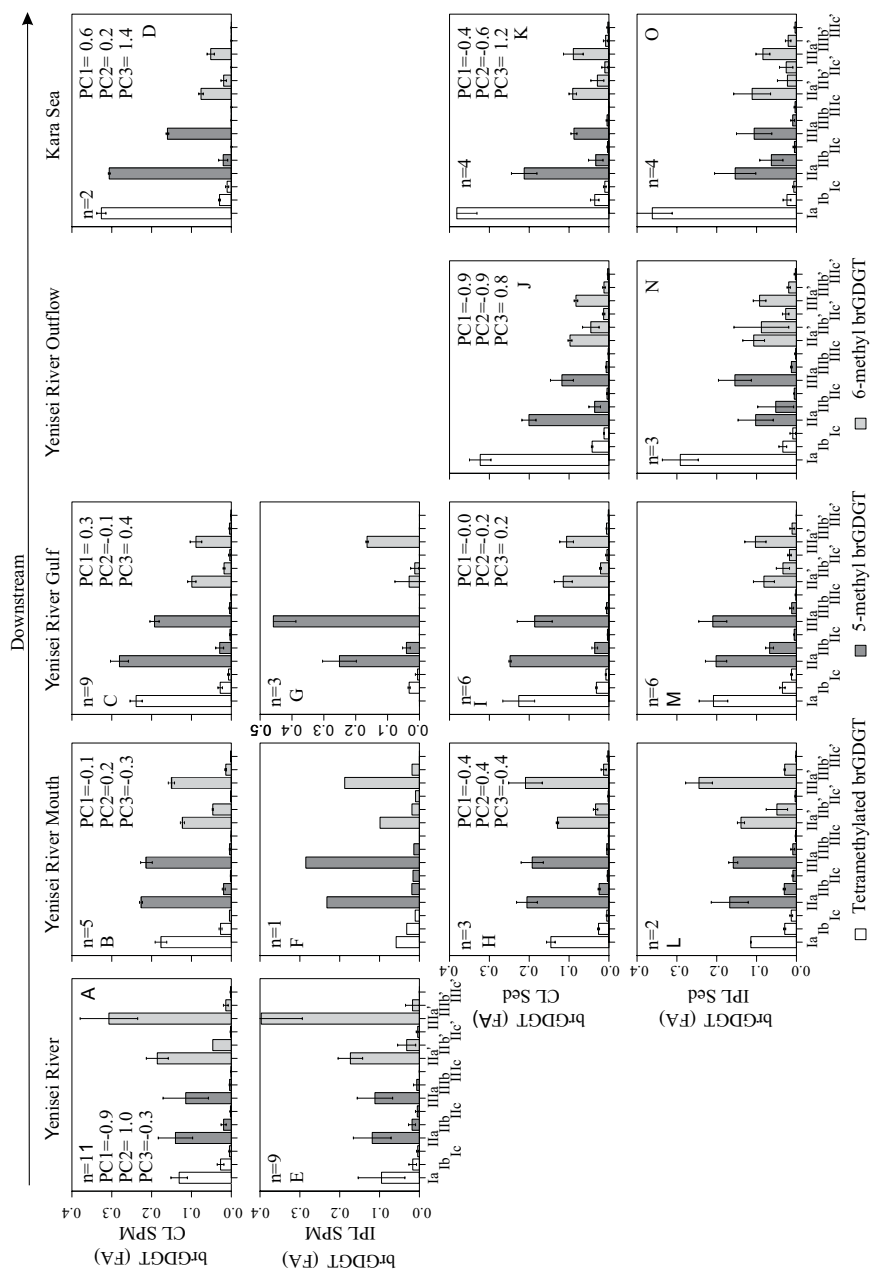


Fig. 4. Bar plots of the fractional abundance of brGDGTs in the CL (A-D and H-K) and IPL (E-G and L-O) fractions of the SPM (A-G) and sediments (H-O), respectively. The fractional abundances are averaged per geographical zone, as defined in Table 1. For the CL fraction, the average score on the first three PC is reported per geographical zone. For clarity, brGDGTs with a large standard deviation (sd) of their fractional abundance (reflecting the variance within the geographical zone) only have the lower half of the range (range = 2 x sd) plotted. The colour of the bars refer to the brGDGT structure, as reflected in the figure legend. As only samples with >8 brGDGTs quantified were plotted, the number of observations per zone is reported, and zones without any samples with >8 compounds, have no corresponding bar plot.

brGDGTs at all studied sites, including the Khalmyer Bay, coastal cliff samples and watershed soils (Fig. 6A, C). We excluded samples that have <9 brGDGTs quantified ($n=8$), mostly due to samples with low brGDGT abundances, to avoid a bias in the PCA. The first three principal components (PC) explain a large part (37, 29 and 13%, respectively) of the variance. The scores provide a summary of the relationship between the stations and the variables (Fig. 6B, D). The strong inverse correlation between the 6-Me brGDGTs IIa', IIb', IIIa', IIIb' and IIIc' on the one hand, and the 5-Me brGDGTs IIa and IIIa on the other hand is captured well by the first principal component (Fig. 6A). This inverse correlation is confirmed by the correlation coefficients (r^2) between the fractional abundances of IIa and IIa' ($r^2=0.70$, $p<0.05$), and, to a lesser extent, between IIIa and IIIa' ($r^2=0.23$, $p<0.05$). Scores on the second PC are predominantly determined by the fractional abundance of a number of minor, cyclopentane containing brGDGTs (i.e. Ib, Ic, IIb, IIc, IIIb, IIIc and IIc'). The third PC (Fig. 6B) is determined by the fractional abundance of brGDGT Ia, that follows an inverse trend as the fractional abundance of brGDGTs IIc, IIIa, IIIb and IIIc, on PC3. We can evaluate downstream trends in the distribution of the 15 brGDGTs by evaluating the scores of the sample sites on these three principal components.

The low scores on PC1 of the Yenisei River SPM (-0.9; Fig. 6B) is in line with the increased abundance of brGDGTs IIa' and IIIa', and consistent with their high IR (0.46-0.77). Compared with the Yenisei River, a strong shift in the brGDGT distribution can be observed in samples collected in the marine system. They show an increasingly higher score on PC1 (except for the Yenisei Outflow and one Kara Sea sediment), indicating a strong shift in the abundance of the 6-Me brGDGTs IIa' and IIIa' (Fig. 6B, E). This is accompanied by lower scores on PC2, related to the increase of the relatively less abundant cyclic brGDGT compounds (i.e. Ib, Ic, IIb, IIc, IIIb, IIIc and IIc'). This decrease of the scores on PC2 is gradual; the SPM and sediments from the Yenisei river Mouth and Gulf score weakly positive, whilst the score on PC2 is negative for the Kara Sea sediments (Fig. 6F), including those sites that underlie the Yenisei River (and Ob River) plume. The scores on PC3 (Fig. 6D, G), mainly reflecting the fractional abundance of brGDGT Ia, increase in the offshore marine Kara Sea sediments (Sed=1.2 and SPM=1.4). This is also the case for the Yenisei Outflow sediments (0.8) and to a lesser degree for the Yenisei Gulf sediments and SPM.

The scores on PC1 (Fig. 6B) of both the Khalmyer Bay and Gulf SPM and sediments indicate an increased amount of the fractional abundance of the brGDGTs IIa and IIIa (Sed = 0.6, SPM = 0.5; Fig. 6B). Compared to the Khalmyer Bay, the Khalmyer Gulf samples also have a relatively higher score on PC2 (Sed = -0.2 and SPM = -0.3), reflecting an increased abundance of cyclopentane-containing brGDGTs. Both the Khalmyer Bay and Gulf samples have a low score on PC3 (Sed = -0.8 and SPM = -0.3), indicating that the fractional abundance of brGDGT Ia is not increased in these samples (Fig. 6D).

The samples collected from the Kara Sea coastal cliffs show a rather variable brGDGT distribution. However, the high scores on PC1 indicate that the high fractional abundances of the 6-Me brGDGTs IIa' and IIIa' encountered in the river SPM, are not encountered in the

coastal cliffs (Fig. 6D). The distributions spans the majority of the variance on PC2, while their low values on PC3 (0.0 on average) indicate that the increased fractional abundance of brGDGT Ia is not encountered in the coastal cliff samples. Both watershed soils have a very different distribution, with the mountainous peat scoring slightly negatively on PC1, contrasting with the positive score of the lowland peat. Both sites have similar scores on PC2, but especially the score on PC3 is radically different, while the mountainous peat has a negative value, the lowland peat has the highest score on PC3 of this dataset.

5. Discussion

5.1. Sources of riverine brGDGTs

In order to use sedimentary brGDGT lipids in palaeoclimate reconstructions, it is essential that the distribution of the brGDGTs does not change between the formation of the signal in soils, their transport through a river system following soil erosion, and their sedimentation in the marine or lacustrine system. In our previous study of the brGDGTs in the Yenisei River SPM (De Jonge et al., 2014a) it was concluded that the majority of the brGDGTs in the Yenisei River SPM were in situ produced, based on the fact that the reconstructed MAT and pH fitted poorly with the soil pH and the MAT imposed on the watershed. However, we employed a soil calibration by Peterse et al. (2012) that was based on a dataset where the 5- and 6-Me brGDGTs were not individually quantified, while the hexamethylated 6-Me brGDGTs were shown to be abundant in the Yenisei River SPM. Re-analysis of the Yenisei SPM samples now allows separating six 6-Me isomers and quantifying all 15 brGDGT components (De Jonge et al., 2014b). The fractional abundance of 6-Me brGDGT in soils increases strongly with increasing pH (De Jonge et al., 2014b). As they are present in high abundance (>50% of summed brGDGTs; Fig. 4) in the Yenisei River water SPM, the novel pH calibration (Eq. 3 and 4; De Jonge et al., 2014b) results in pH values between 6.9 and 7.9 pH units. This is similar to what was obtained previously with the Peterse et al. (2012) calibration, and is significantly higher than the soils present in the Yenisei watershed (De Jonge et al., 2014a). The river water pH values (7.2-7.3) are reconstructed well, taking the calibration's residual standard mean error (RSME) of 0.5 into account. This confirms the dominant influence of aquatic in situ production on the brGDGT distributions in the Yenisei River. The reconstructed MAT, based on the novel MAT_{mr} (Eq. 5; De Jonge et al., 2014b) varies between 3.5 and 7.1 °C. This is on average 4 °C warmer than the reconstructed MAT using the Peterse et al. (2012) soil calibration and on average 9 °C warmer than the measured MAT in the Yenisei watershed. As the calibration by De Jonge et al. (2014b) significantly overestimates the MAT of cold soils, the temperature offset alone is not sufficient to identify the brGDGTs as riverine in situ produced. However, a large temperature gradient is imposed on the watershed soils (De Jonge et al., 2014b), that is absent in the reconstructed temperatures, and it is primarily the lack of this gradient, together with the deviating reconstructed pH values, that indicate that the watershed soils are not the dominant source of brGDGTs. Therefore, the conclusion from De Jonge et al. (2014a) that the Yenisei River brGDGTs are dominantly produced in situ remains valid.

5.2. Sources of brGDGTs in the Yenisei River Mouth and Gulf

The variation in the brGDGT distribution of the SPM and sediments was analysed using a principal component analysis (PCA; Fig. 6). The Yenisei River SPM, especially in the lowland river, has a large fractional abundance of 6-Me brGDGT IIIa' and IIa' (Fig. 4). The high abundance of these brGDGTs, whose fractional abundance was shown to increase with increasing soil pH (De Jonge et al., 2014b), reflects their production in the neutral pH of the Yenisei River water. However, the brGDGTs distribution delivered by the Yenisei River is altered significantly in the Yenisei River Mouth and in the Kara Sea. Firstly, considering the scores on PC1 (Figs. 6B, 6E), both SPM and sediments in the Yenisei River Mouth show a strong decrease in the fractional abundance of the brGDGTs IIIa' and IIa', compared to the upstream Yenisei River values. Also the scores on PC2 (Figs. 6B, 6F) indicate a shift in the brGDGT distribution between the Yenisei River SPM and Yenisei River Mouth. Furthermore, shifts in the brGDGT distribution are observed further downstream the Yenisei River Mouth, in the Yenisei Outflow, but also in the Kara Sea samples that are not directly influenced by the Yenisei Outflow (KS1-KS4). The scores on PC2 decrease for the Yenisei Outflow and some of the Kara Sea samples. Considering the scores on PC3 (Figs. 6D, 6G) we see that the fractional abundance of brGDGT Ia increases downstream from the Yenisei River Mouth samples. This increase happens gradually, first in the Yenisei Gulf, and further in the Kara Sea sediments and SPM (Fig. 6G).

5.2.1. BrGDGTs delivered by the Yenisei River

Although the brGDGT distribution in the lowland Yenisei River is stable throughout August/September, the contrasting brGDGT signature in the Yenisei River Mouth, compared to the signature in the upstream Yenisei River SPM, possibly reflects brGDGTs that were delivered to the marine system earlier in the year. The SPM of the Yenisei River analysed in this study only represents a snapshot in time and may be quite different from the brGDGT composition of SPM transported by the flood that results from snowmelt during the months May-June. Indeed, the majority of terrigenous OM is thought to be supplied to the Kara Sea during the freshet (Lisitsyn, 1995) and the freshet SPM is possibly much more enriched in brGDGTs, as was recently reported by Peterse et al. (2014b) for the Kolyma River (Eastern Siberia), where a 10 times increased amount of brGDGTs was measured during the freshet, compared to the base flow (50 days later), and even a 30-fold increase compared to the season with ice-cover. Large temporal differences in the SPM brGDGT concentration were also observed in the Arctic MacKenzie river, although the highest TOC-normalized values were not only observed during the freshet (Peterse et al., 2014b). As the freshet is accompanied by large amounts of horizontal run-off and soil erosion, the SPM delivered during this period may carry brGDGTs that are more influenced by a contribution of soil-derived brGDGTs. Although this material was delivered to the Yenisei River Mouth several months prior to our sampling campaign, it may still be present as a background signal in the Yenisei River Mouth SPM. Indeed, Gaye et al. (2007) concluded that the main settling fluxes to the sediments do not occur during the freshet, but rather during the months with decreased flow speed (September/October), and especially during the months with ice cover. This is because OM delivered during the freshet will remain in suspension until the flow speed has decreased sufficiently to allow settling of

the particles. The material delivered during the freshet is thus still in suspension, or may have been resuspended (Gaye et al., 2007). The presence of brGDGTs that were delivered to the Yenisei River Mouth since the start of the freshet results in a suspended brGDGTs distribution that is an average of the OM delivered since May. This probably explains why the brGDGT distribution in the surface sediments, that is an average of the settling particle flux over several years, has similar brGDGT distribution as the overlying SPM (Fig. 6C, E). Also the comparable OC-normalized abundances of the brGDGTs indicate a strong coupling between the SPM and sediments in this shallow setting.

Unfortunately, as the brGDGT distribution in the Yenisei River during the freshet is unknown, constraining the amount of riverine and soil-derived brGDGTs in the Yenisei River Mouth is not possible. Although the fractional abundance of 6-Me brGDGTs IIa' and IIIa' decreases compared to the Yenisei River SPM, increased abundances are still encountered in the Yenisei Mouth SPM and sediment, suggesting that at least part of the brGDGT signal is derived from riverine in situ production.

5.2.2. BrGDGTs derived from coastal cliffs

In contrast to many other coastal seas, the shoreline of the Kara Sea is composed of an extensive system of coastal cliffs that are subjected to thermal and wave erosion. These thermoabrasive coasts are frozen for most of the year, with intensive erosion occurring only during the summer months. The Kara Sea coastal cliffs (up to 80 m high) are comprised mainly of Pleistocene marine sandy clays, with only little contribution of continental soils (Streletskaia et al., 2009). In the Kolyma River Basin, a Northeastern Siberian shelf sea similar to the Kara Sea, coastal OM was shown to contribute to 50-60% of surface sediment OM (Vonk et al., 2010). However, Streletskaia et al. (2009) estimate that the amount of OM delivered by coastal erosion into the Kara Sea (defined as the area between Nova Zembyla and Taymyr Peninsula), is about 25 times less than the amount delivered by the rivers. The Khalmyer Bay and Gulf exemplify a setting in the Kara Sea area where the majority of brGDGTs encountered could be primarily derived from coastal cliff erosion, as no major rivers drain into this bay. Although no erosion rates of the coastal cliffs are known for this setting (Lantuit et al., 2012), satellite photos (e.g. Fig. 2A) show that the amount of clastic material deposited in this bay is substantial. Indeed, high concentrations of brGDGTs, coeval with high BIT-values, were encountered in the Khalmyer Bay (Fig. 3D). Although quite variable in composition, the weighted average of the brGDGT distribution of the Kara Sea coastal cliffs (red asterisk in Figs. 6B-D) is similar to the brGDGT distributions encountered in Khalmyer Bay SPM and sediments (cf. Fig. 5D and Figs. 5A-B). Assuming a similar brGDGT distribution for the cliffs of Khalmyer Bay as for the cliffs in the Yenisei River Mouth and Gulf, this strongly suggests that coastal cliffs may be a major source for brGDGTs in the Khalmyer Bay area.

The brGDGTs encountered in the Yenisei Mouth and Gulf, on the other hand, will reflect a mixture of riverine and coastal sources. Slow erosion rates (i.e. 0.2 to 0.4 m.yr⁻¹) are reconstructed for the coastal cliffs at the latitude of YM1, where the coastal cliffs have a height between 20 and 40 m (Streletskaia et al., 2009), while the northeastern coastline of the narrow in the Yenisei Mouth (i.e. Sopochmaya Karga ice complex; in the proximity of sample sites YM2-YM5), was shown to be a site with moderate erosion rates, in the order of 1-2 m.yr⁻¹

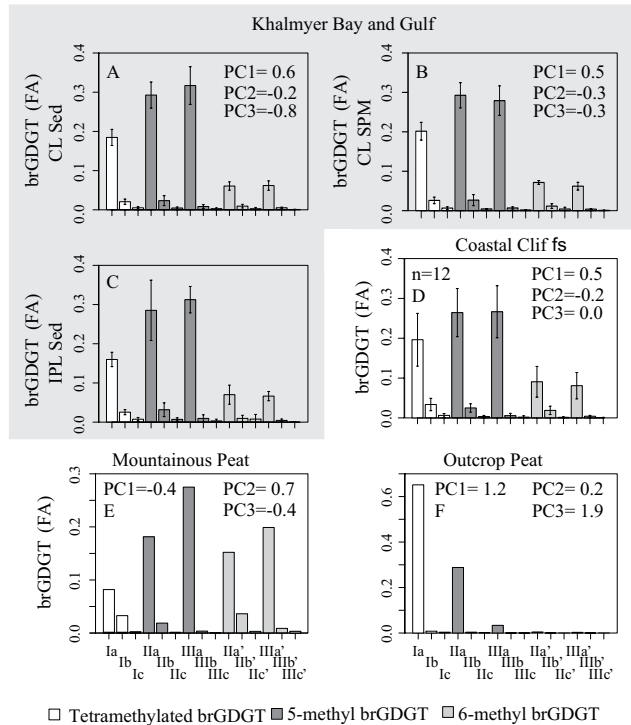


Fig. 5. Bar plots of the fractional abundance of brGDGTs in the CL (A, B, D) and IPL (C) fractions of the Khalmyer Bay and Gulf sediments (A, C) and SPM (B). Furthermore, a number of possible sources of brGDGTs is reported, being the coastal cliffs (D), a mountainous peat sample from the floodplain of a lake (E) and a lowland peat sampled at 2m depth (F). The fractional abundances are averaged for the Khalmyer Bay and Gulf (as defined in Table 1) combined. The number of observations per zone is reported, and to capture the variance between the samples in each dataset, the range indicated with the whiskers equals 2 x standard deviation. For the CL fraction, the average score on the first three PC is reported. The colour of the bars refer to the brGDGT structure, as reflected in the figure legend.

(Lantuit et al., 2012). BrGDGTs derived from coastal cliffs may thus have an influence on the brGDGT distribution, although the extent to which this influences the brGDGT distribution encountered in the Yenisei River Mouth and Gulf is unknown.

5.3. Sources for brGDGTs in the Yenisei Outflow in the Kara Sea

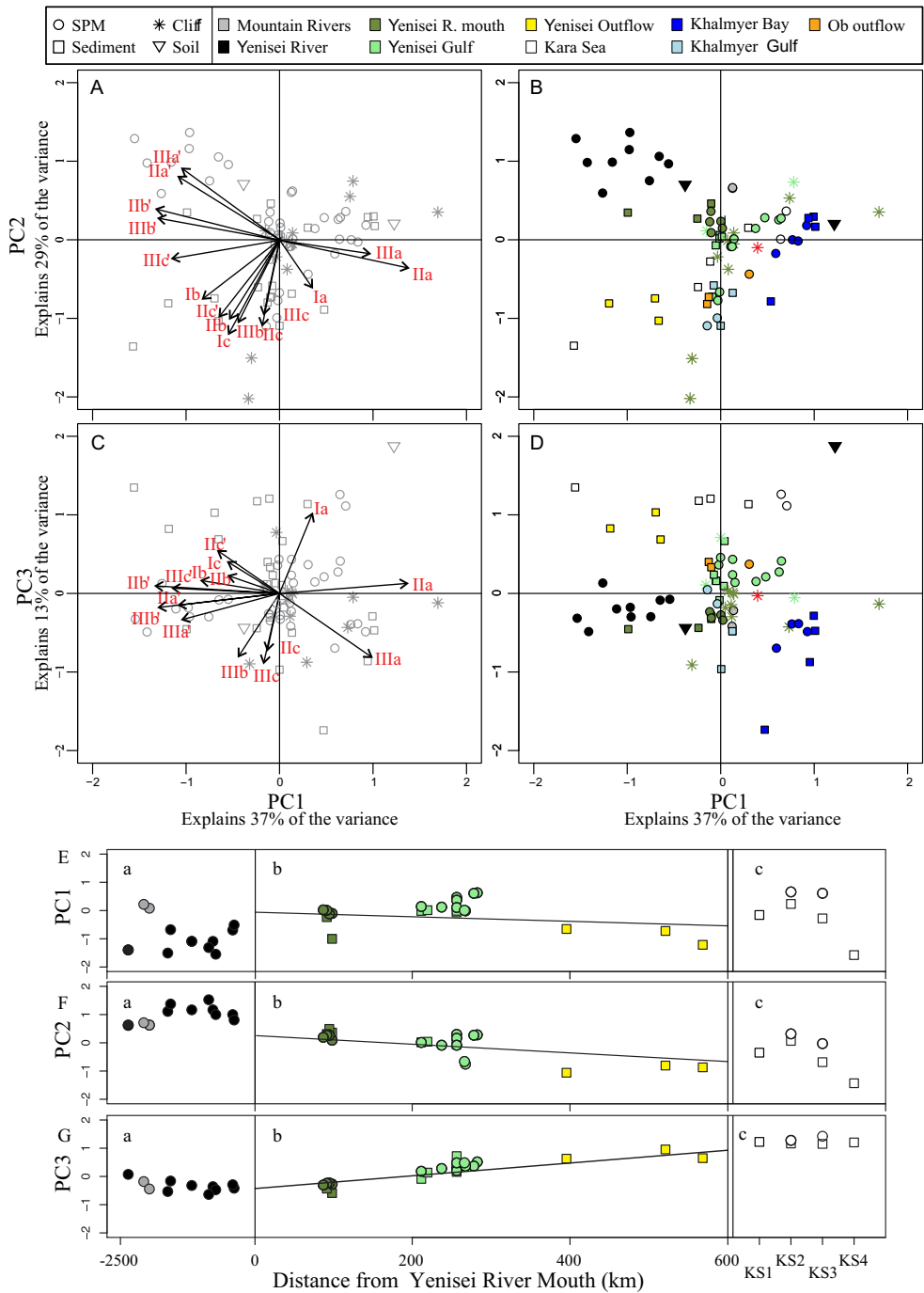
The brGDGT distribution encountered in the Yenisei River Mouth is a mixture of riverine in situ produced brGDGTs, an unknown contribution of soil-derived brGDGTs delivered by the river during the freshet, and an unknown contribution of coastal-cliff derived brGDGTs delivered to the marine system following coastal erosion. This complex mixture is transported eastwards, under the influence of the Greenland current (Fig. 2C). Another major source of brGDGTs in the Kara Sea system is the Ob River. The brGDGT distribution delivered by the Ob River, sampled downstream the Ob Gulf, is similar to some of the Yenisei Gulf distributions (Figs. 6B, 6D), reflecting similar brGDGT sources, as can be expected by the similar geographical extent of the

Ob River. We note that the Kara Sea locations (KS1-4) that are not directly under the influence of the Yenisei River plume probably indirectly receive brGDGTs from the Yenisei River and Ob River outflow, through the anti-clockwise surface current present in the Kara Sea (Fig. 2).

Although the complex origin of the brGDGT mixture in the Yenisei Mouth and Gulf cannot be resolved, this is not the final distribution encountered in the Yenisei Outflow SPM and surface sediments. Moving downstream, we observe a simultaneous decrease of the brGDGT concentration and a shift in the brGDGT distribution, that is reflected in the changing values along PC2 and PC3 (Figs. 6F-G). The largest change is the increase in the fractional abundance of brGDGT Ia in the sediments (up to 43% of all brGDGTs; correlation with distance river Mouth: $r^2 = 0.75$). Also, the concentration of summed brGDGTs decreases strongly downstream of the Yenisei River (negative correlation with distance river Mouth: $r^2 = 0.42$). A mechanistic link between the changing brGDGT distribution and the amount of brGDGTs, or the distance from the river Mouth, seems apparent.

We discuss two mechanisms that may be responsible for changing brGDGT distributions in an increasingly marine system. The first is in situ production of marine brGDGTs. This mechanism has been invoked by a number of authors to explain changing brGDGT distributions in marine coastal sediments (Svalbard fjord, Peterse et al., 2009a; Yangtze River, Zhu et al., 2011a; Pearl River, Zhang et al., 2012; Tagus River and Amazon River; Zell et al., 2014a,b). Overall, these authors describe an increase in the fractional abundance of one or more cyclopentane-containing brGDGTs. The effect of in situ production on the Kara Sea system is probably captured along the second PC, reflected in the increase of a group of minor, cyclopentane-containing brGDGTs, that affect the brGDGT distribution of the Yenisei Outflow and Kara Sea samples (Fig. 6B). The values on PC2 decrease with increasing distance to the Yenisei River, where the Kara Sea samples that are less influenced by the Yenisei Outflow signal, are characterized by the lowest values. Especially the deepest site, KS4, seems to be influenced by an increase of both minor 5-Me cyclopentane-containing brGDGTs (low values on PC2; Fig. 6F), which generally increase with increasing pH, and 6-Me brGDGTs (low values on PC1; Fig. 6E), that have been shown to increase with increasing soil pH (De Jonge et al., 2014b). More information concerning the in situ produced signal can be derived from the intact polar lipid (IPL) fraction. The brGDGTs from living or recently living cells will be present as IPLs, which, after cell death are rapidly degraded into core lipids (CL). The relative abundance of the IPL brGDGTs in the Kara Sea sediments is high (average: 9%), comparable to the IPL percentage in soils (eg. 9-19%; Peterse et al., 2010) and the fractional abundance of the cyclopentane-

Fig. 6. Biplots of the principal components (PC) based on the fractional abundance of CL brGDGTs, for those samples that have more than 8 (out of 15) brGDGTs quantified. The first two (A, B) and first and third PC (C, D) are plotted, representing respectively 37, 29 and 13% of the variance. The loadings of the variables (A, C) and the scores of the sites (B, D) are plotted. The score of each station is calculated using the relative abundance of each compound per station and its loading on the PC. Round symbols indicate SPM brGDGT distributions, rectangles indicate sedimentary brGDGT distributions, asterisks indicate coastal cliff samples and triangles indicate watershed soil samples. The colour of the symbols reflects the geographical zone of the station. The red coloured asterisk gives the score of the weighed average of the coastal cliff brGDGT distributions (n=12). E-G) Plots of the score on the PC1-3. In subplots a and b the scores are plotted against the straight distance from the river Mouth (83°17.0383 N, 70°99.675 E), where subplot a has a different scale compared to subplot b. The 4 Kara Sea samples are plotted in subplot c, as the distance from the river Mouth will be a poor comparison for the length of the flowpath for these samples. ►



containing brGDGTs in the sedimentary IPL fraction is slightly larger than in the CL fraction (25% versus 18% for Yenisei outflow samples, 18% versus 14% for Kara Sea samples).

However, the encountered brGDGT distribution in the Yenisei Outflow and Kara Sea SPM and sediments, cannot be fully attributed to in situ production. In situ produced marine brGDGTs in high-latitude marine sediments were observed by Peterse et al. (2009a) in sediments offshore Svalbard. As Svalbard is located at the same latitude as the most offshore samples in the Kara Sea, we expect an in situ produced marine brGDGT distribution to be comparable. However, the brGDGT distribution Peterse et al. (2009a) observed in Svalbard fjords is clearly distinct from the distributions in the Yenisei outflow system. The Svalbard in situ produced distribution reflects the relatively high pH of the Arctic Ocean, resulting in a brGDGT distribution that was dominated by cyclopentane-containing brGDGTs (60 % of total brGDGTs), in contrast to the off-shore Kara Sea sediments, where the cyclopentane-containing brGDGT comprise on average 14% and at maximum 23% of total brGDGTs. Furthermore, the in situ produced signal in the Arctic sediments off Svalbard reflects the cold conditions with hexa- and pentamethylated brGDGTs representing 88% of the total, while these highly methylated brGDGTs in the offshore Kara Sea sediments amount up to between 55 and 63%. Thus, although in situ production influences the Kara Sea sedimentary brGDGT distribution (as reflected by PC2), it does not fully explain the encountered brGDGT distribution. Especially the increase in the fractional abundance of a 'warm' tetramethylated brGDGT, representing up to 42% of all brGDGTs (as also reflected by the high scores on PC3; Fig. 6G) cannot be attributed to in situ produced marine brGDGTs. Furthermore, the fractional abundance of brGDGT Ia is not increased in the IPL fraction compared to the CL fraction (29% versus 32% for the Yenisei Outflow, 36% versus 38% for the Kara Sea samples), indicating that this brGDGT is probably not in situ produced.

A second mechanism that can cause changing brGDGT distributions in the river outflow, is preferential degradation of different brGDGT pools. The brGDGTs present in the Yenisei River Mouth are a mixture of an in situ produced riverine signal and an unknown amount of pre-aged brGDGTs, both derived from the river watershed and the coastal cliffs. When a mixture of pre-aged and modern (river-derived) OM is delivered to the marine system, the riverine fraction is more labile and will be degraded preferentially (e.g. Blair and Aller, 2012). This is because pre-aged soil-derived material and fossil material, associated with clay particles, will be physically protected from degradation. Thus, the contribution of riverine in situ produced brGDGTs to the Yenisei Outflow and Kara Sea distributions is assumed to be minor. This is also indicated by the offset between the brGDGT distributions encountered in the Yenisei River SPM and the Yenisei Outflow (Fig. 6B, 6D).

Both the watershed soils and coastal cliffs can be the source of pre-aged brGDGTs encountered in the Yenisei Outflow and Kara Sea. We postulate that a coastal cliff source is less probable, as a large offset is observed between the brGDGT distribution present in the coastal cliffs and in the Yenisei Outflow (Fig. 6B, 6D). Secondly, making a rough estimate of the relative contribution of coastal cliff brGDGTs to the total Kara Sea brGDGT pool, reveals that coastal-cliff derived brGDGTs represent only a small fraction of the total brGDGTs delivered to the Kara Sea system. Based on the OC content measured in the cliffs and the erosion rate,

estimates of the amount of OM delivered into the Kara Sea (defined as the area between Nova Zembyla and Taymyr Peninsula) have been made by Streletskaia et al. (2009). These estimates indicated that the amount of OM delivered by coastal erosion to the Kara Sea is about 25 times less than the amount of OM delivered by the rivers. Comparing the brGDGT TOC-normalized concentration in the coastal cliffs with the concentration measured in the Yenisei River allows estimating the relative contributions of both sources to the total Kara Sea brGDGTs. The TOC-normalized concentration of the Yenisei Mouth coastal cliffs ($n=10$, on average $28 \mu\text{g.gTOC}^{-1}$, between 8 and $51 \mu\text{g.gTOC}^{-1}$) slightly exceed the concentration of the Yenisei River baseflow SPM (on average $12 \mu\text{g.gTOC}^{-1}$, up to $20 \mu\text{g.gTOC}^{-1}$). However, this is only a poor estimate of the riverine brGDGT input, as the river SPM does not carry a constant signal year-round and the POC-normalized amount of brGDGTs has been observed to increase during the freshet in another Siberian river system (e.g. Peterse et al., 2014b). Furthermore, we have no information on the concentration of brGDGTs within the Ob River SPM, and thus have to assume a similar contribution as the Yenisei River. As the amount of OC derived from rivers exceeds the coastal cliff-derived OC 25-fold (Streletskaia et al., 2009), we can thus make a very conservative estimate that the contribution of brGDGTs delivered to the Kara Sea system by river will be at least 10 times more than the coastal cliffs input, based on a Yenisei River SPM snapshot that does not reflect freshet conditions.

We thus postulate that the brGDGT distribution in the Kara Sea is probably dominated by pre-aged soil-derived brGDGTs. However, only two watershed soils have been analysed up to date, a mountainous peat sampled in the floodplain of a lake and a lowland peat that was sampled in an outcrop above a buried glacier (Karpov, 1983; Shpolyanskaya, 2003). Although this dataset definitely does not represent a good coverage of the Yenisei watershed soils, it does highlight that watershed soils are a potential source for the brGDGT distribution encountered offshore. Fig. 5 shows the fractional abundance of the brGDGTs encountered in these samples. While the mountainous peat (Fig. 5E) has a brGDGT distribution that is rather different from the offshore distribution (Fig. 4 D, J, K, N and O), the lowland peat sample is characterized by a large fractional abundance of Ia (65%; Fig. 5F), resulting in a fairly comparable distribution as the offshore samples. Although the extent of this soil type is unknown, its contribution to the Yenisei River SPM may explain the observed shift in offshore brGDGTs. In case the brGDGTs encountered in the offshore Kara Sea samples are soil-derived, we would expect that the bulk OM proxies indicate the presence of a terrigenous signal. The following section will discuss how the BIT-index performs as a tracer for terrigenous input, and whether the presence of a terrigenous fingerprint in the sediments and SPM of the Yenisei Outflow and Kara Sea is confirmed by the bulk OM parameters.

5.4. Comparing proxies for terrigenous input in the Kara Sea

The Yenisei River delivers large amounts of OM to the Kara Sea, between $4\text{--}5 \cdot 10^{12} \text{ g} \cdot \text{yr}^{-1}$ (Telang et al., 1990; Lobbes et al., 2000). The supply of OM to the marine system can possibly be traced spatially and reconstructed through time using the GDGT-based BIT-index (Hopmans et al., 2004). This ratio [Eq. 2] calculates the amount of five major brGDGT lipids relative to the amount of crenarchaeol, a membrane lipid that is specific to Thaumarchaeota and

is predominantly produced in the marine system (Sinninghe Damsté et al., 2002). As previous studies assumed that the brGDGTs in marine river fan sediments are derived dominantly from soils, the BIT-index was interpreted to trace the delivery of soil-derived OM to the marine system. As the brGDGTs within the Yenisei River, several months after the freshet, were shown to be dominantly in situ produced (De Jonge et al., 2014a), the BIT index in the Yenisei River outflow should be interpreted as a proxy for both terrigenous and riverine OM transported by the river, rather than soil-derived OM alone. Furthermore, coastal cliff-derived brGDGTs can also be significant, especially in those settings without major river input. This study allows testing the performance of the BIT-index in marine outflow sediments as well as in the overlying SPM.

Although the brGDGT distribution in the Yenisei River SPM reflects an aquatic source, the BIT values of the SPM are close to unity (0.93-0.99; Table 4) and are thus comparable with values typically encountered in soils (generally >0.9 ; Schouten et al., 2013a). Also the coastal cliffs have high BIT values. Although the contribution of brGDGT derived from the river SPM, watershed soils and coastal cliffs cannot be constrained well in the Yenisei River Mouth, all these sources have high BIT-values, resulting in Yenisei River Mouth SPM samples having similar, high BIT values (0.97-0.98). The Khalmyer Bay SPM is also characterized by high BIT values (0.95-0.97; Fig. 3A). The BIT values of the SPM in the Yenisei Gulf decrease with increasing distance to the river Mouth (Fig. 3A).

To evaluate whether the BIT-index is governed by changes in the abundance of crenarchaeol, or by the summed abundance of brGDGTs, previous authors (e.g. Sinninghe Damsté et al., 2012; Smith et al., 2012) have evaluated whether significant correlations can be found with the concentration of these compounds. However, obtaining a significant correlation between the BIT index and the amounts of crenarchaeol and brGDGTs of the SPM is complicated by the phenomenon that some sites with intermediate BIT-values (offshore Oliney Island and in the Yenisei Gulf) have distinctly increased GDGT concentrations, influencing the abundance of both crenarchaeol and brGDGTs (Fig. 3C). Thus, the correlations of BIT with the abundance of crenarchaeol and the summed abundances of brGDGTs have low r^2 values of 0.13 and 0.16, respectively.

In the sediments, the BIT values mimic the pattern observed in the overlying SPM well, decreasing from 0.98 in the Yenisei River Mouth to 0.09 in the offshore marine sediments (Fig. 3B; Table 5). Besides the Yenisei River Mouth, also Khalmyer Bay is characterized by high BIT values (0.95-0.97; Fig. 3B), reflecting the high BIT values in the Khalmyer Bay SPM. Supporting its application as a tracer for terrigenous brGDGTs, the sedimentary BIT values correlate with brGDGT concentration in the sediments ($r^2 = 0.52$; Fig. 3D). However, the BIT-index also correlates negatively with the crenarchaeol concentration ($r^2 = 0.72$; Fig. 3D), indicating that both changes in crenarchaeol and brGDGTs concentration influence the calculated BIT-values. This result is similar to a study tracing terrigenous OM offshore Portugal by Zell et al. (2014a).

To further support the use of the BIT-index for reconstructing terrigenous input in the Yenisei sediments, we compare the BIT values with bulk parameters that have been used to trace the input of terrigenous OM in Kara Sea sediments: stable isotopes ($\delta^{13}\text{C}_{\text{org}}$) and C/N ratios (Fernandes and Sicre, 2000; Krishnamurty et al., 2001). These studies invoked two sources for OM encountered in the Kara Sea sediments, with contrasting $\delta^{13}\text{C}_{\text{org}}$ and C/N values; soil-

derived terrigenous matter (-27‰ and >15, respectively) and in situ produced marine OM (-16 to -19‰ and <6.5, respectively). The influence of coastal cliffs ($\delta^{13}\text{C}_{\text{org}}$ (-26.6 to -24.4 ‰) and C/N signature (median=12)) was previously not taken into account. However, as the $\delta^{13}\text{C}_{\text{org}}$ values confirm a mixed terrigenous and marine OM source, they can't be identified as a third end-member based on their bulk OM characteristics unless radiocarbon ages are taken into account (cf. Vonk et al., 2010).

The range (-29.1 to -23.1‰) of sedimentary $\delta^{13}\text{C}_{\text{org}}$ values calculated in this study (Table 3) agrees with previous studies, although our most positive values exceed the known range for this setting, possibly because of the larger study area which includes more offshore surface sediments. The $\delta^{13}\text{C}_{\text{org}}$ values of the sediments in the Yenisei River Mouth (-26 to -29‰) agree with that of a terrigenous end-member postulated in previous studies (-27‰), that was based on the stable isotopic signal of tundra soils (Naidu et al., 1993), and with the $\delta^{13}\text{C}_{\text{org}}$ value of the lowland peat (-26.4‰). They are, however, slightly offset (more negative) compared to the coastal cliff $\delta^{13}\text{C}_{\text{org}}$ values. The sediments further downstream reveal an increasing $\delta^{13}\text{C}_{\text{org}}$ value, up to -23‰ (Fig. 3D). This latter value is still distinct from the marine Kara Sea end-member calculated in previous studies (Fernandes and Sicre, 2000; between -16 and -19‰), suggesting that even the most offshore sediments do not represent a setting with an exclusively marine input.

The C/N values of the sediments vary between 6.5 and 15, in agreement with previous studies (Fernandes and Sicre, 2000; Krishnamurthy et al., 2001). These authors observed a seaward decrease in C/N ratio, caused by an admixture of marine OM (C/N values <6.5). The C/N ratio in the Yenisei River Mouth sediment varies between 15.0 and 11.6, which agrees with the value of 13.5 Krishnamurthy et al. (2001) obtained at this site, although the range we observe between the values is substantial. Especially station YM4 seems to be characterized a strong terrigenous signal, with a $\delta^{13}\text{C}_{\text{org}}$ value of -29‰ and a C/N ratio of 15. Yenisei Gulf values vary between 6.5 and 12.1, with lower values (6.5-9.3) encountered offshore Oliney Island. The Kara Sea sediments west and north of the Ob and Yenisei outflow (KS2, KS3, KS4), have slightly lower C/N values (7.5 to 8.1) that indicate an increased amount of marine OM, although the C/N ratio confirms that even these sediments do not reflect an exclusive marine OM input. The Kara Sea samples under influence of the Ob and Yenisei outflow (YO and OO) have a C/N ratio (8.5-11.2) that indicates a substantial input of terrigenous OM, which is higher than the most offshore samples collected by Krishnamurthy et al. (2001) and Fernandes and Sicre (2000) (between 5.0 and 9), although our samples were collected even further from the river Mouth. Thus, both the $\delta^{13}\text{C}_{\text{org}}$ and C/N values indicate the presence of terrigenous matter in offshore Kara Sea sediments, even in those sediments that are not directly influenced by the Ob and Yenisei plume (i.e. KS1 - KS4). In the Khalmyer Bay sediments, bulk terrigenous proxies indicate a substantial amount of terrigenous OM. Its sediments are characterized by $\delta^{13}\text{C}_{\text{org}}$ values of -27.0 and -27.7‰, only slightly more negative than the $\delta^{13}\text{C}_{\text{org}}$ values of the coastal cliffs, and C/N ratios between 10.1 and 12.6. The C/N ratio decreases rapidly, varying between 8.4 and 9.8 in the Khalmyer Gulf sediments.

Both bulk terrigenous proxies thus reflect a strong terrigenous signal in the Yenisei River Mouth, that decreases downstream, and a strong terrigenous signal in the Khalmyer Bay. This reflects the spatial pattern of the BIT index. The good correlation between BIT and the bulk

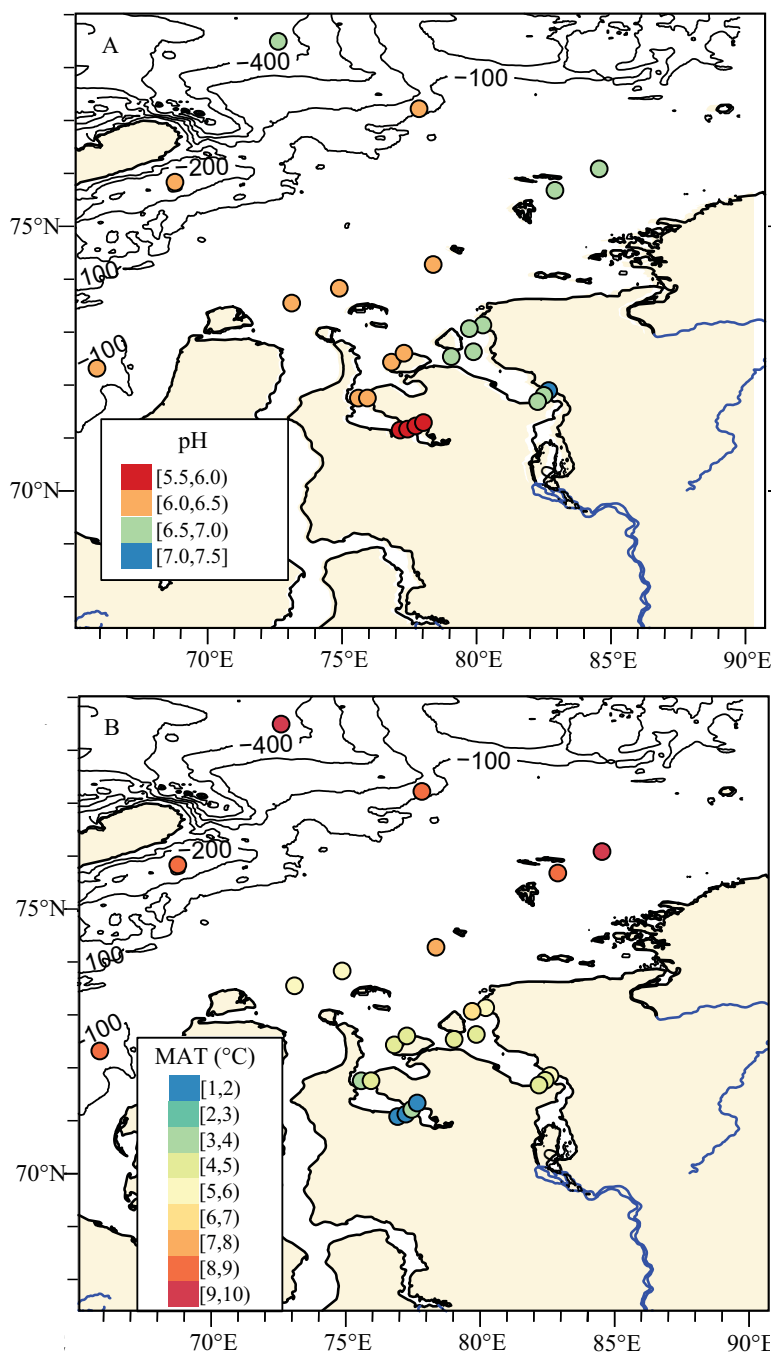


Fig. 7. A) Reconstructed pH [Eq. 3 and 4] and B) reconstructed MAT [Eq. 5], based on the brGDGT distribution in surface sediments.

proxies for terrigenous matter in the marine system (r^2 with $\delta^{13}\text{C}_{\text{org}} = 0.60$, r^2 with $\text{C/N} = 0.50$; after exclusion of one outlier) indicate that the BIT-index is a robust proxy to trace changes in the input of terrigenous OM in the Kara Sea sediments.

5.5. Implications for palaeoclimate reconstructions

The reconstruction of palaeotemperature and soil pH, based on marine sedimentary brGDGTs relies on the conservation of a soil-derived brGDGT signal during its transport in the river and in the marine system. This is, however, not the case in the Yenisei River watershed, where in situ production in the river water and in the marine system influence the brGDGT distributions that are derived from the watershed soils and coastal cliffs. However, preferential degradation of a labile pool of brGDGTs, resulting in an enrichment of pre-aged brGDGTs, possibly results in a dominantly soil-derived brGDGT signal in offshore sediments. The influence of terrigenous material in these offshore sediments is confirmed by the bulk $\delta^{13}\text{C}_{\text{org}}$ values and C/N ratios (see section 5.4).

The possible impact of the changing distributions on palaeoclimate reconstructions is evident when we reconstruct the pH and MAT. Compared to the Yenisei River SPM (reconstructed pH between 6.9 and 7.9), the reconstructed pH [Eq. 2 and 3] is lower (i.e. 6.5-7.0) in the Yenisei River Mouth (Fig. 7A). This decrease is caused by the strong decrease in fractional abundance of the 6-Me brGDGTs IIa' and IIIa' (Fig. 4). Furthermore, the reconstructed pH decreases further downstream (pH 6-7). This is fairly high compared to the soils present in the Yenisei River watershed (average pH = 5; De Jonge et al., 2014a), although some soils fall within this range. As the marine in situ production of brGDGTs increases the fraction of brGDGTs that are typical for high pH conditions (Fig. 6A), this may influence the reconstructed pH. The Khalmir Bay brGDGT distributions reflect a more acidic signal (pH 5.5-6.0; Fig. 7A), reflecting a signal dominated by coastal cliffs.

Using the MAT_{mr} calibration [Eq. 5], the reconstructed MAT in the Yenisei River Mouth varies between 4 and 5 °C. Fig. 7B shows that the reconstructed temperature increases going downstream. In offshore Yenisei Outflow and Kara Sea sediments, the reconstructed MAT is between 8 and 10°C. Although the MAT_{mr} is calibrated against the MAT, this value overestimates the measured MAT in the Yenisei River watershed significantly (measured MAT is between -8°C and 1°C, De Jonge et al., 2014a). However, this is to be expected, as high latitude soils have shown a consistent warm offset using all published soil calibrations (Weijers et al., 2007a, Peterse et al., 2012, De Jonge et al., 2014b). The motivation behind this was the lower metabolism and lipid production of soil bacteria in frozen conditions. Although we expect a large contribution of fossilized brGDGTs in the coastal cliff samples collected at the Yenisei River Mouth (MAT_{mr} between -1 and 8°C, modern measured MAT -11°C), a warm bias in the reconstructed MAT is observed here, but also in the mountainous floodplain and lowland outcrop soil samples (MAT_{mr} 4 and 10 °C, measured MAT between -6 and -6.4 °C, respectively). Following our hypothesis that the majority of brGDGTs in the Kara Sea sediments are derived from watershed soils, our results indicate that the Yenisei watershed soils record a temperature signal that is above the annual average in the Yenisei River catchment, and possibly rather reflect a mean summer temperature (MST measured in the Yenisei River watershed is between 7.5 and 16 °C; De Jonge et al., 2014a). Furthermore, as the geographical extent of the pre-

aged brGDGT pool remains unknown, it is possible that the brGDGT distributions and the reconstructed pH and MAT reflect only a part of the Yenisei watershed.

6. Conclusions

We have quantified the full suite of 15 brGDGT compounds in the Yenisei River and its outflow in the Kara Sea system. BrGDGTs are present throughout the system, both in the SPM and sediments. The brGDGT distribution in the Yenisei River SPM, with a large abundance of 6-Me brGDGTs, confirms its in situ production in the river system, as previously assessed by De Jonge et al. (2014a). However, after remaining fairly constant within the Yenisei River, brGDGTs distributions change drastically in the Yenisei Mouth/Kara Sea system. Firstly, a strong decrease in the fractional abundance of the 6-Me brGDGTs IIa' and IIIa' is observed in the Yenisei River Mouth. This offset can be due to the presence of brGDGTs delivered during the freshet, whose distribution can be offset from the signal present in the Yenisei River base flow in September. Also thermoabrasive coastal cliff sediments contain brGDGTs and can influence the brGDGT distribution, especially in sites with no major river input. Further downstream, the fractional abundance of number of minor, cyclopentane containing brGDGTs and brGDGT Ia increases. Marine in situ production has been invoked to explain changing brGDGT distributions, and is probably the mechanism causing the increase of the pH-sensitive cyclopentane-containing compounds. However, the distribution present in offshore marine Kara Sea sediments is distinct from previously described in situ produced brGDGT distributions in the Arctic Ocean (Peterse et al., 2012), especially as it has a strongly increased fractional abundance of brGDGT Ia. We postulate that preferential degradation of a modern brGDGT subpool can cause a downstream shift in brGDGT distributions. As the most labile brGDGTs subpool, produced in situ in the Yenisei River will be degraded preferentially, this implies that coastal cliff and soil-derived brGDGT lipids possibly dominate the most offshore sediments. Whereas the encountered brGDGT distribution is distinct from the coastal cliffs, it agrees better with a lowland peat. Based on the reconstructed MAT in these sediments, we postulate that the Yenisei watershed soils record a summer temperature. The reconstructed pH is influenced by marine in situ production.

The three invoked terrestrial brGDGT sources (river SPM, watershed soils, coastal cliffs) are characterized by high BIT values. Even though their relative contribution to the marine system is not constrained well, the BIT values are high in both the Yenisei River Mouth and Khatymy Bay. The decrease in the brGDGTs abundance offshore is reflected by a decrease in the BIT-index. As the BIT-index in the Kara Sea sediments correlates well with bulk OM proxies that trace terrigenous matter, the $\delta^{13}\text{C}$ and C/N values, it performs well as a tracer for riverine/terrigenous OM input.

The complex behaviour of brGDGTs in the Yenisei River and Kara Sea, indicates that palaeoclimate reconstructions performed on Kara Sea sediment cores will be challenging. We recommend that sediment cores should be collected in offshore Kara Sea sediments, as the distribution closer to the river Mouth is subjected to strong shifts, probably due to preferential degradation. Climatic changes, resulting in changing sea level and discharge patterns, can influence the geographic location of this process, complicating the interpretation of a climatic

archive collected in the Yenisei River Mouth and Gulf. We postulate that modern sediments collected further offshore are dominated by pre-aged soil-derived brGDGTs. The Kara Sea thus represents a rare situation where the supply of soil-derived brGDGTs is sufficient to dominate a marine in situ produced signal, after the degradation of ‘modern’, aquatic brGDGTs. However, the pre-aged subpool that is represented after the preferential degradation does not necessarily reflect the entire Yenisei watershed. Furthermore, the extent to which this pre-aged subpool responds to climatic changes is unknown. The downcore behaviour of the brGDGTs distribution in the Kara Sea, and its potential to reconstruct palaeoclimate shifts in the Yenisei watershed thus remains to be investigated.

Thus, palaeoclimate reconstructions performed on Kara Sea sediment cores will have to identify the source of the pre-aged brGDGTs, and take the influence of freshwater and marine in situ production of brGDGTs into account. However, our study does indicate that although brGDGT-based palaeoclimate reconstructions in offshore Kara Sea sediments will be complicated, they are still possible.

7. Acknowledgments

We acknowledge the work of Annelieke Mets in the work-up and analysis of the Kara Sea sediment samples. This work was performed in the framework of the memorandum NIOZ-VNIOkeangeologia for Arctic research. The research was funded by research project 819.01.013, financed by the Netherlands Organization for Scientific Research (NWO) and the European Research Council under the EU Seventh Framework Programme (FP7/2007-2013)/ERC grant agreement No. [226600].

Table 4. Summarizes the fractional abundances of the brGDGT compounds of the core brGDGTs per site. The calculated BIT index for the IPL and CL fractions [Eq. 2] and the lipid (CL) and intact polar lipid (IPL) fractions in the SPM. The amounts of CL brGDGTs reconstructed MAT [Eq. 5] and pH [Eq. 3 and 4] for the CL fraction are reported. B.d.l. and crenarchaeol at each station are reported normalized per gram POC, while the IPL indicates that the amounts measured were below detection limit. abundances are expressed as the percentage of IPLs relative to the total amount of

Sample	Fra	Ia	Ib	Ic	IIa	IIb	IIc	IIIa	IIIB	IIIC	IIa'	IIb'	IIc'	IIIa'	IIIB'	IIIC'	Σ brGDGTs (μg. g POC ⁻¹) IPL (%)	crenarchaeol (μg. g POC ⁻¹) IPL (%)	BIT	MAT (°C)	pH
MR1	CL	15	2	0.5	21	2	0.3	21	0.3	b.d.l.	14	2	0.1	22	0.5	b.d.l.	1	0.02	0.98	4.5	6.9
	IPL	15	2	0.7	22	2	1	18	b.d.l.	b.d.l.	13	2	1	24	b.d.l.	b.d.l.	11%	58%	0.85		
MR2	CL	11	2	0.4	22	2	0.4	24	0.3	b.d.l.	15	2	0.3	20	1	b.d.l.	15	0.08	0.99	3.5	6.9
	IPL	b.d.l.	b.d.l.	b.d.l.	b.d.l.	b.d.l.	b.d.l.	49	b.d.l.	b.d.l.	7	b.d.l.	b.d.l.	44	b.d.l.	b.d.l.	1%	45%	0.73		
SR1	CL	12	5	0.7	12	4	0.3	8	0.4	b.d.l.	24	7	0.4	24	1	b.d.l.	4	0.2	0.93	7.3	7.5
	IPL	b.d.l.	b.d.l.	b.d.l.	14	4	1	15	2	b.d.l.	17	0.1	1	41	4	b.d.l.	2%	61%	0.17		
YR1	CL	14	3	1	13	2	b.d.l.	9	0.4	0.1	18	3	b.d.l.	36	1	0.1	10	0.3	0.97	6.8	7.5
	IPL	14	3	1	11	2	b.d.l.	8	0.2	b.d.l.	18	2	b.d.l.	40	0.1	b.d.l.	16%	37%	0.91		
YR2	CL	9	3	0.4	9	2	0.2	7	0.4	0.1	19	7	0.2	42	2	0.4	21	0.2	0.99	7.1	7.9
	IPL	b.d.l.	2	0.3	5	1	1	10	1	b.d.l.	12	b.d.l.	1	62	5	b.d.l.	3%	39%	0.83		
YR3	CL	14	2	0.4	12	1	0.2	8	0.4	0.1	20	5	0.2	35	1	0.2	11	0.2	0.98	6.7	7.6
	IPL	13	2	0.3	10	1	0.4	6	0.1	b.d.l.	21	5	0.4	39	1	b.d.l.	13%	37%	0.94		
YR4	CL	14	2	b.d.l.	11	2	b.d.l.	9	b.d.l.	b.d.l.	19	4	b.d.l.	39	b.d.l.	b.d.l.	3	0.06	0.98	6.8	7.6
	IPL	b.d.l.	b.d.l.	b.d.l.	b.d.l.	b.d.l.	b.d.l.	b.d.l.	b.d.l.	b.d.l.	b.d.l.	b.d.l.	b.d.l.	b.d.l.	b.d.l.	b.d.l.	b.d.l.	38%	n.d.		

YR5	CL	14	3	0	12	2	0.3	9	0.4	0.1	20	6	0.2	32	2	0.3	16	0.2	0.99	7	7.5
	IPL	13	3	1	10	2	0.5	7	0.4	b.d.l.	21	6	1	35	2	b.d.l.	10%	40%	0.93		
YR6	CL	11	3	0.5	10	2	0.3	8	1	0.1	18	6	0.2	37	2	0.3	14	0.2	0.99	7	7.7
	IPL	7	2	0.3	8	2	1	9	1	b.d.l.	18	5	1	43	2	b.d.l.	5%	32%	0.88		
YR7	CL	13	2	0.2	10	1	0.2	8	0.4	0.04	21	5	0.2	37	1	0.2	15	0.1	0.99	7	7.7
	IPL	14	0	0.1	11	1	b.d.l.	9	0.4	b.d.l.	18	4	b.d.l.	41	1	b.d.l.	5%	41%	0.88		
YR8	CL	16	2	1	16	2	0.3	11	1	0.1	18	4	0.2	28	1	0.2	12	0.1	0.99	5.9	7.3
	IPL	13	b.d.l.	1	18	2	b.d.l.	14	b.d.l.	b.d.l.	16	2	b.d.l.	33	b.d.l.	b.d.l.	4%	28%	0.91		
YR9	CL	16	2	1	17	2	b.d.l.	12	1	0.1	18	4	b.d.l.	27	1	0.2	9	0.1	0.99	5.9	7.2
	IPL	11	2	1	14	2	b.d.l.	17	b.d.l.	b.d.l.	18	4	b.d.l.	32	b.d.l.	b.d.l.	4%	91%	0.27		
YM1	CL	15	3	0.5	23	2	0.3	21	0.5	0.1	14	3	0.1	17	1	0.2	16	0.2	0.98	4.2	6.8
	IPL	6	3	1.1	23	2	2	29	1	b.d.l.	10	2	1	19	2	b.d.l.	5%	43%	0.81		
YM2	CL	19	3	0.7	23	3	0.5	20	1	0.1	13	3	0.2	15	1	0.2	39	1	0.97	4.8	6.7
	IPL	b.d.l.	b.d.l.	b.d.l.	b.d.l.	b.d.l.	b.d.l.	b.d.l.	b.d.l.	b.d.l.	b.d.l.	b.d.l.	b.d.l.	b.d.l.	b.d.l.	b.d.l.	b.d.l.	38%	n.d.		
YM3	CL	18	3	0.6	22	2	0.4	20	0.5	0.1	14	3	0.2	15	1	0.2	35	1	0.97	4.8	6.7
	IPL	b.d.l.	b.d.l.	b.d.l.	b.d.l.	b.d.l.	b.d.l.	b.d.l.	b.d.l.	b.d.l.	b.d.l.	b.d.l.	b.d.l.	b.d.l.	b.d.l.	b.d.l.	b.d.l.	36%	n.d.		
YM4	CL	17	3	0.6	23	3	0.4	22	0.5	0.1	13	3	0.2	15	1	0.1	27	1	0.97	4.4	6.7
	IPL	b.d.l.	b.d.l.	b.d.l.	4	b.d.l.	1	65	5	b.d.l.	b.d.l.	b.d.l.	b.d.l.	23	2	b.d.l.	0%	41%	0.05		
YM5	CL	17	3	0.6	23	3	0.5	23	0.5	0.1	13	3	0.2	14	1	0.1	34	1	0.97	4.5	6.7
	IPL	b.d.l.	2	1.2	20	b.d.l.	b.d.l.	41	4	b.d.l.	7	b.d.l.	b.d.l.	20	5	b.d.l.	2%	41%	0.5		

Sample	Fra	Ia	Ib	Ic	Ila	Ilb	Ilc	IIla	IIlb	IIlc	IIIa	IIIb	IIIc	Σ brGDGTs (μg. g POC ⁻¹) IPL (%)	crenarchaeol (μg. g POC ⁻¹) IPL (%)	BIT	MAT (°C)	pH
YG1	CL	22	3	1	26	3	0.4	19	0.5	0.1	11	1	0.1	35	11	0.75	4.4	6.5
	IPL	b.d.l.	b.d.l.	b.d.l.	b.d.l.	b.d.l.	b.d.l.	70	12	b.d.l.	b.d.l.	17	1	b.d.l.	0%	n.d.		
YG2a	CL	23	2	1	29	2	0.3	20	0.4	0.1	10	2	0.2	18	3	0.84	3.6	6.4
	IPL	b.d.l.	3	b.d.l.	30	3	b.d.l.	38	b.d.l.	b.d.l.	8	1	b.d.l.	2%	26%	0.26		
YG2b	CL	26	3	1	26	3	0.3	17	0.4	0.1	11	2	0.4	16	11	0.58	5.1	6.4
	IPL	b.d.l.	b.d.l.	b.d.l.	14	3	b.d.l.	50	b.d.l.	b.d.l.	8	0.5	b.d.l.	1%	38%	0.02		
YG3	CL	22	2	1	29	2	0.3	20	0.3	b.d.l.	10	2	0.2	7	1	0.84	3.5	6.4
	IPL	b.d.l.	3	0.4	26	3	b.d.l.	49	b.d.l.	b.d.l.	1	1	b.d.l.	1%	23%	0.21		
YG4	CL	25	2	0.5	31	2	0.3	20	0.3	0.1	9	1	0.1	13	3	0.83	3.1	6.2
	IPL	b.d.l.	3	1	19	5	b.d.l.	51	b.d.l.	b.d.l.	b.d.l.	3	b.d.l.	0%	27%	0.03		
YG5	CL	26	2	1	32	2	0.2	19	0.3	b.d.l.	9	1	0.2	16	10	0.61	3.4	6.2
	IPL	b.d.l.	0.4	b.d.l.	29	b.d.l.	b.d.l.	43	b.d.l.	b.d.l.	5	b.d.l.	b.d.l.	0%	36%	0.03		
YG6	CL	23	3	0.7	27	3	0.4	19	0.4	0.1	10	2	0.4	4	1	0.8	4.4	6.4
	IPL	b.d.l.	b.d.l.	b.d.l.	b.d.l.	b.d.l.	b.d.l.	b.d.l.	b.d.l.	b.d.l.	b.d.l.	b.d.l.	b.d.l.	b.d.l.	22%	n.d.		
YG7	CL	36	b.d.l.	b.d.l.	30	b.d.l.	b.d.l.	16	b.d.l.	b.d.l.	11	b.d.l.	b.d.l.	9	3	0.75	4.7	6.1
	IPL	b.d.l.	b.d.l.	b.d.l.	b.d.l.	b.d.l.	b.d.l.	b.d.l.	b.d.l.	b.d.l.	b.d.l.	b.d.l.	b.d.l.	b.d.l.	20%	n.d.		
YG8	CL	24	3	1.1	26	4	1	20	1	0.1	9	2	1	19	8	0.67	5.3	6.3
	IPL	b.d.l.	b.d.l.	b.d.l.	b.d.l.	b.d.l.	b.d.l.	b.d.l.	b.d.l.	b.d.l.	b.d.l.	b.d.l.	b.d.l.	b.d.l.	19%	n.d.		

YG9	CL	24	4	1.0	26	5	0.4	20	1	0.1	9	2	1	7	0.4	0.2	30	12	0.68	5	6.3
	IPL	b.d.l.	b.d.l.	b.d.l.	b.d.l.	b.d.l.	b.d.l.	b.d.l.	b.d.l.	b.d.l.	b.d.l.	b.d.l.	b.d.l.	b.d.l.	b.d.l.	b.d.l.	b.d.l.	12%	n.d.		
YO1	CL	32	2	b.d.l.	33	b.d.l.	b.d.l.	18	b.d.l.	b.d.l.	8	b.d.l.	b.d.l.	6	b.d.l.	b.d.l.	1	0.4	0.65	3.7	5.9
	IPL	b.d.l.	b.d.l.	b.d.l.	b.d.l.	b.d.l.	b.d.l.	b.d.l.	b.d.l.	b.d.l.	b.d.l.	b.d.l.	b.d.l.	b.d.l.	b.d.l.	b.d.l.	b.d.l.	12%	n.d.		
YO2	CL	16	b.d.l.	b.d.l.	19	b.d.l.	b.d.l.	34	b.d.l.	b.d.l.	9	b.d.l.	b.d.l.	21	b.d.l.	b.d.l.	0.2	0.4	0.35	4.4	6.6
	IPL	b.d.l.	b.d.l.	b.d.l.	b.d.l.	b.d.l.	b.d.l.	b.d.l.	b.d.l.	b.d.l.	b.d.l.	b.d.l.	b.d.l.	b.d.l.	b.d.l.	b.d.l.	b.d.l.	14%	n.d.		
YO3	CL	25	b.d.l.	b.d.l.	26	b.d.l.	b.d.l.	24	b.d.l.	b.d.l.	13	b.d.l.	b.d.l.	13	b.d.l.	b.d.l.	0.1	0.4	0.22	4	6.4
	IPL	b.d.l.	b.d.l.	b.d.l.	b.d.l.	b.d.l.	b.d.l.	b.d.l.	b.d.l.	b.d.l.	b.d.l.	b.d.l.	b.d.l.	b.d.l.	b.d.l.	b.d.l.	b.d.l.	10%	n.d.		
KS1	CL	35	b.d.l.	b.d.l.	37	b.d.l.	b.d.l.	17	b.d.l.	b.d.l.	6	b.d.l.	b.d.l.	5	b.d.l.	b.d.l.	0.4	0.09	0.84	2.7	5.7
	IPL	b.d.l.	b.d.l.	b.d.l.	b.d.l.	b.d.l.	b.d.l.	b.d.l.	b.d.l.	b.d.l.	b.d.l.	b.d.l.	b.d.l.	b.d.l.	b.d.l.	b.d.l.	b.d.l.	12%	n.d.		
KS2	CL	33	3	0.8	31	1	b.d.l.	16	b.d.l.	b.d.l.	8	2	b.d.l.	5	b.d.l.	b.d.l.	1	0.4	0.75	5.1	6.0
	IPL	b.d.l.	b.d.l.	b.d.l.	b.d.l.	b.d.l.	b.d.l.	b.d.l.	b.d.l.	b.d.l.	b.d.l.	b.d.l.	b.d.l.	b.d.l.	b.d.l.	b.d.l.	b.d.l.	11%	n.d.		
KS3	CL	32	3	1.3	30	3	b.d.l.	16	b.d.l.	b.d.l.	7	1	b.d.l.	6	b.d.l.	b.d.l.	1	1	0.47	5.1	6.0
	IPL	b.d.l.	b.d.l.	b.d.l.	b.d.l.	b.d.l.	b.d.l.	b.d.l.	b.d.l.	b.d.l.	b.d.l.	b.d.l.	b.d.l.	b.d.l.	b.d.l.	b.d.l.	b.d.l.	24%	n.d.		
KS4	CL	31	b.d.l.	b.d.l.	35	b.d.l.	b.d.l.	18	b.d.l.	b.d.l.	10	b.d.l.	b.d.l.	6	b.d.l.	b.d.l.	0.1	0.1	0.53	2.4	6.0
	IPL	b.d.l.	b.d.l.	b.d.l.	b.d.l.	b.d.l.	b.d.l.	b.d.l.	b.d.l.	b.d.l.	b.d.l.	b.d.l.	b.d.l.	b.d.l.	b.d.l.	b.d.l.	b.d.l.	14%	n.d.		
KB1	CL	20	2	0.5	31	2	0.4	29	1	0.1	7	1	0.1	5	0.4	0.04	29	1	0.97	2.4	6.0
	IPL	b.d.l.	b.d.l.	b.d.l.	b.d.l.	b.d.l.	b.d.l.	b.d.l.	b.d.l.	b.d.l.	b.d.l.	b.d.l.	b.d.l.	b.d.l.	b.d.l.	b.d.l.	b.d.l.	60%	n.d.		
KB2	CL	20	2	0.5	31	2	0.5	30	0.4	0.1	6	1	0.1	6	0.2	0.1	28	1	0.97	2.3	5.9
	IPL	b.d.l.	12	b.d.l.	15	b.d.l.	b.d.l.	51	6	b.d.l.	2	b.d.l.	b.d.l.	9	5	b.d.l.	2%	39%	0.44		

Sample	Fra	Ia	Ib	Ic	Ila	Ilb	Ilc	IIla	IIlb	IIlc	IIIa'	IIIb'	IIIc'	IIa'	IIb'	IIc'	IIIa'	IIIb'	IIIc'	Σ brGDGTs (μg. g POC ⁻¹) IPL (%)	crenarchaeol (μg. g POC ⁻¹) IPL (%)	BIT	MAT (°C)	pH
KB3	CL	19	2	1	28	2	1	30	1	0.2	7	1	0.2	8	0.5	0.1	30	1	0.95	3.1	6.1			
	IPL	b.d.l.	8	b.d.l.	b.d.l.	b.d.l.	b.d.l.	60	5	b.d.l.	3	b.d.l.	b.d.l.	18	6	b.d.l.	1%	37%	0.15					
KB4	CL	17	2	0.3	33	2	0.3	32	0.5	0.1	7	1	0.1	6	0.3	0.1	49	2	0.97	1.1	5.9			
	IPL	b.d.l.	b.d.l.	b.d.l.	b.d.l.	b.d.l.	b.d.l.	73	1	b.d.l.	b.d.l.	1	1	21	2	0.3	0%	38%	n.d.					
KG1	CL	23	4	1	26	4	0.5	22	1	0.3	7	2	1	6	0.5	0.2	21	7	0.71	5.2	6.2			
	IPL	b.d.l.	b.d.l.	b.d.l.	b.d.l.	b.d.l.	b.d.l.	b.d.l.	b.d.l.	b.d.l.	b.d.l.	b.d.l.	b.d.l.	b.d.l.	b.d.l.	b.d.l.	b.d.l.	18%	n.d.					
KG2	CL	22	3	1	26	5	1	24	1	0.3	8	2	1	6	1	0.2	21	8	0.71	4.8	6.2			
	IPL	b.d.l.	b.d.l.	b.d.l.	b.d.l.	b.d.l.	b.d.l.	b.d.l.	b.d.l.	b.d.l.	b.d.l.	b.d.l.	b.d.l.	b.d.l.	b.d.l.	b.d.l.	b.d.l.	18%	n.d.					
OO1	CL	27	3	1.2	28	3	1	19	1	b.d.l.	7	1	0.3	8	1	b.d.l.	5	2	0.67	4.8	6.2			
	IPL	b.d.l.	b.d.l.	b.d.l.	b.d.l.	b.d.l.	b.d.l.	b.d.l.	b.d.l.	b.d.l.	b.d.l.	b.d.l.	b.d.l.	b.d.l.	b.d.l.	b.d.l.	b.d.l.	32%	n.d.					
OO2	CL	31	2	b.d.l.	32	2	b.d.l.	19	b.d.l.	b.d.l.	7	1	b.d.l.	7	b.d.l.	b.d.l.	1	0.3	0.73	3.9	6.0			
	IPL	b.d.l.	b.d.l.	b.d.l.	b.d.l.	b.d.l.	b.d.l.	b.d.l.	b.d.l.	b.d.l.	b.d.l.	b.d.l.	b.d.l.	b.d.l.	b.d.l.	b.d.l.	b.d.l.	19%	n.d.					

Table 5. Summarizes the fractional abundances of the brGDGT compounds of the core lipid (CL) and intact polar lipid (IPL) fractions in the sediments. The amounts of CL brGDGTs and crenarchaeol at each station are reported normalized per gram TOC, while the IPL abundances are expressed as the percentage of IPLs relative to the total amount of

Sample	Fraction	Ia	Ib	Ic	Ila	Ilb	Ilc	IIla	IIlb	IIlc	IIla'	IIb'	IIc'	IIIa	IIIb'	IIIc'	Σ brGDGTs (μg. g TOC ⁻¹) IPL (%)	crenarchaeol (μg. g TOC ⁻¹) IPL (%)	BIT	MAT (°C)	pH	
YM2	CL	14	2	1	18	2	0.5	16	1	0.2	13	4	0.3	26	2	0.5	87	1.3	0.98	5.4	7.1	
	IPL	11	3	1	13	3	1	15	1	0.2	15	7	0.3	27	3	0.2	6%	54%	0.75			
YM3	CL	16	2	0.4	22	2	0.3	20	0.5	0.1	13	3	0.1	19	1	0.1	82	1.0	0.99	4.2	6.8	
	IPL	11	3	2	20	3	1	17	1	0.3	13	3	0.3	22	3	0.1	7%	45%	0.85			
YM4	CL	14	3	1	22	3	0.4	22	1	0.1	13	3	0.2	18	1	0.2	36	0.2	0.99	4.3	6.8	
	IPL	b.d.l.	b.d.l.	b.d.l.	b.d.l.	b.d.l.	b.d.l.	b.d.l.	b.d.l.	b.d.l.	b.d.l.	b.d.l.	b.d.l.	b.d.l.	b.d.l.	b.d.l.	b.d.l.	30%	n.d.			
YG1	CL	20	3	1	24	3	0.4	20	1	0.1	12	2	0.3	13	1	0.1	18	2.6	0.86	4.5	6.6	
	IPL	20	4	1	20	8	1	22	1	0.1	9	2	2	9	1	b.d.l.	2%	18%	0.37			
YG2	CL	30	3	1	25	2	0.3	11	0	0.1	15	2	0	10	1	0.1	12	2.5	0.81	6.4	6.6	
	IPL	27	4	1	19	7	1	18	1	b.d.l.	10	2	1	10	1	b.d.l.	5%	9%	0.71			
YG3	CL	23	3	1	25	3	0.4	18	1	0.1	12	2	0	11	1	0.2	15	3.1	0.81	5	6.5	
	IPL	19	3	1	17	8	1	23	1	0.3	12	3	2	10	1	0.1	5%	20%	0.47			
YG7	CL	22	3	1	25	3	0.4	18	1	0.1	13	2	0.3	12	1	0.1	28	3.8	0.87	4.7	6.6	
	IPL	23	3	1	25	5	0.5	20	1	b.d.l.	4	6	1	10	1	b.d.l.	4%	26%	0.42			
YG8	CL	20	3	1	25	5	0.4	23	1	0.1	9	2	1	8	1	0.2	69	20	0.75	4.7	6.4	
	IPL	19	3	1	21	7	1	26	1	0.4	7	3	2	8	1	b.d.l.	6%	13%	0.55			
YG9	CL	21	3	1	25	5	0.4	22	1	0.1	9	2	1	10	1	0.2	62	19	0.74	4.7	6.4	
	IPL	17	5	1	20	6	1	17	2	b.d.l.	7	5	2	15	2	b.d.l.	12%	45%	0.31			

Sample	Fraction	Ia	Ib	Ic	Ila	Ilb	Ilc	IIla	IIlb	IIlc	IIa'	IIb'	IIc'	IIIa'	IIIb'	IIIc'	Σ brGDGTs ($\mu\text{g. g TOC}^{-1}$) IPL (%)	crenarchaeol ($\mu\text{g. g TOC}^{-1}$) IPL (%)	BIT	MAT (°C)	pH
YO1	CL	29	4	1	21	5	1	15	1	0.1	9	3	1	8	1	0.3	12	11	0.47	7.6	6.5
	IPL	33	4	1	13	7	1	14	1	0.2	8	4	2	9	2	0.2	8%	15%	0.28		
YO2	CL	35	4	1	21	3	0.4	10	1	0.2	10	4	1	8	1	0.3	16	14	0.49	8.6	6.5
	IPL	24	2	0.1	5	b.d.l.	0.5	20	1	b.d.l.	14	17	3	11	2	b.d.l.	4%	25%	0.10		
YO3	CL	33	4	1	18	2	0.5	11	1	0.2	10	7	2	9	2	0.4	12	12.8	0.43	9.2	6.7
	IPL	30	4	1	12	8	1	12	1	0.4	11	5	3	8	2	1	12%	20%	0.27		
KS1	CL	39	3	1	22	3	0.2	9	0.4	0.1	10	2	1	8	1	0.2	19	20	0.46	8.8	6.4
	IPL	32	3	0.2	17	10	1	11	2	0.5	9	1	4	7	3	0.5	8%	22%	0.19		
KS2	CL	42	2	1	23	2	0.2	8	0.2	0.03	9	1	0.3	11	0.4	0.1	11	16	0.39	8.5	6.3
	IPL	39	2	1	22	2	0.3	8	1	b.d.l.	10	2	1	11	1	b.d.l.	8%	22%	0.16		
KS3	CL	40	4	1	23	3	0.3	9	1	0.1	8	3	1	6	1	0.2	8.3	8.2	0.46	8.7	6.2
	IPL	32	1	1	11	7	0.3	17	1	0.5	18	0	2	7	2	0.4	6%	12%	0.30		
KS4	CL	31	5	1	17	6	1	9	1	0.1	9	5	2	150	2	0.6	3.9	33	0.08	9.5	6.7
	IPL	42	3	1	11	7	0.4	7	1	0.5	8	6	3	8	2	0.5	14%	14%	0.09		
KB1	CL	19	2	0.3	34	1	0.3	31	0.3	0.1	7	1	0.1	5	0	0.02	83	0.7	0.99	1.3	5.9
	IPL	16	2	0.4	37	2	1	30	0.3	b.d.l.	6	0.5	0.1	6	0	b.d.l.	11%	53%	0.92		
KB2	CL	19	2	0.3	33	1	0.3	33	0.5	0.1	5	1	0.1	5	0	0.04	53	0.3	0.99	1.5	5.7
	IPL	17	2	1	33	2	1	30	0.4	b.d.l.	7	1	b.d.l.	5	0	b.d.l.	11%	53%	0.95		
KB3	CL	20	2	1	28	2	1	32	1	1	5	1	0.1	6	1	0.1	56	1.0	0.98	3.4	5.9
	IPL	17	3	1	28	3	1	31	1	1	7	1	0.1	6	1	0.03	10%	44%	0.88		

Sample	Fraction	Ia	Ib	Ic	IIa	IIb	IIc	IIIa	IIIb	IIIc	IIa'	IIb'	IIc'	IIIa'	IIIb'	IIIc'	Σ brGDGTs (μg. g TOC ⁻¹) IPL (%)	crenarchaeol (μg. g TOC ⁻¹) IPL (%)	BIT	MAT (°C)	pH
KB4	CL	14	1	0.3	29	1	0.3	40	1	0.2	6	1	0.1	6	0	0.1	82	1.0	0.99	1.6	5.9
	IPL	12	2	0.4	33	2	1	37	0.5	0.1	3	0.3	0.1	8	b.d.l.	b.d.l.	5%	40%	0.86		
KG1	CL	19	3	1	27	4	0.4	27	1	0.2	7	2	1	7	1	0.2	56	12	0.81	3.9	6.2
	IPL	17	2	1	24	4	0.4	32	1	b.d.l.	9	1	2	8	1	b.d.l.	4%	11%	0.58		
KG2	CL	20	3	1	25	4	1	27	2	0.4	7	2	1	8	1	0.1	61	11	0.83	4.3	6.2
	IPL	17	4	2	16	6	1	28	3	1	10	3	3	8	1	b.d.l.	4%	25%	0.37		
OO1	CL	28	3	1	25	5	1	18	1	0.2	8	2	1	7	1	0.2	32	16	0.64	5.9	6.3
	IPL	29	4	1	20	8	1	16	1	b.d.l.	7	3	1	6	1	0.1	7%	19%	0.34		
OO2	CL	27	3	1	25	4	0.5	18	1	0.2	8	2	1	7	1	0.2	35	23	0.57	5.8	6.3
	IPL	26	4	1	23	6	1	20	1	0.1	7	2	1	7	1	0.2	11%	21%	0.38		

Table 6. Summarizes the fractional abundances of the brGDGT compounds of [Eq. 2] is reported for the CL and IPL fraction, and the reconstructed MAT [Eq. the watershed soils and the coastal cliffs. The amounts of CL and IPL brGDGTs 5] and pH [Eq. 3 and 4] are reported for the CL fraction. B.d.l. indicates that the and crenarchaeol at each station are reported. The calculated BIT index amounts measured were below detection limit. ▼

Sample	Ia	Ib	Ic	Ila	Ilb	Ilc	IIla	IIlb	IIc	IIIa	IIIb	IIIc	IIla'	IIlb'	IIc'	IIIa'	IIIb'	IIIc'	Σ brGDGTs (μg g OC ⁻¹)	crenarchaeol (μg g OC ⁻¹)	BIT	MAT (°C)	pH
S_1	8	3	0.2	18	2	0.2	27	0.4	0.1	15	4	0.3	20	1	0.3	n.d.	1.00	4	7.0	n.d.	1.00	4	7.0
S_2	65	1	0.4	29	0.4	0.2	3	b.d.l.	b.d.l.	0.5	0.1	b.d.l.	0.3	b.d.l.	b.d.l.	86	0.003	1.00	10	4.1	1.00	10	4.1
CC_YM1	25	4	1	21	3	1	23	2	1	7	2	0.3	9	1	0.1	45	8	0.83	7	6.3	0.83	7	6.3
CC_YM2	14	5	1	24	3	0.2	30	0.5	0.1	10	2	0.1	10	0.5	0.1	13	0.2	0.98	4	6.5	0.98	4	6.5
CC_YM3	28	5	2	21	3	1	20	1	1	8	2	0.2	8	1	0.1	43	9	0.81	8	6.4	0.81	8	6.4
CC_YM4	15	4	1	23	3	0.4	28	0.4	0.1	13	2	0.2	10	0.4	0.1	51	2	0.97	4	6.4	0.97	4	6.4
CC_YM5	24	0.2	b.d.l.	42	1	0.5	32	0.0	b.d.l.	b.d.l.	b.d.l.	b.d.l.	0	b.d.l.	b.d.l.	n.d.	n.d.	1.00	-1	3.2	1.00	-1	3.2
CC_YM6	8	3	0.3	27	2	b.d.l.	40	0.2	b.d.l.	8	0	b.d.l.	11	0.3	0.1	22	0.04	1.00	2	6.4	1.00	2	6.4
CC_YM7	17	4	1	25	3	0.4	25	0.5	0.1	12	3	0.2	9	0.5	0.1	n.d.	n.d.	0.95	4	6.3	0.95	4	6.3
CC_YM8	23	4	1	25	3	0.5	22	1	0.2	10	2	0.2	8	0.5	0.1	23	2	0.91	5	6.5	0.91	5	6.5
CC_YM9	17	5	1	26	3	0.4	25	0.5	0.1	11	3	0.2	9	0.4	0.1	21	0.8	0.96	4	6.2	0.96	4	6.2
CC_YG1	29	4	1	25	3	0.3	13	0.4	0.1	12	2	0.5	9	0.5	0.1	32	11	0.71	6	6.4	0.71	6	6.4
CC_YG2	16	3	b.d.l.	30	2	b.d.l.	31	0.2	b.d.l.	10	2	b.d.l.	7	0.3	b.d.l.	7.6	0.02	0.99	2	4.9	0.99	2	4.9
CC_YG3	16	5	1	25	4	b.d.l.	22	1	0.2	12	3	b.d.l.	10	1	0.2	18	0.8	0.95	4	6.6	0.95	4	6.6



Bacteriohopanepolyol distribution
in Yenisei River and Kara Sea
suspended particulate matter
and sediments traces terrigenous
organic matter input and
submerged permafrost.

7

Cindy De Jonge, Helen M. Talbot, Juliane Bischoff,
Alina Stadnitskaia, Georgy Cherkashov
and Jaap S. Sinninghe Damsté

ABSTRACT

Bacteriohopanepolyols (BHPs) are ubiquitous bacterial membrane lipids, encountered in soils, river and marine suspended particulate matter (SPM) and sediments. Their abundance and distribution provides a direct means to identify bacterial inputs and can be used to trace soil-derived bacterial OM and the presence of bacterial groups and their activities in aquatic systems. We have studied the BHP distribution in the SPM of a major Siberian River (Yenisei River) that crosses a large latitudinal gradient, draining a large part of Mongolia and Siberian Russia. The Yenisei River is the main river to drain into the Kara Sea, a shelf sea of the Arctic Ocean. We show that the BHP distribution and concentration of SPM and sediments of the Yenisei Outflow in the Kara Sea allow to trace soil-marker BHPs and to evaluate the performance of the R'_{soil} index, a proxy developed to trace bacterial soil-derived OM. Soil-marker BHPs are present in the Yenisei River, and their abundance decreases from the Yenisei River Outflow into the offshore marine sediments. The R'_{soil} correlates well with an independent proxy for bacterial OM, the BIT-index ($r^2 = 0.82$) and has a moderate correlation with the $\delta^{13}C_{org}$ values, a bulk OM proxy for terrigenous input ($r^2 = 0.44$). Consequently, the R'_{soil} index performs well in the Kara Sea, strengthening its application in the Arctic Ocean, both in modern and downcore sediments. Furthermore, a suite of BHPs that are characteristic for methanotrophic bacteria, i.e. aminopentol and aminotetrol, is encountered in the Yenisei Outflow sediments. These components are partly sourced from terrigenous sources, but are also produced in situ in the marine sediments. The distribution of the pentafunctionalized cyclitol ether BHP in the marine systems is noteworthy, and indicates that it can possibly be applied as a marker for cyanobacterial biomass in marine sediments.

1. Introduction

The study of the fate of organic carbon (OC) that is delivered to the marine environments by riverine sources is an important topic in environmental sciences (e.g. Blair and Aller, 2012). It is a critical component for models of carbon cycling in the modern coastal ocean and for models of atmospheric compositions over geologic time (Berner et al., 2004). The study of this process in the Arctic is especially important, as up to one third of global soil organic matter (OM) is stored in the Arctic terrestrial regions, predominantly in taiga and tundra soils (Waelbroeck et al., 1997; Oechel et al., 2000). This is one of the so-called global climate vulnerable carbon pools (Field and Raupach, 2004) and climate warming could cause transport of the terrestrial OC, that is now 'locked' in these pan-arctic tundra/taiga areas (Schuur et al., 2009), via the Arctic rivers to the Eurasian Arctic shelves. A second pool of vulnerable OC, that can contribute to atmospheric greenhouse gasses, is the large amount of submerged permafrost stored in the Kara Sea sediments, as reported by a number of authors (e.g. Portnov et al., 2013). As this permafrost is currently degrading, methane, a potent greenhouse gas that is found in permafrost layers near the surface (Rivkina et al., 2007), can be liberated as permafrost thaws (Portnov et al., 2013). Climate models forecast an amplification of global warming in the continental Arctic region (e.g. Zwiers, 2002), and there is already evidence for increasing river discharge and change in the hydrological regime in these regions (Peterson, 2002; Dittmar and Kattner, 2003; Benner et al., 2004). Within the context of the Arctic Ocean, which receives 11% of the freshwater and dissolved organic material globally (Aagaard and Carmack, 1989), the Kara Sea is of special importance, receiving about 50% (ca. $1500 \text{ km}^3 \cdot \text{year}^{-1}$) of the total river runoff discharged into the Eurasian Arctic (Gordeev et al., 1996; Holmes et al., 2002; Peterson, 2002; Stein and Macdonald, 2004). The Yenisei and Ob rivers are the major rivers contributing to this outflow, draining a large part of Mongolia and the Siberian continent (combined watersheds equal $5.6 \times 10^6 \text{ km}^2$).

A fraction of the organic matter delivered to or produced in the marine system will be preserved in sediments after settling. Biomarkers are organic molecules with a characteristic and stable structure, which can be traced back to a specific source. Sources include marine organisms such as algae, (cyano)bacteria and archaea and terrestrial organisms (plants, microbes) living at the time of deposition. Biomarker distributions can reveal information about the environmental conditions, e.g. marine and continental environmental conditions, and the terrigenous supply of OM through time. One such group of biomarkers are the bacteriohopanepolyols (BHPs), membrane constituents that are synthesised by many bacteria (Ourisson and Albrecht, 1992; Pearson et al., 2007). These compounds are structurally diverse as they have polyfunctionalised side chains (e.g. Rohmer, 1993). Possible structures include tetra-, penta- and hexafunctionalised compounds according to the number of functional groups occupying positions C-30 to C-35 of the BHP structure (see Fig. 1 for structures). BHP derivatives have been observed in recent sediments and soils (e.g. Cooke et al., 2008; Cooke et al., 2009; Rethemeyer et al., 2010; Wagner et al., 2014) and older sediments (up to ca. 50 Ma; van Dongen et al., 2006; Cooke et al., 2008a; Handley et al., 2010; Talbot et al., 2014). Commonly occurring BHPs include bacteriohopane-32,33,34,35-tetrol (BHT; **Id**; see Table 1 for used abbreviations), 35-aminobacteriohopane-32-33-34-triol (aminotriol; **Ig**) and BHT-cyclitol ether (**Ie**), which are found widespread among many bacterial species (Talbot et al., 2008 and references therein), while other BHPs are

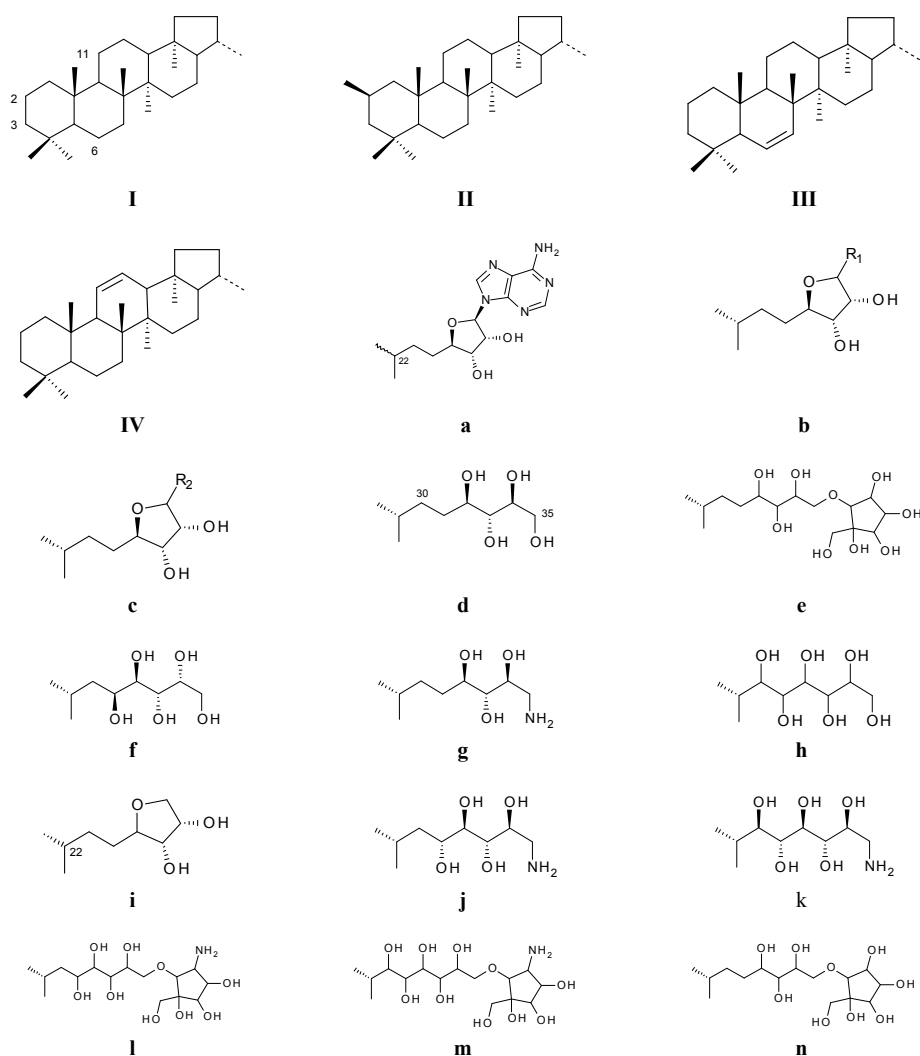


Fig. 1. Ring system (I-IV) and side chains (a-n) of the BHPs observed in the sediments and suspended particulate matter.

more source-specific. For instance 35-aminobacteriohope-31,32,33,34-tetrol (aminotetrol, **Ij**; Talbot and Farrimond, 2007) and, especially, 35-aminobacteriohopane-30,31,32,33,34-pentol (aminopentol, **Ik**; Talbot et al., 2014 and references therein) are produced almost exclusively by aerobic methanotrophic bacteria. Adenosylhopane (**Ia**) and up to five related BHPs (**Ia**, **Ib**, **Ib**, **Ic** and **Ic**) with a similar cyclized side chain have been observed to be particularly common in soils (e.g. Cooke et al., 2008b; Xu et al., 2009; Rethemeyer et al., 2010; Kim et al., 2011) and are, therefore, considered to be ‘soil-markers’, and have been used to trace soil transport to marine sediments, both in recent sediments and through time (e.g. Cooke et al., 2008a; Cooke et al., 2009; Handley et al., 2010; Taylor and Harvey, 2011). Recently Zhu et al. (2011b) successfully applied a BHP-based proxy, R_{soil} , based on the relative abundance of soil marker BHPs against a pseudo-marine end member, i.e. BHT (**Id**), to trace the soil input into

BHP name	Structure number	Base peak ion (<i>m/z</i>)
Adenosylhopane	Ia	788
Meth. Adenosylhopane	IIa	802
G2	Ib	761
Meth. G2	IIb	775
G3	Ic	802
Meth. G3	IIc	816
BHT	Id	655
Meth. BHT	IIId	669
Unsat. BHT	IIId or IVd	653
AnhydroBHT		613
BHPentol	If	713
BHHexol	Ih	771
Aminotriol	Ig	714
Unsat. Aminotriol	IIIg or IVg	712
Aminotetrol	Ij	772
Aminopentol	Ik	830
BHT cyclitol ether	Ie	1002
BHPentol cyclitol ether	II	1060
BHHexol cyclitol ether	Im	1118
BHT Comp	In	943
Meth. BHT Comp	IIIn	957
Unsat. BHT Comp	IIIn or IVn	941

Table 1. Overview of the BHP names used in the manuscript, the corresponding structure number, that refers to Fig. 1, and the dominant base peak ion that is formed analyzing the samples when using the method described in section 3.

surface sediments along a subtropical river–estuary–shelf transect. This ratio was simplified by Doğrul Selver et al. (2012), defining the R'_{soil} . In this ratio, the C-2 methylated soil-marker BHPs (**IIa**, **IIb**, **IIc**) were excluded. A few studies have been performed on BHPs in the Arctic Ocean. The BHP abundance and distribution has been studied in front of a set of Siberian rivers (Cooke et al., 2009), but this study did not allow for evaluation of changes that act on the BHPs before and during their outflow into the marine system and during sedimentation. Taylor and Harvey (2011) reported the BHP composition in surface sediments along two transects offshore two minor Alaskan Rivers ($n = 8$), in the Chukchi Sea, and compared the BHP signature within river sediments ($n = 2$) and watershed soils ($n = 2$), but it remains unclear how a shallow shelf system like the Kara Sea, that is more typical for the Arctic Ocean, compares with this setting.

This study describes, for the first time, the BHP distribution within riverine suspended particulate matter (SPM), over a large latitudinal gradient (Yenisei River, Siberia). The BHP signature is traced in the suspended material during its outflow in the Kara Sea, and compared with the signal preserved in the sediments. We quantify a suite of BHPs, which allows us to trace the soil OM transport in the Yenisei River and in the Kara Sea system, and also evaluate the possibility of an in situ produced BHP fingerprint of aerobic methanotrophic bacteria (Cvejic et al., 2000; Talbot and Farrimond, 2007; Talbot et al., 2014).

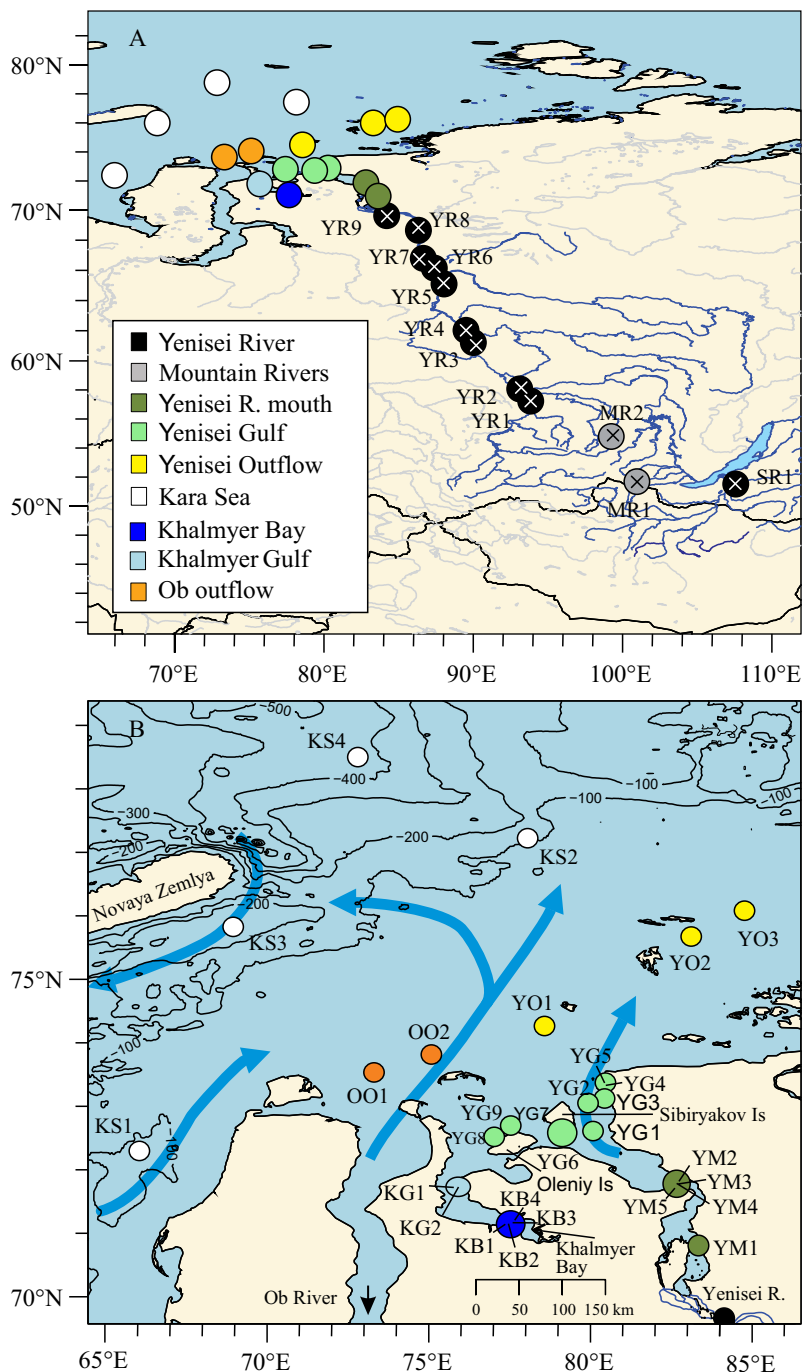


Fig. 2. Map with the sampling locations of A) the Siberian mainland and B) the Kara Sea, with the outflow of the Yenisei and Ob Rivers and Khalmyer Bay indicated. Background colours divide the stations in geographical zones, according to the legend.

2. Geographical setting

The Yenisei River is the longest river in Russia and one of the longest rivers in Asia (Fig. 2A). The river starts in Northern Mongolia, draining a mountainous watershed. Further north, its most important tributary (25% of flow), the Angara River, joins the Yenisei River. Angara River drains Lake Baikal, a large freshwater lake that is fed dominantly (50% of flow) by the Selenga River that drains large parts of Mongolia, a watershed that is dominated by steppe vegetation. The second important tributary for the Yenisei River is the Lower Tunguska (20% of flow), draining large areas of Taiga and Tundra soils. In the lower reaches of the river the Yenisei River flow becomes smooth, the riverbed width reaching several kilometers. The Yenisei River is characterized by a pronounced discharge peak, the freshet, (>30% of annual discharge) in June associated with snowmelt and relatively low water flow between September and April (Stedmon et al., 2011). The Kara Sea (Fig. 2B), where the Yenisei River Mouth is located, is the second largest shelf area of the Arctic Ocean, partially enclosed to the west by the Novaya Zembla and Franz Josef Land and to the south by the Siberian mainland. To the southeast, it is confined by the Zevernaya Archipelago and the Taimyr Peninsula, while the Kara Sea shelf is open to the Arctic Ocean at the north. About one third of the total freshwater discharge into the Arctic Ocean occurs through river run-off (Aagaard and Coachman, 1975). Here, the Kara Sea drains a fifth of the continental run-off of the Eurasian continent into the Arctic Ocean (Lammers et al., 2001). The resulting water discharges of the Ob and Yenisei River reach 400 and 630 km³.yr⁻¹, ranking them thirteenth and sixth in the world in terms of water discharge (Bobrovitskaya et al., 1996). The Gydan Peninsula, where the narrow and deep Khatmyer Bay is situated, separates the Ob and Yenisei River estuaries. North of its shore are a number of islands; e.g. the Oleniy and Sibiriakov Islands.

The Yenisei discharge and Kara Sea circulation are characterized by a strong seasonality. During the summer months, the surface currents in the Kara Sea follow a cyclonic circulation. The Greenland current enters the Kara Sea from the north, and passes along the east coast of Novaya Zembla, flowing southwards. This water body is then joined by the discharge of the Ob and Yenisei Rivers, before flowing further to the northeast (Pavlov and Pfirman, 1995). From mid-October to mid-May, when only 10-15% of the river discharge happens, the Kara Sea and Yenisei River estuary are almost entirely ice-covered. The ice protects the uppermost water layers against wind mixing, and therefore the freshwater layer extends for a large distance under the ice, dispersing the little material delivered over a large distance (Lisitsyn, 1995). Between June and September, when most of the discharge happens (ca. 80%, e.g. Pavlov and Pfirman, 1995), the bulk of suspended load is deposited in front of the estuaries (Lisitsyn, 1995). This causes concentrations of suspended load to decrease by an order of magnitude compared to the estuary (Lisitsyn, 1995), between the surface isohaline of 2 and 20 psu. The high discharge period is characterized by a strong thermal stratification. Below the warm, fresh surface water, a salt-water tongue is present at 6-8 m in the inner Kara Sea, flowing onshore (Pavlov and Pfirman, 1995). Present sedimentation rates in the southern Kara Sea are estimated to range between approximately 0.2 to 1 mm.yr⁻¹, with the exception of shallow areas that are subjected to winnowing (Polyak et al., 2000). Sediment trap studies showed that sedimentation fluxes are highest in autumn and during the ice-covered months (Gaye et al., 2007).

The Kara Sea, like the other Arctic shelf seas, contains large amounts of submarine permafrost, that was submerged due to the eustatic sea-level rise (~120 m) since the last transgression (~7–15 ka). The submarine permafrost is composed of frozen sediments interlayered with the flooded peatland (Romanovskii et al., 2005). The permanent permafrost is mapped to extend offshore in water depths < 20 m, and as it is expected to work as a ‘seal’ for methane release, no extensive methane release is expected above these depths (Shakhova et al., 2010). Discontinuous permafrost can be present in sediment underlying deeper water (>20 m, < 60 m), where large methane flares have indeed been described in the Kara Sea water column (Portnov et al., 2013).

3. Materials and methods

3.1. Collection of environmental samples

The suspended particulate matter (SPM) and sediment samples investigated in this study and location of the sampling stations (Fig. 2) are identical to those described in De Jonge et al. (2014a, Chapter 6). Briefly, surface water (<10 m depth; 1–300 L) was collected and filtered at 30 locations distributed throughout the Kara Sea and at 9 locations along the Yenisei River, from the R/V Sovetskaya Arktika (Aug and Sep 2009). At 15 sites, surface sediment samples were obtained by gravity coring. In September 2011, SPM (120–150 L) and surface sediments (obtained by box cores) were sampled at 9 sites, selected to sample conditions further offshore than the 2009 expedition, from the R/V Akademik Mstislav Keldysh. The SPM from both the 2009 and 2011 expeditions was collected with an in situ pump (McLane Large Volume Water Transfer System Sampler), on 0.7 µm pore size GF/F glass fibre filters. In 2010, three SPM samples were obtained in tributaries of the Angara and in the Selenga River. Surface water was collected in canisters after wading several meters into the river and filtered using the same filters, a peristaltic pump and a titanium tripod system.

3.2. BHP analysis

Freeze-dried sediments (2 g) and filters were extracted as described in De Jonge et al. (Chapter 6). The total lipid extract (TLE) obtained from the sediments and an aliquot (5–10%) of the TLE obtained from the filters was used for BHP analysis. A known amount of internal standard (5 α -pregnane- 3 β ,20 β -diol) was added to the extracts. All lipid extracts were acetylated with acetic anhydride and pyridine (0.5 mL, 1:1 v/v) for 1 h at 50 °C and left at room temperature overnight. The solvent was removed under a continuous N₂ flow, on a 50°C heating block. The acetylated extract was dissolved in methanol:propan-2-ol (3:2, v/v) and filtered over 0.2 µm PTFE filters prior to HPLC–MS analysis.

Reversed-phase high-performance liquid chromatography (HPLC) analysis of the acetylated BHPs was modified after the method described in Cooke et al. (2008a). A Surveyor HPLC system (Thermo Finnigan, Hemel Hempstead, UK) was equipped with a Phenomenex (Macclesfield, UK) Gemini C18 5 µm HPLC column (150 mm, 3 mm internal diameter) and a Phenomenex Security Guard column of the same material. Separation over the column was achieved at a flow rate of 0.5 mL·min⁻¹ at 30 °C with a solvent gradient profile starting at 90% A and 10% B (0–3 min), to 59% A, 1% B and 40% C at 25 min. Then elution was isocratic to 40 min, returning to starting conditions over a span of 5 min (with A = MeOH, B = water, C = propan-2-ol). The starting ratio was allowed to stabilize for 15 min before each run. For HPLC-

MS, a Thermo Finnigan LCQ ion trap MS instrument equipped with an atmospheric pressure chemical ionization (APCI) source operated in positive ion mode was used. HPLC–MS was performed in data-dependent mode with two scan events. While SCAN 1 was performed over the whole spectrum (m/z 300–1300), SCAN 2 was a data-dependent MS² spectrum recorded for the most abundant ion from SCAN 1. Most intact BHPs were identified by comparison of the mass spectra to known BHP mass spectra (Talbot et al., 2001; Talbot et al., 2003; Talbot and Farrimond, 2007). A semi-quantitative estimate of the concentration was obtained, relative to the internal standard, as described in van Winden et al. (2012).

To trace the amount of soil-derived OM, the R'_{soil} was calculated, a ratio based on the relative abundances of soil-marker BHPs against BHT, a pseudo-marine end-member (Doğrul Selver et al., 2012):

$$R'_{soil} = (Ia+Ib+Ic)/(Ia+Ib+Ic+Id) \quad [\text{Eq. 1}]$$

The structures **Ia**, **Ib** and **Ic** refer to soil-marker BHPs, while **Id** refers to BHT (see Fig. 1 for structures).

4. Results

SPM samples from the Yenisei River ($n = 13$) and the SPM ($n = 28$) and sediments ($n = 24$) of its outflow into the marine system were analysed for BHPs (Fig. 2). A total of 22 BHP compounds were quantified (Table 2 and 3). An overview of the abbreviations used and the chemical structures they refer to can be found in Table 1. The summed BHP concentration varied between 180 and 2300 $\mu\text{g.gTOC}^{-1}$ in the sediments, with an average of 1100 $\mu\text{g.gTOC}^{-1}$. The BHPs in the SPM were present in lower absolute abundances, with concentrations varying between 0 and 1500 $\mu\text{g.gPOC}^{-1}$, with an average of 130 $\mu\text{g.gPOC}^{-1}$. The most abundant BHPs in the sediments were: BHT (**Id**), on average 410 $\mu\text{g.gTOC}^{-1}$, followed by adenosylhopane (**Ia**) and BHT cyclitol ether (**Ie**; both on average 160 $\mu\text{g.gTOC}^{-1}$). In the SPM these BHPs also have the highest concentration, although they are present in lower POC-normalized concentrations; BHT (on average 60 $\mu\text{g.gPOC}^{-1}$), adenosylhopane (15 $\mu\text{g.gPOC}^{-1}$) and BHT cyclitol ether (23 $\mu\text{g.gPOC}^{-1}$).

4.1. BHT, BHPentol, BHHexol

BHT (**Id**), and its C-2 methylated (**IId**) and unsaturated counterparts (**IIId** or **IVd**) are encountered both in the sediments and SPM. BHT is a BHP that is produced by a wide variety of source organisms, such as cyanobacteria, purple non-sulfur bacteria, N₂ fixing bacteria and many others (e.g. Talbot et al., 2008 and references therein). BHT is the most abundant compound in the Yenisei and Kara Sea environment, encountered in all sediments and the majority of SPM samples. In the Yenisei Mouth, Gulf and Outflow sediments, the TOC-normalized abundance of BHT (between 120 and 770 $\mu\text{g.gTOC}^{-1}$) remains constant downstream the Yenisei outflow (Fig. 3A). However, as the total amount of BHPs decreases downstream (Table 2), the fractional abundance of BHT increases in the sediments following the Yenisei River outflow (Fig. 3B). In the Yenisei River SPM, the absolute abundance is variable, but does not show a downstream trend (Fig. 4A, between 3 and 30 $\mu\text{g.gPOC}^{-1}$). In marine SPM, BHT is present in concentrations

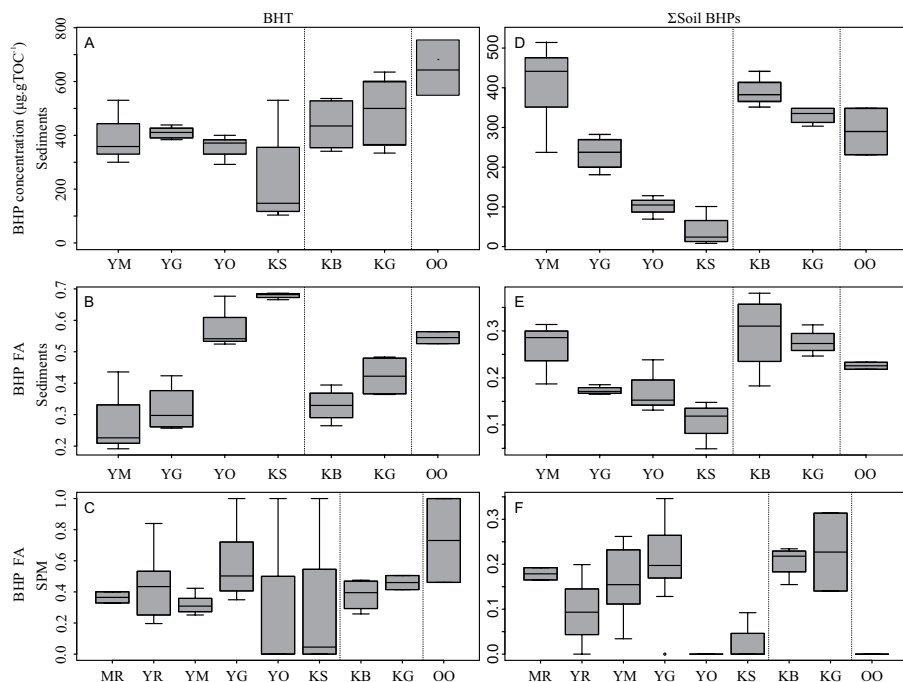


Fig. 3. Box plots showing the variation in the concentration (A-D) and fractional abundances (FA: relative to the total suite of 22 BHPs quantified) of bacteriohopanetetrol (BHT; panels A, B, C) and of the summed concentration of the non-methylated (NM) soil-marker BHPs (Adenosylhopane, G2 and G3 BHPs; **Ia**, **Ib**, **Ic**; panels D, E, F) in sediments (panels A-B, D-E) and SPM (panels C and F). Data are summarized per geographical zone (as defined in Fig. 2), where MR = Mountainous upstream rivers, YR = Lowland Yenisei River, YM = Yenisei Mouth, YG = Yenisei Gulf, YO = Kara Sea sites in Yenisei Outflow, KS = Kara Sea sites distinct from Yenisei outflow, KB = Khalmyer Bay, KG = Khalmyer Gulf, OO = Kara Sea sites in Ob Outflow.

between 0 and 970 $\mu\text{g.gPOC}^{-1}$. Its fractional abundance varies between 0 and 1, but no downstream trend is obvious in the marine SPM (Fig. 3C). The unsaturated BHT is present in 71% of all sediments, in concentrations up to 120 $\mu\text{g.gTOC}^{-1}$ (Table 2). It could be quantified in 14 SPM samples, in concentrations up to 70 $\mu\text{g.gPOC}^{-1}$. The methylated BHT is present in 22 sediments (0-34 $\mu\text{g.gTOC}^{-1}$) and 18 SPM samples (0-33 $\mu\text{g.gTOC}^{-1}$). The quantification of bacteriohopane-31,32,33,34,35-pentol (BHPentol; **If**) was problematic, as it co-elutes with the compound 35-aminobacteriohopane-32,33,34-triol (aminotriol; **Ig**), that is present in much higher abundance. We will thus refrain from discussing changes in the abundance of this BHP. The compound bacteriohopane-30,31,32,33,34,35-hexol (BHHexol; **Ih**) was present in the sediments at 15 sites, in concentrations up to 19 $\mu\text{g.gTOC}^{-1}$, and it was found in the SPM on two occasions (at a maximum abundance of 29 $\mu\text{g.gPOC}^{-1}$, Table 3). The BHP degradation product 32,35-anhydro-bacteriohopanetetrol (anhydroBHT; **Ii**) is observed in 14 sediments, in concentrations up to 10 $\mu\text{g.gTOC}^{-1}$. In the SPM it only amounts up to 5 $\mu\text{g.gPOC}^{-1}$.

4.2. Soil-marker BHPs

Adenosylhopane (**Ia**) is the most abundant component of a group of BHPs that is generally assumed to be derived of bacteria living in soil (e.g. Cooke et al., 2008a,b; Rethemeyer et al., 2011). It is present in all sediments ($n = 24$), in concentrations varying between 9 and 390 $\mu\text{g.gTOC}^{-1}$. Its methylated counterpart (2-methyladenosylhopane; **Ia**) is present in 50% of the sediments, although it is much less abundant (0–29 $\mu\text{g.gTOC}^{-1}$). The adenosylhopane type-2 (colloquially referred to as “soil group 2”; G2; **Ib**), is present in all but one sediment. It is less abundant than adenosylhopane at all sites, with concentrations varying between 0 and 110 $\mu\text{g.gTOC}^{-1}$. Its methylated counterpart (**Ib**) is present in 70% of the sediments, although the concentrations are never $>22 \mu\text{g.gTOC}^{-1}$. The “soil group 3”, G3 BHP (**Ic**), could be quantified in 18 sediments, and occurs in concentrations $<47 \mu\text{g.gTOC}^{-1}$. Its methylated form (**Ic**) is present less frequently ($n = 9$) and in even lower concentrations, with abundances that are in general below 25 $\mu\text{g.gTOC}^{-1}$, although one site (YG8) has a higher concentration of 92 $\mu\text{g.gTOC}^{-1}$. The non-methylated compounds are present in both river and marine SPM, in concentrations up to 240 $\mu\text{g.gPOC}^{-1}$ ($n = 30$; Adenosylhopane), 110 $\mu\text{g.gPOC}^{-1}$ ($n = 30$; G2) and 61 $\mu\text{g.gOC}^{-1}$ ($n = 5$; G3). Their methylated counterparts could be quantified only in a few SPM samples, but they are encountered both in riverine and marine SPM. The highest concentration of the methylated (M; **Ila**, **Ilb**, **Ilc**) and non-methylated (NM; **Ia**, **Ib**, **Ic**) soil-marker BHPs are encountered in the Yenisei Mouth sediments (> 30 and $>300 \mu\text{g.gTOC}^{-1}$, respectively), decreasing towards the Yenisei Gulf (> 20 and between 300 and 150 $\mu\text{g.gTOC}^{-1}$, respectively), while the Yenisei Outflow and Kara Sea samples have concentrations <10 for M soil-marker BHPs and $<150 \mu\text{g.gTOC}^{-1}$ (Fig. 3D) for NM soil-marker BHPs. The fractional abundance of the soil-marker BHPs, compared to the total amount of BHPs also decreases downstream in the SPM (Fig. 3E for NM soil-marker BHPs). Although not part of the Yenisei Outflow system, the Khalmiyer Bay is also characterized by a high concentration of soil-marker BHPs (Fig. 3D; $>20 \mu\text{g.gTOC}^{-1}$ for M soil-marker BHPs, $>350 \mu\text{g.gTOC}^{-1}$ for NM soil-marker BHPs). In the Yenisei River SPM, higher abundances of NM soil-marker BHPs are generally encountered in the Southern Selenga River, decreasing downstream in the Yenisei River, with the exception of YR5 (Fig. 4B). In the SPM of the marine system, the fractional abundance of the NM soil-marker BHPs is slightly increased in the Yenisei Gulf compared with the Yenisei Mouth (and Yenisei River), which is in

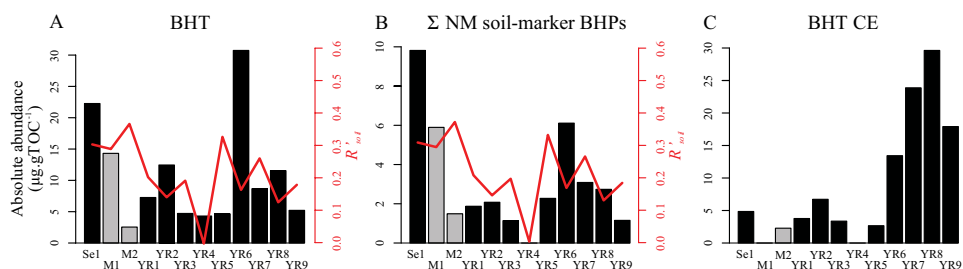


Fig. 4. River SPM BHP distributions showing the concentration of BHT (**Ia**; A), of the sum of the non-methylated (NM) soil-marker BHPs (**Ia** + **Ib** + **Ic**; B), and of BHT CE (**Ic**; C). The R'_{soil} values are plotted in panel A and B in a red line. The grey bars indicate mountainous rivers, while the black bars indicate lowland river settings, reflecting the zones in Fig. 2.

contrast with the decrease observed in the underlying sediments (Fig. 3F). Also, the fractional abundance of the NM soil-marker BHPs is slightly increased compared to the riverine SPM samples, varying between 4 and 35% (Fig. 3F).

4.3. Composite BHPs

Composite BHPs contain an ether-linked functionality at the terminal position of the side-chain moiety (C-35) within the BHP structure. Cyclitol, glycosidic and carbapseudopentose moieties are produced by a variety of source organisms (Talbot et al., 2008 and references therein). Cyclitol ether-containing BHPs were encountered as tetra-, penta- and hexafunctionalized compounds. The tetrafunctionalized BHT cyclitol ether (**Ie**) was present in 18 sediments, with abundances up to $740 \mu\text{g.gTOC}^{-1}$. It was present in the majority of the SPM samples ($n = 18$, up to $30 \mu\text{g.gPOC}^{-1}$). Within the Yenisei River SPM, the concentration of this BHP was increased in the lowland, high latitude sites (Fig. 4C). The BHPentol cyclitol ether (**II**) was less frequently observed ($n = 13$), with concentrations varying up to $100 \mu\text{g.gTOC}^{-1}$ (Table 2). However, it can be found with the same absolute abundances both in sediments with high and low riverine input (Fig. 5A), resulting in increased fractional abundances in the Kara Sea sediments (Table 2; Fig. 5B). It was present in 13 SPM samples (with a maximum concentration of $53 \mu\text{g.gPOC}^{-1}$, Fig. 5A, crossed symbols). Even less common was the hexafunctionalized BHHexol cyclitol ether (**Im**). It was present in only a handful of sediments ($n = 8$), with low concentration, up to $51 \mu\text{g.gTOC}^{-1}$ (Table 2). It could be quantified in 5 SPM samples, albeit in relatively low concentration (up to $8 \mu\text{g.gTOC}^{-1}$; Table 3).

BHT carbapseudopentose (BHT-pseudopentose; **In**) could be quantified in 10 sediment samples, in concentrations varying between 0 and $93 \mu\text{g.gTOC}^{-1}$. In the SPM it could only be quantified at 5 locations, in concentrations up to $88 \mu\text{g.gPOC}^{-1}$. Its unsaturated counterpart (**IIIn** or **IVn**) was present in a small number of sediments ($n = 7$), in a concentration between 0 and $89 \mu\text{g.gTOC}^{-1}$. It was present in 4 SPM samples, albeit in low concentrations (up to $16 \mu\text{g.gOC}^{-1}$). The C-2 methylated BHT-pseudopentose (**IIn**) was present in 5 sediments (concentration up to $33 \mu\text{g.gTOC}^{-1}$). It could be quantified in only 2 SPM samples, in relatively low concentration (up to $10 \mu\text{g.gOC}^{-1}$).

4.4. Aminopolyols

Aminobacterioplanepolyol compounds were encountered as tetra-, penta- and hexafunctionalized compounds. While the tetrafunctionalized compounds are produced by a plethora of source organisms (e.g. Talbot et al., 2008), the penta- and especially the hexafunctionalized compounds are more source-specific, being produced dominantly by methanotrophic bacteria (Talbot and Farrimond, 2007, Talbot et al., 2014 and references therein). Aminotriol (**Ig**) is present in all sediments (9 to $220 \mu\text{g.gTOC}^{-1}$), while its unsaturated counterpart (**IIIg** or **IVg** or containing an unsaturated carbon in the side chain; van Winden et al., 2012) was present in much smaller quantities; it was present above detection limit in only 11 sediments (0 to $28 \mu\text{g.gTOC}^{-1}$). The pentafunctionalized 35-aminobacterioplanetetrol (aminotetrol, **Ij**) was present in the majority of the sediments ($n = 16$; 0 - $48 \mu\text{g.gTOC}^{-1}$), with the highest abundances encountered in the Yenisei Gulf and Khatmyer Bay (Fig. 6A). The hexafunctionalized BHP 35-aminobacterioplanepane-30,31,32,33,34-pentol (aminopentol, **Ik**)

was present in the sediment at 13 sites (0–54 $\mu\text{g.gTOC}^{-1}$), with the highest abundances again in the Yenisei Gulf and Khalmir Bay (Fig. 6B). These BHPs are also present in the SPM, although the concentrations of the tetra-, penta- and hexafunctionalized aminopolyols only amount up to 67 $\mu\text{g.gPOC}^{-1}$ ($n = 21$), 2 $\mu\text{g.gPOC}^{-1}$ ($n = 3$) and 2 $\mu\text{g.gPOC}^{-1}$ ($n = 5$), respectively.

5. Discussion

5.1. BHPs as tracers for soil organic matter in the Kara Sea

The BHP signature in soils has been identified over the past 5 years; temperate soils and peats (Cooke et al., 2008b; Redshaw et al., 2008; Kim et al., 2011; van Winden et al., 2012a, 2012b), tropical soils (Pearson et al., 2009; Wagner et al., 2014), subarctic soils (Xu et al., 2009) and high-latitude soil profiles (Rethemeyer et al., 2010) have been studied. These studies have reported adenosylhopane (Ia) and G2 (Ib) BHPs (and their C-2 methylated homologues) as being present and abundant in all soils, typically averaging 29% of total BHPs (Cooke et al., 2009; Cooke, 2010). These BHPs have been identified in cultures of purple non-sulfur bacteria (Talbot et al., 2007 and references therein), while adenosylhopane is also known to be produced by other Proteobacteria including a dinitrogen-fixing bacterium (*Bradyrhizobium japonicum*; Bravo et al., 2001) and an ammonia-oxidizing bacterium (*Nitrosomonas europaea*; Seemann et al., 1999). In fact, adenosylhopane has been reported to be the precursor for all other side chain elongated BHPs (Bradley et al., 2010) but it is currently unknown why it appears to accumulate so readily in soils compared to other environments. G3 BHP (Ic) and its methylated counterpart (IIc) were first encountered in high latitude soils (Rethemeyer et al., 2010), where they comprised up to 15% of the total BHP concentration. The microbial source of these compounds remains unknown.

To evaluate the transport and sedimentation of soil-derived OM delivered by the Yenisei River, we discuss the abundance of the NM soil-marker BHPs (i.e. Ia, Ib, Ic; Cooke et al., 2010; Rethemeyer et al., 2011) in the SPM of the Yenisei River and the SPM and sediments of the Yenisei Outflow in the Arctic Ocean. This data is compared with previously published data (De Jonge et al., Chapter 6) on the presence of terrigenous OM in the Yenisei River and Kara Sea. Firstly, the results are compared with the abundance and distribution of branched glycerol dialkyl glycerol tetraethers (brGDGTs). Although brGDGTs in the marine system are generally assumed to be soil-derived, De Jonge et al. (Chapter 6) infer that the brGDGTs encountered are derived from several sources, i.e. not only soil-derived and transported by the river, but also influenced by a contribution of brGDGTs that are produced in situ in the Yenisei River and from coastal cliff-derived brGDGTs. The BIT-index, a ratio that contrasts the abundance of 5 major brGDGTs against the marine isoprenoid GDGT crenarchaeol (modified after Hopmans et al., 2004), was found to trace the presence of terrigenous OM in the Kara Sea. A second proxy for the presence of terrigenous OM is the stable carbon isotopic composition of organic matter ($\delta^{13}\text{C}_{\text{org}}$) measured on the same samples (De Jonge et al., 2014a, Chapter 6). $\delta^{13}\text{C}_{\text{org}}$ has been frequently used for tracing terrigenous OM transport in the Kara Sea (Fernandes and Sicre, 2000; Krishnamurthy et al., 2001; Vetrov and Romankevich, 2011; Lein et al., 2012). The performance and applicability of the novel R'_{soil} ratio (Doğrul Selver et al., 2012) can thus be evaluated against two independent proxies for terrigenous OM, the BIT-index and the $\delta^{13}\text{C}_{\text{org}}$ values.

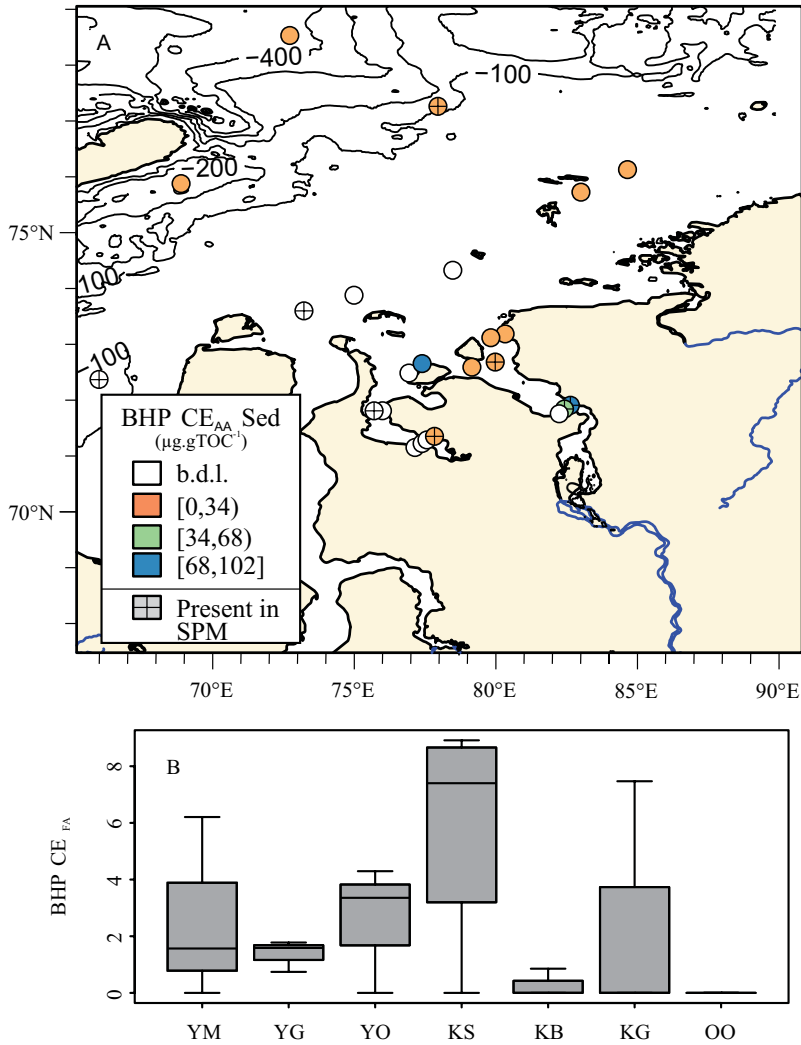


Fig. 5. Occurrence of the BHP CE (II) in the Yenisei/Kara Sea system. A) Geographical variation in the concentration of BHP CE (II) in the sediments. The symbol colour refers to the legend, while a blank symbol indicates a concentration below detection limit (b.d.l.). Crossed symbols indicate the sites where BHP CE (II) was encountered in the SPM. B) Box plots showing the variations in fractional abundance (relative to the summed amount of 22 BHPs) of BHP CE, summarized per geographical zone (see Fig. 2), where YM = Yenisei Mouth, YG = Yenisei Gulf, YO = Kara Sea sites in Yenisei Outflow, KS = Kara Sea sites not directly influenced by the Yenisei outflow, KB = Khalmyer Bay, KG = Khalmyer Gulf, OO = Kara Sea samples in Ob Outflow.

5.1.1. Soil-marker BHPs in Kara Sea surface sediments

The concentration of NM soil-marker BHPs can be compared with the concentrations of brGDGTs, BIT and bulk OM $\delta^{13}\text{C}_{\text{org}}$ values, all indicative for terrigenous input (Fig. 7A-C). The summed concentrations of sedimentary NM soil-marker BHPs possess a good linear correlation ($r^2 = 0.78$) with the concentration of river and soil-derived brGDGTs (Fig. 7A; full line). However, a slightly better fit ($r^2 = 0.81$) can be made when plotting the summed NM soil-marker BHPs as a logarithmic function [$y = \log(x)+x$] against the brGDGT concentration (Fig. 7A; dotted line). The deviation of a linear trend indicates that the concentration of brGDGTs approaches 0 between the Yenisei Gulf and Kara Sea, whereas the soil-marker BHPs still decrease significantly in these offshore sediments (Fig. 7A). This behaviour is slightly offset with the observed difference in degradation by Zhu et al. (2013) in the East China Sea, who describes a stronger resilience of brGDGTs to degradation, compared to soil-marker BHPs. This may be due to differences in the mineral matrix that physically protects the OM in the Yenisei River watershed and Kara Sea (Blair and Aller, 2012), or by the presence of more labile brGDGT pools (e.g. riverine in situ produced brGDGTs).

The pattern in the decrease in abundance of both classes of biomarkers is thus likely to be explained by degradation and dilution (by freshly produced organic matter) in the marine system. The correlation between the BIT values and the concentration of NM soil-marker BHPs ($r^2 = 0.74$, $p < 0.05$; Fig. 7B) is good, as they both trace bacterial OM. Although $\delta^{13}\text{C}_{\text{org}}$ values and the soil-marker BHPs trace different pools of OM (bulk terrigenous-derived OM versus soil-derived OM), the moderate correlation with the concentration of NM soil-marker BHPs ($r^2 = 0.38$, $p < 0.05$; Fig. 7C) indicates that these terrigenous carbon pools are preserved with a similar efficiency in the Kara Sea system.

In marine sediments, the presence of soil-marker BHPs is generally interpreted to be derived from a terrigenous source, delivered to the marine system by riverine transport. Cooke et al. (2009)

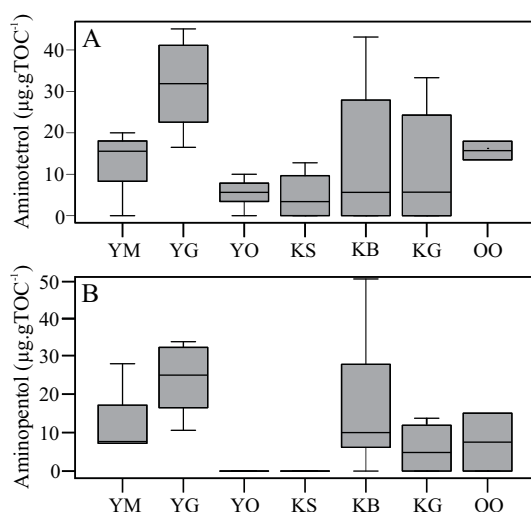


Fig. 6. Box plots showing the variation in concentrations of the BHPs aminotetrol (**Ij**) (A) and aminopentol (**Ik**) (B) per geographical zone (defined as in Fig. 2), where YM = Yenisei Mouth, YG = Yenisei Gulf, YO = Kara Sea sites in Yenisei Outflow, KS = Kara Sea sites not directly influenced by the Yenisei outflow, KB = Khalmyer Bay, KG = Khalmyer Gulf, OO = Kara Sea samples in Ob Outflow.

quantified 4 soil-marker BHPs in the estuaries of 7 major rivers draining into the Arctic Ocean, where their concentration (between 10 and 190 $\mu\text{g.gTOC}^{-1}$) was found to increase eastwards along the Eurasian continent. Zhu et al. (2011b) reported the seaward decrease in concentration of 6 soil-marker BHPs in front of the Yangtze River (400–40 $\mu\text{g.gTOC}^{-1}$) and Doğrul Selver et al. (2012) evaluated seaward trends in concentration changes (500–80 $\mu\text{g.gTOC}^{-1}$) of 6 soil-marker BHPs in the Baltic Sea, in front of the Kalyx River. The two latter studies both identify a seaward decrease in the abundance of soil-marker BHPs. In line with these previous studies, and supporting the riverine transport mechanism of the soil-marker BHPs, we find the full suite of six soil-marker BHPs in the Yenisei River Mouth sediments (Table 2). The concentration of the 6 soil-marker BHPs reported for the Yenisei River outflow in this study (between 10 and 550 $\mu\text{g.gTOC}^{-1}$) compares well with the concentrations encountered in the Kalyx and Yangtze River systems. However, their concentration (between 250 and 550 $\mu\text{g.gTOC}^{-1}$) is high compared to the 77 $\mu\text{g.gTOC}^{-1}$ reported for soil-marker BHPs in the Yenisei River estuary in Cooke et al. (2009). The observed offshore decrease in the concentration of soil-marker BHPs (Fig. 3D) in the Kara Sea, is in agreement with the suggested riverine-derived terrigenous source.

In contrast to many other coastal seas, the shoreline of the Kara Sea is composed of an extensive system of coastal cliffs that are subjected to thermal and wave erosion. The input of coastal-cliff derived OM will be especially significant in those settings where no major river drains. In this study, the Khalmyer Bay is a good example of such a setting. The high

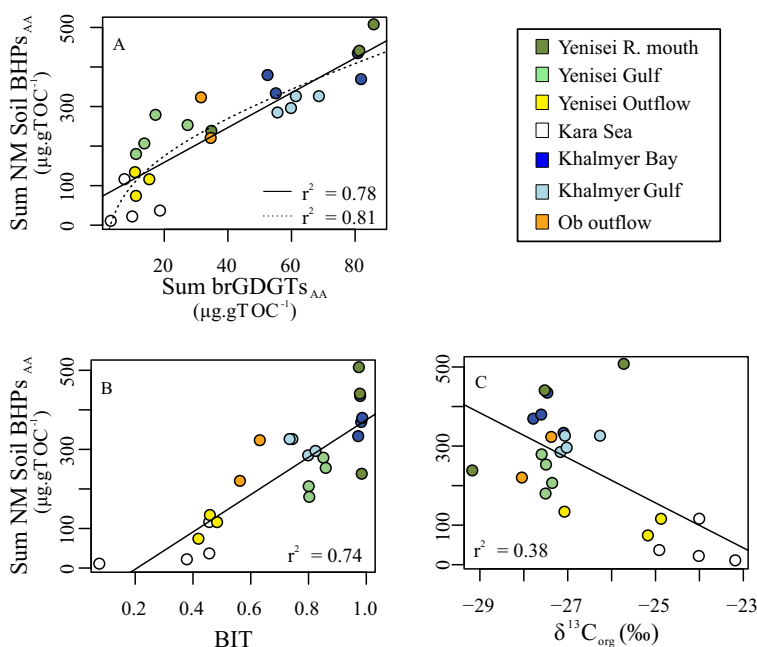


Fig. 7. The concentration (in $\mu\text{g.gTOC}^{-1}$) of the sum of non-methylated soil-marker BHPs (Sum NM Soil BHPs; **Ia** + **Ib** + **Ic**) in surface sediments plotted against A) the concentration of brGDGTs, B) BIT-index values and C) $\delta^{13}\text{C}_{\text{org}}$ values. The squared correlation coefficients (r^2) values are reported. The values for the brGDGT concentrations, BIT-indices and $\delta^{13}\text{C}_{\text{org}}$ values are from De Jonge et al. (Chapter 6). Symbol colours indicate geographical zones, as shown in the legend and defined in Fig. 2.

concentration of soil-marker BHPs encountered in the Khalmalyr Bay (Fig. 3D; $>350 \mu\text{g.gTOC}^{-1}$) indicates that soil-marker BHPs in the Kara Sea can derive in addition to from riverine transport also from coastal cliff erosion.

The R'_{soil} is an index, based on the abundance of 6 soil-marker BHPs relative to BHT, designed to trace soil-derived OM in a river outflow system (Zhu et al., 2011b). The R'_{soil} [Eq. 1] is a similar, but simplified index that excludes three minor C-2 methylated compounds, without losing the source-specific nature of the original ratio (Doğrul Selver et al., 2012). In both ratios, BHT is used as a pseudo-marine end-member, although, being a widespread BHP, it is also present in soils. This results in R_{soil} and R'_{soil} values that are below unity in soils. Zhu et al. (2011b) report that R_{soil} values in soil globally vary between 0.4 and 0.9, with an average value of 0.7 ± 0.1 ($n=30$). This variability within the soil endmember is similar to the BIT-index (Hopmans et al., 2004) that uses crenarchaeol, a tetraether membrane lipid typical for marine Thaumarchaeota as the marine end-member. Crenarchaeol occurs typically in substantially lower concentrations than the brGDGTs, resulting in BIT-values that are generally vary between 0.7 and 1 in soils and peat with an average of 0.9 ± 0.14 ($n=224$) (Schouten et al., 2013). The R_{soil} and R'_{soil} values are strongly correlated in our dataset ($r^2 = 0.99$, both for SPM and sediments), caused by the low abundance of the M soil-marker BHPs in our dataset (Table 2 and 3). Although the presence of the M soil-marker BHPs does not introduce any variation in the index, as observed in Doğrul Selver et al., (2012), the R'_{soil} has typically been applied in northern river systems, and so we will thus discuss variations in the R'_{soil} index. After soil erosion and transport to the marine system, the R'_{soil} values in the Yenisei River Mouth sediments amounts up to 0.62 (Fig. 8A), with slightly lower values in the overlying SPM (up to 0.57; Fig. 8B). These values exceed the R'_{soil} values reported by Doğrul Selver et al. (2012) for the subpolar Kalyx outflow (up to 0.30) and for the tropical Yangtze River outflow (0.43). The spatial pattern in the R'_{soil} values reflects a high input of soil-marker BHPs in the Yenisei Mouth that decreases downstream (Fig. 8A). Although not part of the Yenisei outflow system, the Khalmalyr Bay is characterized by similar R'_{soil} values. In order to interpret changes in R'_{soil} values, both in spatially distributed modern sediments as downcore, it is important to establish the driving factors on the values of this ratio. Instead of recording only changes in the contribution of soil-marker BHPs, the R'_{soil} ratio can also be influenced by changes in the concentration of the pseudo-marine end-member BHT. In this setting, however, the variations in R'_{soil} values are dictated by changes in the abundance of soil-marker BHPs ($r^2 = 0.83$, $p < 0.05$; Fig. 8C), and not by changes in the pseudo marine end-member BHT ($r^2 = 0.05$; Fig. 8D). In the Kara Sea system, R'_{soil} values can thus be interpreted as a tracer for soil-marker BHPs in the marine system, without being influenced by changes in the concentration of BHT.

The R'_{soil} values show a slightly improved correlation with independent terrigenous OM proxies compared to the absolute and fractional abundances of the soil-marker BHPs. It shows a moderate correlation with $\delta^{13}\text{C}_{\text{org}}$ ($r^2 = 0.44$, $p < 0.05$; Fig. 8E) and a good correlation with the BIT ratio ($r^2 = 0.82$, $p < 0.05$; Fig. 8F). The use of a ratio, compared to total abundances is preferred for palaeoclimate proxies, as downcore degradation may influence the absolute concentration of lipids. Indeed, both the BIT-index and the R'_{soil} ratio have been used for reconstructing the delivery of soil OM to the marine system through time (e.g. Weijers et al., 2007; Wagner et al., 2014).

5.1.2. Soil-marker BHPs in riverine and marine SPM

The proposed concept of the R'_{soil} tracing soil-derived OM after soil run-off and transport through a riverine system, implies the presence of soil-marker BHPs in the riverine SPM. As the Yenisei is the largest river in Russia and one of the largest rivers in Asia, it allows evaluation of the BHP distribution in river water crossing several climatic zones (latitudinal range = 5500 km). Furthermore, this study allows comparison of upstream and lowland BHP distributions. We have identified 17 individual BHP compounds in the Yenisei River SPM (Table 3), whereas the maximum diversity of BHPs encountered in a single sample was 9 compounds. To date, only one description of BHPs in riverine SPM has been published (Sáenz et al., 2011), for a small river in Panama. They described the BHP distribution at one site, quantifying 11 compounds. The total BHP abundance encountered in this setting ($0.18 \mu\text{g} \cdot \text{L}^{-1}$) is slightly lower than the highest abundance found in our dataset ($0.31 \mu\text{g} \cdot \text{L}^{-1}$; SR), but higher than the majority of the upstream and lowland sites investigated ($1-3 \cdot 10^{-5} \mu\text{g} \cdot \text{L}^{-1}$).

Both BHT and soil-marker BHPs can be quantified in the Yenisei River SPM, both in upstream and downstream rivers (Fig. 4A, B). The resulting R'_{soil} values are low in the Yenisei River SPM, between 0 and 0.35 (Fig. 4A, B) and are only weakly controlled by changes in the concentration of the NM soil-marker BHPs ($r^2 = 0.17$, $p=0.2$). No correlation is observed for R'_{soil} values and the concentration of BHT. Although the variation in R'_{soil} values in the river SPM are substantial, we can not infer what causes these shifts without further knowledge of the watershed soils BHP distribution. However, the presence of soil-marker BHPs supports the riverine transport of soil-marker BHPs, as part of the Yenisei River SPM. In the Yenisei Mouth and Gulf, a slightly increased amount of soil-marker BHPs is observed, compared to the SPM of the Yenisei River (Fig. 3F). However, taking the average and variance within these groups into account, these small increases are not significant (student t-test, $p>0.05$). As the fractional abundance of BHT shows no significant increase in the Yenisei Mouth and Gulf (Fig. 3C), the resulting average R'_{soil} values in the SPM of the Yenisei Mouth (0.31), is higher than the average R'_{soil} values in the Yenisei River SPM (0.21). This increase in soil-derived OM in the marine system has also been recognized based on brGDGT concentrations and was discussed in the study by De Jonge et al. (Chapter 6). There, it was postulated that it can be due to the presence of an SPM signal that records the signal delivered during the freshet that is possibly increased in soil-derived OM, as the main settling fluxes only occur during the calmer winter months (Gaye et al., 2007). Furthermore, the contribution of coastal-cliff derived soil-marker BHPs may also influence their abundance in the Yenisei River Mouth. Further downstream in the Yenisei Outflow and Kara Sea, soil-marker BHPs are below detection limit in many samples, resulting in R'_{soil} index values that equal 0.

5.2. Other BHPs derived from terrigenous sources

As reported previously (Zhu et al. 2011b; Sáenz et al., 2011; Doğrul Selver et al., 2012), the diversity of BHP compounds is larger in riverine and soil samples, compared to the marine environment (e.g. Blumenberg et al., 2010), indicating that, in addition to the soil-marker BHPs, an additional suite of BHP compounds is produced in the terrigenous system and transported to the marine system. In this section we identify those compounds that are delivered to the marine system via the Yenisei River or coastal erosion, based on their presence in the Yenisei River

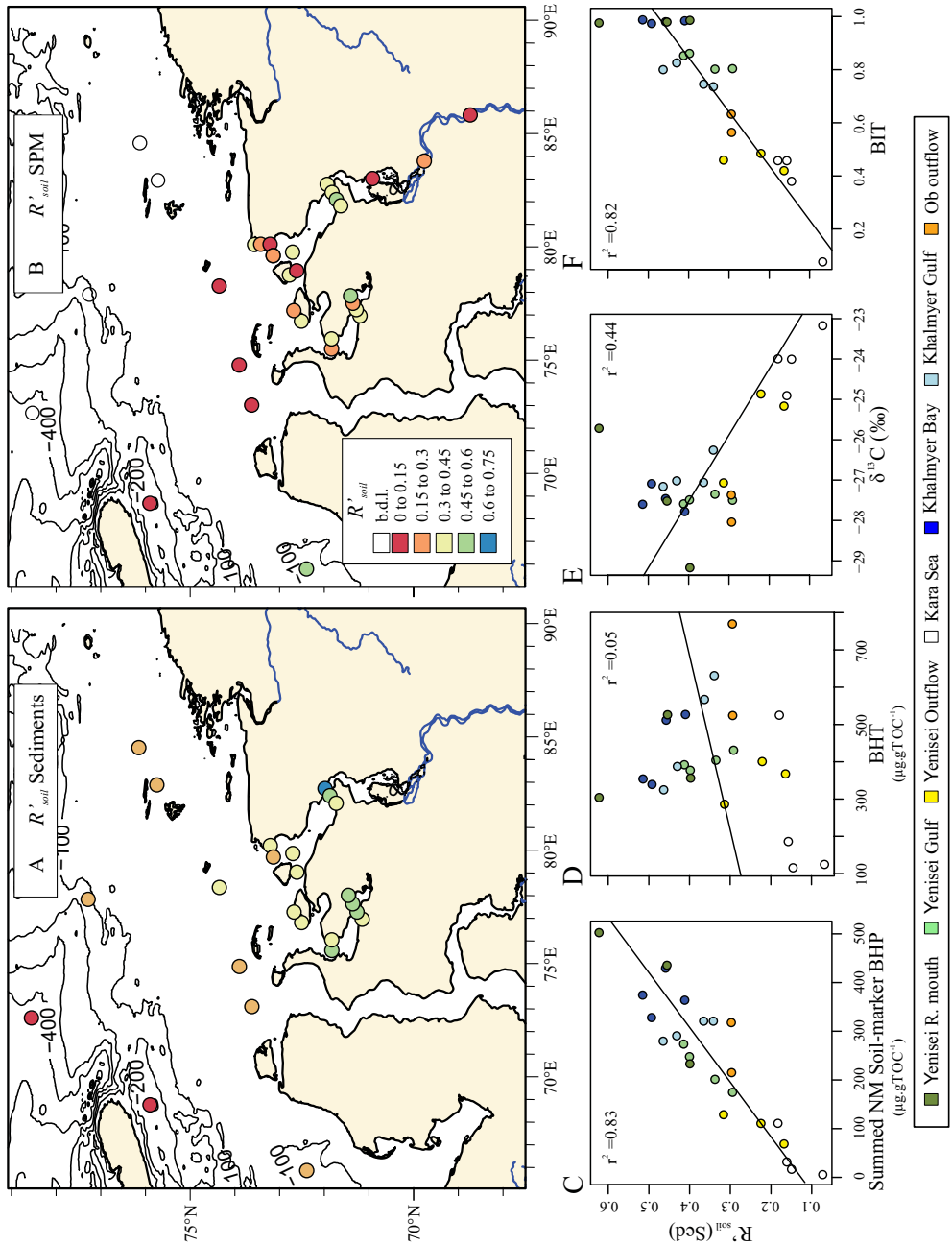


Fig. 8. Geographical distribution of the R'_{soil} index values in (A) surface sediments and (B) SPM of the Yenisei/Kara Sea system. The symbol colours refer to the legend in panel B. B.d.l = below detection limit. The R'_{soil} values of the sediments are plotted against (C) the concentration of the summed non-methylated (NM) soil-marker BHPs (**1a + 1b + 1c**), (D) the concentration of BHT (**1d**), (E) the $\delta^{13}\text{C}_{org}$, and (F) the BIT-index values, a brGDGT-based biomarker proxy for terrigenous material. BIT and $\delta^{13}\text{C}_{org}$ values are reported in Chapter 6. For Panel C-F, the symbol colours indicate geographical zones, as reflected in the legend and in Fig. 2.

SPM and on having a similar geographical distribution as the soil-marker BHPs, i.e. with the largest concentrations in the Yenisei River Mouth and Khalmir Bay.

The BHPs BHT-pseudopentose (**I_n**) and its unsaturated (**III_n** or **IV_n**) and methylated (**II_n**) counterparts are present in the Yenisei mouth and Gulf outflow sediments, with the highest abundance in YM3. Originally shown to be produced by an Arctic cyanobacterium (*Gloeocapsa* sp.; Talbot et al., 2008), they have subsequently been described in the surface layers of peat bogs (van Winden et al., 2012), and also in Arctic soils, where they were found to be particularly abundant in the overlying surface vegetation (organic mat) and river sediments (Rethemeyer et al., 2010). The fractional abundance of the three BHT pseudopentoses is highest in the upstream river SPM samples (Table 3) that have the highest R'_{soil} signal. This pattern fits a dominant source in soils and/or overlying vegetation.

The tetra- and hexafunctionalized BHP cyclitol ethers (**I_e** and **I_m** respectively) show an increased abundance in the Yenisei Mouth sediments, indicating a likely predominantly terrigenous source for these BHPs. The BHHexol cyclitol ether also shows an increased abundance in the upstream rivers and Yenisei outflow SPM, both sites characterised by high R'_{soil} values (Table 3). This BHP has been observed in temperate soils (e.g. Cooke et al., 2008b) but has yet to be identified in bacterial cultures although a related BHHexol mannosamide has been reported from a culture of *Alicyclobacillus acidoterrestris* (Řezanka et al., 2011). The BHT cyclitol ether (**I_e**) is an abundant BHP in both temperate (e.g. Cooke et al., 2008b) and arctic soils (Rethemeyer et al., 2010). It is produced by a variety of organisms, including cyanobacteria, purple non-sulfur bacteria, N_2 -fixing bacteria, *Geobacter* sp. and others (e.g. Talbot et al., 2008; Eickhoff et al., 2013). However, the increase in absolute abundance of BHT cyclitol ether (Fig. 4C) results in their large fractional abundance (between 60 and 70% of all BHPs) in lowland river SPM samples. This points to in situ production in the river water, although input of high-latitude soils cannot be excluded, as the potential source organisms of this BHP are very diverse (Talbot et al., 2008).

The hexafunctionalized BHHexol (**I_h**) is observed in highest abundance in the Khalmir Bay and Yenisei Gulf. It has been described to be the dominant BHP in an enrichment culture of *Methylomirabilis* sp. (Kool et al., 2014), an autotrophic methanotroph. Furthermore, Řezanka et al. (2011) have found BHHexol to be present in the thermophilic bacterium *Alicyclobacillus acidoterrestris*, in abundances up to half of the commonly occurring BHT. This BHP has only occasionally been reported in low abundances in the environment, including lake sediments of Loch Ness, UK (Talbot and Farrimond, 2007), soils (Cooke et al., 2008b), and Amazon shelf and fan sediments (Wagner et al., 2014). Although this BHP could not be quantified in the Yenisei River SPM, we infer a soil source for this minor BHP in the Kara Sea, based on its presence in Yenisei River Mouth sediments.

5.3. Possible marine sources of BHPs

5.3.1. The pseudo-marine end-member BHT

BHT (**I_d**) is a non-specific BHP, it is very common in both terrestrial and marine environments. It has a wide range of source organism (e.g. Talbot et al., 2008). As this compound typically represents around 20% of BHPs in soils (summarized in Zhu et al., 2011b), its presence in the Yenisei River mouth, with a fractional abundance between 20 and 43% (Fig. 3C) is

Absolute abundance (μg·gTOC ⁻¹)																								
	Ii	III d or IV d	Id	II d	Ih	III g or IV g	Ig	Ij	Ik	Ia	IIa	Ib	IIb	Ic	IIc	III n or IV n	In	II n	Ie	II	Im	Sum BHPs μg·gTOC ⁻¹	R' ^{soil}	
<i>m/z</i>	613	653	655	669	771	712	714	772	830	788	802	761	775	802	816	941	943	957	1002	1060	1118			
Site																								
YM2	9.1	120	310	25	9	b.d.l	70	15	6.8	390	27	71	12	47	b.d.l	21	33	b.d.l	310	100	13	1600	0.62	
YM3	b.d.l	52	530	34	13	9.6	110	19	27	300	21	110	22	30	b.d.l	89	93	33	740	37	51	2300	0.45	
YM4	b.d.l	27	360	31	11	b.d.l	32	b.d.l	6.8	150	8.9	60	14	26	9.0	33	37	21	b.d.l	b.d.l	b.d.l	830	0.40	
YG1	2.9	20	400	30	10	23	160	35	33	170	11	80	13	31	11	44	57	19	290	24	25	1500	0.41	
YG2	2.5	22	440	29	11	11	82	16	10	100	b.d.l	56	14	25	11	29	36	11	110	7.6	10	1000	0.29	
YG3	3.5	24	410	24	12	24	130	30	22	130	b.d.l	54	11	20	9.0	31	42	b.d.l	210	20	16	1200	0.33	
YG7	b.d.l	33	380	28	18	28	220	48	34	150	11	76	15	26	10	35	47	16	240	26	23	1500	0.40	
YG8	5.9	28	570	27	13	b.d.l	70	b.d.l	b.d.l	220	b.d.l	79	11	30	93	b.d.l	b.d.l	b.d.l	55	b.d.l	b.d.l	1200	0.36	
YG9	b.d.l	b.d.l	640	b.d.l	b.d.l	b.d.l	57	b.d.l	b.d.l	220	b.d.l	100	b.d.l	b.d.l	b.d.l	b.d.l	b.d.l	b.d.l	200	98	b.d.l	1300	0.34	
YO1	4.8	14	290	14	6.4	5.5	31	5.5	b.d.l	69	b.d.l	44	8.0	19	b.d.l	b.d.l	b.d.l	b.d.l	31	b.d.l	b.d.l	540	0.31	
YO2	7.4	13	410	25	b.d.l	24	77	9.5	b.d.l	68	b.d.l	46	8.4	b.d.l	b.d.l	b.d.l	b.d.l	b.d.l	40	25	b.d.l	750	0.22	
YO3	8.3	b.d.l	370	23	b.d.l	9.9	37	b.d.l	b.d.l	39	b.d.l	33	3.7	b.d.l	b.d.l	b.d.l	b.d.l	b.d.l	b.d.l	24	b.d.l	550	0.16	
KS1	9.6	14	530	25	b.d.l	b.d.l	69	13	b.d.l	66	b.d.l	32	b.d.l	17	b.d.l	b.d.l	b.d.l	b.d.l	b.d.l	b.d.l	b.d.l	780	0.18	
KS2	b.d.l	b.d.l	190	14	b.d.l	b.d.l	22	b.d.l	b.d.l	24	b.d.l	12	b.d.l	b.d.l	b.d.l	b.d.l	b.d.l	b.d.l	b.d.l	24	b.d.l	290	0.16	
KS3	b.d.l	b.d.l	120	b.d.l	b.d.l	3.3	16	6.2	b.d.l	13	b.d.l	7.4	b.d.l	b.d.l	b.d.l	b.d.l	b.d.l	b.d.l	b.d.l	11	b.d.l	180	0.14	
KS4	b.d.l	b.d.l	130	6.7	b.d.l	b.d.l	9.3	b.d.l	b.d.l	9.3	b.d.l	b.d.l	b.d.l	b.d.l	b.d.l	b.d.l	b.d.l	b.d.l	17	17	b.d.l	190	0.07	
KB1	8.8	61	530	34	19	b.d.l	120	46	54	230	19	100	10	33	b.d.l	b.d.l	54	b.d.l	610	b.d.l	24	2000	0.41	
KB2	6.1	59	360	27	9	b.d.l	38	b.d.l	9.0	260	29	92	8.8	23	b.d.l	b.d.l	44	b.d.l	170	b.d.l	b.d.l	1100	0.51	
KB3	9.3	b.d.l	340	19	9	b.d.l	26	b.d.l	b.d.l	220	19	69	13	40	12	b.d.l	b.d.l	b.d.l	79	b.d.l	b.d.l	860	0.49	
KB4	b.d.l	b.d.l	520	30	15	b.d.l	44	13	11	290	20	110	b.d.l	35	b.d.l	b.d.l	52	b.d.l	350	13	10	1500	0.46	
KG1	b.d.l	22	330	11	b.d.l	b.d.l	43	13	11	200	21	53	8.0	33	16	b.d.l	b.d.l	b.d.l	150	b.d.l	b.d.l	910	0.46	
KG2	7.6	30	390	14	b.d.l	b.d.l	89	35	14	190	18	71	11	34	25	b.d.l	b.d.l	b.d.l	130	b.d.l	b.d.l	1100	0.43	
OO1	6.1	29	770	30	16	9.6	110	18	16	210	16	77	20	32	b.d.l	b.d.l	b.d.l	b.d.l	96	b.d.l	b.d.l	1500	0.29	
OO2	b.d.l	27	530	28	12	15	95	14	b.d.l	130	b.d.l	56	b.d.l	34	b.d.l	b.d.l	b.d.l	b.d.l	b.d.l	b.d.l	b.d.l	940	0.29	

Table 2. Concentration of the individual and summed sedimentary BHPs ($\mu\text{g}\cdot\text{gTOC}^{-1}$). The R'_{soil} values are calculated [Eq. 1]. B.d.l. indicates that the concentration was below detection limit.

Absolute abundance (μg.gTOC ⁻¹)																								
	Ii	III d or IV d	Id	II d	Ih	III g or IV g	Ig	Ij	Ik	Ia	IIa	Ib	IIb	Ic	IIc	III n or IV n	In	II n	Ie	II	Im	Sum BHPs μg.gPOC ⁻¹	R' _{soil}	
m/z	613	653	655	669	771	712	714	772	830	788	802	761	775	802	816	941	943	957	1002	1060	1118			
Site																								
M1	b.d.l	b.d.l	14	1.8	b.d.l	b.d.l	1.3	b.d.l	b.d.l	3.0	b.d.l	2.9	1.1	b.d.l	b.d.l	3.0	5.7	2.5	b.d.l	b.d.l	b.d.l	35	0.29	
M2	b.d.l	b.d.l	2.5	b.d.l	0.2	b.d.l	0.1	b.d.l	b.d.l	1.0	b.d.l	0.5	b.d.l	b.d.l	b.d.l	b.d.l	b.d.l	b.d.l	2.3	0.5	0.5	7.6	0.37	
SR1	b.d.l	3.5	22	1.8	b.d.l	b.d.l	5.1	b.d.l	b.d.l	6.4	b.d.l	3.4	2.0	b.d.l	b.d.l	b.d.l	b.d.l	b.d.l	4.9	b.d.l	b.d.l	49	0.31	
YR1	b.d.l	b.d.l	7.3	b.d.l	b.d.l	b.d.l	b.d.l	b.d.l	b.d.l	1.2	b.d.l	0.7	b.d.l	b.d.l	b.d.l	b.d.l	b.d.l	b.d.l	3.8	b.d.l	b.d.l	13	0.20	
YR2	0.6	b.d.l	12	2.8	b.d.l	b.d.l	b.d.l	b.d.l	b.d.l	1.6	b.d.l	0.5	b.d.l	b.d.l	b.d.l	b.d.l	b.d.l	b.d.l	6.7	b.d.l	b.d.l	24	0.14	
YR3	b.d.l	0.6	4.7	0.9	b.d.l	b.d.l	b.d.l	b.d.l	b.d.l	0.9	b.d.l	0.3	b.d.l	b.d.l	b.d.l	b.d.l	b.d.l	b.d.l	3.4	0.6	b.d.l	11	0.19	
YR4	5.1	b.d.l	4.3	b.d.l	b.d.l	b.d.l	b.d.l	b.d.l	0.8	b.d.l	b.d.l	b.d.l	b.d.l	b.d.l	b.d.l	b.d.l	b.d.l	b.d.l	b.d.l	b.d.l	b.d.l	10	0.00	
YR5	0.1	1.1	4.6	0.8	b.d.l	b.d.l	0.4	b.d.l	b.d.l	1.8	b.d.l	0.5	b.d.l	b.d.l	b.d.l	b.d.l	b.d.l	b.d.l	2.7	b.d.l	b.d.l	12	0.33	
YR6	b.d.l	b.d.l	31	6.2	b.d.l	b.d.l	1.2	b.d.l	b.d.l	6.1	b.d.l	b.d.l	b.d.l	b.d.l	b.d.l	b.d.l	b.d.l	b.d.l	13	b.d.l	b.d.l	58	0.17	
YR7	b.d.l	1.0	8.7	0.8	b.d.l	b.d.l	b.d.l	b.d.l	b.d.l	2.4	b.d.l	0.7	b.d.l	b.d.l	b.d.l	b.d.l	b.d.l	b.d.l	24	1.4	b.d.l	39	0.26	
YR8	b.d.l	b.d.l	12	b.d.l	b.d.l	b.d.l	0.7	b.d.l	b.d.l	1.2	1.1	0.5	b.d.l	b.d.l	b.d.l	b.d.l	b.d.l	b.d.l	30	1.3	b.d.l	47	0.13	
YR9	b.d.l	1.0	5.2	b.d.l	b.d.l	b.d.l	0.3	b.d.l	b.d.l	0.9	b.d.l	0.3	b.d.l	b.d.l	b.d.l	b.d.l	b.d.l	b.d.l	18	0.9	b.d.l	27	0.18	
YM1	b.d.l	b.d.l	16	b.d.l	b.d.l	b.d.l	0.8	b.d.l	b.d.l	b.d.l	b.d.l	1.6	b.d.l	b.d.l	b.d.l	b.d.l	b.d.l	b.d.l	27	b.d.l	b.d.l	45	0.09	
YM2	b.d.l	3.1	21	1.9	b.d.l	b.d.l	1.8	b.d.l	1.6	6.9	b.d.l	3.8	0.9	b.d.l	b.d.l	b.d.l	b.d.l	b.d.l	25	1.6	b.d.l	68	0.33	
YM3	b.d.l	2.3	22	2.0	b.d.l	b.d.l	2.0	b.d.l	b.d.l	7.8	b.d.l	2.1	0.7	b.d.l	b.d.l	b.d.l	b.d.l	b.d.l	46	2.6	1.2	89	0.31	
YM4	b.d.l	6.9	100	8.7	b.d.l	3.2	6.6	b.d.l	1.9	65	5.5	23	5.3	8.8	400	16	22	11	71	7.0	3.5	370	0.49	
YM5	b.d.l	b.d.l	20	1.7	b.d.l	b.d.l	b.d.l	b.d.l	0.5	6.8	1.0	3.7	0.8	0.70	b.d.l	b.d.l	b.d.l	b.d.l	13	b.d.l	b.d.l	48	0.35	
YG1	1.3	b.d.l	25	b.d.l	b.d.l	b.d.l	b.d.l	b.d.l	b.d.l	7.8	b.d.l	3.7	1.3	b.d.l	b.d.l	3.6	6.3	b.d.l	14	6.8	b.d.l	70	0.32	
YG2a	b.d.l	b.d.l	7.4	b.d.l	b.d.l	b.d.l	b.d.l	b.d.l	b.d.l	3.3	b.d.l	1.0	b.d.l	b.d.l	b.d.l	b.d.l	b.d.l	b.d.l	9.4	b.d.l	b.d.l	21	0.37	
YG2b	1.4	b.d.l	22	1.8	b.d.l	b.d.l	b.d.l	b.d.l	b.d.l	5.2	b.d.l	3.5	0.9	b.d.l	b.d.l	2.0	2.2	b.d.l	2.9	b.d.l	b.d.l	42	0.29	
YG3	b.d.l	b.d.l	6.2	b.d.l	b.d.l	b.d.l	b.d.l	b.d.l	b.d.l	b.d.l	b.d.l	0.9	b.d.l	b.d.l	b.d.l	b.d.l	b.d.l	b.d.l	b.d.l	b.d.l	b.d.l	7.1	0.13	
YG4	b.d.l	b.d.l	7.1	b.d.l	b.d.l	b.d.l	b.d.l	b.d.l	b.d.l	2.1	b.d.l	0.8	b.d.l	b.d.l	b.d.l	b.d.l	b.d.l	b.d.l	3.9	b.d.l	1.0	15	0.28	
YG5	b.d.l	b.d.l	5.6	b.d.l	b.d.l	b.d.l	0.5	0.2	0.6	2.2	b.d.l	1.0	b.d.l	0.6	b.d.l	b.d.l	b.d.l	b.d.l	b.d.l	b.d.l	b.d.l	11	0.40	
YG6	b.d.l	b.d.l	4	b.d.l	b.d.l	b.d.l	0.5	b.d.l	b.d.l	1.8	b.d.l	0.8	b.d.l	b.d.l	b.d.l	b.d.l	b.d.l	b.d.l	2.6	b.d.l	b.d.l	10	0.39	
YG7	b.d.l	b.d.l	970	b.d.l	b.d.l	b.d.l	b.d.l	b.d.l	b.d.l	b.d.l	b.d.l	b.d.l	b.d.l	b.d.l	b.d.l	b.d.l	b.d.l	b.d.l	b.d.l	b.d.l	b.d.l	970	0.00	
YG8	b.d.l	69.0	600	34	29	20	68	b.d.l	b.d.l	240	b.d.l	110	b.d.l	62	b.d.l	b.d.l	88	b.d.l	160	b.d.l	b.d.l	1500	0.41	
YG9	b.d.l	b.d.l	5.30	0.2	b.d.l	b.d.l	0.5	b.d.l	b.d.l	0.7	b.d.l	0.7	b.d.l	b.d.l	b.d.l	b.d.l	b.d.l	b.d.l	b.d.l	b.d.l	b.d.l	7.4	0.21	
YO1	b.d.l	b.d.l	0.5	b.d.l	b.d.l	b.d.l	b.d.l	b.d.l	b.d.l	b.d.l	b.d.l	b.d.l	b.d.l	b.d.l	b.d.l	b.d.l	b.d.l	b.d.l	b.d.l	b.d.l	b.d.l	0.5	0.00	
YO2	b.d.l	b.d.l	b.d.l	b.d.l	b.d.l	b.d.l	b.d.l	b.d.l	b.d.l	b.d.l	b.d.l	b.d.l	b.d.l	b.d.l	b.d.l	b.d.l	b.d.l	b.d.l	b.d.l	b.d.l	b.d.l	b.d.l	NA	
YO3	b.d.l	b.d.l	b.d.l	b.d.l	b.d.l	b.d.l	b.d.l	b.d.l	b.d.l	b.d.l	b.d.l	b.d.l	b.d.l	b.d.l	b.d.l	b.d.l	b.d.l	b.d.l	b.d.l	b.d.l	b.d.l	b.d.l	NA	
KS1	b.d.l	0.5	0.6	b.d.l	b.d.l	b.d.l	0.3	b.d.l	b.d.l	0.7	b.d.l	b.d.l	b.d.l	b.d.l	b.d.l	b.d.l	b.d.l	b.d.l	0.9	4.1	b.d.l	7.1	0.50	

KS2	b.d.l	b.d.l	b.d.l	b.d.l	b.d.l	b.d.l	b.d.l	b.d.l	b.d.l	b.d.l	b.d.l	b.d.l	b.d.l	b.d.l	b.d.l	b.d.l	b.d.l	b.d.l	b.d.l	b.d.l	b.d.l	0.4	b.d.l	0.6	NA
KS3	b.d.l	b.d.l	b.d.l	b.d.l	b.d.l	b.d.l	b.d.l	b.d.l	b.d.l	b.d.l	b.d.l	b.d.l	b.d.l	b.d.l	b.d.l	b.d.l	b.d.l	b.d.l	b.d.l	b.d.l	b.d.l	b.d.l	b.d.l	0.8	0.00
KS4	b.d.l	b.d.l	b.d.l	b.d.l	b.d.l	b.d.l	b.d.l	b.d.l	b.d.l	b.d.l	b.d.l	b.d.l	b.d.l	b.d.l	b.d.l	b.d.l	b.d.l	b.d.l	b.d.l	b.d.l	b.d.l	b.d.l	b.d.l	0.2	NA
KB1	b.d.l	5.3	38	1.5	b.d.l	b.d.l	b.d.l	b.d.l	13	b.d.l	4.9	b.d.l	b.d.l	b.d.l	b.d.l	b.d.l	b.d.l	b.d.l	b.d.l	b.d.l	b.d.l	18	b.d.l	81	0.32
KB2	b.d.l	15.0	47	4.7	b.d.l	b.d.l	b.d.l	b.d.l	25	b.d.l	6.7	b.d.l	2.70	b.d.l	b.d.l	b.d.l	b.d.l	b.d.l	b.d.l	b.d.l	b.d.l	43	b.d.l	140	0.42
KB3	b.d.l	16.0	99	4.0	b.d.l	b.d.l	b.d.l	6.4	b.d.l	b.d.l	24	b.d.l	9.3	b.d.l	b.d.l	b.d.l	b.d.l	b.d.l	b.d.l	b.d.l	b.d.l	56	b.d.l	220	0.25
KB4	b.d.l	31.0	230	17	b.d.l	b.d.l	b.d.l	17	b.d.l	b.d.l	150	b.d.l	41	b.d.l	b.d.l	b.d.l	b.d.l	b.d.l	b.d.l	b.d.l	b.d.l	330	53	900	0.45
KG1	b.d.l	b.d.l	35	b.d.l	b.d.l	b.d.l	5.2	2.1	b.d.l	7.1	b.d.l	4.8	b.d.l	b.d.l	b.d.l	b.d.l	b.d.l	b.d.l	b.d.l	b.d.l	b.d.l	13	17	84	0.25
KG2	b.d.l	b.d.l	34	b.d.l	b.d.l	b.d.l	4.3	b.d.l	b.d.l	15	b.d.l	5.8	b.d.l	b.d.l	b.d.l	b.d.l	b.d.l	b.d.l	b.d.l	b.d.l	b.d.l	7.7	b.d.l	67	0.38
OO1	b.d.l	b.d.l	1.6	b.d.l	b.d.l	b.d.l	0.5	0.2	b.d.l	b.d.l	b.d.l	b.d.l	b.d.l	b.d.l	b.d.l	b.d.l	b.d.l	b.d.l	b.d.l	b.d.l	b.d.l	0.9	0.2	3.4	0.00
OO2	b.d.l	b.d.l	0.3	b.d.l	b.d.l	b.d.l	b.d.l	b.d.l	b.d.l	b.d.l	b.d.l	b.d.l	b.d.l	b.d.l	b.d.l	b.d.l	b.d.l	b.d.l	b.d.l	b.d.l	b.d.l	b.d.l	b.d.l	0.3	0.00

Table 3. Concentration of the individual and summed BHPs of the suspended particulate matter ($\mu\text{g}\cdot\text{gTOC}^{-1}$). The R'_{sed} values are calculated [Eq. 1]. B.d.l. indicates that the concentration was below detection limit.

probably partly derived from watershed soils. This riverine transport mechanism is confirmed by its presence in the Yenisei River SPM (Figs. 3C, 4A). In contrast to the distribution of the soil-marker BHPs (Fig. 3D), the BHT concentration in marine sediments does not change substantially downstream the Yenisei Outflow (Fig. 3A). This can be based on two mechanisms; i) the simultaneous degradation of soil-derived BHP with marine in situ production, or ii) the significantly better preservation of BHT compared to the soil-marker BHPs. Handley et al. (2010) observed better preservation of BHT, compared to the soil-marker BHPs, in downcore sediments from the Congo deep sea fan. On the other hand, in situ production of BHT in the marine system was observed to occur in modern marine coastal systems. For instance, Pearson et al. (2009), Rethemeyer et al. (2011) and Zhu et al. (2011b) observed an increase of the BHT concentration, and attributed this to in situ production. Based on this dataset, we cannot conclusively state which mechanism is dominant in controlling the observed pattern in the Yenisei outflow BHT concentrations.

5.3.2. Possible cyanobacterial markers produced in the marine system.

The pentafunctionalized BHP cyclitol ether (**II**) is present in similar concentration in sediments with high and low riverine input, resulting in increased fractional abundances in the Kara Sea sediments (Table 2; Fig. 5A, B). This indicates that this BHP is possibly produced in situ in the marine system. This is confirmed by its presence in marine SPM, where it can be present in a high fractional abundance (up to 70% in one sample, on average 30%). This is remarkable, as this compound was so far reported to dominate BHP distributions only in environmental samples from a terrestrial geothermal vent (Champagne Pool; Gibson et al., 2014). The possible source organism in that environment such as *Acidithiobacillus* sp. are chemolithotrophic organisms. Other known source organisms include the acetic acid bacteria (*Acetobacter* spp., *Gluconacetobacter* spp.; Talbot et al., 2007b and references therein). However, these organisms also make the unsaturated and C-3 methylated cyclitol ethers that were not present in our sediments. Also in the acetic acid bacterium *Frateuria aurantica* (Joyeux et al., 2004), the BHPentol cyclitol ether was shown to be the most abundant BHP, although its abundance increased with increased growth temperature, a condition that does not reflect the Arctic Ocean. Furthermore, both the acetic acid bacteria and *Frateuria* sp. thrive at low pH conditions, and are thus unlikely to occur in the high pH Arctic marine system. We postulate, therefore, that the most probable source organism of this compound in the Kara Sea is a cyanobacterium such as *Chlorogloeopsis* sp. (Talbot et al., 2003b). In polar environments, BHPentol cyclitol ether (**II**) was described as a minor compound in an Antarctic lake sediment and microbial mat (Talbot et al., 2008). We thus postulate a cyanobacterial source for the increase in fractional abundance of the pentafunctionalized BHP cyclitol ether, resulting in a dominance of BHP cyclitol ether especially in those sediments that receive almost no terrigenous OM (e.g. KS1).

5.3.3. Methanotrophic markers in the marine system

Large amounts of submerged, degrading permafrost are present in the Kara Sea sediments (Romanovskii et al., 2005). This permafrost was formed on-land during the sea-level lowstand of the last glacial period and inundated with marine water 7-15 ky ago. Substantial amounts of methane are present (trapped in frozen material) or being formed in these sediments. Since

the inundation, this permafrost has been melting, and methane gas can be expelled as large flares of methane bubbles that have been reported to be present between the 20 and 60 m isobaths, where pathways are present within the degrading permafrost that allow the escape of methane (Portnov et al., 2013). Aerobic methanotrophic bacteria have been described to be present and active in permafrost environments (Trotsenko and Khmelenina, 2005, and references therein). As methanotrophic bacteria have the capacity to mitigate CH₄ emissions from melting permafrost, the response of microbial communities on thawing permafrost will determine whether permafrost environments will be a net source of greenhouse gasses in the coming decades (Graham et al.; 2012). The presence of active aerobic methanotrophs in the Kara Sea sediments is to be expected, as methane oxidation was described to occur in the upper sediments throughout the Kara Sea (Savvichev et al., 2010).

Aerobic methanotrophy can be traced using specific BHPs that are known to be markers for methanotrophic bacteria. Aminopentol (**Ik**) is a marker for type I methanotrophs (gammaproteobacteria; Talbot et al., 2014 and references therein) although there is one report of trace levels in one species of sulfate-reducing bacteria (Blumenberg et al., 2012). Aminotetrol (**Ij**) also may reflect the presence of both type I and type II (alphaproteobacteria) methanotrophs, as it was found in most methanotrophs from the alpha- and gammaproteobacteria (Talbot and Farrimond, 2007). Type I methanotrophs (using the ribulose monophosphate carbon assimilation pathway) are generally associated with freshwater and marine aquatic systems, although they have also been shown to dominate Arctic soils (e.g. Martineau et al., 2010; Yergeau et al., 2010), while Type II methanotrophs (employing the Serine pathway for carbon assimilation) are widespread in terrestrial settings, (e.g. Hanson and Hanson, 1996).

Previous research on the distribution of the BHPs aminopentol and aminotetrol in the freshwater and marine realm identified two possible sources. Firstly, the methanotrophic signal can be derived from the continent, as methanotrophy is a process that will occur in the aerobic zones of methanogenic soils, peats and wetlands (e.g. Talbot et al., 2014 and references therein). Van Winden et al. (2012a, 2012b) described the presence of both aminotetrol and aminopentol in UK and Belgian Sphagnum peat, amounting up to 3 and 0.5% of all BHPs quantified, respectively. This is comparable to the fractional abundances encountered in the marine sediments in this study. Bacterial methanotrophy has also been described in the Yenisei River water column (Namsaraev et al., 1995), and the biomarker signal may thus also be produced in situ in the Yenisei River. At least part of the methanotrophic signal encountered in the marine system is derived from the Yenisei River or its watershed, as aminopolyols were detected in the Yenisei River SPM (Table 3). Aminotetrol is present in both the Yenisei River and the Yenisei Gulf. The fractional abundance of aminopentol is highest in lowland Yenisei River SPM, and in the Yenisei River Mouth (Tables 2 and 3). A terrigenous source is in line with previous studies (Talbot et al., 2014, Wagner et al., 2014), where the presence of aminopentol in marine river fan sediments was shown to derive from terrestrial wetland systems in the Congo River catchment and in the Amazon Basin.

However, the increase in concentration of all aminopolyols in the Yenisei Gulf sediments, compared to the upstream Yenisei River Mouth (Table 3; illustrated for aminotetrol and aminopentol in Figs. 6A-B) contrasts with the decrease observed for soil-marker BHPs (Fig. 3D). A possible explanation for the increase of the concentration of all 4 aminopolyols is the in

situ production of these BHPs in the marine sediments. Based on the presence of aminopentol, we postulate that they are produced by a salt-tolerant clade of Type I methanotrophic Bacteria. *Methylovulum* sp. was isolated from an acidic peat has been shown to produce all 4 of these BHPs (van Winden et al., 2012). The aminopolyol signature thus reflects a typical methanotrophic signature that would be expected for a *Methylovulum*-like organism. Also, Taylor and Harvey (2011) describe the presence of aminotetrol and aminopentol in the surface sediments of the Chukhi Sea, a shallow shelf sea comparable to the Kara Sea, although these BHPs were absent from river sediments ($n = 2$) and watershed peat samples ($n = 2$). These data are in favour of an in situ source for these BHPs in the Yenisei Gulf sediments.

Moving further downstream, to the Yenisei River outflow, both the unsaturated and saturated aminotriol compounds and aminotetrol are still present in similar maximum abundances as observed in the Yenisei River mouth sediments (Fig. 6A). However, as aminopentol is not present at these sites, this BHP distribution possibly reflects the in situ production by a methanotrophic community that is dominated by Type II methanotrophs, potentially including *Methylocella* sp., which produces high levels of aminotriol and also BHT (van Winden et al., 2012). In truly marine systems where methanotrophy is encountered, e.g. those associated with methane seeps, aminopentol has not been observed (Jahnke et al., 1995; Burhan et al., 2002; Pancost et al., 2005; Birgel et al., 2011), which has led to the speculation that at least some of these environments are dominated by Type II methanotrophs (e.g. Birgel et al., 2011). However, Coolen et al. (2008) reported 16S ribosomal RNA gene sequences from Type I species in sediments from an Antarctic meromictic lake in which the only aminoBHPs observed were aminotriol and aminotetrol, indicating that some Type I species may not produce aminopentol. Therefore, it is possible that the absence of aminopentol, whilst potentially indicating a change in the methanotroph community, does not necessarily indicate a shift to Type II species. The interspersed nature of the occurrence of the methanotrophic signal, both in the Yenisei River Gulf and Outflow (Fig. 6A-B) indicate that the erosion of the submerged permafrost does not lead to a uniformly increased methanotrophic signal in this setting. Although the presence of methanotrophic biomarkers does not indicate that the source organisms are active in the environment, it does highlight the potential for methanotrophic bacteria to mitigate the export of methane stored and produced within submerged permafrost.

6. Conclusion

This study reports the BHP distribution and abundance in a major Siberian river that spans a large latitudinal gradient, and its outflow in the Kara Sea, a shallow Arctic Ocean shelf sea. In this setting, the R'_{soil} index can be used as a tracer for the delivery of soil OM to modern marine sediments, indicated by its good correlation with the BIT-index ($r^2 = 0.82$). Although the presence of both soil-marker BHPs and BHT in the Yenisei River SPM supports the proposed riverine transport mechanism of BHPs to the marine system, it is unclear to what extent the R'_{soil} values in the River SPM reflect the R'_{soil} values in the watershed soils, as no BHPs were measured on soils in the Yenisei watershed. The increased abundance of soil-marker BHPs in the Khatymy Bay, where no major rivers drain, is probably derived from coastal cliffs erosion. Soil-marker BHPs can thus have two sources in shallow Arctic Seas. The diversity of BHPs was found to decrease from the Yenisei River Mouth into the marine system. The distributions

of the BHPs BHT-pseudopentose (**In**), its unsaturated (**IIIIn** or **IVn**) and methylated (**IIIn**) counterparts, tetra- and hexafunctionalized BHP cyclitol ethers (**Ie** and **Im** respectively) and BHHexol (**Ih**) in the marine sediments mimics that of the soil-marker BHPs in the outflow of the Yenisei River. This suggests that these BHPs are also soil-derived, and delivered to the marine system by riverine transport. The distribution of BHTetrol CE (**Ie**) in the river SPM indicates that it is possibly produced in situ in the lowland Yenisei River, or derived from high-latitude soils. The increased fractional abundance of BHPentol CE in offshore marine samples indicates a probably cyanobacterial, marine source. The spatial distribution of biomarkers for methanotrophic activity (aminotetrol (**Ij**), and especially aminopentol (**Ik**)) in the Kara Sea sediments indicates a mixture of terrigenous and marine sources. Their downstream increase is a strong indication for an in situ produced methanotrophic signal, which can be related to the presence of large amounts of submerged permafrost in the Kara Sea sediments. Overall, the study of riverine and marine BHPs in the Yenisei River/Kara Sea system confirms the potential of BHPs to identify the dominant source of the OM encountered, and even identify specific bacterial groups.

7. Acknowledgments

This work was performed in the framework of the memorandum NIOZ-VNIIOkeangeologia for Arctic research. The research was funded by research project 819.01.013, financed by the Netherlands Organization for Scientific Research (NWO) and the European Research Council under the EU Seventh Framework Programme (FP7/2007-2013)/ERC grant agreement No. [226600] and the Natural Environment Research Council (NERC) grant number NE/I027967/1 to HMT for funding (JB). We also thank the Science Research Investment Fund (SRIF) from HEFCE for funding the purchase of the ThermoFinnigan LCQ ion trap mass spectrometer (Newcastle) and Frances Sidgwick for technical assistance.



Photo by Cindy De Jonge

Branched glycerol dialkyl glycerol
tetraethers and crenarchaeol
record post-glacial sea level rise
and shifts in sources of terrigenous
brGDGTs in the Kara Sea
(Arctic Ocean)

8

Cindy De Jonge, Alina Stadnitskaia,
Georgy Cherkashov
and Jaap S. Sinninghe Damsté

ABSTRACT

The distribution of branched glycerol dialkyl glycerol tetraethers (brGDGTs) was found to correlate with soil pH and mean annual temperature (MAT) in soils. Based on this dependence, calibrations were made that allow the reconstruction of soil pH and MAT, based on the brGDGT distribution in geological archives, e.g. marine sediments. Furthermore, the branched and isoprenoid tetraether (BIT) index was developed to trace terrigenous material in river outflow systems. Following up on a thorough study on the sources and processes acting on the brGDGTs delivered to the Kara Sea, this study evaluates the GDGT distribution in a sediment core (spanning a minimum of 13.3 ka) in the St. Anna Trough (Northern Kara Sea). This site has experienced large fluctuations in the delivery of river-derived OM, caused by eustatic changes in sea level. Both the BIT-index and brGDGT distribution indicate two contrasting sources of brGDGTs. Overall, the deepest sediments (>10 ka) are characterized by riverine-derived brGDGTs that reflect the brGDGT distribution currently encountered in front of the Yenisei River. The most shallow unit (< 10 ka) contains a brGDGT distribution that is strongly influenced by marine, in situ produced brGDGTs. This contribution of marine, in situ produced brGDGTs traces the isoprenoid GDGT crenarchaeol concentration, that is low in the bottom of the core, increasing gradually in the most shallow unit. Overall, the BIT-index follows the same trend, except for a sedimentary horizon (150 – 153 cm below the sea floor) where the brGDGT concentration is strongly decreased, coeval with a pronounced shift in the brGDGT distribution. As the brGDGTs delivered to the current Kara Sea system are composed of several sub-pools, we postulate that a temporary change in the relative importance of the brGDGT sources happened during this interval. This change may have happened during the delivery of terrigenous brGDGTs to the marine system, or through preferential degradation of a more labile brGDGT pool, e.g. riverine in situ produced brGDGTs, during or post sedimentation. Both in situ production and changing brGDGT provenances have large implications for palaeoclimate reconstructions. In situ production of marine brGDGTs will result in a higher reconstructed pH. However, the calibration with soil MAT used (the MAT_{ms}) is independent of the brGDGTs produced in situ. Changes in the relative contribution of brGDGT sub-pools however, were shown to influence both soil pH and MAT reconstructions.

1. Introduction

Branched glycerol dialkyl glycerol tetraethers (brGDGTs) are ubiquitous bacterial membrane lipids that have been found to be produced in soils globally, where their distribution depends on the prevailing mean annual air temperature (MAT) imposed on the soils and the soil pH (Weijers et al., 2007). Based on this dependence, they find an application as palaeoclimate proxy, in palaeosoils (e.g. Zech et al., 2012; Peterse et al., 2011b), lacustrine sediments (e.g. Niemann et al., 2012; Das et al., 2012), but firstly in coastal marine sediments that receive substantial amounts of soil-derived matter (Weijers et al., 2007, 2009b; Bendle et al., 2010). Furthermore, as they are present in high abundance in soils, rivers and river fan sediments, and decrease in concentration in the marine system, their presence in modern and downcore marine sediments was interpreted to reflect the delivery of soil-derived OM (e.g. Kim et al., 2006; Ménot et al., 2006). For this purpose, the Branched and Isoprenoid Tetraether (BIT) index was developed, where the concentration of terrigenous brGDGTs is calculated relative to the marine Thaumarchaeotal lipid crenarchaeol (Hopmans et al., 2004). Although the majority of palaeoclimate reconstructions so far has been based on a dataset of 9 brGDGTs, recent analytical developments (De Jonge et al., 2014a) now allow the separation of 15 brGDGT compounds, including six 5-methyl brGDGT compounds as described by Sinninghe Damsté et al. (2000) and Weijers et al. (2006a), and six recently described 6-methyl compounds (De Jonge et al., 2013; 2014a) that previously co-eluted with the 5-methyl brGDGTs. These 6-methyl compounds were shown to be abundant in the Yenisei River and its outflow into the Kara Sea (De Jonge et al., 2014b; De Jonge et al., Chapter 6).

The Kara Sea is a shallow shelf sea that is connected to the Arctic Ocean. The OM in its sediments is influenced strongly by river-derived terrigenous material, as indicated by bulk OM proxies (e.g. Fernandes and Sicre, 2000; Lein et al., 2012) and by the presence of lipid-based tracers for terrigenous bacterial organic matter in the sediments. Both the brGDGT-based BIT-index (De Jonge et al., Chapter 6) and the R'_{soil} based on bacteriohopanepolyols (De Jonge et al., Chapter 7), reveals the presence of soil-derived bacterial OM in Kara Sea surface sediments. Based on the distribution of brGDGTs in surface sediments of the Kara Sea several possible sources were described; i.e. riverine in situ produced brGDGTs with an unknown contribution of soil-derived and coastal cliff-derived brGDGTs (De Jonge et al., Chapter 6). In modern sediments, in situ production of brGDGTs and preferential degradation of brGDGTs was postulated to influence the brGDGT distributions in the Yenisei River outflow, resulting in large differences in brGDGT-based reconstructed MAT and soil pH.

In this study, we investigate the sedimentary GDGT record of the Kara Sea of at least the last 13.3 kyr. During this period (i.e. Late Weichselian and the Holocene) the Kara Sea has experienced large shifts in sea level resulting in a regression in the position of the Yenisei and Ob River mouths. A sediment core was collected in the St. Anna Trough, a through that was formed by a marine-based glacier during the Last Glacial Maximum (LGM; Polyak et al., 1997). The sedimentological history of the St. Anna Trough has been documented in a number of lithological studies (Polyak et al., 1997; Hald et al., 1999). These studies describe large changes in the sedimentation regimes in this trough, shifting from a glacial sedimentation regime that was dominated by deposition of glacial ice-rafted debris (IRD) and river-derived clastic material, to the modern setting. The GDGT concentration, the brGDGT distribution and

the BIT-index are used to trace changes in the relative contribution of terrigenous and marine OM over time.

2. Study site

The St. Anna Trough is a North to South-facing open ended glacial trough located approximately between 77–82 °N and 65–75 °E at the outer Eurasian continental margin (Fig. 1A). It is bounded by the islands of Franz Joseph Land to the west, Novaya Zemlya to the south, the shallow bank area Central Kara Plateau in the east and the Arctic Ocean to the north. It is a major pathway for the export of water, sediment and ice between the Arctic Ocean and the Kara Sea (Stein et al., 2004). The position where the core was taken is located in the southern basin of the St.-Anne Through, 200 km to the northeast of Novaya Zemlya. The Polar Surface Water in the study area (temperature -1.75 to 0 °C, salinity 34 - 33.2‰; Hald et al., 1999), occupies the upper ca. 100 m of the water column and is formed partly in the Arctic Ocean and partly in the Kara Sea, where fresh water from the large Siberian rivers (Yenisei, Ob) and from sea-ice cover is under the influence of low insolation. During summer, surface salinities are reduced to 32‰ and the temperatures may increase by 2–3 °C. Because of its low salinity, the Polar Surface Water forms a lid upon the warmer Atlantic Water (Aagaard and Carmack, 1989). This intermediate, Atlantic-derived water (33‰, 1.5 °C) can move southwards into the St. Anna Through at depths of 100 to 400 m (Hanzlick and Aagaard, 1980; Hald et al., 1999). More saline (>34.60‰; e.g. Hald et al., 1999) polar water is formed below forming sea ice and forms the bottom waters in the St.-Anna Through (Midttun, 1985). During fall and winter, sea-ice forms in the Kara Sea and eastern and northern part of the Barents Sea (e.g. Aagaard and Carmack).

3. Materials and methods

3.1. Collection of sediments

A gravity core (3.03 m) was collected at 78° 28' 9928 N, 72° 47' 8487 E, at a depth of 473 m, aboard the R/V Akademik Mstislav Keldysh. The core was subsampled (n=32) on-board, after a detailed description of the lithology was made. For this purposes, the grain size classification as employed in Shepard et al. (1954) was used. The color of the downcore sediments was described using a standard Munsell colour chart (Munsell Color ©). The samples were taken from a 1 cm broad slot, where the top of the sediment slot is reported in Table 1 and 2. After subsampling, the sediments were immediately stored at -20°C.

3.2. Lipid extraction and GDGT analysis

2.5 to 3 g of freeze dried, homogenized sediment was extracted using a Dionex accelerated solvent extractor (ASE), with a 9:1 (v/v) mixture of dichloromethane and methanol (100 °C, 3x). The extract was separated according to polarity, and the polar fraction was analyzed using high-performance liquid chromatography/atmospheric pressure chemical ionization-mass spectrometry (HPLC/APCI-MS), as described in De Jonge et al. (2014a). Detection was achieved in selected ion monitoring mode (SIM; Schouten et al., 2007a) using m/z 744 for the internal standard, m/z 1292 for crenarchaeol and m/z 1050, 1048, 1046, 1036, 1034, 1032, 1022, 1020 and 1018 for branched GDGTs. Agilent Chemstation software was used to integrate peak areas in the mass chromatograms of the protonated molecule ($[M+H]^+$). However, visual

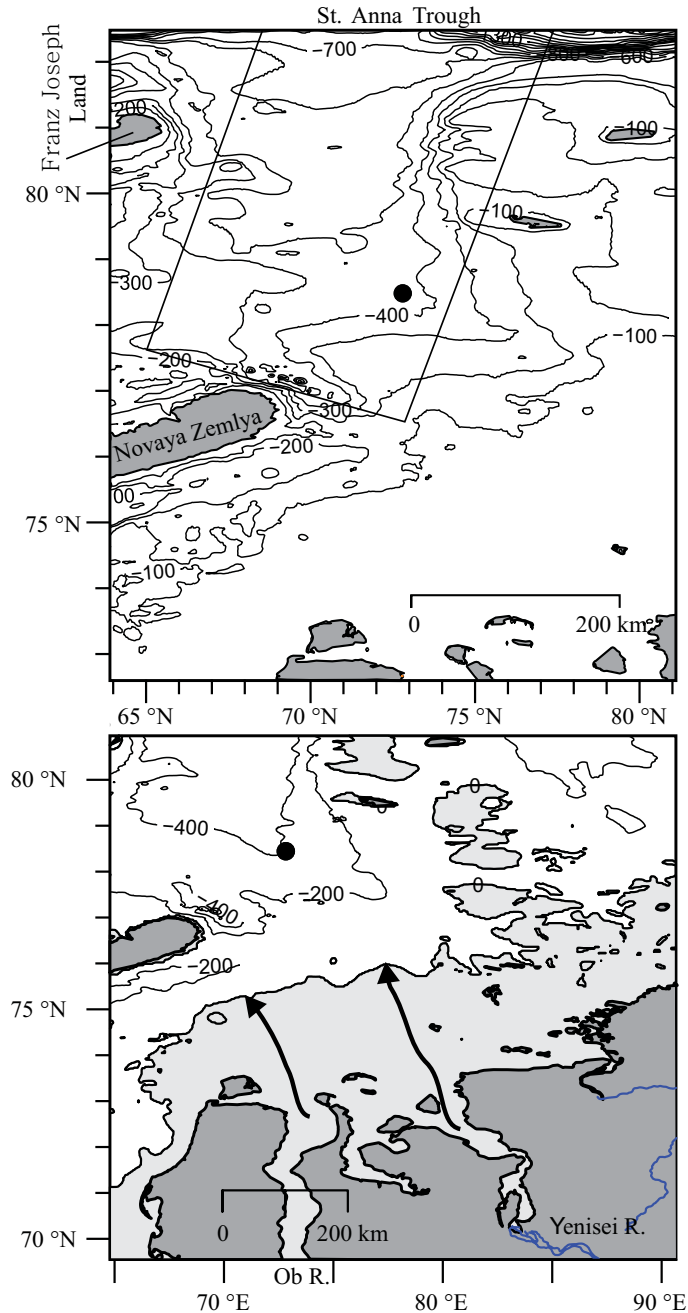


Fig. 1. A) Map showing the bathymetry of the central part of the Kara Sea, with the approximate boundaries of the St. Anna Trough indicated. The location of the core site is indicated. B) Map showing the current distribution of land masses (dark grey), with the extent of the coastline during a sealevel drop of 50 m, reflecting the conditions at 11 ka (Fairbanks, 1989; Bauch et al., 2001), indicated in light grey. This map is simplified, as it is based on the current 50 m isobath, and assumes that isostatic rebound was negligible. The course of the palaeo Yenisei and Ob Rivers is indicated with an arrow, after Stein et al. (2004).

inspection of the base peak traces, revealed that the brGDGT with m/z 1020 often co-eluted with an unidentified compound that was present as a broad peak, and its concentration should be interpreted with caution.

3.3. Calculation of GDGT-based proxies

The BIT index was calculated according to Hopmans et al. (2004). The inclusion of 6-methyl brGDGTs (De Jonge et al., 2013) is mentioned explicitly:

$$\text{BIT index} = (\text{Ia} + \text{IIa} + \text{IIIa} + \text{IIa}' + \text{IIIa}') / (\text{Ia} + \text{IIa} + \text{IIIa} + \text{IIa}' + \text{IIIa}' + \text{IV}). \quad [\text{Eq. 1}]$$

The roman numerals refer to the fractional abundances of GDGTs indicated in Fig. 1. Here, Ia, IIa and IIIa are 5-Me brGDGTs, IIa' and IIIa' are 6-methyl brGDGTs and IV is the isoprenoid GDGT (iGDGT) crenarchaeol, a GDGT specific for Thaumarchaeota (Sinninghe Damsté et al., 2002).

The isomer ratio (IR) represents the fractional abundance of the penta- and hexamethylated 6-Me brGDGTs, compared to the total of penta- and hexamethylated brGDGTs (modified after De Jonge et al., 2014a):

$$\text{IR} = (\text{IIabc}' + \text{IIIabc}') / (\text{IIabc} + \text{IIIabc} + \text{IIabc}' + \text{IIIabc}'). \quad [\text{Eq. 2}]$$

Xabc means that this index includes both the non-cyclopentane containing (Xa) and the cyclopentane containing (Xb,c) components (Fig. 1).

We calculated a reconstructed pH using the CBT' index following De Jonge et al. (2014a):

$$\text{CBT}' = {}^{10}\log[(\text{Ic} + \text{IIa}' + \text{IIb}' + \text{IIc}' + \text{IIIa}' + \text{IIb}' + \text{IIIc}') / (\text{Ia} + \text{IIa} + \text{IIIa})]. \quad [\text{Eq. 3}]$$

$$\text{pH} = 7.15 + 1.59 * \text{CBT}' \quad [\text{Eq. 4}]$$

The MAT_{mrs} was calculated as a multiple linear regression, based on the abundance of only the major brGDGTs Ia, IIa and IIIa (De Jonge et al., 2014a):

$$\text{MAT}_{\text{mrs}} (^{\circ}\text{C}) = 5.58 + 17.91 * [\text{Ia}] - 18.77 * [\text{IIa}] \quad [\text{Eq. 5}]$$

The square brackets in this formula indicate that the fractional abundance of brGDGT Ia and IIa is calculated relative to the sum of the three major brGDGTs ($\text{Ia} + \text{IIa} + \text{IIIa}$). This calibration was chosen over the MAT_{mr} calibration, that is based on the fractional abundance of the brGDGTs Ia, Ib, Ic and IIa, relative to all 15 brGDGTs, to exclude the brGDGT compound Ib, which was observed to co-elute with an unknown compound, based on the peak shape.

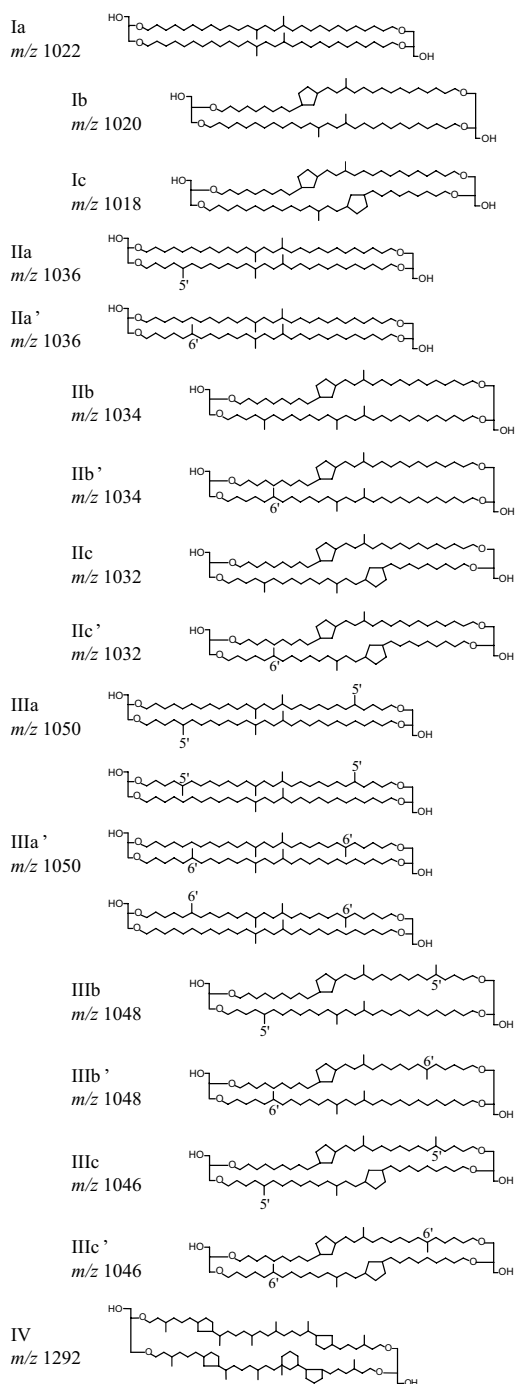
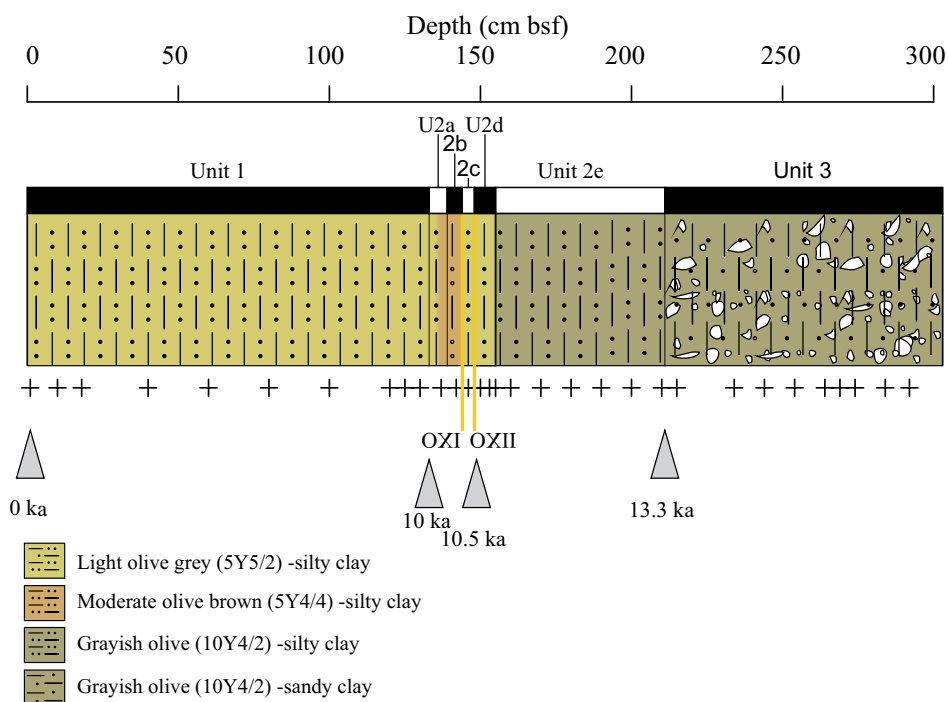


Fig. 2. Chemical structures of branched GDGTs (I-III) and crenarchaeol (IV). The chemical structures of the hexa- and pentamethylated brGDGTs with cyclopentyl moiety(ies) IIb', IIc', IIIb' and IIIc' are tentatively assigned.

4. Results

4.1. Stratigraphy of the core

The core (303 cm) consist of a number of clearly defined lithological units (Fig. 3; Table 1), based on a visual description of the core. Underlying a fluffy top layer, a large lithological unit (Unit 1: 0-133 cm below sea floor; bsf) is present, composed of light olive gray (5Y5/2) silty clay. Multiple ferrous and shell fragments are encountered. This unit overlies a second unit (133-210 cm bsf), that is composed of 4 thin subunits (Unit 2a-d), and a thicker Unit 2e. Unit 2a (133-139 cm bsf), is composed of silty clay laminae. No ferrous iron deposits are encountered in this section. Unit 2b (139-144 cm bsf) is characterized by a slightly different coloration, as it is composed of silty clay sediments with a colour between moderate olive brown (5Y4/4) and light olive brown (5Y5/6). The lower boundary of this section contains an oxidized lens, with an aberrant colour (OX I). Also Unit 2c is only a few cm thick (144-148 cm bsf) and is composed of light olive gray (5Y5/2) silty clay. At the bottom of this section a second oxidized lens is present (OX II: 147.5 – 148 cm bsf), that is characterized by a moderate yellowish brown (10YR5/4) sandy clay, and contains gravel particles and lenses of greyish-black sand. Unit 2d (148 – 155 cm bsf) is a light olive grey (5Y5/2), massive silty clay containing gravel particles. It overlies a much thicker Unit 2e (155-210 cm bsf) that is composed of a darker, greyish olive (10Y4/2), silty clay, with extensive banded ferrous precipitates. Especially towards the lower boundary, rock material is present, containing pieces of up to 4 cm long. The basal unit of this core, Unit 3 (210 – 303 cm bsf) is described as diamicton, and is mainly composed of a sandy clay, with gravel fragments of variable size.



Unit	Depth (cm, bsf)	TOC (%)	TN (%)	C/N	$\delta^{13}\text{C}_{\text{org}}$ (‰)	$\delta^{15}\text{N}$ (‰)
1	1	1.25	0.17	8	-22.8	5.1
	10	1.25	0.16	8	-23.1	5.2
	18	1.21	0.15	8	-23.4	5.3
	40	1.06	0.13	8	-23.4	5.3
	60	0.63	0.08	8	-24.2	4.7
	80	0.94	0.07	13	-24.5	3.3
	100	0.79	0.07	12	-25.7	3.4
	120	0.57	0.06	10	-24.6	2.4
	125	0.54	0.05	10	-25.0	3.0
2a	130	1.03	0.06	17	-24.6	3.3
	137	0.82	0.10	8	-24.1	5.2
	142	1.54	0.08	19	-24.7	3.8
	146	0.64	0.05	12	-25.9	4.1
	148	0.68	0.06	12	-25.9	4.0
	150	0.63	0.06	11	-25.2	3.4
	153	0.80	0.05	15	-24.8	3.7
	155	0.97	0.12	8	-23.9	5.4
	160	0.86	0.06	15	-24.8	3.7
	170	0.67	0.05	12	-25.0	3.7
2e	180	0.57	0.06	10	-25.0	3.5
	190	0.47	0.05	9	-25.2	3.4
	200	1.45	0.08	19	-24.5	3.6
3	210	0.84	0.06	14	-24.7	4.0
	215	1.28	0.16	8	-23.2	5.3
	234	1.09	0.12	9	-23.8	5.8
	244	0.69	0.09	8	-24.5	5.4
	254	0.31	0.04	7	-24.7	5.3
	264	0.44	0.05	10	-25.6	4.6
	269	0.52	0.05	10	-25.5	3.9
	274	0.70	0.06	12	-26.1	4.0
	284	0.72	0.06	12	-26.2	3.9
	292	0.68	0.06	12	-26.1	4.0

Table 1. Bulk OM characteristics of the depths sampled. The lithological unit and the depth (cm, below sea floor (bsf)) at which the sample was taken is indicated. The total organic carbon content (TOC (%)), the total nitrogen content (TN (%)), the carbon/nitrogen (C/N) ratio, the stable organic carbon isotope value ($\delta^{13}\text{C}_{\text{org}}$, ‰) and the stable nitrogen isotope value ($\delta^{15}\text{N}$, ‰) are reported.

◀ Fig. 3. Overview of the lithological description of the 303 cm long gravity core obtained from the St Anna Trough of the Kara Sea. The sediments are sampled over an interval of 1 cm, and the top of each interval is indicated with a cross symbol. The arrows indicate characteristic horizons that allowed interpolation with dated horizons as reported in Polyak et al. (1997) or Hald et al. (1999) based on radiocarbon determinations reported in these studies. The color and pattern per lithological unit refers to the legend. The boundaries of the lithological units discussed and the depth (cm below sea floor) are indicated on the scale on the left, yellow lines indicate the presence of oxidized lenses, based on the lithological description.

4.2. Downcore variations in bulk OM properties

The bulk OM proxies (total organic carbon (TOC) and total nitrogen (TN) contents), the ratio of TOC over TN (C/N ratio) and the stable organic carbon and nitrogen isotopes ($\delta^{13}\text{C}_{\text{org}}$ and $\delta^{15}\text{N}$) were measured to trace potential downcore changes in the delivery of terrigenous and marine OM (Fig. 4A-E, Table 1). The TOC and TN content vary between 0.3 and 1.5% and 0.04 and 0.2 % of the dry weight, respectively. The highest TOC content is encountered in Unit 2b and the lower part of Unit 2e and upper part of Unit 3. Furthermore, increased values are encountered in the most recent sediments (Fig. 4A). The TN content does not mimic this downcore pattern in TOC content completely. Although increased values are also observed in recent sediments, the highest TN content are encountered in the upper layers of the diamictic Unit 3. Furthermore, increased values are present in Unit 2a and at the boundary between Unit 2d and 2e (Fig. 4B). Overall, the TOC and TN contents downcore are not coeval with the observed changes in lithology. Values of the C/N ratio (Fig. 4C), commonly used to differentiate between marine and terrigenous OM (e.g. Thornton and McManus, 1994), vary between 7 and 18. The highest values are encountered in Unit 2b and in the deeper part of Unit 2e. They decrease from the bottom to the top of Unit 1, remaining relatively stable in the upper 60 cm bsf. Also stable isotopic values ($\delta^{13}\text{C}_{\text{org}}$ and $\delta^{15}\text{N}$) have been measured to trace the source of the bulk sedimentary OM in the Kara Sea (e.g. Krishnamurthy et al., 2001). The $\delta^{13}\text{C}_{\text{org}}$ has less negative values both in recent sediments, and in the upper part of diamicton (Unit 3). The interval containing the oxidized layers (although the oxidized layers themselves have not been sampled) is characterized by more negative $\delta^{13}\text{C}_{\text{org}}$ values (Fig. 4D). The $\delta^{15}\text{N}$ values are lower in horizons that have a decreased TN content; the lower part of Unit 1, throughout the Units 2b, 2c, 2d and in Unit 2e, excluding the boundary between Unit 2d and Unit 2e.

4.3. GDGT abundance and distribution

Both brGDGTs and crenarchaeol are present in all examined sediments (Fig. 4F, G; Table 2). BrGDGTs have TOC-normalized abundances between 7 and 60 $\mu\text{g.gTOC}^{-1}$, with the majority of the samples having brGDGT concentrations below 30 $\mu\text{g.gTOC}^{-1}$. Crenarchaeol is present in comparable concentrations, varying between 3 and 190 $\mu\text{g.gTOC}^{-1}$, with substantially higher values in the upper part of the core. Values higher than 20 $\mu\text{g.gTOC}^{-1}$ are only encountered in Unit 1. The contrasting downcore behaviour of brGDGTs and crenarchaeol is reflected in a distinct record of the BIT ratio (Fig. 4H; [Eq. 1]), with values varying between 0.01 and 0.87, with low (<0.2) values in Unit 1 and higher values in all other units. Unit 2d, however, is characterized by lower BIT ratios than those of the sandwiching Units 2c and 2e.

To identify the end-members of the brGDGT distributions in the St. Anna Trough sediments, the variance in the brGDGT distribution can be described in a principal component analysis

Table 2 summarizes the fractional abundances of the brGDGT compounds downcore in the St. Anna Trough sediments. The score on the first 2 PCs of PCA_{SAT}, based on the fractional abundance of the 15 brGDGTs in the St. Anna Trough core, is indicated. The TOC-normalized summed amount of 15 brGDGTs and crenarchaeol are reported ($\mu\text{g.g TOC}^{-1}$). The calculated BIT index [Eq. 1], the IR values [Eq. 2], the reconstructed pH [based on the CBT': Eq. 3 and 4] and the reconstructed MAT [based on the MAT_{mrs}: Eq. 5] are reported. ►

Unit	Depth (cm, bsf)	Fractional abundances										IIIc'	IIIb'	IIIa'	IIb'	IIc'	IIa'	IIIb	IIIc	IIa	IIb	IIc	IIIa	IIIb	IIIc	PC _{1SAT}	PC _{2SAT}	Concentration brGDGTs ($\mu\text{g g TOC}^{-1}$)	Concentration crenarchaeol ($\mu\text{g g TOC}^{-1}$)	BIT	IR	pH	MAT (°C)			
1	1	23	5	2	10	3	1	11	1	0	7	4	15	4	2	-1.8	0.3	9	80	0.07	0.38	7.2	11													
	10	24	5	2	10	1	1	13	1	0	7	12	4	16	2	1	-1.4	0.4	11	120	0.06	0.40	7.1	11												
	18	16	37	2	7	1	1	8	1	0	5	9	3	9	1	1	-1.1	0.1	9	81	0.05	0.39	7.1	11												
	40	18	24	3	8	1	1	9	1	0	6	12	4	12	2	1	-1.4	-0.1	15	140	0.05	0.36	7.2	11												
	60	19	19	2	11	2	1	10	1	0	6	12	3	11	2	1	-1.3	-0.1	15	140	0.06	0.41	7.1	9												
	80	20	9	3	13	2	1	13	1	0	7	14	3	9	2	2	-1.5	-0.3	12	100	0.07	0.45	7.1	8												
	100	20	17	3	10	4	1	11	1	0	6	11	4	8	2	1	-1.4	-0.4	17	190	0.05	0.46	7.1	10												
	120	21	22	2	12	3	1	9	1	0	8	9	3	7	2	1	-0.9	0.1	20	100	0.11	0.47	6.9	9												
	125	24	17	2	15	2	0	10	1	0	10	7	3	8	1	1	-0.5	0.6	15	48	0.17	0.48	6.9	9												
	130	25	12	1	16	4	0	11	1	0	13	4	2	9	1	0	-0.1	1	8	24	0.20	0.52	6.8	9												
2a	137	28	11	1	18	2	0	12	0	0	14	3	1	9	1	0	0.4	1.2	7	6	0.45	0.55	6.7	8												
	142	26	6	1	22	3	0	16	0	0	11	3	1	9	1	0	0.4	1.3	10	5	0.65	0.63	6.5	6												
	2c	146	30	5	1	23	3	0	15	0	0	10	3	1	7	1	0	0.4	0.8	26	9	0.71	0.65	6.4	7											
	2d	148	34	10	2	20	3	1	13	0	0	6	2	1	6	1	0	0.3	-0.3	13	9	0.53	0.70	6.2	9											
		150	56	6	3	13	3	1	8	0	0	0	2	1	5	1	0	0.3	-2.6	12	12	0.44	0.76	5.8	16											
		153	49	8	4	17	3	1	6	0	0	4	2	0	4	1	0	0.3	-2.1	8	7	0.47	0.72	6.0	13											
	2e	155	31	13	2	20	3	0	13	0	0	8	2	1	6	0	0	0.3	0.1	20	11	0.59	0.69	6.3	8											
		160	35	3	2	26	3	0	13	0	0	9	2	0	6	0	0	0.7	0.3	28	4	0.87	0.71	6.2	8											
		170	31	6	1	25	3	0	15	0	0	9	2	0	6	0	0	0.6	0.6	34	7	0.81	0.71	6.3	7											
		180	30	5	1	25	3	0	16	0	0	9	2	0	6	0	0	0.6	0.7	44	9	0.81	0.71	6.3	7											
3	190	30	2	1	26	3	0	18	0	0	8	2	0	7	0	0	0.6	0.7	57	12	0.80	0.74	6.2	6												
	200	29	2	1	26	3	0	19	0	0	8	2	0	7	0	0	0.6	0.9	20	5	0.79	0.73	6.2	6												
	3	210	31	5	1	26	3	0	15	0	0	9	2	0	6	0	0	0.7	0.6	26	5	0.81	0.71	6.2	7											
		215	36	7	2	24	3	1	15	0	0	6	1	0	5	0	0	0.6	-0.4	7	3	0.71	0.76	6.1	8											
		234	38	6	2	23	2	1	13	0	0	7	2	0	5	0	0	0.5	-0.4	15	3	0.79	0.74	6.1	9											
		244	37	6	2	24	2	1	14	0	0	7	1	0	5	1	0	0.6	-0.4	15	4	0.76	0.74	6.1	9											
		254	36	8	2	24	3	1	14	0	0	6	1	0	5	0	0	0.6	-0.5	28	9	0.73	0.76	6.1	8											
		264	38	7	2	24	3	1	14	0	0	6	1	0	4	0	0	0.6	-0.7	12	5	0.68	0.77	6.0	9											
		269	38	7	2	25	3	1	13	0	0	4	1	0	4	0	0	0.5	-0.9	16	6	0.70	0.81	5.9	8											
		274	37	5	2	25	2	1	15	0	0	6	1	0	5	1	0	0.6	-0.3	10	3	0.73	0.76	6.0	8											
	284	36	6	2	24	2	0	14	0	0	7	2	0	5	1	0	0.6	-0.2	20	5	0.78	0.73	6.1	8												
	292	35	6	2	24	3	0	14	0	0	8	2	0	6	0	0	0.5	0	23	6	0.77	0.72	6.2	8												

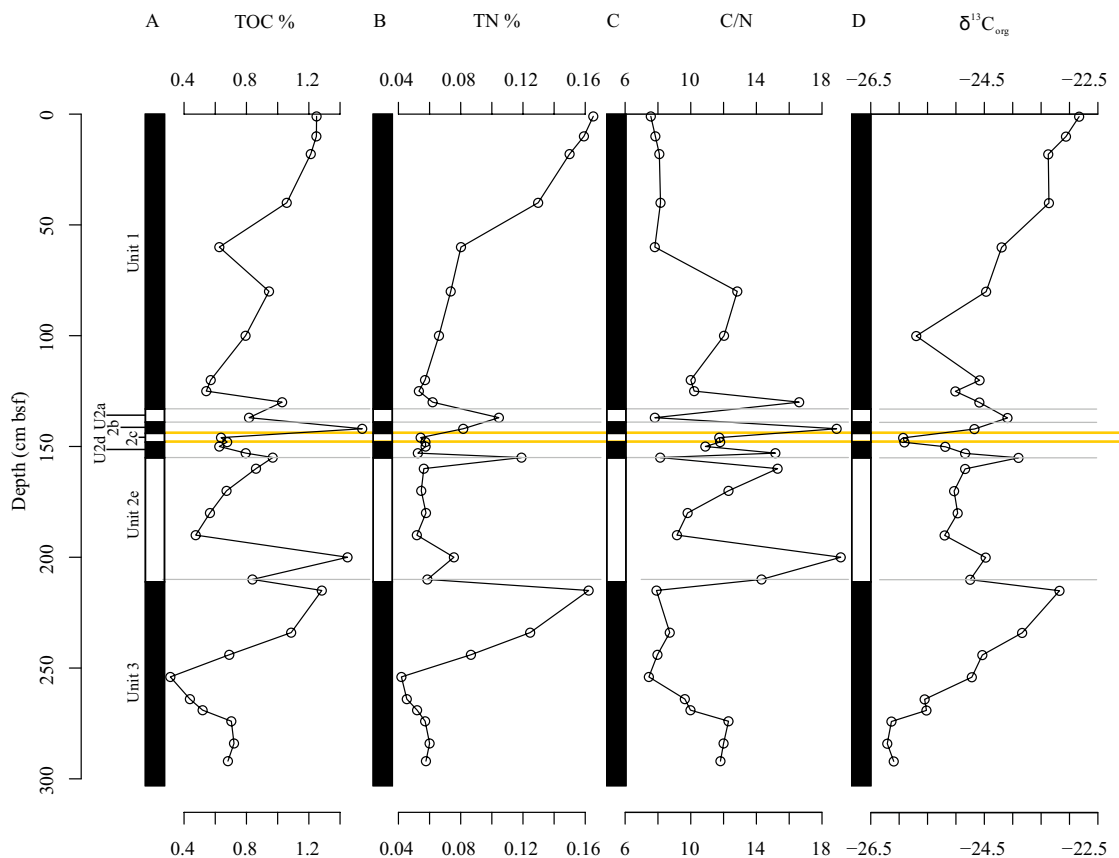
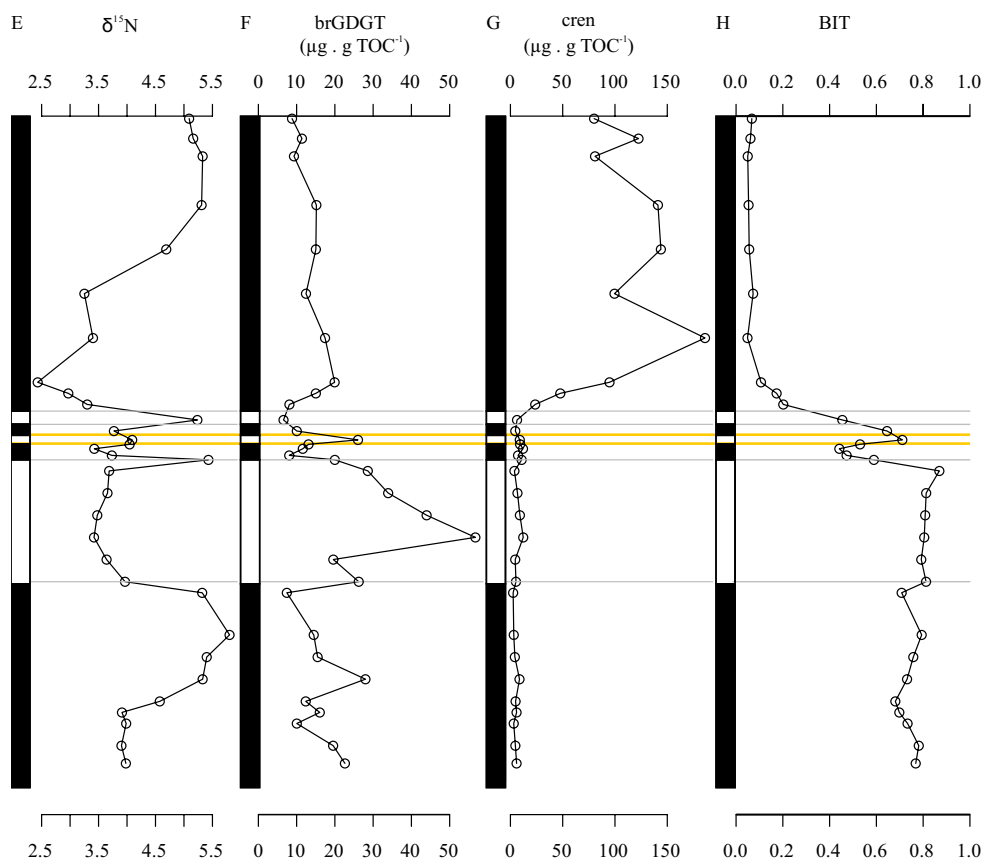


Fig. 4. The downcore distribution of the A) total organic carbon content (TOC (%)), B) the total nitrogen content (TN (%)), C) the bulk carbon/nitrogen ratio (C/N), D) the stable organic carbon isotopic signal ($\delta^{13}\text{C}_{\text{org}}$), E) the stable nitrogen isotopic signal ($\delta^{15}\text{N}$), F) the TOC-normalized concentration of summed brGDGTs ($\mu\text{g} \cdot \text{g TOC}^{-1}$), G) the TOC-normalized concentration of crenarchaeol (GDGT IV; $\mu\text{g} \cdot \text{g TOC}^{-1}$), H) the branched and isoprenoid tetrather (BIT)- index values [Eq. 1]. The boundaries of the lithological units and depths (cm below sea floor) discussed are indicated on the scale on the left, yellow lines indicate the presence of oxidized lenses, based on the lithological description.

(PCA_{SAT}: PCA of St. Anna Trough sediments), based on the standardized abundances of the 15 brGDGTs (Table 2). The first two principal components (PCs) explain a large part of the variance in this dataset, explaining 58 and 20% of the variance, respectively (Fig. 5A). The first principal component (PC1SAT) highlights the good correlation between the fractional abundance of brGDGTs IIb, IIc, IIb', IIc', IIIa', IIb', IIc'. In general, the fractional abundances of these brGDGTs possess a negative correlation with that of brGDGT IIa (e.g., r^2 between brGDGT IIa and IIIa' = 0.46). The second principal component (PC2_{SAT}) indicates that the fractional abundance of brGDGTs Ia, Ic and IIc follow a different trend, that anti-correlates with that of the brGDGT IIa' and, to a lesser extent, IIIa and IIIa'.



The downcore trends in brGDGTs, as captured by $PC1_{SAT}$ and $PC2_{SAT}$, are shown in Fig. 5B-C. The sediments of Unit 1 all plot negatively on the first PC, indicating that the brGDGTs with a negative score on $PC1_{SAT}$ are relatively increased in the shallow sediments. The deeper sediments of Units 2 and 3 all score positively on $PC1_{SAT}$. In the lower part of Unit 1 the score on PC1 gradually increases towards the values of PC1 in Unit 2 and 3. While the score on $PC2_{SAT}$ is generally constant downcore (Fig. 5C), and close to 0 for the majority of the samples, the brGDGT distribution encountered at the depths 150 and 153 cm bsf (Unit 2d), have highly negative values on this PC. The contrasting behaviour of the 5- and 6-methyl brGDGTs along PC1 is also reflected by the large variability in the IR values [Eq. 2], that generally traces the downcore scores on PC1 (Fig. 5D). This illustrates the necessity to quantify the 5- and 6-methyl compounds separately when studying downcore brGDGT variations.

Based on the PCA of the brGDGT distributions, we can thus identify three clear brGDGT end-members (Unit 1; Unit 2d (especially 150 and 153 cm bsf); and the remaining sections of Units 2 and 3). These distributions can be exemplified by those at 1, 153 and 200 cm bsf, shown in Fig. 5D-F. The tetramethylated brGDGT Ia was the most abundant brGDGT at all

three depths. The brGDGT distribution in Unit 1 (Fig. 5E; Table 2) is further characterized by large fractional abundances of the 6-methyl brGDGTs, with IIb' present in larger fractional abundance than IIa', which is an uncommon distribution. The brGDGT distribution present in Unit 2d (Fig. 5F) has a high fractional abundance of brGDGT Ia (49-56% of all brGDGTs), with low abundances of the 6-methyl brGDGTs. The “deep” brGDGT distribution (Fig. 5G) shows a contrasting brGDGT distribution that is dominated by non-cyclopentane-containing brGDGTs but with Ia less abundant (<38%) and with the 5-methyl brGDGTs present in larger abundances compared to the 6-methyl brGDGTs but not as extreme as in Unit 2d.

To evaluate the brGDGT distributions encountered downcore with those in suspended particulate matter (SPM) and surface sediments in the Yenisei River and its outflow in the Kara Sea, an extended dataset, composed of the standardized fractional abundances of the 15 brGDGTs in both the modern setting (De Jonge et al., Chapter 6) and in the downcore St. Anna Trough sediments, was used to calculate the PCA_{EXT}. The scores on the first two PCs (explaining 40 and 23% of the variance, respectively) of both brGDGTs and the various sites are indicated in Fig. 6. The PC1_{EXT} (Fig. 6) generally captures the same variance as captured by PC1_{SAT} in the PCA of the downcore distributions only (Fig. 5A), with cyclopentane-containing brGDGTs Ib, Ic, IIc, IIIb, IIb', IIc', IIIb' and IIIc' having low scores and 5-methyl brGDGTs IIa and IIIa having high scores. Especially the sediments from Unit 1 have a highly negative value on this PC, while the sediments from other units have scores close to 0. PC2_{EXT} captures the different trend in the fractional abundance of brGDGT Ia, and the contrasting behaviour of the 6-methyl brGDGTs IIa' and IIIa'. On this second PC, the scores for the sediments of Units 1 to 2c are all close to 0, while the sediments of Units 2e, 3 and 2d have increasingly positive values, reflecting a decrease in the fractional abundance of the brGDGTs IIa' and IIIa', and a corresponding increase in the fractional abundance of brGDGT Ia. The modern Yenisei River SPM has a highly negative loading on this PC2_{EXT}, reflecting the high fractional abundance of the brGDGTs IIa' and IIIa' (De Jonge et al., 2014b; Chapter 6).

5. Discussion

5.1. Interpolation of dated horizons

Although no horizons were dated for this core, careful interpolation of the lithological strata with other dated St. Anna Trough cores (Polyak et al., 1997; Hald et al., 1999) allows deriving an age for a few horizons (Fig. 2). The deepest sedimentary facies described by Hald et al. (1999) and Polyak et al. (1997) was formed underneath a marine-based glacier, or in associating with an icesheet grounding line, locally disturbed by iceberg tracks. These sediments are present at 140 to >400 cm bsf in the trough, and at a depth between 150 and >250 cm bsf in cores taken in the vicinity of our coring site (cf. Hald et al., 1999). The lithology of these sediments was described to be massive diamict with a high sand content (Polyak et al., 1997). The similar lithology and depth as the deepest unit encountered in our core (Unit 3; 210 cm bsf)

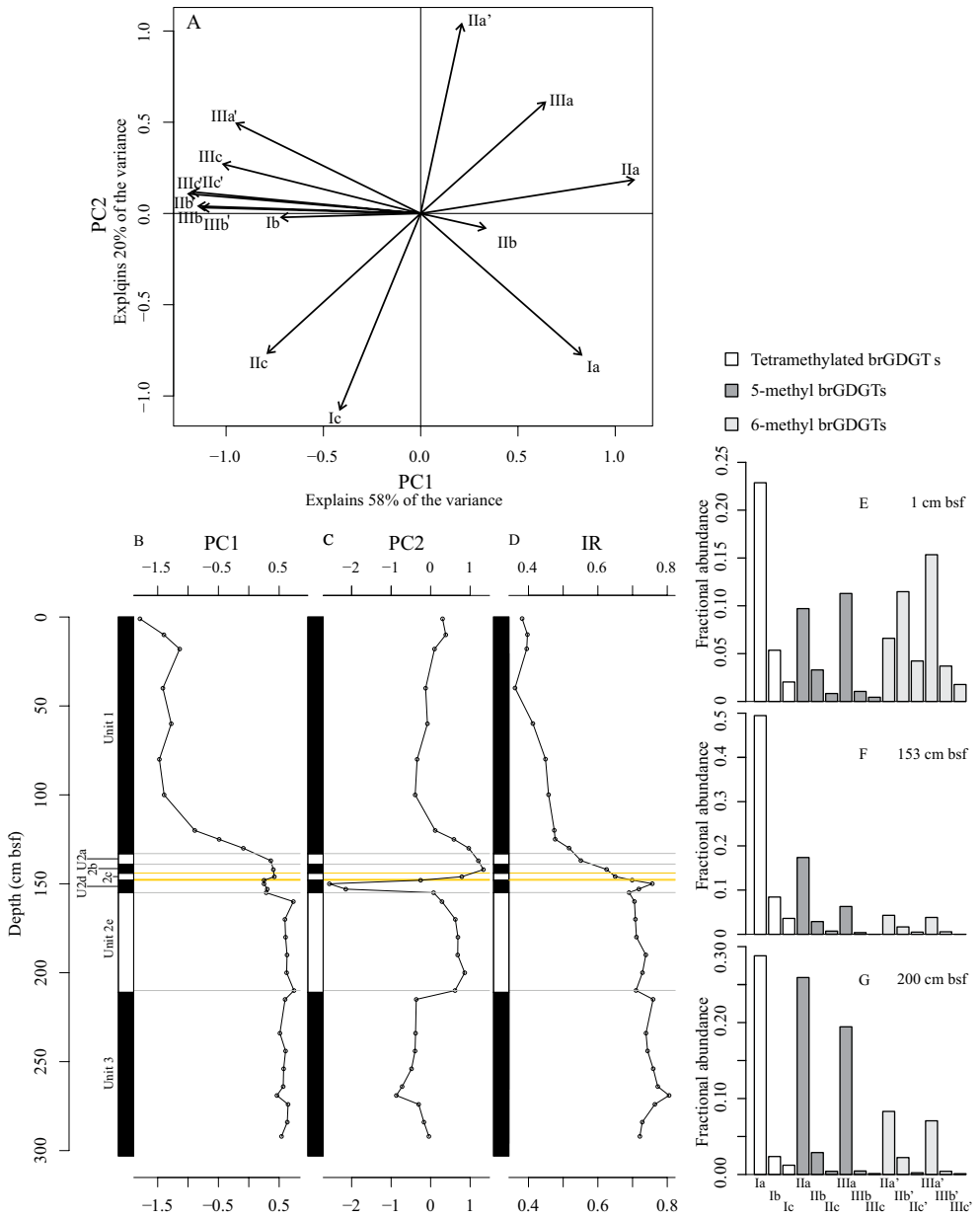


Fig. 5. Principal component analysis based on the standardized fractional abundances of the 15 brGDGTs in the St. Anna Trough core, plotting A) the scores of the brGDGT compounds on the first two principal components (PC). The scores of the downcore distributions are plotted against the depth (cm, below sea floor) in panel B and C. The IR values are plotted against depth in panel D. For B-D) the depth (cm below sea floor) and the boundaries of the lithological units discussed are indicated on the scale on the left, yellow lines indicate the presence of oxidized lenses, based on the lithological description. Panels E-G) show the brGDGT distribution of three depths (1, 153 and 200 cm below the sea floor) that are characteristic for the three end-members of the brGDGT distributions encountered in this core. The color of the bars refers to the brGDGT structure, as reflected by the legend.

indicate that this unit probably corresponds with the deepest horizons encountered in Polyak et al. (1997) and Hald et al. (1999).

These authors further postulate that the top of this unit is coeval with the onset of the ice retreat, that has a minimum age of 13.3 ka in the St. Anna Trough. In the sediment core studied here, this transition is probably the boundary between Unit 3 and Unit 2e. Overlying this basal unit, an intermediate section is described in Polyak et al. (1997) of <1 m in thickness, that is comprised of several lithological units, wherein alternating glacial deposits were described, whose characteristics indicated forwards and backwards shifts in the proximity of the St. Anna Trough and Novaya Zemlya glaciers (Hald et al., 1999). The heterogeneity within the intermediate unit in this core (Unit 2), thus probably reflects the complex deglaciation sequence on Novaya Zemlya and in the St. Anna Trough. In these transitional sediment horizons, Hald et al. (1999) reported the presence of laminations, indicating the periodic input of sediments, with little bioturbation. Similar laminations are encountered in the Unit 2a. Another feature that is found throughout the St. Anna Trough (Polyak et al., 1997), is the presence of clear oxidized lenses within this sedimentary section. Their formation suggests relatively low deposition rates and oxic bottom waters, perhaps associated with a reduction of calving/melting of the glacier front, or with a permanent sea-ice cover (Hebbeln and Wefer, 1991; Polyak et al., 1997). In the Bering Streat, the presence of oxidized layers in the sediments was related to the presence of substantial amounts of seasonal sea ice, associated with a decreased organic productivity during summer and intensive downwelling of oxygen-rich brine water during the winter months (Gardner et al., 1982). Two oxidized lenses are described in this core (OXI and OXII), based on the characteristic brown colour of these oxidized sediments. This colour shift can be attributed to the formation of manganese and iron oxides, and the dissolution of biogenic carbonates in the subsurface sediment (e.g. Wilson et al., 1986), although downcore oxidized layers (6 ka) from the Bering Strait were described to be enriched only in manganese (Gardner et al., 1982). The widespread presence of two oxidized beds and two sandy beds, results in their use as lithostratigraphic markers (Polyak et al., 1999). One oxidised layer was especially easily recognized, as it was described to directly overlie a dark-grey sandy bed. It was dated to have been deposited between 10 and 11 ka, by extrapolation of available radiocarbon ages in Polyak et al. (1997). Based on the similar lithology, we propose that the layer OXII encountered in our core, overlying a distinct sandy bed (147.5-148 cm bsf; Unit 2c), was deposited at an estimated age of 10.5 ka in this core.

The upper sedimentary unit in the St. Anna Trough has been described by both Polyak et al. (1997) and Hald et al. (1999) to be a homogenous, soft clayey mud, lacking glacial deposits and deposited in similar oceanic conditions as observed today. Overlying an initial phase with increased sedimentation speed that was related to a lower sea level, increased coastal erosion, and increased river discharge, an oxidized layer is described within the upper unit (Polyak et al., 1997), that was inferred to have an age of 8 ka. However, if this age is interpolated for the OXI layer observed in our core, Late Holocene sediments have a linear sedimentation rate of 18 cm.ky⁻¹, while the Early Holocene sediments have a linear sedimentation rate of only 1.6 cm.ky⁻¹. We thus postulate that the oxidized front observed in cores collected deeper in the St. Anna Trough (>600 m) is not observed here. Based on the homogenous nature of Unit 1, we postulate that the onset of the marine sedimentation regime, which was dated around 10 ka (e.g.

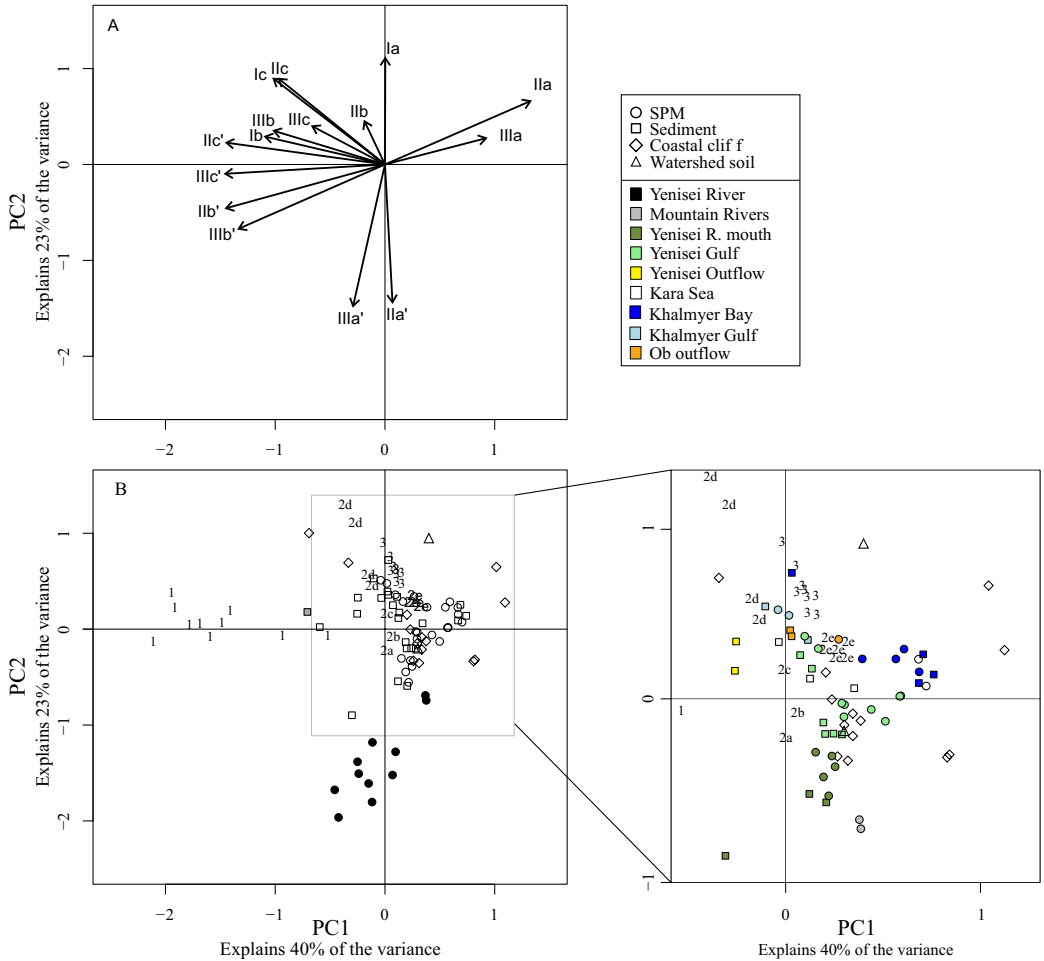


Fig. 6. Principal component analysis based on the standardized fractional abundances of the 15 brGDGTs in the St. Anna Trough core and the modern Yenisei and Kara Sea SPM, sediments, coastal cliff and soil samples, that have been described in De Jonge et al. (Chapter 6). Panel A shows the scores of the 15 brGDGT compounds on the first 2 principal components (PC). Panel B shows the scores of the sites and depths studied. The St. Anna Trough downcore distributions are indicated with a number (1-3) that corresponds with the lithological unit, as defined in Figure 3.

Polyak et al., 1997), is coeval with the lower boundary of Unit 1. As the fluffy nature of the surface sediments indicates that the gravity core was successful in collecting the most recent sediments, the top of the core is assumed to be of a recent age (0 ka).

Based on these four dating points (Fig. 3), the linear sedimentation rates are estimated to be 14 cm.ky⁻¹ for the modern sedimentation regime (average for Unit 1), amounting up to 23 (average for Unit 2a, b, c) and 24 cm.ky⁻¹ (average for Unit 2d, e) in deeper sediments. This agrees with the average Holocene sedimentation rate, that was estimated to approach 12 cm.ky⁻¹ in a core sampled close to the site studied (0-11 ka; Stein et al., 2004). These authors further state that the sedimentation rate during the Early Holocene (roughly corresponding with Unit 2), exceeds the sedimentation rate in the Late Holocene roughly corresponding with Unit 1). Thus, although our dated horizons are based only on interpolated radiocarbon ages, the resulting linear sedimentation rates agree well with published values, and we are therefore confident that we are evaluating a minimum of 13.3 ka of sedimentation in the St. Anna Trough.

5.2. Terrigenous and marine sources of brGDGTs

Based on the GDGT concentrations and the BIT-index values (Hopmans et al., 2004: Table 2), three main phases can be identified in the sediments of the St. Anna trough (Fig. 4F, G, H); i) high brGDGT and low crenarchaeol concentrations and high (>0.7) BIT-values throughout Unit 2e and Unit 3, ii) low brGDGT and increasing crenarchaeol concentrations result in decreasing, generally low (<0.2) BIT-values in Unit 1, and iii) low crenarchaeol concentrations and variable brGDGT concentrations and BIT-values in the Units 2a-2d. This latter section reflects a transitional zone between Unit 3 and 2e and Unit 1.

The highest brGDGT concentrations, encountered in Unit 2e (up to 50 µg.g TOC⁻¹), approach the brGDGT concentration in front of the Yenisei River Mouth in surface sediments (i.e. between 12 and 87 µg.g TOC⁻¹; De Jonge et al, Chapter 6). The concentration of the marine end-member crenarchaeol is low throughout the Units 2e to 3 (<5 µg.g TOC⁻¹), comparable with concentrations in surface sediments in front of the Yenisei River Mouth (i.e. between 0.2 and 20 µg.g TOC⁻¹; De Jonge et al, Chapter 6). Although the brGDGT concentrations in the basal sediments (Unit 3) are lower compared to Unit 2e, the resulting BIT values in both units vary between 0.7 and 0.85. These values are comparable to BIT-values encountered in modern Yenisei Gulf surface sediments, between 200 and 300 km distance from the river mouth (De Jonge et al, Chapter 6). Assuming a sea level drop of 50 m at 11 ka (Fairbanks et al., 1989; Bauch et al., 2001), the distance between the core location and the presumed mouth of the palaeo Yenisei and Ob Rivers (Stein et al., 2004; Dittmers et al., 2008) was ca. 350 km. The brGDGT and crenarchaeol concentration in the Units 2e and 3 thus reflect a setting where the core site was much closer to the Yenisei River Mouth. We can further constrain the source of the brGDGTs encountered in Unit 2e and Unit 3 by studying their distribution (Fig. 4). The sediments in Unit 2e and 3 have a similar brGDGT fingerprint, as reflected in their similar scores on both PC1_{SAT} and PC2_{SAT}. Compared to the brGDGT distribution in modern Yenisei and Kara Sea sediments and SPM, the Units 2e and 3 have similar scores on PC1_{EXT} and PC2_{EXT} (and thus similar brGDGT distributions; Fig. 6B) as the Yenisei Gulf samples, although especially the distribution encountered in Unit 3 shows an enrichment of the brGDGTs that have a high score on PC2_{EXT} (increase of brGDGT Ia). Thus, the brGDGT concentrations, as well as the high BIT-

indices and the comparable brGDGT distributions reflect the deposition of brGDGTs in a setting where the core site was significantly closer to the mouth of the palaeorivers Yenisei and Ob, comparable to the current situation in the Yenisei Gulf (± 250 km distance from river Mouth), where riverine transport delivered brGDGTs with a comparable distribution as encountered in the modern Yenisei River Gulf sediments.

A contrasting GDGT content is present in the most recent sedimentary horizon; Unit 1. It contrasts with the Units 2d and 3, as it is characterized by low (<0.2) BIT values that are caused by a strongly decreased amount of brGDGTs and a crenarchaeol concentration that increases from the bottom to the top of this unit, reaching maximum levels at 100 cm bsf (Fig. 4G). The brGDGT concentrations ($5\text{--}20 \mu\text{g.g TOC}^{-1}$) and BIT-values (between 0.05 and 0.1) encountered in this unit are similar to the modern values encountered in offshore sediments in the Kara Sea (i.e. $4\text{--}20 \mu\text{g.g TOC}^{-1}$ and BIT values down to 0.09; De Jonge et al, Chapter 6), suggesting that conditions during this period resembled those of the current marine system throughout most of Unit 1. However, the crenarchaeol concentrations ($30\text{--}180 \mu\text{g.g TOC}^{-1}$) are significantly higher than the concentrations encountered in modern Kara Sea sediments, which are $30 \mu\text{g.g TOC}^{-1}$ at maximum (De Jonge et al, Chapter 6). Regarding the brGDGT distributions, Unit 1 has highly negative values on PC1_{SAT} (Fig. 5B), with increased amounts of the cyclopentane-containing brGDGTs Ib, IIb, IIc, IIIb, IIIc, IIb', IIc', IIIa', IIIb' and IIIc' (Fig. 5A). The downcore decrease of the scores on PC1_{SAT} is coeval with the increase in concentration of the marine iGDGT crenarchaeol ($r^2 = 0.85$), a specific biomarker for marine Thaumarchaeota, reflecting the increased production of these cyclopentane-containing brGDGTs in a system with increasing marine in situ production. Several authors have inferred in situ production of brGDGTs in the marine coastal and distal sediments as a mechanism to influence the brGDGT delivered from the continent (Svalbard fjord, Peterse et al., 2009a; Yangtze River, Zhu et al., 2011; Pearl River, Zhang et al., 2012; Tagus River and Amazon River; Zell et al., 2014a,b; globally distributed sediments, Weijers et al., 2014). Overall, these authors describe an increase in the fractional abundance of one or more cyclopentane-containing brGDGTs. As such, in situ production of marine brGDGTs is in line with the observed increase of the cyclopentane-containing brGDGTs along PC1_{SAT} (Fig. 5A). Although minor cyclopentane containing brGDGTs were often below detection limit in the modern Kara Sea sediments, in situ production was shown to increase the cyclopentane-containing brGDGTs Ib, Ic, IIb, IIc, IIIb, IIIc and IIc', which generally agrees with the increase of these brGDGTs in Unit 1. The gradually increasing marine signature of brGDGTs, as observed in the decreasing values on PC1_{SAT} , the increasing crenarchaeol concentrations and the decreasing BIT-values indicate an increasingly marine influence on the southern St. Anna Through during deposition of Unit 1. Indeed, the rise in sea level has been documented to continue until between 5-8 ka (Bauch et al., 2001 and Stein et al., 2004, respectively), and can thus be traced in the lower part of the sediments in Unit 1.

The palaeoenvironmental changes from the Units 2e and 3, with a strong river-derived terrigenous sedimentary signal, to Unit 1, with a stronger marine signal, can clearly be recognized from the GDGT concentrations and distributions and is consistent with evidence based on sediment-core and seismic-reflection data (e.g. Polyak et al., 2000; Stein et al., 2004). Units 2a-2d reflect the main phase of transition from one phase to the other, although some changes are evident in the upper part of Unit 2e (i.e. the start in the decrease of the BIT index values; Fig.

4H) and the lowermost part of Unit 1 (i.e. the increase in the crenarchaeol concentration; Fig. 4G). In Units 2a-2d, the crenarchaeol concentration is still low, but the brGDGT concentration and the resulting BIT-index values are showing distinct trends. The relatively high brGDGT concentrations in Unit 2e decrease strongly in Unit 2d, but increase in Unit 2c again, before the onset of the gradual decrease in brGDGT concentrations in Unit 2b and 2a, that continues into the lowest part of Unit 1. Since the concentration of the marine iGDGT crenarchaeol is low throughout these units, and the scores on the $PC1_{SAT}$ remain high, there are no indications for a contribution of marine in situ produced brGDGTs in the sediments of Unit 2. In the Units 2a-c the brGDGT distributions are similar to the terrigenous, river-derived brGDGTs in the sedimentary Units 2e and 3, as they have similar scores on $PC1_{SAT}$ and $PC2_{SAT}$. This indicates that the contribution of river-derived terrigenous brGDGTs remains strong in these sediments. However, the strong decrease in the brGDGT concentration in Unit 2d corresponds with a remarkable shift in the brGDGT distribution, that is characterized by a shift along the $PC2_{SAT}$, most apparent from the substantial increase in the fractional abundance of the brGDGTs Ia (Fig. 4C). We postulate that the strong shift in the brGDGT distribution in Unit 2d is related to a shift in the provenance of terrigenous brGDGTs. The brGDGT signature in the modern Kara Sea sediments was described to be a mixture of riverine in situ produced, soil-derived and coastal-cliff derived brGDGTs (De Jonge et al., Chapter 6). These different sources, but also different sub-pools of brGDGTs within the Yenisei River watershed are characterized by different brGDGT distributions and BIT-values (De Jonge et al., Chapter 6).

Enrichment in a brGDGT subpool can be caused by two processes. Firstly, a change in the relative contribution of the subpools, can happen during soil and coastal cliff erosion and riverine transport, prior to their delivery to the marine system. Secondly, the brGDGT distribution of terrigenous OM can be modified after its delivery to the marine system, if the brGDGT subpools differ in degradability. The nature of the brGDGT sub-pool enriched in the sediments of Unit 2d may be constrained by comparing this brGDGT distribution with the modern brGDGT signatures in the Kara Sea (Fig. 6B). However, the high score of Unit 2d on $PC2_{EXT}$ driven by the large fractional abundance of brGDGT Ia, sets them apart from all modern brGDGT distributions. They contrast especially with the brGDGT distribution produced in situ in the Yenisei River SPM, where the fractional abundance of the 6-methyl brGDGTs IIa' and IIIa' is strongly increased, and the fractional abundance of brGDGT Ia is decreased. Based on the PCA_{SAT} and the PCA_{EXT} the shift in brGDGT distribution can thus possibly be caused by an increased contribution of a brGDGT sub-pool predominantly enriched in the brGDGTs Ia, or a substantial decrease of the contribution of riverine in situ produced brGDGTs, characterized by a relatively high abundance of 6-methyl brGDGTs. A temporary increase in the erosion of continental brGDGTs during the Early Holocene, possibly limited to only part of the Yenisei watershed, or a decrease in the production of in situ produced brGDGTs may be related to the increased soil erosion during the deglaciation. Indeed, a 'peak' in meltwater run-off, dated between 10 and 13ka, was recognized in the Laptev Sea sedimentary record (Kleiber and Niessen, 2000). This observation was based on an increase in magnetic minerals sourced by the basaltic Putoran Massif, a plateau in the northern reaches of the Yenisei River watershed that was glaciated during the LGM. The brGDGT distribution encountered in a peat overlying a

buried glacier at a similar latitude as the Putoran Massif, is similar to the brGDGT distribution in the Unit 2d (Fig; 6B), as it is also characterized by a high fractional abundance of brGDGT Ia (63%; De Jonge et al., Chapter 6). However, as the geographical extent of brGDGT sub-pools enriched in brGDGTs Ia is unknown, we can not constrain whether this meltwater pulse may have influenced the brGDGTs delivered to the Kara Sea during the formation of Unit 2d.

The presence of oxidized lenses in Unit 2 of the Kara Sea sediments (Fig. 3) reflect a marine system wherein post-depositional oxic degradation may have modified the OM delivered to the site to a variable extent. Unit 2d directly underlies OXII (which was not analysed preventing the direct analysis of the impact of the oxidation on the brGDGT distribution), an oxidized lens that is present throughout the Kara Sea. The bulk OM parameters in the sediments underlying this oxidized lens, indicate that oxygen possibly penetrated the surface sediments during the formation of the oxidized front, and possibly oxidized the brGDGT distribution in the subsurface. This is reflected in a slight decrease of the TOC and TN content, from 1 to 0.6% and from 0.08 to 0.06% respectively. A shift in the $\delta^{13}\text{C}_{\text{org}}$ and $\delta^{15}\text{N}$ values at the depths of the oxidized lenses, from -24.5 to -26 ‰ and from 5 to 3.5 ‰ respectively, can also be attributed to degradation of the OM present in the sediments (e.g. Lehmann et al., 2002; Prahl et al., 2003; Robinson et al., 2012). The effect of degradation is also reflected in the C/N ratios, where increased values may reflect degradation of OM (e.g. Mariotti et al., 1984; Thornton and McManus, 1994). However, the extent of degradation, based on the bulk OM proxies, does not completely agree with the interval in the core where a different brGDGT provenance is observed. Furthermore, previous studies on the effect of oxic degradation on GDGTs, indicated a strong increase in the BIT-index in oxidized sediments, following the preferential degradation of marine in situ produced crenarchaeol (Huguet et al., 2008; Lengger et al., 2013). The decreasing BIT-values observed in Unit 2d can only be caused by oxic degradation if crenarchaeol is dominantly derived from terrigenous sources, and differs between brGDGT sub-pools. Nonetheless, preferential degradation was inferred to explain the increase in brGDGT Ia in offshore Kara Sea sediments, and was thus already inferred to act on the brGDGT distribution during transport and incorporation into the sediments (De Jonge et al., Chapter 6). The increase in the fractional abundance of brGDGT Ia, Ic and IIc in Unit 2d indicates that a similar mechanism may further influence the brGDGT distribution delivered to a marine sediment. Furthermore, if degradation acts on the brGDGT distribution, it is expected to act specifically on the brGDGTs that are produced in situ in the Yenisei River, as this modern brGDGT pool will be degraded preferentially (Blair and Aller, 2012; Arndt et al., 2013). The contrasting score on PC2_{EXT} of the Yenisei River SPM and Unit 2d distributions, respectively, indicate that brGDGTs IIa' and IIIa', that are strongly enriched in the Yenisei River SPM, have a decreased fractional abundance in Unit 2d. This observation can be explained invoking the mechanism of preferential degradation. Although we can not conclude on the mechanism causing the observed shift in the provenance of terrigenous brGDGTs, the score on the PC2_{EXT} may reflect this shift. Thus, the brGDGT distribution of Unit 2d represents the most intensely enriched/degraded distribution encountered in the modern and downcore Kara Sea distributions.

5.3. Implications for brGDGT-based palaeoclimate reconstructions

In the modern Kara Sea SPM and sediments, the brGDGT distribution was shown to be influenced by in situ production and by the contribution of several sub-pools of brGDGTs (De Jonge et al., Chapter 6). In recent sediments, preferential degradation of a labile brGDGT pool, e.g. the in situ produced riverine brGDGTs, and possibly also less refractory sub-pools of soil-derived brGDGTs was inferred to explain the changing provenance of brGDGTs in offshore sediments. This study indicates that these processes can also act on longer timescales. The in situ production of marine brGDGTs was shown to be coeval with the increase of the marine iGDGT crenarchaeol, and both parameters trace the production of marine OM, and the increasingly marine nature of the St. Anna Trough. Although in situ production in sediments apparently did not influence the brGDGT distributions in Unit 2 and 3, these were in their turn influenced by changes in the provenance of the terrigenous brGDGTs.

To evaluate the influence these various processes may have on the brGDGT-based palaeoclimate distributions, we can evaluate the reconstructed pH and MAT (Fig. 7). For the pH reconstruction, we employ the CBT' calibration, a calibration based on a log-ratio [Eq. 3 and 4] of the 6-methyl brGDGTs IIa', IIb', IIc', IIIa', IIIb' and IIIc' and brGDGT Ic, relative to the brGDGT compounds Ia, IIa and IIIa. The MAT temperature will be reconstructed using the MAT_{ms} [Eq. 5], that is based only on the abundances of the three major non-cyclopentane containing brGDGTs Ia, IIa and IIIa, as brGDGT Ib was found to co-elute with an unknown compound in some samples (n=15). Both these calibrations are based on a dataset of globally distributed soils (De Jonge et al., 2014a). Overall, the reconstructed pH is relatively stable throughout Units 3 and 2e (between 5.9 and 6.3), sharply decreases in Unit 2d to a pH values of 5.8, and subsequently increases in the transitional Units 2c-a, towards constant values of ca. 7.1 in Unit 1. Both in situ production of marine brGDGTs and changes in the provenance of terrigenous brGDGTs will have an effect on the reconstructed pH. BrGDGTs predominantly produced in situ in the marine sediments (i.e. Unit 1) reflect the increased pH of the marine production site, although the reconstructed pH still underestimates the marine (pore)water pH, that is typically between 7.8 to 8.4 (e.g. Polukhin and Makkaveev, 2014). An extended dataset of brGDGTs in marine sediments, that were inferred to be in situ produced in the sediments (Weijers et al., 2014), reported reconstructed pH values between 6.1 and 9.9. These authors postulated that the brGDGT distribution possibly reflected the more variable sedimentary porewater pH values, rather than the more stable pH of the water column. Furthermore, this apparent offset may be due to the fact that the soil pH calibration may not be applicable to marine in situ produced brGDGTs. Alternatively, it may also indicate that the brGDGTs in Unit 1 represent a mixture of in situ produced and terrestrial brGDGTs. The sediments in Unit 2d and 3 resemble the current brGDGT distribution in the Yenisei Gulf, and thus reflect a mixture of riverine-in situ produced and coastal-cliff derived brGDGTs. The brGDGT distribution in Unit 2d probably represent a strongly enriched brGDGT subpool. The reconstructed pH in this unit approaches the average pH encountered in the watershed soils (pH=5; De Jonge et al., 2014a,b).

Based on a soil calibration, the reconstructed temperatures in the deepest part of the core

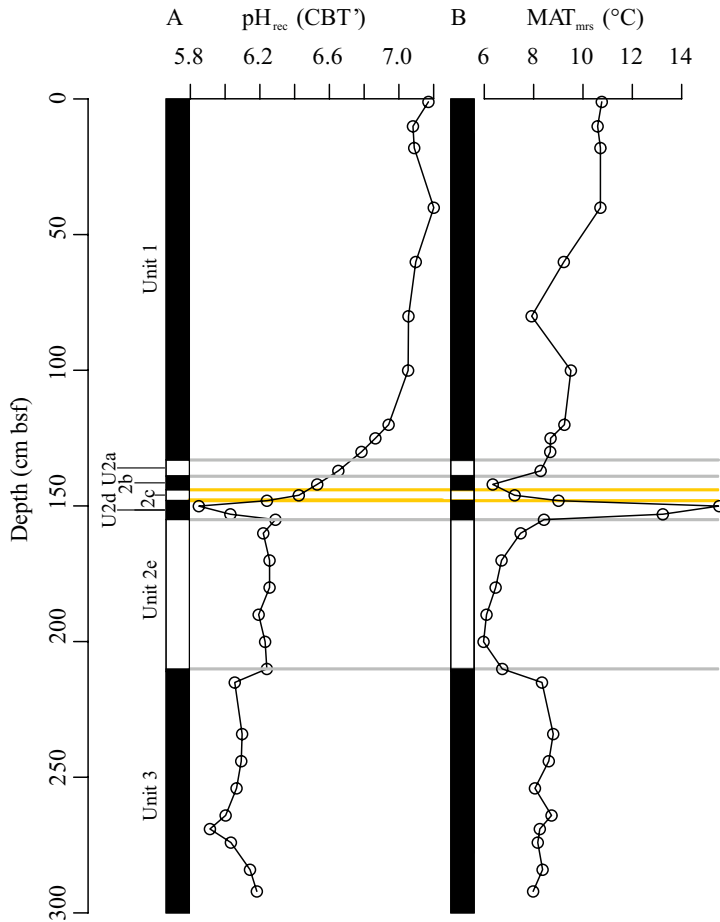


Fig. 7. A) The downcore reconstructed soil pH [based on the CBT': Eq. 3, 4] and B) the reconstructed mean annual temperature (MAT) [based on the MAT_{mrs}: Eq. 5]. The scale on the left indicates the depth (cm below sea floor) and the lithological units as described in Fig. 3, yellow lines indicate the presence of oxidized lenses, based on the lithological description.

(Units 2d and 3; between 6 and 9 °C) are slightly below those calculated for Unit 1 (between 8 and 11 °C). The distinct brGDGT distribution in Unit 2d results in a strongly increased reconstructed MAT at these depths (13-16 °C). As the increase in cyclopentane-containing and 6-methyl brGDGTs, that is typical for marine in situ production, does not influence the MAT_{mrs}-based temperatures, it may possibly be a proper palaeothermometer for the reconstruction of temperatures in marine sediments where in situ production is probable. However, the effect of a changing provenance of terrigenous brGDGTs has a large effect (> 4 °C) on the reconstructed temperature in the Kara Sea system. As in situ production of riverine brGDGT has been documented in rivers globally (e.g. Kim et al., 2012; Zell et al., 2014a, 2014b), and

the watershed of large rivers drains several different soil types, the brGDGT distribution delivered to the marine system globally, can be assumed to consist of several sub-pools with different brGDGT distribution. In the case these sub-pools are exported to a different extent on a geological timescale, or if they differ in degradability, this mechanism has to be taken into account when reconstructing palaeotemperatures.

6. Conclusion

The brGDGT distribution has been analyzed in the St. Anna Trough, reflecting large changes in terrigenous material delivered since the last regression of marine glaciers from this trough (minimum age of 13.3 ka). The brGDGT and crenarchaeol concentration and the BIT-index, reflect the transition from a sedimentation regime during a sea level lowstand, where the proximity of the palaeo Yenisei and Ob River Mouth to the core site, results in a strong signal of terrigenous river-derived brGDGTs. The rising sea level caused the increase of the fractional abundance of marine in situ produced brGDGTs (Ib, IIb, IIc, IIIb, IIIc, IIb', IIc', IIIa', IIIb' and IIIc') and crenarchaeol. This increase of marine production is reflected by an increase in the marine in situ produced brGDGTs. A clear shift in the provenance of terrigenous brGDGTs can be observed at a depth of 150-153 cm bsf, characterized by an increase in fractional abundance of predominantly brGDGT Ia. The mechanism causing this shift is unknown as both increased continental erosion and increased degradation in the marine sediments can result in this enrichment.

Both in situ production of brGDGTs and shifts in the provenance of terrigenous brGDGTs have to be taken into account when reconstructing continental palaeoenvironments. Separating these processes from palaeoclimate-induced changes is a challenge for palaeoclimate reconstructions that can only be solved using a multi-proxy approach, studying several (lipid-based) biomarkers and sedimentary characteristics.

7. Acknowledgments

We acknowledge the work of Annelieke Mets and Jort Ossebaer in the work-up and in the analysis of the samples and Ellen Hopmans for helpful discussions. This work was performed in the framework of the memorandum NIOZ-VNIOkeangeologia for Arctic research. The research was funded by research project 819.01.013, financed by the Netherlands Organization for Scientific Research (NWO) and the European Research Council under the EU Seventh Framework Programme (FP7/2007-2013)/ERC grant agreement No. [226600].



Photo by Cindy De Jonge

References, Summaries and Acknowledgments



- Aagaard K. and Carmack E. C. (1989) The role of sea ice and other fresh water in the Arctic circulation. *Journal of Geophysical Research-Oceans* **94**, 14485–14498.
- Aagaard K. and Coachman L. K. (1975) Toward an ice-free Arctic ocean. *Eos, Transactions American Geophysical Union* **56**, 484–486.
- Adams H. D. and Kolb T. E. (2005) Tree growth response to drought and temperature in a mountain landscape in northern Arizona, USA: Tree growth response to drought and temperature. *Journal of Biogeography* **32**, 1629–1640.
- Anderson-Teixeira K. J., Snyder P. K., Twine T. E., Cuadra S. V., Costa M. H. and DeLucia E. H. (2012) Climate-regulation services of natural and agricultural ecoregions of the Americas. *Nature Climate Change* **2**, 177–181.
- Arndt S., Jørgensen B. B., LaRowe D. E., Middelburg J. J., Pancost R. D. and Regnier P. (2013) Quantifying the degradation of organic matter in marine sediments: A review and synthesis. *Earth and Science Reviews* **123**, 53–86.
- Auguet J.-C., Nomokonova N., Camarero L. and Casamayor E. O. (2011) Seasonal Changes of Fresh-water Ammonia-Oxidizing Archaeal Assemblages and Nitrogen Species in Oligotrophic Alpine Lakes. *Appl. Environmental Microbiology* **77**, 1937–1945.
- Bailey I. W. and Sinnott E. W. (1915) A Botanical Index of Cretaceous and Tertiary Climates. *Science* **41**, 831–834.
- Barns S. M., Takala S. L. and Kuske C. R. (1999) Wide Distribution and Diversity of Members of the Bacterial Kingdom Acidobacterium in the Environment. *Appl. Environ. Microbiol.* **65**, 1731–1737.
- Barns S. M., Cain E. C., Sommerville L. and Kuske C. R. (2007) Acidobacteria Phylum Sequences in Uranium-Contaminated Subsurface Sediments Greatly Expand the Known Diversity within the Phylum. *Applied and Environmental Microbiology* **73**, 3113–3116.
- Bauch H. ., Mueller-Lupp T., Taldenkova E., Spielhagen R. ., Kassens H., Grootes P. ., Thiede J., Heinemeier J. and Petryashov V. . (2001) Chronology of the Holocene transgression at the North Siberian margin. *Global and Planetary Change* **31**, 125–139.
- Bendle J. A., Weijers J. W. H., Maslin M. A., Sinninghe Damsté J. S., Schouten S., Hopmans E. C., Boot C. S. and Pancost R. D. (2010) Major changes in glacial and Holocene terrestrial temperatures and sources of organic carbon recorded in the Amazon fan by tetraether lipids. *Geochemistry Geophysics Geosystems* **11**, Q12007.
- Benner R., Benitez-Nelson B., Kaiser K. and Amon R. M. W. (2004) Export of young terrigenous dissolved organic carbon from rivers to the Arctic Ocean: Age of Arctic dissolved organic carbon. *Geophysical Research Letters* **31**, L05305.
- Berner R. A. (2004) *The phanerozoic carbon cycle: CO₂ and O₂*, Oxford University Press, Oxford ; New York.
- Birgel D., Feng D., Roberts H. H. and Peckmann J. (2011) Changing redox conditions at cold seeps as revealed by authigenic carbonates from Alaminos Canyon, northern Gulf of Mexico. *Chemical Geology* **285**, 82–96.
- Bisseret P., Zundel M. and Rohmer M. (1985) Prokaryotic triterpenoids 2. 2β-Methylhopanoids from *Methylobacterium organophilum* and *Nostoc muscorum*, a new series of prokaryotic triterpenoids. *European Journal of Biochemistry* **150**, 29–34.
- Blaga C. I., Reichart G. J., Heiri O. and Sinninghe Damsté J. S. (2009) Tetraether membrane lipid distributions in water-column particulate matter and sediments: a study of 47 European lakes along a north-south transect. *Journal of Paleolimnology* **41**, 523–540.
- Blaga C. I., Reichart G. J., Schouten S., Lotter A. F., Werne J. P., Kosten S., Mazzeo N., Lacerot G. and Sinninghe Damsté J. S. (2010) Branched glycerol dialkyl glycerol tetraethers in lake sediments: Can they be used as temperature and pH proxies? *Organic Geochemistry* **41**, 1225–1234.
- Blaga C. I., Reichart G.-J., Vissers E. W., Lotter A. F., Anselmetti F. S. and Sinninghe Damsté J. S. (2011) Seasonal changes in glycerol dialkyl glycerol tetraether concentrations and fluxes in a perialpine lake: Implications for the use of the TEX₈₆ and BIT proxies. *Geochimica et Cosmochimica Acta* **75**, 6416–6428.
- Blaga C. I., Reichart G.-J., Lotter A. F., Anselmetti F. S. and Sinninghe Damsté J. S. (2013) A TEX₈₆ lake record suggests simultaneous shifts in temperature in Central Europe and Greenland during the last deglaciation. *Geophysical Research Letters* **40**, 948–953.
- Blair N. E. and Aller R. C. (2012) The Fate of Terrestrial Organic Carbon in the Marine Environment. *Annual Review of Marine Science* **4**, 401–423.

- Blumenberg M., Hoppert M., Krüger M., Dreier A. and Thiel V. (2012) Novel findings on hopanoid occurrences among sulfate reducing bacteria: Is there a direct link to nitrogen fixation? *Organic Geochemistry* **49**, 1–5.
- Blumenberg M., Krüger M., Nauhaus K., Talbot H. M., Oppermann B. I., Seifert R., Pape T. and Michaelis W. (2006) Biosynthesis of hopanoids by sulfate-reducing bacteria (genus *Desulfovibrio*). *Environmental Microbiology* **8**, 1220–1227.
- Blyth A. J. and Schouten S. (2013) Calibrating the glycerol dialkyl glycerol tetraether temperature signal in speleothems. *Geochimica et Cosmochimica Acta* **109**, 312–328.
- Bobrovitskaya N. N., Zubkova C. and Meade R. H. (1996) Discharges and yields of suspended sediment in the Ob and Yenisey Rivers of Siberia. In *Erosion and sediment yield : global and regional perspectives ; proceedings of an international symposium held at Exeter, UK, from 15 to 19 July 1996* IAHS Publication. Desmond E Walling. pp. 115–123.
- Boucsein B., Knies J. and Stein R. (2002) Organic matter deposition along the Kara and Laptev Seas continental margin (eastern Arctic Ocean) during last deglaciation and Holocene: evidence from organic–geochemical and petrographical data. *Marine Geology* **183**, 67–87.
- Branco R., Chung A.-P., Veríssimo A. and Morais P. V. (2005) Impact of chromium-contaminated wastewaters on the microbial community of a river. *FEMS Microbiology Ecology* **54**, 35–46.
- Broström A., Nielsen A. B., Gaillard M.-J., Hjelle K., Mazier F., Binney H., Bunting J., Fyfe R., Meltsov V., Poska A., Räsänen S., Soepboer W., Stedingk H., Suutari H. and Sugita S. (2008) Pollen productivity estimates of key European plant taxa for quantitative reconstruction of past vegetation: a review. *Vegetation History and Archaeobotany* **17**, 461–478.
- Buckles L. K., Villanueva L., Weijers J. W. H., Verschuren D. and Sinninghe Damsté J. S. (2013) Linking isoprenoidal GDGT membrane lipid distributions with gene abundances of ammonia-oxidizing Thaumarchaeota and uncultured crenarchaeotal groups in the water column of a tropical lake (Lake Challa, East Africa). *Environmental Microbiology* **15**, 2445–2462.
- Buckles L. K., Weijers J. W. H., Verschuren D. and Sinninghe Damsté J. S. (2014a) Sources of core and intact branched tetraether membrane lipids in the lacustrine environment: Anatomy of Lake Challa and its catchment, equatorial East Africa. *Geochimica et Cosmochimica Acta* **140**, 106–126.
- Buckles L. K., Weijers J. W. H., Tran X.-M., Waldron S. and Sinninghe Damsté J. S. (2014b) Provenance of tetraether membrane lipids in a large temperate lake (Loch Lomond, UK): implications for GDGT-based palaeothermometry. *Biogeosciences* **11**, 5539–5563.
- Buckley D. H. and Schmidt T. M. (2003) Diversity and dynamics of microbial communities in soils from agro-ecosystems. *Environmental Microbiology* **5**, 441–452.
- Burhan R. Y. P., Trendel J. M., Adam P., Wehrung P., Albrecht P. and Nissenbaum A. (2002) Fossil bacterial ecosystem at methane seeps: Origin of organic matter from Be’eri sulfur deposit, Israel. *Geochimica et Cosmochimica Acta* **66**, 4085–4101.
- Chapin F. S., Randerson J. T., McGuire A. D., Foley J. A. and Field C. B. (2008) Changing feedbacks in the climate–biosphere system. *Frontiers in Ecology and the Environment* **6**, 313–320.
- Chapin F. S., McFarland J., McGuire A. D., Euskirchen E. S., Ruess R. W. and Kielland K. (2009) The changing global carbon cycle: linking plant–soil carbon dynamics to global consequences. *Journal of Ecology* **97**, 840–850.
- Chappe B., Michaelis W., Albrecht P. and Ourisson G. (1979) Fossil evidence for a novel series of archaeobacterial lipids. *Naturwissenschaften* **66**, 522–523.
- Chong P. L.-G. (2010) Archaeobacterial bipolar tetraether lipids: Physico-chemical and membrane properties. *Chemistry and Physics of Lipids* **163**, 253–265.
- Cook E. and Kairiūkštis L. [Eds.] (1990) *Methods of dendrochronology: applications in the environmental science.*, Kluwer Academic Publishers ; International Institute for Applied Systems Analysis, Dordrecht, The Netherlands.
- Cooke M. P., Talbot H. M. and Wagner T. (2008a) Tracking soil organic carbon transport to continental margin sediments using soil-specific hopanoid biomarkers: A case study from the Congo fan (ODP site 1075). *Organic Geochemistry* **39**, 965–971.
- Cooke M. P., Talbot H. M. and Farrimond P. (2008b) Bacterial populations recorded in bacteriohopanepolyol distributions in soils from Northern England. *Organic Geochemistry* **39**, 1347–1358.
- Cooke M. P., van Dongen B. E., Talbot H. M., Semiletov I., Shakhova N., Guo L. and Gustafsson Ö. (2009) Bacteriohopanepolyol biomarker composition of organic matter exported to the Arctic Ocean by seven of the major Arctic rivers. *Organic Geochemistry* **40**, 1151–1159.

- Cooke M. P. (2010) *The role of bacteriohopanepolyols as biomarkers for soil bacterial communities and soil derived organic matter*. PhD thesis, Newcastle University.
- Cowling S. A. (1999) Plants and Temperature-CO₂ Uncoupling. *Science* **285**, 1500.
- Cvejić J. H., Bodrossy L., Kovács K. L. and Rohmer M. (2000) Bacterial triterpenoids of the hopane series from the methanotrophic bacteria *Methylocaldum* spp.: phylogenetic implications and first evidence for an unsaturated aminobacteriohopanepolyol. *FEMS Microbiology Letters* **182**, 361–365.
- Das S. K., Bendle J. and Routh J. (2012) Evaluating branched tetraether lipid-based palaeotemperature proxies in an urban, hyper-eutrophic polluted lake in South Africa. *Organic Geochemistry* **53**, 45–51.
- Davidson E. A. and Janssens I. A. (2006) Temperature sensitivity of soil carbon decomposition and feedbacks to climate change. *Nature* **440**, 165–173.
- Davis M. B. and Shaw R. G. (2001) Range shifts and adaptive responses to quaternary climate change. *Science* **292**, 673–679.
- Dedysh S. N., Pankratov T. A., Belova S. E., Kulichevskaya I. S. and Liesack W. (2006) Phylogenetic analysis and in situ identification of bacteria community composition in an acidic sphagnum peat bog. *Applied Environmental Microbiology* **72**, 2110–2117.
- De Jonge C., Hopmans E. C., Stadnitskaia A., Rijpstra W. I. C., Hofland R., Tegelaar E. and Sinninghe Damsté J. S. (2013) Identification of novel penta- and hexamethylated branched glycerol dialkyl glycerol tetraethers in peat using HPLC–MS², GC–MS and GC–SMB–MS. *Organic Geochemistry* **54**, 78–82.
- De Jonge C., Stadnitskaia A., Hopmans E. C., Cherkashov G., Fedotov A. and Sinninghe Damsté J. S. (2014a) In situ produced branched glycerol dialkyl glycerol tetraethers in suspended particulate matter from the Yenisei River, Eastern Siberia. *Geochimica et Cosmochimica Acta* **125**, 476–491.
- De Jonge C., Hopmans E. C., Zell C. I., Kim J.-H., Schouten S. and Sinninghe Damsté J. S. (2014b) Occurrence and abundance of 6-methyl branched glycerol dialkyl glycerol tetraethers in soils: Implications for palaeoclimate reconstruction. *Geochimica et Cosmochimica Acta* **141**, 97–112.
- De Rosa M., Gambacorta A., Lanzotti V., Trincone A., Harris J. E. and Grant W. D. (1986) A range of ether core lipids from the methanogenic archaeobacterium *Methanosarcina barkeri*. *Biochimica et Biophysica Acta - Lipids and Lipid Metabolism* **875**, 487–492.
- Dirghangi S. S., Pagani M., Hren M. T. and Tipple B. J. (2013) Distribution of glycerol dialkyl glycerol tetraethers in soils from two environmental transects in the USA. *Organic Geochemistry* **59**, 49–60.
- Dittmar T. and Kattner G. (2003) The biogeochemistry of the river and shelf ecosystem of the Arctic Ocean: a review. *Marine Chemistry* **83**, 103–120.
- Dittmers K., Niessen F. and Stein R. (2008) Late Weichselian fluvial evolution on the southern Kara Sea Shelf, North Siberia. *Global and Planetary Change* **60**, 327–350.
- Dobson M. (1998) *Ecology of aquatic systems*. Longman, Harlow, Essex, England.
- Doğrul Selver A., Talbot H. M., Gustafsson Ö., Boulton S. and van Dongen B. E. (2012) Soil organic matter transport along an sub-Arctic river–sea transect. *Organic Geochemistry* **51**, 63–72.
- Donders T. H., Weijers J. W. H., Munsterman D. K., Hoeve M. L. K., Buckles L. K., Pancost R. D., Schouten S., Sinninghe Damsté J. S. and Brinkhuis H. (2009) Strong climate coupling of terrestrial and marine environments in the Miocene of northwest Europe. *Earth and Planetary Science Letters* **281**, 215–225.
- Dong H., Zhang G., Jiang H., Yu B., Chapman L. R., Lucas C. R. and Fields M. W. (2006) Microbial diversity in sediments of saline Qinghai Lake, China: linking geochemical controls to microbial ecology. *Microbial Ecology* **51**, 65–82.
- Dunbar J., Takala S., Barns S. M., Davis J. A. and Kuske C. R. (1999) Levels of bacterial community diversity in four arid soils compared by cultivation and 16S rRNA gene cloning. *Applied Environmental Microbiology* **65**, 1662–1669.
- Dunbar J., Barns S. M., Ticknor L. O. and Kuske C. R. (2002) Empirical and theoretical bacterial diversity in four Arizona soils. *Applied Environmental Microbiology* **68**, 3035–3045.
- Edwards R. T. and Meyer J. L. (1986) Production and turnover of planktonic bacteria in two southeastern blackwater rivers. *Applied and Environmental Microbiology* **52**, 1317–1323.
- Eggermont H. and Heiri O. (2012) The chironomid-temperature relationship: expression in nature and palaeoenvironmental implications. *Biological Reviews of the Cambridge Philosophical Society* **87**, 430–456.
- Eickhoff M., Birgel D., Talbot H. M., Peckmann J. and Kappler A. (2013) Bacteriohopanoid inventory of *Geobacter sulfurreducens* and *Geobacter metallireducens*. *Organic Geochemistry* **58**, 107–114.

- Fairbanks R. G. (1989) A 17,000-year glacio-eustatic sea level record: influence of glacial melting rates on the Younger Dryas event and deep-ocean circulation. *Nature* **342**, 637–642.
- Fernandes M. B. and Sicre M.-A. (2000) The importance of terrestrial organic carbon inputs on Kara Sea shelves as revealed by n-alkanes, OC and $\delta^{13}\text{C}$ values. *Organic Geochemistry* **31**, 363–374.
- Fialkov A.B., Gordin A., Amirav A. (2008). Hydrocarbons and fuels analyses with the supersonic gas chromatography mass spectrometry - The novel concept of isomer abundance analysis. *Journal of Chromatography A* **1195**, 127–135.
- Field C. B. and Raupach M. R. [Eds.] (2004) *The global carbon cycle: integrating humans, climate, and the natural world*. Island Press, Washington.
- Fierer N. and Jackson R. B. (2006) The diversity and biogeography of soil bacterial communities. *Proceedings of the National Academy of Sciences* **103**, 626–631.
- Fierer N., Bradford M. A. and Jackson R. B. (2007) Toward an ecological classification of soil bacteria. *Ecology* **88**, 1354–1364.
- Fietz S., Martínez-García A., Huguet C., Rueda G. and Rosell-Melé A. (2011) Constraints in the application of the Branched and Isoprenoid Tetraether index as a terrestrial input proxy. *Journal of Geophysical Research: Oceans* **116**, C10032.
- Fox J. and Weisberg S. (2011). An {R} Companion to applied regression, second edition. Thousand Oaks CA: Sage. <http://socserv.socsci.mcmaster.ca/jfox/Books/Companion>.
- Fracchia L., Dohrmann A. B., Martinotti M. G. and Tebbe C. C. (2006) Bacterial diversity in a finished compost and vermicompost: differences revealed by cultivation-independent analyses of PCR-amplified 16S rRNA genes. *Applied Microbiology and Biotechnology* **71**, 942–952.
- Gao L., Nie J., Clemens S., Liu W., Sun J., Zech R. and Huang Y. (2012) The importance of solar insolation on the temperature variations for the past 110kyr on the Chinese Loess Plateau. *Palaeogeography, Palaeoclimatology, Palaeoecology* **317–318**, 128–133.
- Gardner J. V., Dean W. E., Klise D. H. and Baldauf J. G. (1982) A climate-related oxidizing event in deep-sea sediment from the Bering Sea. *Quaternary Research* **18**, 91–107.
- Gascoyne M. (1992) Palaeoclimate determination from cave calcite deposits. *Quaternary Science Reviews* **11**, 609–632.
- Gaye B., Fahl K., Kodina L. A., Lahajnar N., Nagel B., Unger D. and Gebhardt A. C. (2007) Particulate matter fluxes in the southern and central Kara Sea compared to sediments: Bulk fluxes, amino acids, stable carbon and nitrogen isotopes, sterols and fatty acids. *Continental Shelf Research* **27**, 2570–2594.
- Gebhardt A. C., Gaye-Haake B., Unger D., Lahajnar N. and Ittekkot V. (2004) Recent particulate organic carbon and total suspended matter fluxes from the Ob and Yenisei Rivers into the Kara Sea (Siberia). *Marine Geology* **207**, 225–245.
- Gibson R. A., Sherry A., Kaur G., Pancost R. D. and Talbot H. M. (2014) Bacterioplanepolyols preserved in silica sinters from Champagne Pool (New Zealand) indicate a declining temperature gradient over the lifetime of the vent. *Organic Geochemistry* **69**, 61–69.
- Gordeev V. V., Martin J. M., Sidorov I. S. and Sidorova M. V. (1996) A reassessment of the Eurasian river input of water, sediment, major elements, and nutrients to the Arctic Ocean. *American Journal of Science* **296**, 664–691.
- Graham D. E., Wallenstein M. D., Vishnivetskaya T. A., Waldrop M. P., Phelps T. J., Pfiffner S. M., Onstott T. C., Whyte L. G., Rivkina E. M., Gilichinsky D. A., Elias D. A., Mackelprang R., VerBerkmoes N. C., Hettich R. L., Wagner D., Wulfschleger S. D. and Jansson J. K. (2012) Microbes in thawing permafrost: the unknown variable in the climate change equation. *The ISME Journal* **6**, 709–712.
- Hald M., Kolstad V., Polyak L., Forman S. L., Herlihy F. A., Ivanov G. and Nescheretov A. (1999) Late-glacial and Holocene paleoceanography and sedimentary environments in the St. Anna Trough, Eurasian Arctic Ocean margin. *Palaeogeography, Palaeoclimatology, Palaeoecology* **146**, 229–249.
- Handley L., Talbot H. M., Cooke M. P., Anderson K. E. and Wagner T. (2010) Bacterioplanepolyols as tracers for continental and marine organic matter supply and phases of enhanced nitrogen cycling on the late Quaternary Congo deep sea fan. *Organic Geochemistry* **41**, 910–914.
- Hanson R. S. and Hanson T. E. (1996) Methanotrophic bacteria. *Microbiological Reviews* **60**, 439–471.
- Hanzlick D. and Aagaard K. (1980) Freshwater and Atlantic water in the Kara Sea. *Journal of Geophysical Research* **85**, 4937.
- Hartmann, D.L., A.M.G. Klein Tank, M. Rusticucci, L.V. Alexander, S. Brönnimann, Y. Charabi, F.J. Dentener, E.J. Dlugokencky, D.R. Easterling, A. Kaplan, B.J. Soden, P.W. Thorne, M. Wild and P.M. Zhai (2013) Observations: atmosphere and surface. In: *Climate Change 2013: The Physical Science*

Basis. Contribution of Working Group I to the Fifth Assessment Report of the Intergovernmental Panel on Climate Change [Stocker, T.F., D. Qin, G.-K. Plattner, M. Tignor, S.K. Allen, J. Boschung, A. Nauels, Y. Xia, V. Bex and P.M. Midgley [Eds.]]. Cambridge University Press, Cambridge, United Kingdom and New York, NY, USA.

- Herfort L., Schouten S., Boon J. P., Woltering M., Baas M., Weiers J. W. H. and Sinninghe Damsté J. S. (2006) Characterization of transport and deposition of terrestrial organic matter in the southern North Sea using the BIT index. *Limnology and Oceanography* **51**, 2196–2205.
- Herrmann D., Bissleret P., Connan J. and Rohmer M. (1996) A non-extractable triterpenoid of the hopane series in *Acetobacter xylinum*. *FEMS Microbiology Letters* **135**, 323–326.
- Holmes R. M., McClelland J. W., Peterson B. J., Shiklomanov I. A., Shiklomanov A. I., Zhulidov A. V., Gordeev V. V. and Bobrovitskaya N. N. (2002) A circumpolar perspective on fluvial sediment flux to the Arctic ocean. *Global Biogeochemical Cycles* **16**, 45–1–45–14.
- Hopmans E. C., Schouten S., Pancost R. D., van der Meer M. T. J. and Sinninghe Damsté J. S. (2000) Analysis of intact tetraether lipids in archaeal cell material and sediments by high performance liquid chromatography/atmospheric pressure chemical ionization mass spectrometry. *Rapid Communications in Mass Spectrometry* **14**, 585–589.
- Hopmans E. C., Weijers J. W. H., Schefuß E., Herfort L., Sinninghe Damsté J. S. and Schouten S. (2004) A novel proxy for terrestrial organic matter in sediments based on branched and isoprenoid tetraether lipids. *Earth and Planetary Science Letters* **224**, 107–116.
- Hu A., Yang X., Chen N., Hou L., Ma Y. and Yu C.-P. (2014) Response of bacterial communities to environmental changes in a mesoscale subtropical watershed, Southeast China. *Science of The Total Environment* **472**, 746–756.
- Huguet C., Hopmans E. C., Febo-Ayala W., Thompson D. H., Sinninghe Damsté J. S. and Schouten S. (2006) An improved method to determine the absolute abundance of glycerol dibiphytanyl glycerol tetraether lipids. *Organic Geochemistry* **37**, 1036–1041.
- Huguet C., de Lange G. J., Gustafsson O., Middelburg J. J., Sinninghe Damsté J. S. and Schouten S. (2008) Selective preservation of soil organic matter in oxidized marine sediments (Madeira Abyssal Plain). *Geochimica et Cosmochimica Acta* **72**, 6061–6068.
- Jahnke L. L., Summons R. E., Dowling L. M. and Zahiralis K. D. (1995) Identification of methanotrophic lipid biomarkers in cold-seep mussel gills: chemical and isotopic analysis. *Applied Environmental Microbiology* **61**, 576–582.
- Jakobsson M., Andreassen K., Bjarnadóttir L. R., Dove D., Dowdeswell J. A., England J. H., Funder S., Hogan K., Ingólfsson Ó., Jennings A., Krog Larsen N., Kirchner N., Landvik J. Y., Mayer L., Mikkelsen N., Möller P., Niessen F., Nilsson J., O'Regan M., Polyak L., Nørgaard-Pedersen N. and Stein R. (2014) Arctic Ocean glacial history. *Quaternary Science Reviews* **92**, 40–67.
- Janssen P. H. (2006) Identifying the dominant soil bacterial taxa in libraries of 16S rRNA and 16S rRNA genes. *Applied Environmental Microbiology* **72**, 1719–1728.
- Jewell W. J. and McCarty P. L. (1971) Aerobic decomposition of algae. *Environmental Science and Technology* **5**, 1023–1031.
- Johnsen S. J., Dahl-Jensen D., Gundestrup N., Steffensen J. P., Clausen H. B., Miller H., Masson-Delmotte V., Sveinbjörnsdóttir A. E. and White J. (2001) Oxygen isotope and palaeotemperature records from six Greenland ice-core stations: Camp Century, Dye-3, GRIP, GISP2, Renland and NorthGRIP. *Journal of Quaternary Science* **16**, 299–307.
- Jordan G. J. (1997) Uncertainty in palaeoclimatic reconstructions based on leaf physiognomy. *Australian Journal of Botany* **45**, 527–547.
- Joyeux C., Fouchard S., Llopiz P. and Neunlist S. (2004) Influence of the temperature and the growth phase on the hopanoids and fatty acids content of *Frateuria aurantia* (DSMZ 6220). *FEMS Microbiology Ecology* **47**, 371–379.
- Kaneko M., Kitajima F., Naraoka H. (2011) Stable hydrogen isotope measurement of archaeal ether-bound hydrocarbons. *Organic Geochemistry* **42**, 166–172.
- Karpov E. G. (1984) About the origin of an underground massive ice within the mouth of the Yenisei River (in Russian). *Geologia I Geophisika* **1**, 1–5.
- Kim J.-H., Schouten S., Buscail R., Ludwig W., Bonnin J., Sinninghe Damsté J. S. and Bourrin F. (2006) Origin and distribution of terrestrial organic matter in the NW Mediterranean (Gulf of Lions): Exploring the newly developed BIT index. *Geochemistry, Geophysics, Geosystems* **7**, Q11017.
- Kim J.-H., Ludwig W., Schouten S., Kerherve P., Herfort L., Bonnin J. and Sinninghe Damsté J. S. (2007)

- Impact of flood events on the transport of terrestrial organic matter to the ocean: A study of the Têt River (SW France) using the BIT index. *Organic Geochemistry* **38**, 1593–1606.
- Kim J.-H., van der Meer J., Schouten S., Helmke P., Willmott V., Sangiorgi F., Koç N., Hopmans E. C. and Sinninghe Damsté J. S. (2010a) New indices and calibrations derived from the distribution of crenarchaeal isoprenoid tetraether lipids: Implications for past sea surface temperature reconstructions. *Geochimica et Cosmochimica Acta* **74**, 4639–4654.
- Kim J.-H., Zarzycka B., Buscail R., Peterse F., Bonnín J., Ludwig W., Schouten S. and Sinninghe Damsté J. S. (2010b) Contribution of river-borne soil organic carbon to the Gulf of Lions (NW Mediterranean). *Limnology and Oceanography* **55**, 507–518.
- Kim J.-H., Talbot H. M., Zarzycka B., Bauersachs T. and Wagner T. (2011) Occurrence and abundance of soil-specific bacterial membrane lipid markers in the Têt watershed (southern France): Soil-specific BHPs and branched GDGTs. *Geochemistry, Geophysics, Geosystems* **12**, Q02008.
- Kim J.-H., Zell C., Moreira-Turcq P., Perez M. A. P., Abril G., Mortillaro J.-M., Weijers J. W. H., Meziane T. and Sinninghe Damsté J. S. (2012) Tracing soil organic carbon in the lower Amazon River and its tributaries using GDGT distributions and bulk organic matter properties. *Geochimica et Cosmochimica Acta* **90**, 163–180.
- Kissin Y.V., Feulmer G.P. (1986) Gas chromatographic analysis of alkyl-substituted paraffins. *Journal of Chromatographic Science* **24**, 53–59.
- Kleiber H. P. and Niessen F. (2000) Variations of continental discharge pattern in space and time: implications from the Laptev Sea continental margin, Arctic Siberia. *International Journal of Earth Sciences* **89**, 605–616.
- Knappy C.S., Chong J.P.J., Keely B.J. (2009) Rapid discrimination of Archaeal tetraether lipid cores by liquid chromatography-tandem mass spectrometry. *Journal of the American Society for Mass Spectrometry* **20**, 51–59.
- Kool D. M., Talbot H. M., Rush D., Ettwig K. and Sinninghe Damsté J. S. (2014) Rare bacteriohopanepolyols as markers for an autotrophic, intra-aerobic methanotroph. *Geochimica et Cosmochimica Acta* **136**, 114–125.
- Kravchinsky V. A., Krainov M. A., Evans M. E., Peck J. A., King J. W., Kuzmin M. I., Sakai H., Kawai T. and Williams D. F. (2003) Magnetic record of Lake Baikal sediments: chronological and paleoclimatic implication for the last 6.7 Myr. *Palaeogeography, Palaeoclimatology, Palaeoecology* **195**, 281–298.
- Krishnamurthy R. V., Machavaram M., Baskaran M., Brooks J. M. and Champ M. A. (2001) Organic carbon flow in the Ob, Yenisey Rivers and Kara Sea of the Arctic region. *Marine Pollution Bulletin* **42**, 726–732.
- Lammers R.B. and Shiklomanov A.I. (2000) *R-ArcticNet, a regional hydrographic data network for the Pan-Arctic region*, Durham, NH: Water Systems Analysis Group, University of New Hampshire; distributed by the National Snow and Ice Data Center.
- Lammers R. B., Shiklomanov A. I., Vörösmarty C. J., Fekete B. M. and Peterson B. J. (2001) Assessment of contemporary Arctic river runoff based on observational discharge records. *Journal of Geophysical Research* **106**, 3321–3334.
- Langworthy T. A., Mayberry W. R. and Smith P. F. (1976) A sulfonolipid and novel glucosamidyglycolipids from the extreme thermoacidophile *Bacillus acidocaldarius*. *Biochimica et Biophysica Acta - Lipids and Lipid Metabolism* **431**, 550–569.
- Lantuit H., Overduin P. P., Couture N., Wetterich S., Aré F., Atkinson D., Brown J., Cherkashov G., Drozdov D., Forbes D. L., Graves-Gaylord A., Grigoriev M., Hubberten H.-W., Jordan J., Jorgenson T., Ødegård R. S., Ogorodov S., Pollard W. H., Rachold V., Sedenko S., Solomon S., Steenhuisen F., Streletskaia I. and Vasiliev A. (2012) The arctic coastal dynamics database: a new classification scheme and statistics on arctic permafrost coastlines. *Estuaries and Coasts* **35**, 383–400.
- Lauber C. L., Hamady M., Knight R. and Fierer N. (2009) Pyrosequencing-based assessment of soil pH as a predictor of soil bacterial community structure at the continental scale. *Applied and Environmental Microbiology* **75**, 5111–5120.
- Lee S.-H., Ka J.-O. and Cho J.-C. (2008) Members of the phylum Acidobacteria are dominant and metabolically active in rhizosphere soil. *FEMS Microbiology Letters* **285**, 263–269.
- Lein A. Y., Kravchishina M. D., Politova N. V., Savvichev A. S., Vesopolova E. F., Mitskevich I. N., Ul'yanova N. V., Shevchenko V. P. and Ivanov M. V. (2012) Transformation of particulate organic matter at the water-bottom boundary in the Russian Arctic seas: Evidence from isotope and radioisotope data. *Lithology and Mineral Resources* **47**, 99–128.

- Lengger S. K., Hopmans E. C., Sinninghe Damsté J. S. and Schouten S. (2014) Fossilization and degradation of archaeal intact polar tetraether lipids in deeply buried marine sediments (Peru Margin). *Geobiology* **12**, 212–220.
- Leng M. J. and Marshall J. D. (2004) Palaeoclimate interpretation of stable isotope data from lake sediment archives. *Quaternary Science Reviews* **23**, 811–831.
- Leng M. J. and Barker P. A. (2006) A review of the oxygen isotope composition of lacustrine diatom silica for palaeoclimate reconstruction. *Earth-Science Reviews* **75**, 5–27.
- Lisitsyn A. P. (1995) Marginal Filter of the Ocean. *Oceanology* **34**, 671–682.
- Liu X.-L., Leider A., Gillespie A., Gröger J., Versteegh G. J. M. and Hinrichs K.-U. (2010) Identification of polar lipid precursors of the ubiquitous branched GDGT orphan lipids in a peat bog in Northern Germany. *Organic Geochemistry* **41**, 653–660.
- Liu X.-L., Summons R. E. and Hinrichs K.-U. (2012) Extending the known range of glycerol ether lipids in the environment: structural assignments based on tandem mass spectral fragmentation patterns. *Rapid Communications in Mass Spectrometry* **26**, 2295–2302.
- Llirós M., Gich F., Plasencia A., Auguet J.-C., Darchambeau F., Casamayor E. O., Descy J.-P. and Borrego C. (2010) Vertical Distribution of ammonia-oxidizing crenarchaeota and methanogens in the epipelagic waters of Lake Kivu (Rwanda-Democratic Republic of the Congo). *Applied and Environmental Microbiology* **76**, 6853–6863.
- Lobbés J. M., Fitznar H. P. and Kattner G. (2000) Biogeochemical characteristics of dissolved and particulate organic matter in Russian rivers entering the Arctic Ocean. *Geochimica et Cosmochimica Acta* **64**, 2973–2983.
- Longinelli A. (1984) Oxygen isotopes in mammal bone phosphate: A new tool for paleohydrological and paleoclimatological research? *Geochimica et Cosmochimica Acta* **48**, 385–390.
- Loomis S. E., Russell J. M. and Sinninghe Damsté J. S. (2011) Distributions of branched GDGTs in soils and lake sediments from western Uganda: Implications for a lacustrine paleothermometer. *Organic Geochemistry* **42**, 739–751.
- Loomis S. E., Russell J. M., Ladd B., Street-Perrott F. A. and Sinninghe Damsté J. S. (2012) Calibration and application of the branched GDGT temperature proxy on East African lake sediments. *Earth and Planetary Science Letters* **357–358**, 277–288.
- Loomis S. E., Russell J. M., Heuroux A. M., D'Andrea W. J. and Sinninghe Damsté J. S. (2014a) Seasonal variability of branched glycerol dialkyl glycerol tetraethers (brGDGTs) in a temperate lake system. *Geochimica et Cosmochimica Acta* **144**, 173–187.
- Loomis S. E., Russell J. M., Eggermont H., Verschuren D. and Sinninghe Damsté J. S. (2014b) Effects of temperature, pH and nutrient concentration on branched GDGT distributions in East African lakes: Implications for paleoenvironmental reconstruction. *Organic Geochemistry* **66**, 25–37.
- Lumley T. using Fortran code by Miller A. (2009). Leaps: regression subset selection. R package version 2.9, <http://CRAN.R-project.org/package=leaps>.
- Maksimenko S. Y., Zemskaya T. I., Pavlova O. N., Ivanov V. G. and Buryukhaev S. P. (2008) Microbial community of the water column of the Selenga River-Lake Baikal biogeochemical barrier. *Microbiology* **77**, 587–594.
- Mariotti A., Lancelot C. and Billen G. (1984) Natural isotopic composition of nitrogen as a tracer of origin for suspended organic matter in the Scheldt estuary. *Geochimica et Cosmochimica Acta* **48**, 549–555.
- Martineau C., Whyte L. G. and Greer C. W. (2010) Stable isotope probing analysis of the diversity and activity of methanotrophic bacteria in soils from the Canadian High Arctic. *Applied Environmental Microbiology* **76**, 5773–5784.
- McDermott F. (2004) Palaeo-climate reconstruction from stable isotope variations in speleothems: a review. *Quaternary Science Reviews* **23**, 901–918.
- McMahon S. K., Wallenstein M. D. and Schimel J. P. (2009) Microbial growth in Arctic tundra soil at –2°C. *Environmental Microbiology Reports* **1**, 162–166.
- Menges J., Huguet C., Alcañiz J. M., Fietz S., Sachse D. and Rosell-Melé A. (2013) Water availability determines branched glycerol dialkyl glycerol tetraether distributions in soils of the Iberian Peninsula. *Biogeochemistry* **11**, 2571–2581.
- Ménot G., Bard E., Rostek F., Weijers J. W. H., Hopmans E. C., Schouten S. and Sinninghe Damsté J. S. (2006) Early reactivation of European rivers during the last deglaciation. *Science* **313**, 1623–1625.

- Midttun L. (1985) Formation of dense bottom water in the Barents Sea. *Deep Sea Research Part A. Oceanographic Research Papers* **32**, 1233–1241.
- Milliman, J.D. (1991). Flux and fate of fluvial sediment and water in coastal seas. In: *Ocean margin processes in global change: report of the Dahlem Workshop on Ocean Margin Processes in Global Change, Berlin, 1990, March 18–23, Dahlem workshop reports*. [Mantoura, R.F.C., Martin, J.-M. and Wollast, R. [Eds.]] Wiley, Chichester ; New York, 69–89.
- Montgomery D. C., Peck E. A. and Vining, G. G. (2007) *Introduction to linear regression analysis*. Wiley, John Wiley, Hoboken, N.J.; Chichester.
- Naidu A. S., Scanlan R. S., Feder H. M., Goering J. J., Hameedi M. J., Parker P. L., Behrens E. W., Caughey M. E. and Jewett S. C. (1993) Stable organic carbon isotopes in sediments of the north Bering-south Chukchi seas, Alaskan-Soviet Arctic Shelf. *Continental Shelf Research* **13**, 669–691.
- Namsaraev B. B., Rusanov I. I., Mitskevich I. N., Veslopolova E. F., Bol'shakov A. M. and Egorov A. V. (1995) Bacterial oxidation of methane in the Yenisei River estuary and the Kara Sea. *Oceanology* **35**.
- Neunlist S. and Rohmer M. (1985a) A novel hopanoid, 30-(5'-adenosyl) hopane, from the purple non-sulphur bacterium *Rhodospseudomonas acidophila*, with possible DNA interactions. *Biochemical Journal* **228**, 769.
- Neunlist S. and Rohmer M. (1985b) Novel hopanoids from the methylotrophic bacteria *Methylococcus capsulatus* and *Methylomonas methanica*. (22S)-35-aminobacteriohopane-30, 31, 32, 33, 34-pentol and (22S)-35-amino-3 beta-methylbacteriohopane-30, 31, 32, 33, 34-pentol. *Biochemical Journal* **231**, 635–639.
- Newton R. J., Jones S. E., Eiler A., McMahon K. D. and Bertilsson S. (2011) A guide to the natural history of freshwater lake bacteria. *Microbiology and Molecular Biology Reviews* **75**, 14–49.
- Niemann H., Stadnitskaia A., Wirth S. B., Gilli A., Anselmetti F. S., Sinninghe Damsté J. S., Schouten S., Hopmans E. C. and Lehmann M. F. (2012) Bacterial GDGTs in Holocene sediments and catchment soils of a high Alpine lake: application of the MBT/CBT-paleothermometer. *Climate of the Past* **8**, 889–906.
- Nimick D. A., Gammons C. H. and Parker S. R. (2011) Diel biogeochemical processes and their effect on the aqueous chemistry of streams: A review. *Chemical Geology* **283**, 3–17.
- Oechel W. C., Vourlitis G. L., Hastings S. J., Zulueta R. C., Hinzman L. and Kane D. (2000) Acclimation of ecosystem CO₂ exchange in the Alaskan Arctic in response to decadal climate warming. *Nature* **406**, 978–981.
- Oksanen J., F. Blanchet G., Kindt R., Legendre P., Minchin P. R., O'Hara R. B., Simpson G. L., Solymos P., Stevens M. H. H. and Wagner H. (2013). Vegan: community ecology package. R package version 2.0-8, <http://CRAN.R-project.org/package=vegan>.
- Oppermann B. I., Michaelis W., Blumenberg M., Frerichs J., Schulz H. M., Schippers A., Beaubien S. E. and Krüger M. (2010) Soil microbial community changes as a result of long-term exposure to a natural CO₂ vent. *Geochimica et Cosmochimica Acta* **74**, 2697–2716.
- Ouirsson G. and Albrecht P. (1992) Hopanoids. 1. Geohopanoids: the most abundant natural products on Earth? *Accounts of Chemical Research* **25**, 398–402.
- Pancost R. D. and Sinninghe Damsté J. S. (2003) Carbon isotopic compositions of prokaryotic lipids as tracers of carbon cycling in diverse settings. *Chemical Geology* **195**, 29–58.
- Pancost R. D., Zhang C. L., Tavacoli J., Talbot H. M., Farrimond P., Schouten S., Sinninghe Damsté J. S. and Sassen R. (2005) Lipid biomarkers preserved in hydrate-associated authigenic carbonate rocks of the Gulf of Mexico. *Palaeogeography, Palaeoclimatology, Palaeoecology* **227**, 48–66.
- Pavlov V. K. and Pfirman S. L. (1995) Hydrographic structure and variability of the Kara Sea: Implications for pollutant distribution. *Deep Sea Research Part II: Topical Studies in Oceanography* **42**, 1369–1390.
- Pearson A., Huang Z., Ingalls A. E., Romanek C. S., Wiegel J., Freeman K. H., Smittenberg R. H. and Zhang C. L. (2004) Nonmarine crenarchaeol in Nevada hot springs. *Applied and Environmental Microbiology* **70**, 5229–5237.
- Pearson A., Flood Page S. R., Jorgenson T. L., Fischer W. W. and Higgins M. B. (2007) Novel hopanoid cyclases from the environment. *Environmental Microbiology* **9**, 2175–2188.
- Pearson A., Leavitt W. D., Sáenz J. P., Summons R. E., Tam M. C.-M. and Close H. G. (2009) Diversity of hopanoids and squalene-hopene cyclases across a tropical land-sea gradient. *Environmental Microbiology* **11**, 1208–1223.

- Pearson E. J., Juggins S., Talbot H. M., Weckstrom J., Rosen P., Ryves D. B., Roberts S. J. and Schmidt R. (2011) A lacustrine GDGT-temperature calibration from the Scandinavian Arctic to Antarctic: Renewed potential for the application of GDGT-paleothermometry in lakes. *Geochimica et Cosmochimica Acta* **75**, 6225–6238.
- Penn K., Wu D., Eisen J. A. and Ward N. (2006) Characterization of bacterial communities associated with deep-sea corals on Gulf of Alaska seamounts. *Applied Environmental Microbiology* **72**, 1680–1683.
- Peppe D. J., Royer D. L., Cariglino B., Oliver S. Y., Newman S., Leight E., Enikolopov G., Fernandez-Burgos M., Herrera F., Adams J. M., Correa E., Currano E. D., Erickson J. M., Hinojosa L. F., Hoganson J. W., Iglesias A., Jaramillo C. A., Johnson K. R., Jordan G. J., Kraft N. J. B., Lovelock E. C., Lusk C. H., Niinemets Ü., Peñuelas J., Rapson G., Wing S. L. and Wright I. J. (2011) Sensitivity of leaf size and shape to climate: global patterns and paleoclimatic applications. *New Phytologist* **190**, 724–739.
- Peterse F., Kim J. H., Schouten S., Kristensen D. K., Koc N. and Sinninghe Damsté J. S. (2009a) Constraints on the application of the MBT/CBT palaeothermometer at high latitude environments (Svalbard, Norway). *Organic Geochemistry* **40**, 692–699.
- Peterse F., Van Der Meer M. T. J., Schouten S., Jia G., Ossebaar J., Blokker J. and Sinninghe Damsté J. S. (2009b) Assessment of soil n-alkane δD and branched tetraether membrane lipid distributions as tools for paleoelevation reconstruction. *Biogeosciences* **6**, 2799–2807.
- Peterse F., Nicol G. W., Schouten S. and Sinninghe Damsté J. S. (2010) Influence of soil pH on the abundance and distribution of core and intact polar lipid-derived branched GDGTs in soil. *Organic Geochemistry* **41**, 1171–1175.
- Peterse F., Hopmans E. C., Schouten S., Mets A., Rijpstra W. I. C. and Sinninghe Damsté J. S. (2011a) Identification and distribution of intact polar branched tetraether lipids in peat and soil. *Organic Geochemistry* **42**, 1007–1015.
- Peterse F., Prins M. A., Beets C. J., Troelstra S. R., Zheng H., Gu Z., Schouten S. and Sinninghe Damsté J. S. (2011b) Decoupled warming and monsoon precipitation in East Asia over the last deglaciation. *Earth and Planetary Science Letters* **301**, 256–264.
- Peterse F., van der Meer J., Schouten S., Weijers J. W. H., Fierer N., Jackson R. B., Kim J.-H. and Sinninghe Damsté J. S. (2012) Revised calibration of the MBT–CBT paleotemperature proxy based on branched tetraether membrane lipids in surface soils. *Geochimica et Cosmochimica Acta* **96**, 215–229.
- Peterse F., Martínez-García A., Zhou B., Beets C. J., Prins M. A., Zheng H. and Eglinton T. I. (2014a) Molecular records of continental air temperature and monsoon precipitation variability in East Asia spanning the past 130,000 years. *Quaternary Science Reviews* **83**, 76–82.
- Peterse F., Vonk J. E., Holmes R. M., Giosan L., Zimov N. and Eglinton T. I. (2014b) Branched glycerol dialkyl glycerol tetraethers in Arctic lake sediments: Sources and implications for paleothermometry at high latitudes. *Journal of Geophysical Research: Biogeosciences*, 119, 1738–1754.
- Peterson B. J. (2002) Increasing river discharge to the Arctic Ocean. *Science* **298**, 2171–2173.
- Pitcher A., Hopmans E. C., Schouten S. and Sinninghe Damsté J. S. (2009) Separation of core and intact polar archaeal tetraether lipids using silica columns: Insights into living and fossil biomass contributions. *Organic Geochemistry* **40**, 12–19.
- Polukhin, A. A., Makkaveev, P., 2014. Long-term dynamics of pH and total alkalinity in the Kara Sea. In: *Abstract Volume Arctic Ocean acidification*, Bergen, Norway, 27.
- Polyak L., Forman S. L., Herlihy F. A., Ivanov G. and Krinitsky P. (1997) Late Weichselian deglacial history of the Svyataya (Saint) Anna Trough, northern Kara Sea, Arctic Russia. *Marine Geology* **143**, 169–188.
- Polyak L., Levitan M., Gataullin V., Khusid T., Mikhailov V. and Mukhina V. (2000) The impact of glacial, river-discharge and sea-level change on Late Quaternary environments in the southwestern Kara Sea. *International Journal of Earth Sciences* **89**, 550–562.
- Polymenakou P. N., Bertilsson S., Tselepides A. and Stephanou E. G. (2005) Bacterial community composition in different sediments from the Eastern Mediterranean Sea: a comparison of four 16S ribosomal DNA clone libraries. *Microbial Ecology* **50**, 447–462.
- Poralla K., Muth G. and Härtner T. (2000) Hopanoids are formed during transition from substrate to aerial hyphae in *Streptomyces coelicolor* A3(2). *FEMS Microbiology Letters* **189**, 93–95.
- Portnov A., Smith A. J., Mienert J., Cherkashov G., Rekant P., Semenov P., Serov P. and Vanshtein B. (2013) Offshore permafrost decay and massive seabed methane escape in water depths >20 m at the

- South Kara Sea shelf. *Geophysical Research Letters* **40**, 3962–3967.
- Pouliot J., Galand P. E., Lovejoy C. and Vincent W. F. (2009) Vertical structure of archaeal communities and the distribution of ammonia monooxygenase A gene variants in two meromictic High Arctic lakes. *Environmental Microbiology* **11**, 687–699.
- Powers L. A., Werne J. P., Johnson T. C., Hopmans E. C., Sinninghe Damsté J. S. and Schouten S. (2004) Crenarchaeotal membrane lipids in lake sediments: A new paleotemperature proxy for continental paleoclimate reconstruction? *Geology* **32**, 613–616.
- Powers L., Werne J. P., Vanderwoude A. J., Sinninghe Damsté J. S., Hopmans E. C. and Schouten S. (2010) Applicability and calibration of the TEX₈₆ paleothermometer in lakes. *Organic Geochemistry* **41**, 404–413.
- Prahl, F.G., Cowie, G.L., de Lange, G.J., Sparrow, M.A., 2003. Selective organic matter preservation in “burn-down” turbidites on the Madeira Abyssal Plain. *Paleoceanography*, **18** (2), 30–1.
- Pross J., Contreras L., Bijl P. K., Greenwood D. R., Bohaty S. M., Schouten S., Bendle J. A., Röhl U., Tauxe L., Raine J. I., Huck C. E., Van De Flierdt T., Jamieson S. S. R., Stickley C. E., Van De Schootbrugge B., Escutia C., Brinkhuis H., Dotti C. E., Klaus A., Fehr A., Williams T., Bendle J. A. P., Carr S. A., Dunbar R. B., González J. J., Hayden T. G., Iwai M., Jimenez-Espejo F. J., Katsuki K., Soo Kong G., Mckay R. M., Nakai M., Olney M. P., Passchier S., Pekar S. F., Riesselman C. R., Sakai T., Shrivastava P. K., Sugisaki S., Tuo S., Welsh K. and Yamane M. (2012) Persistent near-tropical warmth on the Antarctic continent during the early Eocene epoch. *Nature* **487**, 73–77.
- Rampen S. W., Datema M., Rodrigo-Gámiz M., Schouten S., Reichart G.-J. and Sinninghe Damsté J. S. (2014) Sources and proxy potential of long chain alkyl diols in lacustrine environments. *Geochimica et Cosmochimica Acta* **144**, 59–71.
- Redshaw C. H., Cooke M. P., Talbot H. M., McGrath S. and Rowland S. J. (2008) Low biodegradability of fluoxetine HCl, diazepam and their human metabolites in sewage sludge-amended soil. *Journal of Soils and Sediments* **8**, 217–230.
- Rethemeyer J., Schubotz F., Talbot H. M., Cooke M. P., Hinrichs K.-U. and Mollenhauer G. (2010) Distribution of polar membrane lipids in permafrost soils and sediments of a small high Arctic catchment. *Organic Geochemistry* **41**, 1130–1145.
- Řezanka T., Siristova L., Melzoch K. and Sigler K. (2011) N-acylated bacteriohopanohexol-mannosamides from the thermophilic bacterium *Alicyclobacillus acidoterrestris*. *Lipids* **46**, 249–261.
- Rivkina E., Shcherbakova V., Laurinavichius K., Petrovskaya L., Krivushin K., Kraev G., Pecheritsina S. and Gilichinsky D. (2007) Biogeochemistry of methane and methanogenic archaea in permafrost. *FEMS Microbiology Ecology* **61**, 1–15.
- Robinson R. S., Kienast M., Luiza Albuquerque A., Altabet M., Contreras S., De Pol Holz R., Dubois N., Francois R., Galbraith E., Hsu T.-C., Ivanochko T., Jaccard S., Kao S.-J., Kiefer T., Kienast S., Lehmann M., Martinez P., McCarthy M., Möbius J., Pedersen T., Quan T. M., Ryabenko E., Schmittner A., Schneider R., Schneider-Mor A., Shigemitsu M., Sinclair D., Somes C., Studer A., Thunell R. and Yang J.-Y. (2012) A review of nitrogen isotopic alteration in marine sediments: N isotopic alteration in marine sediment. *Paleoceanography* **27**, PA4203.
- Rohmer M., Bouvier-Nave P. and Ourisson G. (1984) Distribution of hopanoid triterpenes in prokaryotes. *Journal of General Microbiology* **130**, 1137–1150.
- Rohmer M., Knani M., Simonin P., Sutter B. and Sahn H. (1993) Isoprenoid biosynthesis in bacteria: a novel pathway for the early steps leading to isopentenyl diphosphate. *Biochemistry Journal* **295**, 517–524.
- Romanovskii N. N., Hubberten H.-W., Gavrillov A. V., Eliseeva A. A. and Tipenko G. S. (2005) Offshore permafrost and gas hydrate stability zone on the shelf of East Siberian Seas. *Geo-Marine Letters* **25**, 167–182.
- Sáenz J. P. (2010) Hopanoid enrichment in a detergent resistant membrane fraction of *Crocospaera watsonii*: Implications for bacterial lipid raft formation. *Organic Geochemistry* **41**, 853–856.
- Sáenz J. P., Eglinton T. I. and Summons R. E. (2011) Abundance and structural diversity of bacteriohopanepolyols in suspended particulate matter along a river to ocean transect. *Organic Geochemistry* **42**, 774–780.
- Santruckova H., Bird M. I., Kalaschnikov Y. N., Grund M., Elhottova D., Simek M., Grigoryev S., Gleixner G., Arneith A., Schulze E. D. and Lloyd J. (2003) Microbial characteristics of soils on a latitudinal transect in Siberia. *Global Change Biology* **9**, 1106–1117.
- Savvichev A. S., Zakharova E. E., Veslopolova E. F., Rusanov I. I., Lein A. Y. and Ivanov M. V. (2010) Microbial processes of the carbon and sulfur cycles in the Kara Sea. *Oceanology* **50**, 893–908.

- Schoon P. L., de Kluijver A., Middelburg J. J., Downing J. A., Sinninghe Damsté J. S. and Schouten S. (2013) Influence of lake water pH and alkalinity on the distribution of core and intact polar branched glycerol dialkyl glycerol tetraethers (GDGTs) in lakes. *Organic Geochemistry* **60**, 72–82.
- Schouten S., Hoefs M.J.L., Koopmans M.P., Bosch H.-J., Sinninghe Damsté J.S. (1998) Structural characterization, occurrence and fate of archaeal ether-bound acyclic and cyclic biphytanes and corresponding diols in sediments. *Organic Geochemistry* **29**, 1305–1319.
- Schouten S., Hopmans E. C., Pancost R. D. and Sinninghe Damsté J. S. (2000) Widespread occurrence of structurally diverse tetraether membrane lipids: Evidence for the ubiquitous presence of low-temperature relatives of hyperthermophiles. *Proceedings of the National Academy of Sciences* **97**, 14421–14426.
- Schouten S., Hopmans E. C., Schefuß E. and Sinninghe Damsté J. S. (2002) Distributional variations in marine crenarchaeotal membrane lipids: a new tool for reconstructing ancient sea water temperatures? *Earth and Planetary Science Letters* **204**, 265–274.
- Schouten S., Huguet C., Hopmans E. C., Kienhuis M. V. M. and Sinninghe Damsté J. S. (2007a) Analytical methodology for TEX₈₆ paleothermometry by high-performance liquid chromatography/atmospheric pressure chemical ionization-mass spectrometry. *Analytical Chemistry* **79**, 2940–2944.
- Schouten S., Weijers J. W. H., Peterse F., van der Meer M. T. J. and Sinninghe Damsté J. S. (2007b) Development and application of novel organic proxies. *Geochimica et Cosmochimica Acta* **71**, A905–A905.
- Schouten S., Ossebaer J., Brummer G. J., Elderfield H. and Sinninghe Damsté J. S. (2007c) Transport of terrestrial organic matter to the deep North Atlantic Ocean by ice rafting. *Organic Geochemistry* **38**, 1161–1168.
- Schouten S., Eldrett J., Greenwood D. R., Harding I., Baas M. and Sinninghe Damsté J. S. (2008) Onset of long-term cooling of Greenland near the Eocene-Oligocene boundary as revealed by branched tetraether lipids. *Geology* **36**, 147–150.
- Schouten S., Hopmans E. C., van der Meer J., Mets A., Bard E., Bianchi T. S., Diefendorf A., Escala M., Freeman K. H., Furukawa Y., Huguet C., Ingalls A., Menot-Combes G., Nederbragt A. J., Oba M., Pearson A., Pearson E. J., Rosell-Melé A., Schaeffer P., Shah S. R., Shanahan T. M., Smith R. W., Smittenberg R., Talbot H. M., Uchida M., Van Mooy B. A. S., Yamamoto M., Zhang Z. H. and Sinninghe Damsté J. S. (2009) An interlaboratory study of TEX₈₆ and BIT analysis using high-performance liquid chromatography-mass spectrometry. *Geochemistry Geophysics Geosystems* **10**, 13.
- Schouten S., Rijpstra W. I. C., Durisch-Kaiser E., Schubert C. J. and Sinninghe Damsté J. S. (2012) Distribution of glycerol dialkyl glycerol tetraether lipids in the water column of Lake Tanganyika. *Organic Geochemistry* **53**, 34–37.
- Schouten S., Hopmans E. C. and Sinninghe Damsté J. S. (2013a) The organic geochemistry of glycerol dialkyl glycerol tetraether lipids: A review. *Organic Geochemistry* **54**, 19–61.
- Schouten S., Hopmans E. C., Rosell-Melé A., Pearson A., Adam P., Bauersachs T., Bard E., Bernasconi S. M., Bianchi T. S., Brooks J. J., Carlson L. T., Castañeda I. S., Derrén S., Selver A. D., Dutta K., Eglinton T., Fosse C., Galy V., Grice K., Hinrichs K.-U., Huang Y., Huguet A., Huguet C., Hurley S., Ingalls A., Jia G., Keely B., Knappy C., Kondo M., Krishnan S., Lincoln S., Lipp J., Mangelsdorf K., Martínez-García A., Ménot G., Mets A., Mollenhauer G., Ohkouchi N., Ossebaer J., Pagani M., Pancost R. D., Pearson E. J., Peterse F., Reichert G.-J., Schaeffer P., Schmitt G., Schwark L., Shah S. R., Smith R. W., Smittenberg R. H., Summons R. E., Takano Y., Talbot H. M., Taylor K. W. R., Tarozo R., Uchida M., van Dongen B. E., Van Mooy B. A. S., Wang J., Warren C., Weijers J. W. H., Werne J. P., Woltering M., Xie S., Yamamoto M., Yang H., Zhang C. L., Zhang Y., Zhao M. and Damsté J. S. (2013b) An interlaboratory study of TEX₈₆ and BIT analysis of sediments, extracts, and standard mixtures. *Geochemistry Geophysics Geosystems* **14**, 5263–5285.
- Schuur E. A. G., Vogel J. G., Crummer K. G., Lee H., Sickman J. O. and Osterkamp T. E. (2009) The effect of permafrost thaw on old carbon release and net carbon exchange from tundra. *Nature* **459**, 556–559.
- Shakhova N., Semiletov I., Salyuk A., Yusupov V., Kosmach D. and Gustafsson O. (2010) Extensive methane venting to the atmosphere from sediments of the East Siberian Arctic Shelf. *Science* **327**, 1246–1250.
- Shepard F. P. (1954) Nomenclature based on sand-silt-clay ratios. *Journal of Sedimentary Research* **24**, 151–158.
- Shpolyanskaya N. A. (2003) Massive ground ice as a basis for paleogeographic reconstruction. In *Permafrost: proceedings of the 8th International Conference on Permafrost, Zurich, Switzerland*, 21–25

- July 2003. M. Phillips, S. M. Springman, and L. U. Arenson, A.A. Balkema [Eds.] Lisse, Exton, PA.
- Sievert S. M., Kuever J. and Muyzer G. (2000) Identification of 16S Ribosomal DNA-Defined Bacterial Populations at a Shallow Submarine Hydrothermal Vent near Milos Island (Greece). *Applied and Environmental Microbiology* **66**, 3102–3109.
- Sigman D. M., Jaccard S. L. and Haug G. H. (2004) Polar ocean stratification in a cold climate. *Nature* **428**, 59–63.
- Simankova M. V., Kotsyurbenko O. R., Lueders T., Nozhevnikova A. N., Wagner B., Conrad R. and Friedrich M. W. (2003) Isolation and characterization of new strains of methanogens from cold terrestrial habitats. *Systematic and Applied Microbiology* **26**, 312–318.
- Sinninghe Damsté J. S., Hopmans E. C., Pancost R. D., Schouten S. and Geenevasen J. a. J. (2000) Newly discovered non-isoprenoid glycerol dialkyl glycerol tetraether lipids in sediments. *Chemical Communications*, 1683–1684.
- Sinninghe Damsté J. S., Schouten S., Hopmans E. C., van Duin A. C. T. and Geenevasen J. A. J. (2002) Crenarchaeol: the characteristic core glycerol dibiphytanyl glycerol tetraether membrane lipid of cosmopolitan pelagic crenarchaeota. *Journal of Lipid Research* **43**, 1641–1651.
- Sinninghe Damsté J. S., Rijpstra W. I. C., Schouten S., Fuerst J. A., Jetten M. S. M. and Strous M. (2004) The occurrence of hopanoids in planctomycetes: implications for the sedimentary biomarker record. *Organic Geochemistry* **35**, 561–566.
- Sinninghe Damsté J. S., Ossebaar J., Abbas B., Schouten S. and Verschuren D. (2009) Fluxes and distribution of tetraether lipids in an equatorial African lake: Constraints on the application of the TEX₈₆ palaeothermometer and BIT index in lacustrine settings. *Geochimica et Cosmochimica Acta* **73**, 4232–4249.
- Sinninghe Damsté J. S., Rijpstra W. I. C., Hopmans E. C., Weijers J. W. H., Foesel B. U., Overmann J. and Dedysh S. N. (2011) 13, 16-dimethyl octacosanedioic acid (iso-diabolic acid), a common membrane-spanning lipid of Acidobacteria subdivisions 1 and 3. *Applied and Environmental Microbiology* **77**, 4147–4154.
- Sinninghe Damsté J. S., Ossebaar J., Schouten S. and Verschuren D. (2012) Distribution of tetraether lipids in the 25-ka sedimentary record of Lake Challa: Extracting reliable TEX₈₆ and MBT/CBT palaeotemperatures from an equatorial African lake. *Quaternary Science Reviews* **50**, 43–54.
- Sinninghe Damsté J. S., Rijpstra W. I. C., Hopmans E. C., Foesel B. U., Wüst P. K., Overmann J., Tank M., Bryant D. A., Dunfield P. F., Houghton K. and Stott M. B. (2014) Ether- and ester-bound iso-diabolic acid and other lipids in members of Acidobacteria subdivision 4. *Applied and Environmental Microbiology* **80**, 5207–5218.
- Smith L. C. and Pavelsky T. M. (2008) Estimation of river discharge, propagation speed, and hydraulic geometry from space: Lena River, Siberia. *Water Resources Research* **44**, W03427.
- Smith P., Fang C., Dawson J. J. C. and Moncrieff J. B. (2008) Impact of global warming on soil organic carbon. In *Advances in Agronomy* Elsevier. pp. 1–43.
- Smith R. W., Bianchi T. S. and Li X. (2012) A re-evaluation of the use of branched GDGTs as terrestrial biomarkers: Implications for the BIT Index. *Geochimica et Cosmochimica Acta* **80**, 14–29.
- Smittenberg R.H., Hopmans E.C., Schouten S., Sinninghe Damsté J.S. (2002) Rapid isolation of biomarkers for compound specific radiocarbon dating using high-performance liquid chromatography and flow injection analysis-atmospheric pressure chemical ionisation mass spectrometry. *Journal of Chromatography A* **978**, 129–140.
- Smol J. P. and Cumming B. F. (2000) Tracking long-term changes in climate using algal indicators in lake sediments. *Journal of Phycology* **36**, 986–1011.
- Sorokovikova L. M. (1997) Gaseous regime of the Yenisei River under present conditions. *Water Resources* **24**, 80–83.
- Sorokovikova L. M., Popovskaya G. I., Belykh O. I., Tomberg I. V., Maksimenko S. Y., Bashenkhaeva N. V., Ivanov V. G. and Zemskaya T. I. (2012) Plankton composition and water chemistry in the mixing zone of the Selenga River with Lake Baikal. *Hydrobiologia* **695**, 329–341.
- Stedmon C. A., Amon R. M. W., Rinehart A. J. and Walker S. A. (2011) The supply and characteristics of colored dissolved organic matter (CDOM) in the Arctic Ocean: Pan Arctic trends and differences. *Marine Chemistry* **124**, 108–118.
- Stein R., Dittmers K., Fahl K., Kraus M., Matthiessen J., Niessen F., Pirrung M., Polyakova Y., Schoster F., Steinke T. and Fütterer D. K. (2004) Arctic (palaeo) river discharge and environmental change: evidence from the Holocene Kara Sea sedimentary record. *Quaternary Science Reviews* **23**, 1485–1511.

- Stolbovoi V. I. S. and Sheremet B. (2002) General soil characteristics. In *Land Resources of Russia CD-ROM* International Institute for Applied Systems Analysis and the Russian Academy of Science, Laxenburg, Austria.
- Streletskaia I. D., Vasiliev A. A. and Vanstein B. G. (2009) Erosion of sediment and organic carbon from the Kara Sea Coast. *Arctic, Antarctic, and Alpine Research* **41**, 79–87.
- Sun Q., Chu G. Q., Liu M. M., Xie M. M., Li S. Q., Ling Y. A., Wang X. H., Shi L. M., Jia G. D. and Lu H. Y. (2011) Distributions and temperature dependence of branched glycerol dialkyl glycerol tetraethers in recent lacustrine sediments from China and Nepal. *Journal of Geophysical Research-Bio-geosciences* **116** G01008.
- Talbot H. M., Watson D. F., Murrell J. C., Carter J. F. and Farrimond P. (2001) Analysis of intact bacteriohopanepolyols from methanotrophic bacteria by reversed-phase high-performance liquid chromatography–atmospheric pressure chemical ionisation mass spectrometry. *Journal of Chromatography A* **921**, 175–185.
- Talbot H. M., Squier A. H., Keely B. J. and Farrimond P. (2003) Atmospheric pressure chemical ionisation reversed-phase liquid chromatography/ion trap mass spectrometry of intact bacteriohopanepolyols. *Rapid Communications in Mass Spectrometry* **17**, 728–737.
- Talbot H. M. and Farrimond P. (2007) Bacterial populations recorded in diverse sedimentary biohopanoid distributions. *Organic Geochemistry* **38**, 1212–1225.
- Talbot H. M., Summons R. E., Jahnke L. L., Cockell C. S., Rohmer M. and Farrimond P. (2008) Cyanobacterial bacteriohopanepolyol signatures from cultures and natural environmental settings. *Organic Geochemistry* **39**, 232–263.
- Talbot H. M., Handley L., Spencer-Jones C. L., Dinga B. J., Schefuß E., Mann P. J., Poulsen J. R., Spencer R. G. M., Wabakhanghanzi J. N. and Wagner T. (2014) Variability in aerobic methane oxidation over the past 1.2 Myrs recorded in microbial biomarker signatures from Congo fan sediments. *Geochimica et Cosmochimica Acta* **133**, 387–401.
- Tarasov P. E., Bezrukova E. V. and Krivonogov S. K. (2009) Late Glacial and Holocene changes in vegetation cover and climate in southern Siberia derived from a 15 kyr long pollen record from Lake Kotokel. *Climate of the Past* **5**, 285–295.
- Taylor K. A. and Harvey R. H. (2011) Bacterial hopanoids as tracers of organic carbon sources and processing across the western Arctic continental shelf. *Organic Geochemistry* **42**, 487–497.
- Telang S. A., Pocklington R., Naidu A. S., Romankevich E. A., Gitelson I. I. and Gladyshev M. I. (1990) Carbon and mineral transport in major North American, Russian, and Siberian rivers: the St Lawrence, the Mackenzie, the Yukon, the Arctic Alaskan rivers, the Arctic Basin rivers, and the Yenisei. In *Biogeochemistry of Major World Rivers SCOPE*. John Wiley & sons. pp. 75–104.
- Thornton S. F. and McManus J. (1994) Application of organic carbon and nitrogen stable isotope and C/N ratios as source indicators of organic matter provenance in estuarine systems: evidence from the Tay Estuary, Scotland. *Estuarine, Coastal and Shelf Science* **38**, 219–233.
- Tierney J. E., Russell J. M., Huang Y., Sinninghe Damsté J. S., Hopmans E. C. and Cohen A. S. (2008) Northern Hemisphere controls on tropical Southeast African climate during the past 60,000 years. *Science* **322**, 252–255.
- Tierney J. E. and Russell J. M. (2009) Distributions of branched GDGTs in a tropical lake system: Implications for lacustrine application of the MBT/CBT paleoproxy. *Organic Geochemistry* **40**, 1032–1036.
- Tierney J. E., Russell J. M., Eggermont H., Hopmans E. C., Verschuren D. and Sinninghe Damsté J. S. (2010) Environmental controls on branched tetraether lipid distributions in tropical East African lake sediments. *Geochimica et Cosmochimica Acta* **74**, 4902–4918.
- Tierney J. E., Schouten S., Pitcher A., Hopmans E. C. and Sinninghe Damsté J. S. (2012) Core and intact polar glycerol dialkyl glycerol tetraethers (GDGTs) in Sand Pond, Warwick, Rhode Island (USA): Insights into the origin of lacustrine GDGTs. *Geochimica et Cosmochimica Acta* **77**, 561–581.
- Trotsenko Y. A. and Khmelenina V. N. (2005) Aerobic methanotrophic bacteria of cold ecosystems. *FEMS Microbiology Ecology* **53**, 15–26.
- Turner R. R. and Harris R. C. (1970) The distribution of non-detrital iron and manganese in two cores from the Kara Sea. *Deep Sea Research and Oceanographic Abstracts* **17**, 633–636.
- Tyler J. J., Nederbragt A. J., Jones V. J. and Thurow J. W. (2010) Assessing past temperature and soil pH estimates from bacterial tetraether membrane lipids: Evidence from the recent lake sediments of Lochnagar, Scotland. *Journal of Geophysical Research: Biogeosciences* **115**, G01015.
- van de Vossen J. L. C. M., Driessen A. J. M. and Konings W. N. (1998) The essence of being extremophilic.

- philic: the role of the unique archaeal membrane lipids. *Extremophiles* **2**, 163–170.
- van Dongen B. E., Talbot H. M., Schouten S., Pearson P. N. and Pancost R. D. (2006) Well preserved Palaeogene and Cretaceous biomarkers from the Kilwa area, Tanzania. *Organic Geochemistry* **37**, 539–557.
- van Dongen B. E., Semiletov I., Weijers J. W. H. and Gustafsson O. R. (2008) Contrasting lipid biomarker composition of terrestrial organic matter exported from across the Eurasian Arctic by the five great Russian Arctic rivers. *Global Biogeochemical Cycles* **22**, 1011.
- Van Winden J. F., Talbot H. M., Kip N., Reichart G.-J., Pol A., McNamara N. P., Jetten M. S. M., Op den Camp H. J. M. and Sinninghe Damsté J. S. (2012a) Bacteriohopanepolyol signatures as markers for methanotrophic bacteria in peat moss. *Geochimica et Cosmochimica Acta* **77**, 52–61.
- Van Winden J. F., Talbot H. M., De Vleeschouwer F., Reichart G.-J. and Sinninghe Damsté J. S. (2012b) Variation in methanotroph-related proxies in peat deposits from Misten Bog, Hautes-Fagnes, Belgium. *Organic Geochemistry* **53**, 73–79.
- Verschuren D., Damsté J. S. S., Moernaut J., Kristen I., Blaauw M., Fagot M. and Haug G. H. (2009) Half-precessional dynamics of monsoon rainfall near the East African Equator. *Nature* **462**, 637–641.
- Vetrov A. A. and Romankevich E. A. (2011) Genesis of organic matter in the Kara Sea bottom sediments. *Oceanology* **51**, 608–615.
- Vonk J. E., Sánchez-García L., Semiletov I., Dudarev O., Eglinton T., Andersson A. and Gustafsson O. (2010) Molecular and radiocarbon constraints on sources and degradation of terrestrial organic carbon along the Kolyma paleoriver transect, East Siberian Sea. *Biogeosciences* **7**, 3153–3166.
- Votintsev K. K. (1985) Main features of the hydrochemistry of Lake Baikal. *Water Resources* **12**, 106–116.
- Votintsev, K. K., Mescheryakova A. I. and G. I. Popovskaya [Eds.] (1975). *Cycle of Organic Matter in Lake Baikal*. Nauka, Novosibirsk.
- Waelbroeck C., Monfray P., Oechel W. C., Hastings S. and Vourlitis G. (1997) The impact of permafrost thawing on the carbon dynamics of tundra. *Geophysical Research Letters* **24**, 229–232.
- Wagner T., Kallweit W., Talbot H. M., Mollenhauer G., Boom A. and Zabel M. (2014) Microbial biomarkers support organic carbon transport from methane-rich Amazon wetlands to the shelf and deep sea fan during recent and glacial climate conditions. *Organic Geochemistry* **67**, 85–98.
- Walker I. R., Smol J. P., Engstrom D. R. and Birks H. J. B. (1991) An assessment of chironomidae as quantitative indicators of past climatic change. *Canadian Journal of Fisheries and Aquatic Sciences* **48**, 975–987.
- Wang H., Liu W., Zhang C. L., Wang Z., Wang J., Liu Z. and Dong H. (2012) Distribution of glycerol dialkyl glycerol tetraethers in surface sediments of Lake Qinghai and surrounding soil. *Organic Geochemistry* **47**, 78–87.
- Weijers J. W. H., Schouten S., Hopmans E. C., Geenevasen J. A. J., David O. R. P., Coleman J. M., Pancost R. D. and Sinninghe Damsté J. S. (2006a) Membrane lipids of mesophilic anaerobic bacteria thriving in peats have typical archaeal traits. *Environmental Microbiology* **8**, 648–657.
- Weijers J. W. H., Schouten S., Spaargaren O. C. and Sinninghe Damsté J. S. (2006b) Occurrence and distribution of tetraether membrane lipids in soils: Implications for the use of the TEX₈₆ proxy and the BIT index. *Organic Geochemistry* **37**, 1680–1693.
- Weijers J. W. H., Schouten S., van den Donker J. C., Hopmans E. C. and Sinninghe Damsté J. S. (2007a) Environmental controls on bacterial tetraether membrane lipid distribution in soils. *Geochimica et Cosmochimica Acta* **71**, 703–713.
- Weijers J. W. H., Schefuß E., Schouten S. and Sinninghe Damsté J. S. (2007b) Coupled thermal and hydrological evolution of tropical Africa over the last deglaciation. *Science* **315**, 1701–1704.
- Weijers J. W. H., Schouten S., Sluijs A., Brinkhuis H. and Sinninghe Damsté J. S. (2007c) Warm arctic continents during the Palaeocene–Eocene thermal maximum. *Earth and Planetary Science Letters* **261**, 230–238.
- Weijers J. W. H., Panoto E., van Bleijswijk J., Schouten S., Rijpstra W. I. C., Balk M., Stams A. J. M. and Sinninghe Damsté J. S. (2009a) Constraints on the biological source(s) of the orphan branched tetraether membrane lipids. *Geomicrobiology Journal* **26**, 402–414.
- Weijers J. W. H., Schouten S., Schefuß E., Schneider R. R. and Sinninghe Damsté J. S. (2009b) Disentangling marine, soil and plant organic carbon contributions to continental margin sediments: A multi-proxy approach in a 20,000 year sediment record from the Congo deep-sea fan. *Geochimica et Cosmochimica Acta* **73**, 119–132.

- Weijers J. W. H., Wiesenberg G. L. B., Bol R., Hopmans E. C. and Pancost R. D. (2010) Carbon isotopic composition of branched tetraether membrane lipids in soils suggest a rapid turnover and a heterotrophic life style of their source organism(s). *Biogeosciences* **7**, 2959–2973.
- Weijers J. W. H., Steinmann P., Hopmans E. C., Schouten S. and Sinninghe Damsté J. S. (2011a) Bacterial tetraether membrane lipids in peat and coal: Testing the MBT–CBT temperature proxy for climate reconstruction. *Organic Geochemistry* **42**, 477–486.
- Weijers J. W. H., Bernhardt B., Peterse F., Werne J. P., Dungait J. A. J., Schouten S. and Sinninghe Damsté J. S. (2011b) Absence of seasonal patterns in MBT–CBT indices in mid-latitude soils. *Geochimica et Cosmochimica Acta* **75**, 3179–3190.
- Weijers J. W. H., Schefuß E., Kim J.-H., Sinninghe Damsté J. S. and Schouten S. (2014) Constraints on the sources of branched tetraether membrane lipids in distal marine sediments. *Organic Geochemistry* **72**, 14–22.
- White D. C., Davis W. M., Nickels J. S., King J. D. and Bobbie R. J. (1979) Determination of the sedimentary microbial biomass by extractable lipid phosphate. *Oecologia* **40**, 51–62.
- Woltering M., Werne J. P., Kish J. L., Hicks R., Sinninghe Damsté J. S. and Schouten S. (2012) Vertical and temporal variability in concentration and distribution of thaumarchaeotal tetraether lipids in Lake Superior and the implications for the application of the TEX₈₆ temperature proxy. *Geochimica et Cosmochimica Acta* **87**, 136–153.
- Xu Y., Cooke M. P., Talbot H. M. and Simpson M. J. (2009) Bacteriohopanepolyol signatures of bacterial populations in Western Canadian soils. *Organic Geochemistry* **40**, 79–86.
- Yang G., Zhang C. L., Xie S., Chen Z., Gao M., Ge Z. and Yang Z. (2013) Microbial glycerol dialkyl glycerol tetraethers from river water and soil near the Three Gorges Dam on the Yangtze River. *Organic Geochemistry* **56**, 40–50.
- Yang H., Ding W., Zhang C. L., Wu X., Ma X., He G., Huang J. and Xie S. (2011) Occurrence of tetraether lipids in stalagmites: Implications for sources and GDGT-based proxies. *Organic Geochemistry* **42**, 108–115.
- Yang H., Pancost R. D., Dang X., Zhou X., Evershed R. P., Xiao G., Tang C., Gao L., Guo Z. and Xie S. (2013) Correlations between microbial tetraether lipids and environmental variables in Chinese soils: Optimizing the paleo-reconstructions in semi-arid and arid regions. *Geochimica et Cosmochimica Acta* **126**, 49–69.
- Yergeau E., Hogues H., Whyte L. G. and Greer C. W. (2010) The functional potential of high Arctic permafrost revealed by metagenomic sequencing, qPCR and microarray analyses. *ISME Journal* **4**, 1206–1214.
- Yoshii K. (1999) Stable isotope analyses of benthic organisms in Lake Baikal. *Hydrobiologia* **411**, 145–159.
- Yoshii K., Melnik N. G., Timoshkin O. A., Bondarenko N. A., Anoshko P. N., Yoshioka T. and Wada E. (1999) Stable isotope analyses of the pelagic food web in Lake Baikal. *Limnology and Oceanography* **44**, 502–511.
- Zech R., Gao L., Tarozo R. and Huang Y. (2012) Branched glycerol dialkyl glycerol tetraethers in Pleistocene loess-paleosol sequences: Three case studies. *Organic Geochemistry* **53**, 38–44.
- Zell C., Kim J.-H., Moreira-Turcq P., Abril G., Hopmans E. C., Bonnet M.-P., Sobrinho R. L. and Sinninghe Damsté J. S. (2013) Disentangling the origins of branched tetraether lipids and crenarchaeol in the lower Amazon river: Implications for GDGT-based proxies. *Limnology and Oceanography* **58**, 343–353.
- Zell C., Kim J.-H., Balsinha M., Dorhout D., Fernandes C., Baas M. and Sinninghe Damsté J. S. (2014a) Transport of branched tetraether lipids from the Tagus River basin to the coastal ocean of the Portuguese margin: consequences for the interpretation of the MBT/CBT paleothermometer. *Biogeosciences* **11**, 5637–5655.
- Zell C., Kim J.-H., Hollander D., Lorenzoni L., Baker P., Silva C. G., Nitttrouer C. and Sinninghe Damsté J. S. (2014b) Sources and distributions of branched and isoprenoid tetraether lipids on the Amazon shelf and fan: implications for the use of GDGT-based proxies in marine sediments. *Geochimica et Cosmochimica Acta* **139**, 293–312.
- Zhang C. L., Wang J., Wei Y., Zhu C., Huang L. and Dong H. (2012) Production of branched tetraether lipids in the lower Pearl River and estuary: effects of extraction methods and impact on bGDGT proxies. *Frontiers in Microbiology* **2**, 274.
- Zhu C., Weijers J. W. H., Wagner T., Pan J. M., Chen J. F. and Pancost R. D. (2011a) Sources and distributions of tetraether lipids in surface sediments across a large river-dominated continental margin. *Organic Geochemistry* **42**, 376–386.

- Zhu C., Talbot H. M., Wagner T., Pan J.-M. and Pancost R. D. (2011b) Distribution of hopanoids along a land to sea transect: Implications for microbial ecology and the use of hopanoids in environmental studies. *Limnology and Oceanography* **56**, 1850–1865.
- Zhu C., Wagner T., Talbot H. M., Weijers J. W. H., Pan J.-M. and Pancost R. D. (2013) Mechanistic controls on diverse fates of terrestrial organic components in the East China Sea. *Geochimica et Cosmochimica Acta* **117**, 129–143.
- Zwiers F. W. (2002) Climate change: The 20-year forecast. *Nature* **416**, 690–691.

SUMMARY

Understanding and predicting climate variability is a major scientific challenge, especially as climate-induced environmental change will impact on human society. In order to constrain the magnitude of this impact, models to predict future climates are increasingly complex, and partly based on what is known of the climate in the past, both from the recent instrumental and historical records as well as from geological climate archives. In this thesis so-called proxies are used to estimate past air temperatures, soil pH, and the amount of terrigenous organic matter delivered to the marine system by rivers. To reconstruct these changes, the quantity and distributions of two groups of lipids is studied; bacterial branched glycerol dialkyl glycerol tetraether lipids (brGDGTs) and bacteriohopanepolyols (BHPs).

BrGDGTs are membrane-spanning lipids that are produced most likely by Acidobacteria. These ubiquitous bacteria occur in soil, peat bogs, and lake and coastal marine sediments and the water column. In soils, the number of methyl groups on the alkyl chains was shown to depend on the mean annual air temperature (MAT) and soil pH, while the number of cyclopentane moieties correlates with soil pH. Based on this observation, the methylation index of branched tetraethers (MBT) and the cyclisation index of branched tetraethers (CBT) were introduced to reconstruct MAT and soil pH. As brGDGTs are found in large quantities in soil and peat, it was assumed that their presence in freshwater and marine environments followed soil erosion and transport through river systems. Hence, changes in the brGDGT composition in river fan sediments, were assumed to reflect fluctuations in the past MAT and soil pH of the drainage basin of a river system. Furthermore, their presence allows reconstructing the relative contribution of soil-derived organic matter in the marine system, using the branched and isoprenoid tetraether (BIT) index. A second group of lipids studied are BHPs, lipids that are produced by a variety of (cyano)bacteria. The relative concentration of a set of soil-marker BHPs, expressed as the R'_{soil} index, allows tracing the delivery of terrigenous organic matter to the marine system. Furthermore, the presence of some BHPs can imply a more or less specific chemotaxonomic source.

Previous studies of brGDGTs, described the abundance of only 9 brGDGT compounds, the 5-methyl brGDGTs, where the penta- and hexamethylated brGDGTs have a methylation on the 5 and/ or ω -5 position. In this thesis, the abundance of 15 brGDGT compounds is described, including 6 compounds that were previously partially or fully co-eluting with these 5-methyl compounds. The chemical structure of these novel compounds was determined, following the isolation of penta- and hexamethylated brGDGTs from a Siberian peat. They were described to contain a methylation on the 6 and/ or ω -6 position, and are therefore referred to as 6-methyl brGDGTs. Using improved chromatography, these 6-methyl compounds were shown to be

abundant in soils globally, where their relative concentration was strongly related to the soil pH. Their presence has an impact on the interpretation of currently used brGDGT palaeoclimate proxies, as their separate quantification results in a significantly improved soil pH proxy, and a pH-independent temperature proxy.

The Siberian mainland, a region that is particularly vulnerable to climate change, contains a vast amount of frozen permafrost. The current and accelerating rise in the concentration of greenhouse gasses in the atmosphere, that cause the warming of the globe, can lead to the mobilization of this stock of fossil organic carbon. In a warmer climate, large changes in the export of water and organic carbon to the Arctic Ocean are to be expected. The Yenisei River is the largest river of the Siberian mainland, draining the Mongolian steppe and highlands and vast areas of Siberian temperate forests and taiga, before flowing into the Kara Sea, a shallow shelf sea of the Arctic Ocean. To perform informed palaeoclimate reconstructions of the Yenisei River watershed in particular, but also of Siberian watersheds in general, the source (i.e. soil-derived, riverine or marine) of the bacterial organic matter was determined in the modern Yenisei River and its outflow in the Kara Sea.

Although the Yenisei River crosses several climatic zones, the brGDGTs suspended in the water column of the Yenisei River show very little variation downstream the river. The reconstructed temperature and pH using brGDGTs was distinct from the air temperature and soil pH. The strong temperature gradient imposed on the watershed soils was thus not reflected in the riverine brGDGT distribution. However, the reconstructed water temperature and pH approached those of the Yenisei River water, indicating that the Yenisei River brGDGTs are dominated by riverine in-situ produced lipids.

The prevalent assumption that the riverine brGDGT signal delivered to the ocean represents an average of the watershed was challenged by a study performed on Lake Baikal. Here, it is described how the contrasting brGDGT distribution of its main inflowing river, Selenga River, is strikingly different compared to that from the lake. A detailed study of this outflow system indicates that degradation or in-situ production of brGDGTs takes place. However, the brGDGTs exported from the lake do not contribute to the brGDGT signal encountered in the Yenisei River. Consequently, the watershed of Lake Baikal does not seem to contribute GDGTs to the marine system.

Following up on this, the fate of riverine brGDGTs after their introduction in the marine environment was reconstructed. Moving downstream in the Yenisei River outflow, a strong shift is observed in the brGDGT distribution. It is postulated that this can be explained by degradation, which will affect different brGDGT pools to a different extent. The performance of the BIT index as a tracer for terrigenous and riverine bacterial organic matter was also tested. Although the contribution of the different brGDGT pools present (soil-derived, coastal cliff-derived and produced in-situ in the river) is unknown, the BIT-index performs well in the Kara Sea system. These findings were compared with an independent set of bacteriohopanepolyols lipids. Six BHPs that are generally enriched in soils, i.e. the so-called soil-marker BHPs, are encountered both in the Yenisei River as its outflow. Both pools of bacterial OM show the same decrease in concentration in the marine system.

Although in-situ production of brGDGTs only affects the modern sediments to a minor extent, it clearly influences downcore sediments, as was shown in the Kara Sea Trough. Here, sediments deposited since the deglaciation of this site (13 ka), illustrate that in-situ production of marine brGDGTs can strongly influence their distribution. The shift from a system in front of the river outflow to a system dominated by marine brGDGTs resulting from the substantial rise in sealevel since the last Glacial is also evident from the BIT index record. During this shift substantial changes in the terrigenous sources of brGDGTs have occurred, resulting in changing brGDGT distributions. Both processes strongly influence brGDGT-based palaeoclimate reconstructions.

Overall, the work presented in this thesis has implications for brGDGT-based palaeoclimate reconstructions, not only in Siberian river systems, but also for brGDGTs encountered in river fan sediments worldwide. Analytical developments allow performing palaeoclimate reconstructions with improved accuracy. However, the source of brGDGTs encountered in river fan sediments was shown to be a complex mixture of riverine, marine and soil-derived brGDGTs. In modern sediments, their relative abundance can be influenced by degradation of bacterial organic matter. On geological timescales, changes in sea level affect the importance of marine in-situ produced brGDGTs. The provenance of terrigenous brGDGTs delivered to and stored in the marine sediments can be modified by changes in the erosion of watershed soils, by the presence of large lakes in the flowpath of the river, and by preferential degradation of more labile brGDGT pools. BrGDGT-based palaeoclimate reconstructions thus have to be performed taking these processes in mind.

SAMENVATTING

Toekomstige klimaatveranderingen zullen een grote invloed hebben op de samenleving. Het begrijpen en voorspellen van klimaatveranderingen is daarom een belangrijke uitdaging voor de wetenschap. Om deze klimaatveranderingen te kunnen kwantificeren worden klimaatmodellen gebruikt. Deze uiterst complexe modellen worden onder andere gekalibreerd op basis van klimaatreconstructies van het verleden, gebaseerd op zowel historische metingen en op klimaatreconstructies met behulp van geologische klimaatarchieven. In dit proefschrift worden zogenaamde ‘proxies’ gebruikt om de luchttemperatuur en bodem pH uit het verleden te reconstrueren, evenals de hoeveelheid terrigeen organisch materiaal getransporteerd door rivieren naar het marien milieu. Om deze parameters te reconstrueren, worden twee groepen lipiden bestudeerd; bacteriële vertakte glycerol dialkyl glycerol tetraethers (vGDGTs) en bacteriële hopanepolyolen (BHP).

vGDGTs zijn membraan-overspannende lipiden die meest waarschijnlijk worden geproduceerd door Acidobacteria. Deze alomtegenwoordige bacteriën worden teruggevonden in bodems, veen, en in de lacustriene en mariene water kolom en sedimenten. In bodems was aangetoond dat het aantal methyl groepen van de alkylketens afhankelijk is van de jaargemiddelde luchttemperatuur en de bodem pH, terwijl het aantal cyclopentaan groepen een verband vertoont met de pH van de bodem. Gebaseerd op deze observatie werden de

‘methylation of branched tetraethers (MBT)’ en de ‘cyclization of branched tetraethers (CBT)’ indices geïntroduceerd om de jaargemiddelde luchttemperatuur en de bodem pH te kunnen reconstrueren. Aangezien vGDGTs in hoge concentraties aangetroffen worden in bodems en venen, werd hun aanwezigheid in rivier, lacustriene en mariene systemen verondersteld het gevolg te zijn van bodemerosie en -afspoeling. Veranderingen in de vGDGT verdeling in de sedimenten van de uitstroomdelta zouden dus de klimaatverandering in het stroombekken van de rivier reflecteren. Daarnaast kunnen we de hoeveelheid bodemmateriaal in het marien milieu, aangeleverd met de rivier, reconstrueren met de ‘branched and isoprenoid tetraether (BIT)’ index, waarin de hoeveelheid vGDGTs vergeleken wordt met die van GDGTs geproduceerd in het mariene milieu. Een tweede groep bestudeerde lipiden, de BHP, worden geproduceerd door een verscheidenheid aan (cyano)bacteriën. De relatieve concentratie van een groep BHP kenmerkend voor bodems, wordt uitgedrukt in de R'_{soil} ratio, waarmee de hoeveelheid bodemmateriaal die aangeleverd wordt in het marien milieu kan worden getraceerd. Bovendien hebben sommige BHP componenten een meer of minder specifieke chemotaxonomische bron.

Eerdere studies van vGDGTs beschreven de distributie van negen vGDGT componenten, de 5-methyl vGDGTs, waarbij de penta- en hexa-gemethyleerde vGDGTs een methylgroep hebben op de 5- en/of de ω -5 positie van de alkylketen. In dit proefschrift wordt de distributie van vijftien individuele vGDGTs beschreven, inclusief zes componenten die voorheen volledig of gedeeltelijk co-elueerden met de 5-methyl vGDGTs. De chemische structuur van deze nieuwe penta- en hexa-gemethyleerde moleculen werd bepaald na hun isolatie uit een Siberisch veen. Deze componenten bleken gemethyleerd te zijn op de 6 en/of ω -6 positie, en er wordt dus naar gerefereerd als de 6-methyl vGDGTs. Gebruik makend van verbeterde chromatografie, werd aangetoond dat deze 6-methyl vGDGTs abundant zijn in bodems wereldwijd en dat hun fractionele abundantie afhangt van de bodem pH. Hun aanwezigheid heeft een impact op bestaande vGDGT paleoklimaat proxies, en wanneer zij apart gekwantificeerd worden resulteert dat in een significant verbeterde proxy voor bodem pH en een pH-onafhankelijke temperatuur proxy.

Het Siberische continent, een regio die erg gevoelig is voor klimaatveranderingen, bevat een grote hoeveelheid permafrost. De huidige en versnellende toename in de concentratie van broeikasgassen in de atmosfeer, die de planeet opwarmen, kan leiden tot de mobilisatie van dit fossiel koolstof. In een warmer klimaat verwachten we een sterke toename in de export van water en organisch materiaal naar de Arctische Oceaan. De Yenisei, de grootste rivier van het Siberische continent, watert de Mongoolse steppe en hooglanden en uitgestrekte gebieden met Siberisch loofwoud en taiga af, en mondt uit in de Kara Zee, een kustzee van de Arctische Oceaan. Om gegronde paleoklimaat reconstructies te kunnen maken van het stroombekken van de Yenisei in het bijzonder, en van Siberische stroombekkens in het algemeen, werd de bron van de bacteriële organische materie in de huidige Yenisei en zijn uitstroom in de Kara Zee bepaald.

Ook al doorkruist de Yenisei verschillende klimaatzones, toch tonen de vGDGTs van het gesuspendeerd particulier materiaal weinig verandering in samenstelling als we de rivier stroomafwaarts volgen. De gereconstrueerde temperatuur en pH, gebaseerd op de vGDGT verdeling, verschilde aanzienlijk van de gemeten jaargemiddelde lucht temperatuur en bodem

pH. De sterke temperatuurgradiënt die inwerkt op de bodems van het stroombekken wordt dus niet herkend in de riveriene vGDGT verdeling. In tegendeel, de gereconstrueerde water temperatuur en pH benaderen die van het rivier water, wat er op wijst dat deze lipiden in-situ in het rivierwater zijn geproduceerd.

De heersende aanname dat riveriene vGDGTs die aangeleverd worden aan het mariene milieu, afkomstig zijn uit het hele stroomgebied, wordt betwist in een studie uitgevoerd in het meer Baikal. Hier wordt beschreven hoe de vGDGT distributie van de grootste instromende rivier, de Selenga, sterk afwijkt van het vGDGT signaal in het meer zelf. Een gedetailleerde studie van het uitstroomsysteem geeft aan dat degradatie of in-situ productie van vGDGTs plaats vindt. Daarnaast blijkt de vGDGTs distributie in het meer aanzienlijk te verschillen van die van vGDGTs stroomafwaarts in de Yenisei. Het stroombekken van het Baikal meer lijkt dus niet bij te dragen aan het vGDGT signaal in de rivier dat uiteindelijk geëxporteerd wordt naar het mariene systeem.

In opvolging hiervan werd het lot van vGDGTs na hun introductie in het mariene systeem bestudeerd. Als de uitstroom van de Yenisei in de Kara zee gevolgd wordt, dan wordt een sterke verandering geobserveerd in de verdeling van de vGDGTs. Dit kan worden verklaard door degradatie, wat verschillende vGDGT bronnen in verschillende mate zal beïnvloeden. Hoewel de relatieve contributie van de verschillende vGDGT bronnen (afkomstig van bodems, van kustkliffen, of geproduceerd in de rivier) onbekend, toch presteert de BIT index als indicator van bacterieel organisch materiaal geproduceerd in de bodem of rivier zelf goed in de Kara Zee. Deze bevinding werd gestaafd met een onafhankelijke set lipiden, bacteriohopanepolyolen. Zes BHP die normaal verrijkt zijn in bodems, de zogenaamde bodem-merker BHP, werden zowel in de Yenisei als in zijn uitstroom in de Kara Zee teruggevonden. BHPs en vGDGTs tonen dezelfde afname in concentratie in het mariene systeem.

Ook al bleek de in-situ productie van mariene vGDGT in oppervlakesedimenten slechts miniem te beïnvloeden, het had duidelijk wel een sterke invloed op diepere sedimenten, zoals aangetoond werd in de Kara Zee Trog. Hier werden sedimenten afgezet sinds de deglaciatie in de laatste 13 duizend jaar, die illustreren dat in-situ productie van mariene vGDGTs hun distributie sterk kan beïnvloeden. De shift van een systeem vlak voor de uitstroom van een rivier naar een systeem gedomineerd door mariene vGDGTs, veroorzaakt wordt door de substantiële stijging in zeeniveau sinds het laatste Glaciaal, wordt ook gereflecteerd in de verandering van de BIT index. Tijdens deze shift hebben wezenlijke veranderingen in de bron van het terrigene materiaal plaatsgevonden, die resulteren in veranderingen in de verdeling van vGDGTs. Beide processen hebben een sterke invloed op paleoklimaat reconstructies gebaseerd op vGDGTs.

In besluit heeft het werk gepresenteerd in deze thesis implicaties voor paleoklimaat reconstructies gebaseerd op vGDGTs, niet enkel in Siberische riviersystemen, maar ook voor vGDGTs in de sedimenten van uitstroomdelta's wereldwijd. Analytische ontwikkelingen maken het mogelijk om paleoklimaatreconstructies met een vergrote nauwkeurigheid uit te voeren. Er werd echter ook aangetoond dat vGDGTs in de sedimenten van uitstroomdelta's een complex mengsel van riveriene, mariene en terrigene vGDGTs is. In oppervlakesedimenten werd hun verdeling beïnvloed door degradatie van het bacteriële organisch materiaal. Op een geologische

tijdsschaal zullen zeespiegelschommelingen de contributie van mariene in-situ geproduceerde vGDGTs beïnvloeden. De herkomst van terrigene vGDGTs die worden aangeleverd en opgeslagen in mariene sedimenten kan worden beïnvloed door veranderingen in de erosie van het stroombekken, door de aanwezigheid van grote meren in het stroomtraject van de rivier, en door preferentiële degradatie van meer labiele vGDGT bronnen. Paleoklimaatreconstructies gebaseerd op vGDGTs kunnen enkel uitgevoerd worden wanneer rekening gehouden wordt met deze processen.

РЕЗЮМЕ

Понимание и прогнозирование изменения климата является крупной научной задачей, в особенности, когда проявление климатической нестабильности отображается на условиях окружающей среды, непосредственно воздействуя на человеческое общество. Чтобы ограничить величину этого воздействия, модели для прогнозирования будущих климатических изменений становятся все более сложными и, отчасти, основаны на том, что уже известно об изменении климата в прошлом, опираясь на новейшие результаты аналитических исследований, исторические записи, а так же данные полученные из природных «геологических архивов». В данной работе, так называемые «прокси» используются для оценок прошлых температур воздуха, pH почвы, и количества терригенного органического вещества, поставляемого в Карское море речной системой Енисея. Для их реконструкции, были изучены количество и распределение двух групп липидных органических соединений: бактериальных разветвлённых глицеролдиалкил-глицеролтетраэфиров (branched glycerol dialkyl glycerol tetraether lipids или brGDGTs) и бактериальных гопанополиолов (bacteriohopanepolyols или BHPs).

BrGDGTs являются трансмембранными липидами, которые, скорее всего, производятся Ацидобактериями. Этих повсюду встречающиеся бактерий находили и в почвах, и в торфяниках, в озёрных и прибрежных морских осадках, а также в водной толще. Было выявлено, что в почвах, количество метильных групп в алкильной цепи BrGDGTs коррелируется со средней годовой температурой воздуха (СГТ) и pH почвы, в то время как количество циклопентановых фрагментов коррелируется только лишь с pH почвы. Основываясь на этом наблюдении, для восстановления СГТ и pH почвы были введены индексы метилирования разветвлённых глицеролдиалкил-глицеролтетраэфиров (the **m**ethylation index of **b**ranched **t**etraethers - MBT) и циклизации разветвлённых глицеролдиалкил-глицеролтетраэфиров (the **c**yclisation index of **b**ranched **t**etraethers - CBT). Так как brGDGTs были обнаружены в больших количествах в почвах и торфах, было предположено, что их наличие в пресноводных и морских условиях является результатом почвенной эрозии с последующим переносом речными системами. Таким образом, изменения в составе brGDGTs в осадках конусов выноса рек были прокоррелированы с прошлыми колебаниями CBT и pH почвы водосборного бассейна речной системы. Более того, применение ещё одного индекса разветвлённых и изопреноидных глицеролдиалкил-глицеролтетраэфиров (the **b**ranched and **i**soprenoid **t**etraether - BIT) позволяет реконструировать относительный вклад органического вещества почв в морскую систему.

Вторая группа исследованных липидов представлена BHPs, которые производятся различными группами (циано)бактерий. Относительное содержание некоторых почвенных BHPs определяются индексом R^{soil}, который позволяет проследить перенос терригенного органического вещества в морскую систему. Кроме того, присутствие определённых

ВНPs может относительно точно указывать на их конкретный хемо-таксономический источник.

Предыдущие исследования brGDGTs, показали преобладание всего девяти brGDGT соединений, включая 5-метил-brGDGTs, где пента- и гекса-метилированные brGDGTs содержат метильные группы в α и/или ω -5 положении. В данной работе, описано преобладание пятнадцати brGDGT соединений, включая шесть соединений, которые ранее были частично или полностью ко-элюируемы с 5-метил-brGDGTs соединениями. Химическая структура этих новых соединений была определена после изолирования пента- и гекса-метилированных brGDGTs из сибирского торфа. Эти соединения содержали метильные группы в α и/или ω -6 положении, и, следовательно, были названы 6-метил-brGDGTs. Используя усовершенствованный хроматографический метод, полученные 6-метил-соединения были обнаружены в изобилии в почвах всего мира, где их преобладание чётко связывалось с показателями почвенных pH. Присутствие 6-метил-brGDGTs оказывает влияние на интерпретацию палеоклиматических brGDGT прокси используемых в настоящее время. Исключение их из современных brGDGT прокси в значительной степени улучшает показатели почвенного pH и pH-независимый температурный индекс.

Сибирь особенно уязвима к климатическим изменениям и вмещает огромное количество вечной мерзлоты. Современный увеличивающийся рост концентраций парниковых газов в атмосфере, вызывающий глобальное потепление, может привести к мобилизации захороненного органического углерода. В более теплом климате предполагаются заметные изменения в переносе общего количества воды и органического углерода в Северный Ледовитый океан. Енисей является крупнейшей речной системой Сибири начинающейся в монгольской степи и, перед тем как впасть в Северный Ледовитый океан через Карское море, протекает через высокогорье, обширные территории Сибирских лесов умеренного пояса, тайгу, лесо-тундру, тундру и арктическую пустыню. Для осуществления обоснованных палеоклиматических реконструкций реки Енисей, источник (т.е. почвенного, речного или морского) бактериального органического вещества определялся вдоль современного течения реки Енисей, в системе река Селенга – озеро Байкал, в Енисейском Заливе и в Карском море.

Несмотря на то, что Енисей пересекает несколько климатических зон, brGDGTs из водной толщи показывают крайне незначительное изменение вниз по течению реки. Реконструированные температура и pH воды с использованием brGDGTs были отличны оттемпературы воздуха и почвенного pH. Сильный температурный градиент, выявленный на почвенных водоразделах, в распределении речных brGDGT выявлен не был. Тем не менее, реконструированные значения температуры и pH воды достаточно близки к современным значениям температуры и pH воды в Енисее. Это указывает на то, что преобладающими brGDGTs Енисея являются липиды сформированные непосредственно в водной толще енисейской речной системы.

Распространённое представление о том, что речной brGDGT сигнал привнесённый в океан представляет собой усреднённое значение brGDGT сигнала водораздела, было оспорено исследованиями берегового раздела озера Байкал. В этой работе описывается как контрастные распределения brGDGT из водной толщи основного притока Байкала, реки Селенга, разительно отличаются от распределений brGDGT воды озера Байкал. Детальное изучение системы река Селенга – озеро Байкал показывает, что деградация или производство brGDGTs осуществляются непосредственно на месте. Тем не менее,

brGDGTs экспортируемые из озера Байкал в Енисей не оказывают влияние на brGDGT сигнал измеренный в реке. Следовательно, водораздел озера Байкал, скорее всего, не влияет на привнос GDGTs в морскую систему.

Вслед за этим, была осуществлена реконструкция дальнейшей судьбы речных brGDGTs, после того как они были привнесены в морскую среду. Вниз по течению Енисея, в распределении brGDGT наблюдается заметное изменение. Было предположено, что подобный сдвиг может быть объяснён за счёт деградации липидов, которая будет в различной степени влиять на многообразные резервуары brGDGT. Также тестировали эффективность индекса BIT в качестве индикатора переноса терригенного и речного бактериального органического вещества. Хотя вклад различных резервуаров brGDGT, таких как почва, прибрежные скалы, непосредственно сформированные в реке липиды, неизвестно, BIT-индекс показал высокую эффективность в системе Карского моря. Эти данные были сопоставлены с независимым набором липидов BHPs. Шесть BHPs, которые, как правило, в обилие встречаются в почвах, то есть, так называемые, почвенные-биомаркеры BHPs, были обнаружены как в Енисее, так и в его устье. В морской системе, оба резервуара бактериального органического вещества показывают один и тот же тренд снижения их концентраций.

Хотя производство речных brGDGTs в незначительной степени влияет на речные со-временные отложения, в морских отложениях прогиба Карского моря влияние речных brGDGTs было явно выражено. Морские постгляциальные отложения, (13 кА), показывают, что производство морских brGDGTs может сильно влиять на общее распределение brGDGTs. В результате значительного повышения уровня моря со времени последнего оледенения, переход от системы устья реки к системе доминирующей морскими brGDGTs был чётко определён. Запись BIT-индекса также подтвердила этот факт. Во время этого перехода произошли существенные изменения в терригенных источниках brGDGTs, в результате чего общие распределения brGDGT также изменились. Оба процесса сильно влияют на палеоклиматические реконструкции основанные на brGDGTs.

В целом, работа представленная в данной диссертации, имеет потенциал для проведения палеоклиматических реконструкций на основе brGDGTs не только для Сибирских речных систем, но и для brGDGTs встречающихся в отложениях речных конусов выноса по всему миру. Аналитические разработки и усовершенствования позволяют проводить палеоклиматические реконструкции с повышенной точностью. Тем не менее, источник brGDGTs в речных конусах выноса является сложной смесью речных, морских и почвенных brGDGTs. В современных отложениях, их относительное содержание может зависеть от деградации бактериального органического вещества. На геологических масштабах времени, изменения уровня моря влияют на производительность морских brGDGTs. Происхождение терригенных brGDGTs привносимых и захороненных в морских отложениях могут быть изменены в результате процессов эрозии почвенных водоразделов, присутствием крупных озёр на пути течения реки, и избирательной деградации более лабильных резервуаров brGDGTs. Таким образом, палеоклиматические реконструкции на основе brGDGTs должны с большим вниманием учитывать эти факторы.

ACKNOWLEDGMENTS

This PhD thesis is the product of a lifelong interest in the world, its biology and geology, and I'm very proud of what I achieved. Mama, papa, dankjewel om mij altijd te steunen, zelfs toen ik naar 'Holland' vertrok om te gaan werken, of was het nu studeren? However, a passion for the subject is not all it takes to finish a thesis, and the work presented here has definitely been shaped by the inputs of many of you.

First and foremost, Jaap! Thank you for all the expert advice I got during these years, I have learnt so much about GDGTs and about science in general. You've been a great and very supportive mentor, and your quick replies really helped me wrapping this manuscript up, especially as we were getting closer to some "deadlines"!

Ellen 'lefty loosey, righty tighty', your office was always open, for musing about science or life, or for HPLC emergencies. You've been called the "mom" of the bgc students before, and that indeed reflects your eagerness to get involved and shed your light on, well, anything! Whether we were talking babies or branched GDGTs, it has been very much appreciated.

Alina, I still treasure the time we spent together in Russia, thank you for taking a novice PhD student all the way there. You were always happy to advice and to introduce me to new people, which helped me to feel at home on Texel in no time at all. Of course, you had nowhere to hide, we were sharing an office! Here, I would also like to take the opportunity to thank all the people that helped Alina and me get our hands on the precious Siberian samples described in the book, Georgy Cherkachov, Alexander Vasiliev, Irina Streletskaya, Andrey Fedotov, Ilya Enushchenko, and the many collaborators that I did not get to meet in person.

Stefan, although we only worked together for one chapter of this thesis, fortunately there was plenty of opportunity to interact and learn, working on conference talks, during the literature discussions, etc., which I enjoyed a lot!

Helen, Juliane, Frances, thank you for inviting me over to Newcastle and help me with the analysis of a whole new set of lipids. It was nice to see our work resulting in an interesting chapter of my thesis.

Erik Tegelaar and Ron Hofland, you were so kind to allow me to measure branched alkyl chains on your GC-SMB-MS, with excellent results. I have never seen a group of people so proliferate in the multiplication of 14, thank you for the good cooperation back then, and I hope to meet again at the conferences.

Here, I would like to thank the assessment and reading committees of this thesis: Prof. Dr. Gesine Mollenhauer, Dr. Helen Talbot, Dr. Francien Peterse, Dr. Jorien Vonk, Prof. Dr. Appy Sluijs, Prof. Dr. Stefan Schouten, Prof. Dr. Lex Bouwman, Prof. Dr. Gert-Jan Reichart and Prof. Dr. James Russell.

I was so lucky to learn a lot of new tricks during my PhD. *Labtricks* that I learnt from Anhelique, Michiel, Monique, Irene, Marianne and Denise. A PhD requires a lot of time in the lab, and I really enjoyed working with you. Anhelique, special thanks for the care with which you analysed my samples during my pregnancy. *HPLC-tricks* that I learnt ‘on the job’, thanks to Jort and Ellen. Thank you for letting me play around with your toys, I discovered that I really like to fiddle with tubing and retention times! *R-tricks*, thanks to Jaap van der Meer, who sat down with me to dust off my statistical skills from University, with succes! Many of the figures presented in this thesis were made in R.

I also want to thank everybody who made the lunch breaks, coffee breaks, department outings, evenings out and conferences so enjoyable. Nicole, Yvo, Darci, Sabine, Raquel, Petra, Santi, David, Paul, Lennart, Luke, Nikky, Cécile, Rik, Julie, Craig, Francien, Marcel, Sebastiaan, Maarten K., Laura, Douwe, Marta, Martina, Sandra, Yvonne, Elisabeth, Dorien, Lisa, Eli, Evgenia, Rodrigo and family, Claudia, Els, Loes, Irene, Jort, Sharyn, John, Monique, Kim, Marc, Sebastian (gains!), Taco, Jolanda, and many more.

A special mention here for the scientist-moms, Cécile, Sofia, Julie, it was lovely having you around, always happy to talk about bits and bobs (and science!). Ook dankjewel aan de trouwe bezoekers van het ochtendlijke Nederlandse koffie uurtje, het was voor mij echt een moment om eens rustig neer te zitten, en eindelijk mijn Nederlandse cultuur wat bij te schaven. Ik zeg nog steeds ‘Doei!’ als ik een winkel uit loop...

Claudia, we were meant to be PhD-buddies, working on the same kind of project (unfortunately almost never with the same conclusions), living in the same house, and I’m glad you agreed to be my paranymph. Freija, after we moved to Antwerp you made us feel at home in a ‘foreign’ city that was so unlike Texel, thank you for that. I hope you’ll enjoy being a paranymph.

Robert, thanks a lot! For everything, but especially for your patience during this process of writing up. I’m so glad I have you by my side. Ralph, Margaux, ik zie jullie erg graag, jullie maken het plaatje compleet.^{3e}

When I arrived on Texel for the first time, as a masterstudent, I knew little of what I was getting myself into... As I’m writing this, almost five years later, I can only say that my time at the NIOZ has been filled with fun and exciting science. But of course I also made loads of friends, met Robert, and we got Ralph and Margaux. We all take something along from our time on Texel. Whether it’s a bunch of new friends, whether it’s the discovery of its impressive cloud formations, whether it’s the love(s) of your life, it’s definitely more than a book and a title. And thank you all for that.

CURRICULUM VITAE

Cindy De Jonge was born on the 31st of December 1987, in Ghent, Belgium. She completed a bachelor of Biology at the University of Ghent, with a minor specialising in functional biology and in evolution (2005-2008). Following up on this, she obtained a Master in Marine and Lacustrine Sciences (2008-2010), also at the University of Ghent. She performed a masterthesis project at the Renard Centre of Marine Geology, on the reconstruction of palaeoclimatic changes recorded in the Gulf of Cadiz sediments. It was during this research project that her promotor, Prof. Dr. David Van Rooij, encouraged her to perform part of the research at the Royal NIOZ (Texel, The Netherlands), in the group of Jaap S. Sinninghe Damsté. She decided to continue research in this group, starting as a PhD student in 2010.

During her PhD, her focus was on the testing and improving of lipid-based palaeoclimate proxies, working on analytical improvements and studying environmental datasets (Siberia, Russia). The results of this project are presented in this manuscript.

Cindy currently lives in Antwerp, with her partner Robert, and their two children Ralph and Margaux.

